

ナノクリスタルドープ光導波路及び
次世代フォトニックデバイスへの適用

(研究課題番号 09305021)

平成12年度科学研究費補助金 (基板研究 (A))

研究成果報告書

平成13年5月

研究代表者 加藤 勇

(早稲田大学理工学部・教授)

研究分担者 宇高勝之

(早稲田大学理工学部・教授)

目次

1. はしがき	1
2. 研究発表	
2-1 学会誌、国際会議等	3
2-2 口頭発表	7
3. 研究成果	
3-1 研究の背景	12
3-2 研究目的	18
3-3 研究成果概要	19
4. 添付論文	25

1 はしがき

近年、光通信の各種光デバイスの開発が急速に進みつつある。しかし、新しい光子材料の研究、およびそれを用いた新しい発想の光デバイスの研究開発はあまり進んでいない。そこで本研究では、これまでに開発した二重管式同軸線路形マイクロ波プラズマ CVD 装置において原料ガスの超精密流量制御やチャンバー内のガス圧制御により、プラズマ CVD 装置内におけるプラズマ状態の測定、アモルファスシリコン膜、 $a\text{-Si:H/Si}_3\text{N}_4$ 多層膜やシリコンナノボール膜等を作製し、その膜特性の研究やフォトニックデバイスとしての応用を図った。

さらに、発光デバイスや光変調デバイスなどによるフォトニックデバイスの高性能化や新機能の発現を目的として、高い光学利得と非線形性を有する高品質ナノクリスタルを化合物半導体系により光導波路内に形成するための基本技術を開発すべく、高密度でかつ位置制御された高品質化合物半導体ナノクリスタルの電子ビーム露光や気相エッチングを用いたナノ加工及び分子線エピタキシャル成長法を用いた高精度結晶成長などの作成技術について検討するとともに、これら作成された非線形材料が適用される光スイッチや波長変換素子などの新規フォトニックスイッチングデバイスの提案並びに基本デバイス特性の評価を行った。さらに化合物半導体光導波路及びシリコン系フォトニック材料の融合を図った機能素子の検討を行った。

本報告書は以上を目的として、平成9年 - 12年度の4年間にわたり行われた研究において得られた成果をまとめたものである。

<研究組織>

研究代表者	加藤 勇	(早稲田大学理工学部・教授)
研究分担者	宇高勝之	(早稲田大学理工学部・教授)

<研究経費>

平成 9 年度	13,200 千円
平成 10 年度	12,300 千円
平成 11 年度	7,700 千円
平成 12 年度	1,900 千円
計	35,100 千円

2. 研究発表

2-1 学会誌、国際会議等

- (1) 加藤 勇、匂坂雅彦、菅井貴義、上垣内岳司：“2重管式同軸線路形 MPCVD 装置を用いて作製した a-Si:H/Si₃N₄ 多層膜の膜質とその光回路素子への応用” 電子情報通信学会論文誌、Vol.J84-C No.4、PP245-250、2001.
- (2) 松本貴之、加藤 勇：“Dependence of PL Characteristics of a-Si:H Nanoball Films Fabricated By Double Tubed Coaxial Line Type MPCVD System On Substrate Position”第 18 回プラズマプロセッシング研究会プロシーディングス、PP.425-426、2001.
- (3) 菅井貴義、加藤 勇：“Quality Of a-Si:H/Si₃N₄ Multilayer Films Fabricated By Double Tubed Coaxial Line Type MPCVD System(Ⅱ)”第 18 回プラズマプロセッシング研究会プロシーディングス、PP427-428、2001.
- (4) 匂坂雅彦、菅井貴義、田丸直幸、加藤 勇：“Film Quality Of a a-Si:H/Si₃N₄ Multilayer Films And Propagate Properties Of Optical Waveguides Using The Multilayer Films”第 18 回プラズマプロセッシング研究会プロシーディングス、pp429-430、2001.
- (5) Isamu Kato, Yuuki Nakano, Nobuhiko Yamaguchi: "Effect of Ar⁺ Ion Bombardment During Hydrogenated Amorphous Silicon Film Growth in Plasma Chemical Vapor Deposition System2000",Jpn. J. Appl. Phys. ,Vol.3 No.9,PP.6404-6409,2000.
- (6) Masahiko Sagisaka, Isamu Kato : "Polarization Properties of a-Si:H/Si₃N₄ Multilayers Optical Waveguides"、第 17 回プラズマプロセッシング研究会プロシーディングス、pp.243-246、2000.
- (7) Takeshi Kamigaichi, Isamu Kato : “ Quality of a-Si:H/Si₃N₄ Multilayer Films Fabricated by Double Tubed Coaxial Line Type MPCVD System”、第 17 回プラズマプロセッシング研究会プロシーディングス、PP.239-242、2000.
- (8) Yoshio Kawahara, Isamu Kato : “Dependence of PL Characteristics of

- a-Si:H Nanoball Films Fabricated by Double Tubed Coaxial Line Type MPCVD System on Ion Bombardment Energy”、第 17 回プラズマプロセッシング研究会プロシーディングス、PP.641-644、2000.
- (9) Takashi Ootsuka, Isamu Kato : “Fabrication of Polymer - Like a-C:H Films by Double Tubed Coaxial Line Type MPCVD System”、第 17 回プラズマプロセッシング研究会プロシーディングス、PP.223-226、2000.
- (10) Yuuki Nakano, Isamu Kato : "Fabrication of a-Si:H Film Using H₂/SiH₄ Plasma by Longitudinal Magnetic Field Applied MPCVD System(II)"、第 17 回プラズマプロセッシング研究会プロシーディングス、PP.141-144、2000.
- (11) Isamu Kato, Yoshio Kawahara, O.P.Agnihotri: " Photo Luminescence from a-Si:H Nanoball Films Fabricated by Double Tubed Coaxial Line Type Microwave Plasma CVD system", Proceedings of the Tenth International Workshop on the Physics of Semiconductor Devices II , PP.1107-1114, 1999.
- (12) Isamu Kato, Yoshio Kawahara, "Photo Luminescence from Si Films Fabricated by Double Tubed Coaxial Line Type Microwave Plasma CVD Apparatus", International Conference on Reactive Plasmas and Symposium on plasma Proceeding, PP.109-110,1998.
- (13) Isamu Kato、Toshihiro Yamagishi, Yoshinori Morita, and Taro Kamiko : “Stabilization of Ar Plasma by Applying Longitudinal Magnetic Field”, Electronics and Communications in Japan Part2,Vol.81 No.3、PP10-16、1998.
- (14) Hidetaka Iizuka, Masayuki Usuda, Isamu Kato : “Fabrication Of a-Si:H Film Using H₂/SiH₄ Plasma by Longitudinal Magnetic Field Applied MPCVD System”、第 15 回プラズマプロセッシング研究会プロシーディングス、PP. 406-409、1998.
- (15) Nobuyuki Koshiji, Kazuhiro Watanabe, ISAMU KATO : “Si Luminescence Material Fabricated Using MPCVD Coaxial Line Type”、第 15 回プラズマプロセッシング研究会プロシーディングス、PP.

140-143, 1998.

- (16) Hirotaka Ogihara, Naoyuki Iwata, ISAMU KATO : "Effect of Bombardment During a-Si:H Film Growth", 第15回プラズマプロセッシング研究会プロシーディングス, PP.84-87, 1998.
- (17) 加藤 勇、山岸俊浩、森田義則、神子太郎 : "縦磁界印加による Ar プラズマの安定化" 電子情報通信学会論文誌、Vol.J80-C-II No.11、PP378-383、1997.
- (18) Hirokazu Inayoshi, Seitaro Yagi, Shuichi Nagai, and Katsuyuki Utaka: "Analysis and fabrication of current-defined multi mode interference photonic switches with partial index-modulation regions (MIPS-P)", 6th Optoelectronics and Communications Conference / Integrated Optics and Optical Communication Conference (OECC/IOOC2001), Sydney, PO. 2.03 , 2001.
- (19) Shuichi Takahashi, Masaru Otaka, and Katsuyuki Utaka: "Fundamental evaluation of semiconductor waveguide-type in-line wavelength selective filters with Fabry-Perot etalon resonator", 13th International Conference on Indium Phosphide and Related Materials (IPRM'01), Nara, WP-11, 2001.
- (20) Shuichi Takahashi, Masaru Otaka, Katsuyuki Utaka, Masayoshi Horita, and Tomonori Yazaki: "Fabrication and fundamental evaluation of semiconductor waveguide-type in-line wavelength selective filters with Fabry-Perot etalon resonator", SubOptic 2001 International Convention, Kyoto, P4.3.8, 2001.
- (21) Mikito Yagi, Shuichi Nagai, Hirokazu Inayoshi, and Katsuyuki Utaka: "Proposal of versatile multi-mode interference photonic switches with partial-index modulation regions (MIPS-P)", Electron. Lett., Vol.36, No.6, pp.533-534, 2000.
- (22) Shuichi Nagai, Mikito Yagi, Jin Suzuki, Katsuyuki Utaka, and Shinsuke Tanaka: "Novel wavelength converter using multi-mode interference semiconductor optical amplifier (MIWC)", 25th European Conference on Optical Communication (ECOC'99), Nice, P2.15, 1999.
- (23) Katsuyuki Utaka, Shuichi Nagai, Mikito Yagi, and Hirokazu Inayoshi: "New structure of multi mode interference photonic switches with partial index-modulation regions (MIPS-P)", 5th Asia-Pacific Conference on

Communications / 4th Optoelectronics and Communications Conference (APCC/OECC'99), Beijing, C2S4, 1999.

- (24) Shuichi Nagai, Goh Morishima, Mikito Yagi, and Katsuyuki Utaka, "InGaAsP/InP multi-mode interference photonic switches for monolithic photonic integrated circuits", Japanese J. Appl. Phys., Part 1, Vol.38, No.2B, pp.1269 - 1272, 1999.
- (25) Shuichi Nagai, Norihito Kogure, Goh Morishima, and Katsuyuki Utaka: "Proposal of novel InGaAsP/InP multi-mode interference photonic switches", 10th International Conference on Indium Phosphide and Related Materials (IPRM '98), Tsukuba, ThP-45, 1998.

2-2 口頭発表

- (1) 山口誠彦、中野有喜、加藤 勇：“二重管式同軸線路型 MPCVD 装置において基板温度が a-Si:H 膜に与える影響 (Ⅲ)”、第 48 回応用物理学関係連合講演会講演予稿集、31p-ZQ-5、2001.
- (2) 匂坂雅彦、小山慎一、篠原正仁、田丸 直幸、加藤 勇：“a-Si:H/Si₃N₄ 多層膜光導波路の偏光特性(Ⅲ)”、第 48 回応用物理学関係連合講演会予稿集、31p-H-3、2001.
- (3) 菅井貴義、加藤 勇：“二重管式同軸線路形 MPCVD 装置による a-Si:H/Si₃N₄ 多層膜の作成 (Ⅲ)”、第 48 回応用物理学関係連合講演会講演予稿集、30a-ZT-1、2001.
- (4) 松本貴之、加藤 勇、毛塚博史、鈴木恒則：“二重管式同軸線路形 MPCVD 装置を用いて作製した Si 系発光材料の研究(Ⅷ)”、第 48 回応用物理学関係連合講演会講演予稿集、28p-YL-4、2001.
- (5) 野田俊成、加藤 勇：“二重管式同軸線路形 MPCVD 装置における H₂-Ar 混合プラズマの空間分布、およびカーボン系薄膜の作成”、第 48 回応用物理学関係連合講演会講演予稿集、28a-N-9、2001.
- (6) 菅井貴義、加藤 勇：“同軸線路形 MPCVD 装置において、放電ガスとして Ne ガスを用いた a-Si:H 膜の作製(Ⅱ)”、第 61 回応用物理学学会学術講演会予稿集、3p-ZR-15、2000.
- (7) 中野有喜、山口誠彦、加藤 勇：“二重管式同軸線路型 MPCVD 装置におけるシース電圧の制御(Ⅱ)”、第 61 回応用物理学学会学術講演会予稿集、3p-ZR-14、2000.
- (8) 匂坂雅彦、田丸直幸、加藤 勇：“a-Si:H/Si₃N₄ 多層膜光導波路の偏光特性 (Ⅱ)”、第 61 回応用物理学学会学術講演会予稿集、3a-Q-31、2000.
- (9) 松本貴之、加藤 勇：“二重管式同軸線路形 MPCVD 装置を用いて作製した Si 系発光材料の研究(Ⅶ)”、第 61 回応用物理学学会学術講演会予稿集、6a-ZK-5、2000.
- (10) 松本貴之、河原吉男、加藤 勇：“二重管式同軸線路形 MPCVD 装置を用いて作製した Si 系発光材料の研究(Ⅵ)”、第 47 回応用物理学関係連合講演

- 会予稿集、31a-YC-II、、2000.
- (11) 野田俊成、加藤 勇：“二重管式同軸線路形 MPCVD 装置を用いたカーボン系薄膜の作製(II)”、第 47 回応用物理学関係連合講演会予稿集、28a-YE-I、、2000.
- (12) 菅井貴義、上垣内岳司、加藤 勇：“同軸線路形 MPCVD 装置において放電ガスとして Ne ガスを用いた a-Si:H 膜の作製”、第 47 回応用物理学関係連合講演会予稿集、30p-C-I、、2000.
- (13) 中野有喜、山口誠彦、加藤 勇：“縦磁界印加同軸線路形 MPCVD 装置において基盤温度が a-Si:H 膜に与える影響(II)”、第 47 回応用物理学関係連合講演会予稿集、30p-ZF-II、、2000.
- (14) 匂坂雅彦、加藤 勇：“a-Si:H/Si₃N₄ 多層膜光導波路の偏光特性”、第 47 回応用物理学関係連合講演会予稿集、30p-B-III、、2000.
- (15) 大塚 崇、加藤 勇：“二重管式同軸線路形 MPCVD 装置を用いた a-C:H 膜の作製”、第 60 回応用物理学学会学術講演会予稿集、4a-L-11、、1999.
- (16) 河原吉男、加藤 勇：“二重管式同軸線路形 MPCVD 装置を用いて作製した Si 系発光材料の研究(V)”、第 60 回応用物理学学会学術講演会予稿集、3p-ZN-17、、2000.
- (17) 上垣内岳司、匂坂雅彦、加藤 勇：“二重管式同軸線路形 MPCVD 装置による a-Si:H/Si₃N₄ 多層膜の作製とその応用”、第 60 回応用物理学学会学術講演会予稿集、1p-ZS-9、、1999.
- (18) 白田雅之、中野有喜、加藤 勇：“縦磁界印加同軸線路形 MPCVD 装置において基板温度が a-Si:H 膜に与える影響”、第 46 回応用物理学関係連合講演会予稿集、31p-YB-5、、1999.
- (19) 中野有喜、白田雅之、加藤 勇：“縦磁界印加同軸線路形 MPCVD 装置においてシース電圧が a-Si:H 膜に与える影響”、第 46 回応用物理学関係連合講演会予稿集、31p-YB-3、、1999.
- (20) 匂坂雅彦、上垣内岳司、加藤 勇：“二重管式同軸線路形 MPCVD 装置による a-Si:H/Si₃N₄ 多層膜の作製法の検討”、第 46 回応用物理学関係連合講演会予稿集、30p-D-7、、1999.

- (21) 大塚 崇、加藤 勇：“二重管式同軸線路形 MPCVD 装置を用いた a-C:H 膜の作製”、第 46 回応用物理学関係連合講演会予稿集、30p-D-1、、1999.
- (22) 上垣内岳司、匂坂雅彦、加藤 勇：“二重管式同軸線路形 MPCVD 装置による a-Si:H/Si₃N₄ 多層膜の作成 (II)”、第 46 回応用物理学関係連合講演会予稿集、29a-YD-4、、1999.
- (23) 河原吉男、加藤 勇：“二重管式同軸線路形 MPCVD を用いて作製した Si 系発光材料の研究(IV)”、第 46 回応用物理学関係連合講演会予稿集、28a-P2-8、、1999.
- (24) 岩田直之、加藤 勇：“二重管式同軸線路形 MPCVD 装置におけるシー
ス電圧の制御”、第 59 回応用物理学会学術講演会予稿集、18a-ZC-8、、1998.
- (25) 上垣内岳司、加藤 勇：“二重管式同軸線路形 MPCVD 装置による
a-Si:H/Si₃N₄ 多層膜の作成”、第 59 回応用物理学会学術講演会予稿集、
15p-Z-6、、1998.
- (26) 河原吉男、渡辺一博、加藤 勇：“二重管式同軸線路形 MPCVD を用
いて作製した Si 系発光材料の研究(III)”、第 59 回応用物理学会学術講演
会予稿集、16p-ZE-16、、1998.
- (27) 臼田雅之、加藤 勇：“縦磁界印加同軸線路形 MPCVD 装置において水
素ガス流量が a-Si:H 膜に与える影響”、第 59 回応用物理学会学術講演会
予稿集、15a-Q-3、、1998.
- (28) 岩田直之、荻原博隆、上垣内岳司、加藤 勇：“a-Si:H 膜中のイオン
衝撃効果について(III)”、第 45 回応用物理学関係連合講演会予稿集、
30a-SKY-5、、1998.
- (29) 臼田雅之、飯塚英孝、森和彦、加藤 勇：“磁界印加型同軸線路形
MPCVD 装置における H₂/SiH₄ プラズマを用いた a-Si:H 膜の作製”、第 45
回応用物理学関係連合講演会予稿集、30p-H-13、、1998.
- (30) 飯塚英孝、臼田雅之、加藤 勇：“二重管式同軸線路形 MPCVD 装置に
おける水素プラズマへの磁界印加の効果(II)”、第 58 回応用物理学会学術
講演会予稿集、4a-B-1、、1997.
- (31) 荻原博隆、岩田直之、加藤 勇：“a-Si:H 膜中のイオン衝撃効果につ

- いて(II)”、第 58 回応用物理学会学術講演会予稿集、3p-YD-8、1997.
- (32) 越路信行、加藤 勇：“二重管式同軸線路形 MPCVD を用いて作製した Si 系発光材料の研究(II)”、第 58 回応用物理学会学術講演会予稿集、2p-A-10、1997.
- (33) 西村寿郎、桑島秀幸、宇高勝之：“MMI 導波路及び SOA を利用したマルチビーム半導体光源の基礎検討”、第 48 回応用物理学会学術講演会(春季)、30a-ZS-10、2001.
- (34) 高橋修一、大高潤、宇高勝之：“ファブリ・ペロ共振器構造を用いたインライン型波長選択フィルタの基本動作特性”、第 48 回応用物理学会学術講演会(春季)、28p-YF-7、2001.
- (35) 山本慎哉、下里二郎、宇高勝之：“アドレス識別を指向した全光型半導体フォトニックデバイス”、第 48 回応用物理学会学術講演会(春季)、28p-YF-13、2001.
- (36) 稲吉弘和、八木清太郎、永井秀一、宇高勝之：“電流狭窄構造による部分屈折率変調多モード干渉型光スイッチの基本特性”、第 48 回応用物理学会学術講演会(春季)、28p-YF-3、2001.
- (37) 永井秀一、稲吉弘和、森島郷、八木清太郎、宇高勝之：“多モード干渉型半導体光スイッチ”、電子情報通信学会光エレクトロニクス研究会、OPE2000-139、2月、2001.
- (38) 池田晴申、高畑正浩、井卷克哉、宇高勝之、坂田治久：“ナノ加工基板上への MBE 成長のための基礎検討”、第 61 回応用物理学会学術講演会(秋季)、5a-ZA-5、2000.
- (39) 永井秀一、鈴木仁、宇高勝之：“多モード干渉型半導体光増幅器の利得飽和特性の解析”、第 47 回応用物理学会学術講演会(春季)、29p-ZF-10、2000.
- (40) 八木幹人、永井秀一、稲吉弘和、宇高勝之：“部分屈折率変調多モード干渉型光スイッチ(MIPS-P) のスイッチング特性”、第 60 回応用物理学会学術講演会(秋季)、3p-ZB-5、1999.
- (41) 鈴木仁、永井秀一、八木幹人、宇高勝之、田中信介：“多モード干渉を利用した波長変換素子(MIWC)の試作”、第 60 回応用物理学会学術講演会(秋季)、4a-ZB-6、1999.
- (42) 森島郷、永井秀一、平島希彦、宇高勝之：“広角 FD-BPM 法による多モード干

- 渉型光スイッチの特性解析”、1999 年電子情報通信学会総合大会(春季)、C-3-165、1999.
- (43) 永井秀一、稲吉弘和、平島希彦、八木幹人、宇高勝之：“多モード干渉型光スイッチ(MIPS)の試作とスイッチ特性(I)”、第59回応用物理学会講演会(秋季)、17a-X-9、1998.
- (44) 永井秀一、稲吉弘和、平島希彦、八木幹人、宇高勝之：“多モード干渉型光スイッチ(MIPS)の試作とスイッチ特性(I)”、第59回応用物理学会講演会(秋季)、17a-X-9、1998.
- (45) 永井秀一、森島郷、平島希彦、宇高勝之：“MIPS (Multi-Mode Interference Photonic Switches)の基本特性の解析(I)”、第45回応用物理学関係連合講演会(春季)、29a-SZL-8、1998.
- (46) 港武嗣、野口善清、宇高勝之：“斜め回折格子を用いたモード変換による波長フィルタの基礎検討”、第45回応用物理学関係連合講演会(春季)、29a-SZL-13、1998.
- (47) 伊藤暁、宇高勝之：“グレーティング密度変調による逆方向結合導波路型光フィルタのサイドローブ抑圧”、第45回応用物理学関係連合講演会(春季)、29a-SZL-18、1998.
- (48) 木暮徳人、森島郷、今城克樹、宇高勝之：“多モード干渉導波路を用いた半導体レーザの低出射角化”、第45回応用物理学関係連合講演会(春季)、30a-ZH-6、1998.

3. 研究成果

3-1 研究の背景

次世代光交換システムを実現する上で、デバイスのみならず材料に立ち戻った研究が不可欠である。当研究室では以前より、光子工学と光子材料の研究を行っており、光子材料としての薄膜作製法としてはマイクロ波プラズマ CVD 法を開発し主として用いてきた^[1]。

ここで開発された二重管式同軸線路形マイクロ波プラズマ CVD (MPCVD) 装置では、マイクロ波放電によってプラズマを発生するが、これは空間的均一性のよい、高電子温度、高電子密度のプラズマを容易に得られること、そして無電極放電であるために純粋なプラズマが得られることを着目したことによる^{[2][3]}。

また本 MPCVD 装置ではマイクロ波の波長が短い事を生かして、キャビティ構造を用いてマイクロ波電力を所定の空間に閉じ込める事により、マイクロ波電力の注入されている放電プラズマを所定の空間内にのみ発生させる事ができることにあるこの装置により初めて薄膜を放電プラズマの外で作製できるようになった^{[1][4]}。すなわち、放電プラズマに接続された膜堆積室にはプラズマの拡散と流れによって空間的に分離によって作られたエネルギー注入のないプラズマ、すなわち空間的アフターグロープラズマが作られている。この空間的アフターグロープラズマ内で成膜する事により、プラズマ照射による基板あるいは膜への損傷を防ぐ事が可能になった。さらに、それ自体では堆積物を生じない原子または分子状ガス(放電ガス)とプラズマ中に混入されると解離反応等を起こして堆積物を生じる原子又は分子状ガス(材料ガス)を膜堆積室内に独立して送り込むことができる。そこで種々のガスの組み合わせにより、種々の薄膜を作製することができるという特徴を持つ。

現在、放電ガスとして、 Ar , N_2 , H_2 ガスを用い、材料ガスとしては SiH_4 ガス、 CH_4 ガスを用い、放電時におけるプラズマパラメータの測定^{[7][8][9][10][11][13][14]}、および各種薄膜等の作製研究を行ってきた^{[4][5][6][12][15]}。またより低いガス圧、または放電しにくいガスにおいてもプラズマ CVD に適する安定な、高い電子密度

のプラズマを得るために、縦方向直流磁界をプラズマに印加して、成膜を行った^[13]。これにより、 H_2 ガスを放電ガスとした場合無磁界では a-Si:H 膜の堆積速度が非常に遅いものであったが、高堆積速度を得ることが期待できる。

そこで本研究では、前述の二重管式同軸線路型マイクロ波プラズマ CVD 装置において、その堆積室内におけるプラズマパラメータの測定、アモルファスシリコン(a-Si:H)膜及び窒化シリコン(Si_3N_4)膜、さらにそれらの多層構造である a-Si:H/ Si_3N_4 多層膜を製膜して、成膜条件による膜質の違いの検討やその光子材料への応用を図った。また、a-Si:H 膜を 250[Torr]という高ガス圧において作製したシリコンナノボール膜などのフォトルミネッセンス (PL) 測定などにより光デバイスへの可能性への知見が得られた^[16]。これらの点を踏まえて新たな光子材料・光デバイスへの応用として、本研究を立案した。

他方、化合物半導体系では、これまでに液相エピタキシャル成長 (LPE) 法や気相エピタキシャル成長 (VPE) 法を用いて長距離大容量光ファイバ通信用半導体レーザ^{[17]-[21]}や光変調器^[22]、さらに光交換用光スイッチ、機能フィルタなど各種フォトニックデバイスの研究を進めてきたが、一層の高機能化を目指して分子線エピタキシャル成長 (MBE) 法を用いた光情報処理用半導体超薄膜光機能素子などの研究を行い、その有用性を提示してきた^{[23]-[26]}。今後これら光デバイスの著しい特性向上、さらには新規な光非線形機能を実現するためには量子効果が著しく大きく光学利得特性が優れた低次元、特に 0 次元量子構造の導入が不可欠であることは周知の事実である^{[27], [28]}。この観点から、化合物半導体によるナノクリスタル構造の作製法について多面的に調査を進めてきた。その結果、高品質な 0 次元量子構造、すなわち量子ドットを実現するためには、サイズや組成が制御され、かつ基板上の定められた位置に生成されることが重要であることから、これを実現するためにナノ加工された基板上へ MBE 成長を行うことにより位置制御された高品質量子ドットの作成が実現できることに着想した。同様な方法は各所で試みられているが^[29]、まだ十分良好な結果を得ているとは言い難い。そこで電子ビーム露光法によるナノオーダー基板加工及び MBE 成長による高品質量子ドットの作成の基本技術の確立の観点から研究を開始した。同時に、このような非線形材料が適用される機能フォトニックデバイスとして光スイッチ、波長変換素子、半導体レーザ、光フィルタなどについて

ても、並行してデバイス技術の確立を目指した。

研究の背景における参考文献

- [1]Isamu Kato, Shin-ichi Wakana and Shinnji Hara ;"Microwave Plasma CVD System to Fabricate α -Si Thin Films out of Plasma", JJAP, Vol.22 No.1, PP.40-42,1983.
- [2]加藤勇、若菜伸一;“新しいマイクロ波プラズマ化学気相堆積装置”,真空,Vo1.26-7,PP.30-38, 1983.
- [3]Isamu Kato, Shinji Hara and Shin-ichi Wakana,"Analysis of Radial Distribution of Plasma Parameters in a Coaxial-Line Microwave Discharge Tube", J.Appl.Phys., Vo1.54 No.9, PP.4883-4888, 1983.
- [4]加藤勇、矢野元康、“同軸線路形マイクロ波プラズマ CVD 法によるプラズマ内外での a-Si:H 薄膜の作成”,電子通信学会論文誌,Vo1.69-C No.5, PP.662-668, 1986.
- [5]加藤勇、上田哲也、畑中和久;“二重管式同軸線路形マイクロ波水素プラズマ CVD による a-Si:H 膜の作成”,電子情報通信学会論文誌,Vol.J70-C No.1,1987,PP.78-88.
- [6]伊藤尚己、加藤聖隆、加藤勇;“RF バイアス印加マイクロ波プラズマ CVD による薄膜の形成”,電子情報通信学会論文誌,Vol.74-C- II No.1,1991.
- [7]加藤勇、臼井隆志、坂本匠;“マイクロ波プラズマ CVD におけるプラズマパラメータの空間分布”,Trans. IEEE of Japan, Vol.112-A No.5,1992.
- [8]Isamu Kato, Tadashi Sakamoto, and Tsuyoshi Shimoda, "Method of Probe Measurement in N₂/SiH₄ Microwave Plasma", JJAP, Vol.33 Part I No.1, PP307-310, 1994.
- [9]Isamu Kato, Tsuyoshi Sakamoto, and Toshihiro Yamagishi; "Removal Conditions of Films Deposited on Probe Surface", JJAP, Vol.33 Part1 No.6A, PP3586-3589, 1994.
- [10]加藤勇、米田俊之、松下亨;“マイクロ波プラズマにおける DC バイアスと基板テーブル面積のプラズマパラメータへの影響”,Trans. IEEE of Japan,

Vol.114-A No.5, PP375-380, 1994.

[11] 加藤勇、米田俊之、松下亨、山下真; “マイクロ波プラズマ CVD におけるラジカル種の制御”, 電子情報通信学会論文誌、 Vol.J78-C- II No.4, PP142-148, 1995.

[12] Xuantong Ying, Yoshiori Morita, Taro Kamiko, Isamu Kato; “Fabrication of SiN Film by Using Coaxial Line Type MPCVD System with Longitudinal Magnetic Field”, Proceedings of ICRP-3/SPP-14, PP144-145, 1997.

[13] Taro Kamiko, Yoshinori Morita, Tadahiro Ando, Isamu Kato; “Influence of Longitudinal Magnetic Field Applied to Coaxial Line Type of Micro Wave Plasma(IV)”, Proceedings of ICRP-3/SPP-14, PP403-404, 1997.

[14] 加藤勇、下田毅、山岸俊浩; “二重管式同軸線路形マイクロ波プラズマ CVD における N₂/SiH₄ プラズマのパラメーターの空間分布”, 電気学会論文誌, Vol.116-A No.2, PP.617-622, 1996.

[15] 森田義則、加藤勇; “RF バイアス印加同軸線路形マイクロ波プラズマ CVD による SiN 膜の低温作製”, 電子情報通信学会論文誌, Vol.J79-C- II , PP.303-310, 1996.

[16] 越路信行、加藤勇; “2重管式同軸線路型 MPCVD 装置を用いて作製した Si 系発行材料の研究”, 第 44 回応用物理学関係連合講演会予稿集、30p-B-15、1997.

[17] K.Utaka, S.Akiba, K.Sakai, and Y.Matsushima, “Room-temperature cw operation of distributed-feedback buried-heterostructure InGaAsP/InP lasers emitting at 1.57 μ m”, Electron. Lett., Vol.17, No.25/26, pp.961-963, 1981.

[18] Katsuyuki Utaka, Shigeyuki Akiba, Kazuo Sakai, and Yuichi Matsushima, “Effect of mirror facets on lasing characteristics of distributed feedback InGaAsP/InP laser diodes at 1.5 μ m range”, IEEE J. Quantum Electron., Vol.QE-20, No.3, pp.236-245, 1984.

[19] Katsuyuki Utaka, Shigeyuki Akiba, Kazuo Sakai, and Yuichi Matsushima, “ $\lambda/4$ -shifted InGaAsP/InP DFB lasers”, IEEE J. Quantum Electron., Vol.QE-22, No.7, pp.1042-1051, 1986.

- [20] Masayoshi Horita, Katsuyuki Utaka, and Yuichi Matsushima, "Novel wavelength-tunable active-filter-type laser diodes", *IEEE J. Quantum Electron.*, Vol.27, No.6, pp.1625-1629, 1986.
- [21] T.R.Chen, K. Utaka, Y.H.Zhuang, Y.Y.Liu, and A.Yariv, "Vertical integration of an InGaAsP/InP heterojunction bipolar transistor and a double heterostructure laser", *Appl. Phys. Lett.*, Vol.50, No.14, pp.874-876, 1987.
- [22] M.Suzuki, H.Tanaka, K.Utaka, N.Edagawa, and Y.Matsushima, "Transform-limited 14ps optical pulse generation with 15GHz repetition rate by InGaAsP electroabsorption modulator", *Electron. Lett.*, Vol.28, No.11, pp.1007-1008, 1992.
- [23] Y.Matsushima, K.Utaka, K.Sakai, and O.Takeuchi, "Room-temperature cw operation of MBE-grown GaInAs/AlInAs MQW lasers in 1.55 μ m range", *Electron. Lett.*, Vol.23, No.24, pp.1271-1273, 1987.
- [24] Yuichi Matsushima, Hiroshi Kato, Katsuyuki Utaka, and Kazuo Sakai, "MBE growth of InAs/AlInAs strained-layer multi quantum wells for optical device applications", *J. Crystal Growth*, Vol.95, pp.210-214, 1989.
- [25] H.Sakata, K.Utaka, and Y.Matsushima, "Novel bistable device; resonant-tunneling triangular-barrier optoelectronic switch (R-TOPS)", *Electron. Lett.*, Vol.30, No.20, pp.1714-1716, 1994.
- [26] H.Sakata, K.Utaka, and Y.Matsushima, "High sensitivity and high gain optical functional device: triangular-barrier optoelectronic switch (TOPS)", *Electron. Lett.*, Vol.30, No.21, pp.1792-1793, 1994.
- [27] Y.Arakawa and H.Sakaki, "Multidimensional quantum well lasers and temperature dependence of its threshold current", *Appl. Phys. Lett.*, Vol.40, pp939-941, 1982.
- [28] M.Asada, M.Miyamoto, and Y.Suematsu, "Gain and threshold of three dimensional quantum dot lasers", *IEEE J. Quantum Electron.*, Vol.QE-22, pp.1915-1933, 1986.
- [29] Shigeru Kohmoto, Hitoshi Nakamura, Tomonori Ishikawa, and Kiyoshi

Asakawa, "Site-controlled self-organization of individual InAs quantum dots by scanning tunneling probe-assisted nanolithography", *Appl. Phys. Lett.*, Vol.75, No.22, pp.3488-3490, 1999.

3-2 研究目的

本研究では、組成及び膜厚均一性の優れた水素化アモルファスシリコン (**a-Si:H**)膜を作製時の成膜条件を変えることによる更なる膜質の向上や、その作成時における MPCVD 装置内の各種プラズマパラメータの測定を通じて光子材料としての応用、**a-Si:H** 膜と窒化シリコン (**Si₃N₄**)膜を交互に積層した **a-Si:H/Si₃N₄** 多層膜の作製においてもコンピュータによるプラズマ放電状態の制御や精密ガスフロー制御を行うことによりナノオーダーでの各層の厚さ制御ができる良質な超精密多層構造膜の作製と各種光学定数の測定、さらに多層膜のフォトニックデバイスへの応用として、同多層膜を光導波路として用いた時の伝搬特性の研究、さらにシリコンナノボール膜の成膜条件の変化および成膜後の処理方法による発光ピーク波長、発光強度などの発光特性やナノボール膜内にあるシリコンナノクリスタルの粒径制御に関する研究を行う事により、新しい光子材料の開発やフォトニックデバイスへの応用を図ることを目的としている。

また、粒径・組成、さらに位置制御された高品質量子ドットからなる化合物半導体ナノクリスタルを開発するために、従来の自己組織化量子ドット技術に位置制御を導入することにより粒径制御も同時に達成されるであろうとの着想から、まず基板加工パターンの最適化を目指して電子ビーム露光法とドライエッチングによるナノオーダーの基板加工技術、そして **MBE** 成長条件、作成された位置制御微細構造の光学測定などの評価を通して高品質量子ドットの基本作成技術の開発、さらに、量子ドットが適用される機能フォトニックデバイスである光スイッチ、波長変換素子、波長フィルタなどについて、デバイスの基本構造の設計、作製条件の確立、デバイスの基本特性の評価により次世代光ファイバ通信用機能フォトニックデバイスの要素技術の確立を目的とした。

3-3 研究成果概要

当研究室では以前より、光子工学と光子材料の研究を行っており、光子材料としての薄膜作製法としてはマイクロ波プラズマ CVD 法を主として用いてきた。ここで開発された二重管式同軸線路形マイクロ波プラズマ CVD 装置では、マイクロ波放電によってプラズマを発生するが、それ自体では堆積物を生じない原子または分子状ガス(放電ガス)とプラズマ中に混入されると解離反応等を起こして堆積物を生じる原子又は分子状ガス(材料ガス)を膜堆積室内に独立して送り込むことができる。そこで種々のガスの組み合わせにより、種々の薄膜を作製することができるという特徴を持つ。まず、放電ガスとして、Ar, N₂, H₂ ガスを用い、材料ガスとしては SiH₄ ガスを用い、a-Si:H, SiN 膜の作製研究を行ってきた。さらに、膜中にシリコンナノクリスタルを含むシリコンナノボール膜を作製しその発光特性、膜作製時において CVD 装置をコンピュータ制御する事により a-Si:H 膜と Si₃N₄ 膜を交互に積層した超薄膜多層構造膜を作製し、その膜質やその応用として光導波路として用いて、偏光・導波特性を調べる等の研究を行った。

その詳細は本書の添付論文に記載されているが、添付論文にしたがって以下にその内容をまとめる。文中の括弧数字は参照する添付論文番号である。

- (1) 二重管式同軸線路形マイクロ波プラズマ化学気相堆積 (MPCVD) 装置において、より低いガス圧、または放電しにくいガスにおいてもプラズマ CVD に適する安定な、高い電子密度のプラズマを得るために、縦方向直流磁界をプラズマに印加して、成膜を行った。これにより、SiN 膜では堆積速度が数倍となった。また、H₂ ガスを放電ガスとした場合無磁界では a-Si:H 膜の堆積速度が非常に遅いものであったが、磁界印加により 7 Å/s という高堆積速度を得た。さらに、MPCVD 装置内の各種プラズマパラメータの測定を行い、膜堆積室内でのプラズマの均一性を明らかにした^{[9][13][14][17]}。
- (2) a-Si:H 膜成膜中のイオン衝撃効果には膜表面の格子振動を励起する膜表面加熱効果と打ち込まれたイオンが膜中にとどまり、結合するという化学的な

効果とがあるが、イオン衝撃がない状態で基板温度を変えて成膜することにより、膜表面加熱効果を定量的に明らかにし、化学的な効果との分離に成功した。その結果、イオン衝撃がなければ、より低温プロセスが可能となることを明らかにした^{[5][10][16]}。

(3) 前述のイオン衝撃を低減させるために、水素を放電ガスとして用いて a-Si:H 膜を作製し、水素ガス流量、基板温度、シース電圧を変化させ各パラメータが a-Si:H 膜質に与える影響について検討した。結果、 $V_{sh}=-30[V]$ ($V_{dc}=0[V]$) の場合には、基板温度を $150[^\circ C]$ にすることによりダングリングボンド密度を最小にすることができた。また、基板を室温にした場合には、シース電圧をマイナスから $0[V]$ に近づけることによりダングリングボンド密度を小さくすることができることを明らかにした^{[10][14]}。

(4) MPCVD 装置を用いてシリコンナノクリスタル (Si-nc) を内部に含む a-Si:H ナノボール膜の作製法の検討を行い、フォトルミネッセンスを出す膜の作成条件を明らかにした。その条件の下で a-Si:H ナノボール膜の作製を行い、イオン衝撃が膜質、発光特性に与える影響を検討した。その結果、基板電位を $-80[V] \sim +40[V]$ に変化させることによりシース電圧が $-110[V] \sim -20[V]$ に変化し、イオン衝撃エネルギーを制御できることが分かった。また、Si-nc 生成後の酸化条件 (酸化時間, 酸化温度) を変える事により発光効率が上昇することなどの知見を得た^{[2][8][12][15]}。

(5) また、 Ar^+ イオンが a-Si:H ナノボール膜に打ち込まれると、そのエネルギーが a-Si:H ナノボールに供給され、a-Si:H の一部が水素脱離される。それが結晶化することにより、Si ナノクリスタルが形成される。つまり、Si ナノクリスタルの生成にイオン衝撃が関係していると考えられるが、生成過程を解析することによりこれを明らかにした。さらに、 Ar^+ イオンのポテンシャルエネルギーおよび a-Si:H ナノボールの温度を考慮して、Si ナノクリスタルの数を計算することにより、解析の妥当性も明らかにした^{[2][8][11][12]}。

(6) コンピュータ制御によりガス流量やガス圧などの精密制御を可能とした上記 MPCVD 装置を用いて、**a-Si:H** と **Si₃N₄** からなる多層膜を作製し膜質の評価を行った。作製した多層膜の SEM 写真から、多層膜作製時における **SiH₄** ガス流量を少なくする事によって、堆積速度を遅くすることにより基板温度を変化させても界面が均一で鮮明な多層膜を作製できる事が分かった。さらに X 線回折ピークから算出した多層膜 1 周期の層の厚さから、多層膜の層の厚さを nm 単位で制御できることが分かった。**Si₃N₄** 層の厚さを一定にし、**a-Si:H** 層の厚さを変化させて作製した多層膜の光学的エネルギーバンドギャップの理論曲線と実験値はよく一致しており、良質な多層膜が作製できた。逆に **a-Si:H** 層の厚さを一定にし、**Si₃N₄** 層の厚さを変化させて作製した多層膜の光学的エネルギーバンドギャップから、**Si₃N₄** 層の厚さが 10[nm]より厚くなると、電子の光学的遷移が **Si₃N₄** 層に大きく影響を及ぼすことが分かった^{[1][3][7]}。

(7) 上記多層膜の応用として、これを光導波路として用いた。導波光としては光通信で一般的に用いられている、波長 $1.55\ \mu\text{m}$ のレーザ光を用いた。導波路の波長 λ より十分薄い超薄膜多層構造をもつ光導波路には特異な伝搬特性をもつことが期待できる。当研究室のこれまでの研究で、本多層膜スラブ導波路には **TM** モードは透過し、**TE** モードはカットするという偏光特性をもつことを明らかにした。さらに、本スラブ導波路に光を照射し、**a-Si:H** 層を光ポンピングすることにより、導波路の伝搬特性が変化することを見い出している。これを利用することで、本多層膜光導波路はモードフィルタとしてだけでなく、光—光変調器や光スイッチングデバイスなどの導波型光回路素子への応用が期待できることがわかった^{[1][4][6]}。

高品質化合物半導体ナノクリスタルの、高密度形成並びに基板上の所望位置への精密配列制御の基礎的な検討を行った。GaAs 基板上に電子ビーム (EB) 露光法によりナノオーダーのディップを形成し、その上に分子線エピタキシャル (MBE) 成長を行った。2重交差露光法の採用やエッチング条件などの改良の結果、直径約 300nm、深さ約 20nm のディップの作成が可能となり、その加工基板

上に InAs をガスソース MBE 法により成長し、ディップ沿ってリング状に位置制御された高さ約 25nm のナノクリスタルを得ることができた。その際、ディップのレプリカ成長構造が現れ、積層化が可能であるなどの知見が得られた。作成した InAs パターン構造から室温における PL によりピーク波長 $1.4\mu\text{m}$ の発光を確認するとともに、安全性の優れた固体ソースを用いた MBE 法による成長条件を把握した。現在直径 100nm 以下のさらなる細径化を目指し、超薄膜である自己組織化単分子層 (SAM) を EBX 用マスクに利用した新たな加工方法について検討を行っている。これらの結果から、ナノ加工基板による位置制御半導体ナノクリスタル作成の目途を得た。他方、化合物半導体ナノクリスタルが適用される機能フォトニックデバイスとして、半導体光増幅器を利用した多モード干渉型光スイッチや波長変換素子の基本動作を達成し、動作原理についての解析を通して高効率動作の指針を得るとともに、高機能半導体レーザやフォトニックスイッチングデバイスについても検討を行い、デバイス応用のための技術的な課題を解決した。

以下にその内容を項目ごとにまとめる。

(1) 位置制御量子ドット

目標とする数 10nm サイズの量子ドットの位置制御のためには、量子ドットと同程度のサイズのパターンを基板に形成する必要がある、そのために電子ビーム (EB) 露光並びに CH_4/H_2 ガスによる反応性イオンエッチング (RIE) を用いた。基板として GaAs を用い、その上に Si_3N_4 をプラズマ化学気相堆積 (PCVD) 法により堆積し、電子線レジストとして ZEP-520 を用いた。使用した電子ビーム露光装置のビームの不安定性・解像度の限界を考慮し、またナノオーダーの加工基板上への成長過程の基本的検討を主たる目的であることから、微細化が困難なスポット状露光ではなくライン状の交差 2 重露光法を導入してによりできるだけ微少パターン化を図った。電子線レジストの塗布条件や電子ビーム露光における露光エリアやビーム電流など条件の最適化の結果、直径約 300nm のパターンの露光が可能となった。さらに所望の数 nm オーダーの深さのディップの形成は Si_3N_4 マスク厚や RIE 条件の最適化により達成した。このように形成されたナノオーダーディップを有する GaAs 基板上に MBE 法により

GaAs、InAs 及びそれらの多層構造の成長を行った。まずガスソース MBE 法により InAs を成長を試み、成長条件の検討を行った結果、ディップに沿って高さ約 10nm、幅約 30nm、直径約 400nm のリング状の微細構造が得られた。これは In 及び As₂ のマイグレーションにより、成長ポテンシャルの小さいナノディップの円周に沿って優先的に成長した結果と推定される。また、リングの内側は成長速度が遅いことに加えて極めて平坦性の良い成長面が得られた。さらに続けて固体ソースを用いた MBE 法により、同様の InAs 単層構造並びに GaAs/InAs/GaAs 多層構造の成長を検討した。固体ソースの場合は分子線として As₄ となることや基板温度制御の問題から本方法がガスソース MBE 法の場合ほど表面状態が良くなかったが、それでも加工形状に対応した優先的成長が確認された。これらの結果より、ナノオーダーディップの加工基板上に MBE 成長を行う本方法が、基板上に指定された位置に選択的に量子ドット構造を形成するために極めて有効な方法であることを証明することができた^[27]。

現在、これまでの研究結果を踏まえ、波長 1 μm 帯で発光する量子ドット構造の実現を目指して、基板上へのパターン形成に関しては、直径数 10nm 程度の細径化を図るべく、従来 Si では実績のある自己組織化単分子層 (SAM) による超薄膜を EB 露光用マスクとして用いる作成方法の GaAs 基板への適用の開発や、高効率発光を達成するためにパターン間隔を直径と同程度とするなどの密度度化への検討を、さらに MBE 成長においては安全な固体ソース法による成長条件の把握、及び積層構造による高密度微細径パターン加工基板上への高品質量子ドットの成長の検討を進めている。

(2) 機能フォトニックデバイスの基礎検討

量子ドットの有する非線形性が活用されうるフォトニックデバイスとして、波長多重光ファイバ通信において重要な光スイッチ、波長変換素子そして波長フィルタを取り上げ、量子ドット構造の導入に先立ち、それぞれデバイスの基本構造の確立、基本特性を実現した。

光スイッチについては、機能性に優れた多モード干渉導波路の長手方向の部分的な屈折率を電流注入により変調する新規なデバイス構造である多モード干渉導波路型光スイッチ (MIPS) を提案し、波長 1.55 μm 帯で動作する

InGaAsP/InP 系で 2×2 構造を作製し、 -13dB という低クロストーク特性を実験的に達成した^{[19], [20]}。さらに、屈折率を変調する部分領域をさらに小さくし、また複数カ所設けることにより 3×3 構成以上の多ポート化にも拡張可能な新たな部分変調多モード干渉導波路型光スイッチ (MIPS-P) を提案し、解析により 4×4 においてもポートからの出力に自由度のある機能光スイッチングが得られることを示した。また実験的にも 2×2 構造により基本的なスイッチングを実現した^{[21]-[23]}。これら光スイッチは高品質量子ドットを導入することにより、低い電流で大きな屈折率変化が得られるため、一層の高性能化が期待できる。現在、MIPS-P の機能の拡張性について解析により検討を行うとともに、実験的に電流狭窄構造の導入によるスイッチング特性の一層の高性能化を進めている。

波長変換素子は、多モード干渉導波路を半導体光増幅器 (SOA) とし、SOA の非線形効果である相互利得変調 (XGM) を利用したデバイスを InGaAsP/InP 系で作製し、実際に 3dB の利得飽和特性を達成し、波長変換素子としての動作を実現した^[24]。さらに他の非線形効果であり、より高効率動作が期待できる SOA の相互位相変調効果 (XPM) を用いたデバイス構造を作製し、やはり波長変換動作が達成された。これら SOA を用いた波長変換素子は、量子ドット構造を導入することによりさらに高い非線形性が得られるため、高効率波長変換動作が期待できる。現在、XPM による波長変換素子の高性能化の検討を進めている。

波長フィルタについては、半導体光導波路に一对の狭幅の溝を設けたファブリ・ペロ型半導体インラインフィルタについて検討し、所望の 0.8nm (100GHz) の波長間隔のフィルタリング動作を実現した^{[25], [26]}。今後温度変化を利用した波長可変動作を行う上で、量子ドット構造は有望である。現在、フィルタリング特性の高コントラスト化及び波長可変化について検討を行っている。

いずれもデバイスも、位置制御された高品質高密度量子ドットが開発され次第導入し、低消費電力・高効率動作を目標として研究を進める予定である。

4. 添付論文

- (1) 加藤 勇、匂坂雅彦、菅井貴義、上垣内岳司：“2重管式同軸線路形 MPCVD 装置を用いて作製した a-Si:H/Si₃N₄ 多層膜の膜質とその光回路素子への応用” 電子情報通信学会論文誌、Vol.J84-C No.4、PP245-250、2001.
- (2) 松本貴之、加藤 勇：“Dependence of PL Characteristics of a-Si:H Nanoball Films Fabricated By Double Tubed Coaxial Line Type MPCVD System On Substrate Position”第 18 回プラズマプロセッシング研究会プロシーディングス、PP.425-426、2001.
- (3) 菅井貴義、加藤 勇：“Quality Of a-Si:H/Si₃N₄ Multilayer Films Fabricated By Double Tubed Coaxial Line Type MPCVD System(Ⅱ)”第 18 回プラズマプロセッシング研究会プロシーディングス、PP427-428、2001.
- (4) 匂坂雅彦、菅井貴義、田丸直幸、加藤 勇：“Film Quality Of a a-Si:H/Si₃N₄ Multilayer Films And Propagate Properties Of Optical Waveguides Using The Multilayer Films”第 18 回プラズマプロセッシング研究会プロシーディングス、pp429-430、2001.
- (5) ISAMU KATO,YUUKI NAKANO,NOBUHIKO YAMAGUCHI:”Effect of Ar⁺ Ion Bombardment During Hydrogenated Amorphous Silicon Film Growth in Plasma Chemical Vapor Deposition System2000”,Jpn. J. Appl. Phys. ,Vol.3 No.9,PP.6404-6409,2000.
- (6) MASAHIKO SAGISAKA, ISAMU KATO : "POLARIZATION PROPERTIES OF a-Si:H/Si₃N₄ MULTILAYERS OPTICAL WAVEGUIDES"、第 17 回プラズマプロセッシング研究会プロシーディングス、pp.243-246、2000.
- (7) TAKESI KAMIGAICHI,ISAMU KATO : “ QUORITY OF a-SI:H/Si₃N₄ MULTILAYER FILMS FABRICATED BY DOUBLE TUBED COAXIAL LINE TYPE MPCVD SYSTEM”、第 17 回プラズマプロセッシング研究会プロシーディングス、PP.239-242、2000.
- (8) YOSHIO KAWAHARA,ISAMU KATO : “DEPENDENCE OF PL CHARACTERISTICS OF a-Si:H NANOBALL FILMS FABRICATED BY

- DOUBLE TUBED COAXIAL LINE TYPE MPCVD SYSTEM ON ION BOMBAEDMENT ENERGY”、第 17 回プラズマプロセッシング研究会プロシーディングス、PP.641-644、2000.
- (9) TAKASHI OOTSUKA, ISAMU KATO : “ FABRICATION OF POLYMER-LIKE a-C:H FILMS BY DOUBLE TUBED COAXIAL LINE TYPE MPCVD SYSTEM”、第 17 回プラズマプロセッシング研究会プロシーディングス、PP.223-226、2000.
- (10) YUUKI NAKANO, ISAMU KATO : "FABRICATION OF a-Si:H FILM USING H₂/SiH₄ PLASMA BY LONGITUDINAL MAGNETIC FIELD APPLIED MPCVD SYSTEM(II)"、第 17 回プラズマプロセッシング研究会プロシーディングス、PP.141-144、2000.
- (11) Isamu Kato, Yoshio Kawahara, O.P.Agnihotri: " Photo Luminescence from a-Si:H Nanoball Films Fabricated by Double Tubed Coaxial Line Type Microwave Plasma CVD system", Proceedings of the Tenth International Workshop on the Phisics of Semiconductor Devices II, PP.1107-1114, 1999.
- (12) Isamu Kato, Yoshio Kawahara, "Photo Luminescence from Si Films Fabricated by Double Tubed Coaxial Line Type Microwave Plasma CVD Apparatus", International Conference on Reactive Plasmas and Symposium on plasma Proceeding, PP.109-110,1998.
- (13) Isamu Kato、Toshihiro Yamagishi, Yoshinori Morita, and Taro Kamiko : "Stabilization of Ar Plasma by Applying Longitudinal Magnetic Field", Electronics and Communications in Japan Part2, Vol.81 No.3、PP10-16、1998.
- (14) Hidetaka Iizuka, Masayuki Usuda, Isamu Kato : "Fabrication Of a-Si:H Film Using H₂/SiH₄ Plasma by Longitudinal Magnetic Field Applied MPCVD System”、第 15 回プラズマプロセッシング研究会プロシーディングス、PP. 406-409、1998.
- (15) Nobuyuki Koshiji, Kazuhiro Watanabe, ISAMU KATO : "Si Luminescence Material Fabricated Using MPCVD Coaxial Line

- Type”、第 15 回プラズマプロセッシング研究会プロシーディングス、PP. 140-143、1998.
- (16) Hirotaka Ogihara, Naoyuki Iwata, ISAMU KATO : “Effect of Bombardment During a-Si:H Film Growth”、第 15 回プラズマプロセッシング研究会プロシーディングス、PP.84-87、1998.
- (17) 加藤 勇、山岸俊浩、森田義則、神子太郎 : “縦磁界印加による Ar プラズマの安定化” 電子情報通信学会論文誌、Vol.J80-C-II No.11、PP378-383、1997.
- (18) 池田晴申、高畑正浩、井巻克哉、宇高勝之、坂田治久 : “ナノ加工基板上への MBE 成長のための基礎検討”、第 61 回応用物理学会学術講演会(秋季)、5a-ZA-5、2000.
- (19) Shuichi Nagai, Goh Morishima, Mikito Yagi, and Katsuyuki Utaka, "InGaAsP/InP multi-mode interference photonic switches for monolithic photonic integrated circuits", Japanese J. Appl. Phys., Part 1, vol.38, No.2B, pp.1269 - 1272, February 1999.
- (20) Shuichi Nagai, Norihito Kogure, Goh Morishima, and Katsuyuki Utaka: "Proposal of novel InGaAsP/InP multi-mode interference photonic switches", 10th International Conference on Indium Phosphide and Related Materials (IPRM '98), Tsukuba, ThP-45, May, 1998.
- (21) Hirokazu Inayoshi, Seitaro Yagi, Shuichi Nagai, and Katsuyuki Utaka: "Analysis and fabrication of current-defined multi mode interference photonic switches with partial index-modulation regions (MIPS-P)", 6th Optoelectronics and Communications Conference / Integrated Optics and Optical Communication Conference (OECC/IOOC2001), Sydney, PO. 2.03 , July, 2001.
- (22) Mikito Yagi, Shuichi Nagai, Hirokazu Inayoshi, and Katsuyuki Utaka: "Proposal of versatile multi-mode interference photonic switches with partial-index modulation regions (MIPS-P)", Electronics Letters, vol.36, No.6, pp.533-534, March 2000.
- (23) Katsuyuki Utaka, Shuichi Nagai, Mikito Yagi, and Hirokazu Inayoshi: "New structure of multi mode interference photonic switches with partial

index-modulation regions (MIPS-P)", 5th Asia-Pacific Conference on Communications / 4th Optoelectronics and Communications Conference (APCC/OECC'99), Beijing, C2S4, October, 1999.

(24) Shuichi Nagai, Mikito Yagi, Jin Suzuki, Katsuyuki Utaka and Shinsuke Tanaka: "Novel wavelength converter using multi-mode interference semiconductor optical amplifier (MIWC)", 25th European Conference on Optical Communication (ECOC'99), Nice, P2.15, September, 1999.

(25) Shuichi Takahashi, Masaru Otaka, and Katsuyuki Utaka: "Fundamental evaluation of semiconductor waveguide-type in-line wavelength selective filters with Fabry-Perot etalon resonator", 13th International Conference on Indium Phosphide and Related Materials (IPRM'01), Nara, WP-11, May, 2001.

(26) Shuichi Takahashi, Masaru Otaka, Katsuyuki Utaka, Masayoshi Horita, and Tomonori Yazaki: "Fabrication and fundamental evaluation of semiconductor waveguide-type in-line wavelength selective filters with Fabry-Perot etalon resonator", SubOptic 2001 International Convention, Kyoto, P4.3.8, May, 2001.

2重管式同軸線路形MPCVD装置を用いて作製したa-Si:H/Si₃N₄多層膜の膜質とその光回路素子への応用

加藤 勇^{†,††} 匂坂 雅彦[†] 菅井 貴義[†] 上垣内岳司[†]

Quality of a-Si:H/Si₃N₄ Multilayer Films Fabricated by Double Tubed Coaxial Line Type MPCVD System and Application of the Films to Optical Circuit Element

Isamu KATO^{†,††}, Masahiko SAGISAKA[†], Takayoshi SUGAI[†], and Takeshi KAMIGAICHI[†]

あらまし 本研究は、新しい光子材料として、超薄膜多層構造をもつ良質な a-Si:H/Si₃N₄ 多層膜の作製及びその膜質の評価とその光子工学への応用を目的としている。我々は、a-Si:H/Si₃N₄ 多層膜の X 線回折ピークから、サブナノオーダーで多層膜の厚さを制御することに成功した。Si₃N₄ 層の厚さを一定にし、a-Si:H 層の厚さを变化させて作製した多層膜の光学的エネルギーバンドギャップの理論曲線と実験値はよく一致しており、良質な多層膜が作製できた。そこで、本多層膜の応用としてこれを光導波路として用いた。導波光の波長よりも十分に薄い超薄膜多層構造をもつ光導波路は特異な伝搬特性をもつことが期待できる。我々は本多層膜スラブ導波路が TM モードを透過し、TE モードはカットするという偏光特性をもつことを見出した。

キーワード マイクロ波プラズマ CVD, 多層膜, 光学的エネルギーバンドギャップ, 光導波路, TM モード透過型光回路素子

1. ま え が き

近年、光通信の各種デバイスの開発が急速に進みつつある。しかし、新しい光子材料の開発、及び、それを用いた新しい発想の光デバイスの研究開発はあまり進んでいない。当研究室では、2重管式同軸線路型マイクロ波プラズマ CVD 装置を用いて、新しい光子材料を研究開発してきた。従来の高周波プラズマ CVD 法においては、薄膜基板がプラズマに接触して置かれるため、基板表面及び成長中の薄膜は高エネルギーのプラズマ中にさらされることになる。高エネルギーのプラズマ粒子を被爆した膜は、表面の荒れが目立ち、更にはピンホールなどを含みやすいとされている。そ

れに対して、2重管式同軸線路型マイクロ波プラズマ CVD 装置は、周波数が高いので、質量の重いイオンはその交流電界に応答した運動ができなくなり、イオンの加熱は起きずコールドプラズマが得られることや、空洞構造をもつマイクロ波放電管を用いて、プラズマを所定の空間内に閉じ込め、プラズマ空間と堆積空間との分離を図れることなどといった特徴をもつ。また、同軸線路型にすることで、マイクロ波の管内モードが同軸線路の基本モードになっているので、放電管内において円周方向に沿ってのマイクロ波電界強度分布の変化はなく、円周方向に沿って均一なプラズマが得られるため、良質な薄膜を作製できることなどの特徴が挙げられる [1]~[3]。

我々が研究開発を行ってきた光子材料の一つとして、低ガス圧下において、良質な a-Si:H 膜と Si₃N₄ 膜を用いて 1 層の厚さを 1[nm] 以下の精度で制御して、これを交互に積層して、超薄膜多層構造のスラブ光導波路の作製に成功している。

異種の物質を原子間隔オーダーで多層構造にすること

[†] 早稲田大学理工学部電子情報通信学科, 東京都

School of Science and Engineering, Waseda University, 3-4-1 Ohkubo, Shinjuku-ku, Tokyo, 169-0072 Japan

^{††} 早稲田大学バイオ・フォトンクス新素材研究施設, 東京都

Materials Research Laboratory for Bioscience and Photonics, Waseda University, 3-4-1 Ohkubo, Shinjuku-ku, Tokyo, 169-0072 Japan

で、個々の物質がもち合わせていた本来の物性とは全く異なった性質をもち合わせてくる。それ故、今までの個々の物質では得られなかった全く新しい電氣的、光学的特性をもつ物質を人工的に作製することができる。

本研究は、まず a-Si:H/Si₃N₄ 多層膜の作製法についての研究を行っている。その作製した多層膜について、SEM による断面の観察と X 線回折、光学的エネルギーバンドギャップ、光吸収係数を測定し、膜質の評価を行った。更に、本多層膜の光子材料としての応用としてこれを光導波路として用いた場合の研究を行っている。

2. 実験

図 1 に実験で用いた 2 重管式同軸線路形マイクロ波プラズマ CVD 装置の概略図を示す。本装置はガス流に沿って放電領域、ラジカル生成領域、ラジカル輸送領域の三つの領域からなっている [1],[2]。

本研究では、Ar ガス、N₂ ガスを放電ガスとして用いている。放電ガスは放電領域において、マイクロ波電力により電離される。マイクロ波電力は円筒キャビティ内に閉じ込められているので、電力の注入されている放電プラズマはキャビティ領域内でのみ生成されている。すなわち、これが放電領域である (図 1 参照)。

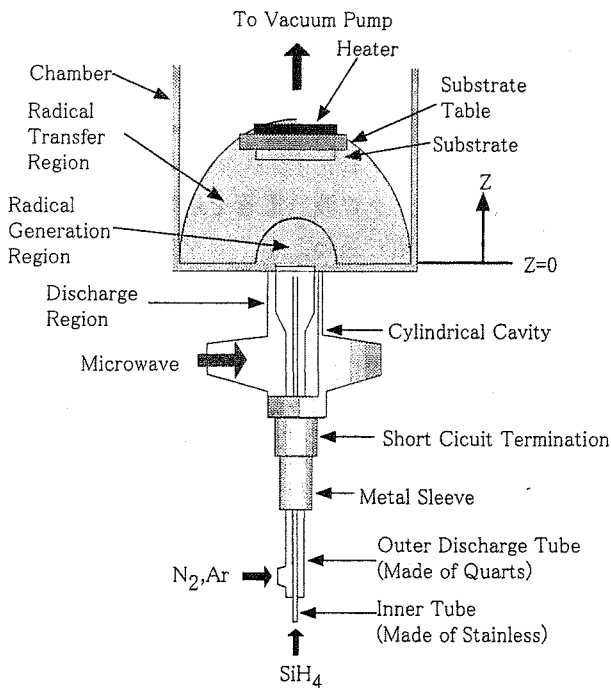


図 1 2 重管式同軸線路型 MPCVD 装置

Fig. 1 The double tubed coaxial line type MPCVD system.

ここで、放電管端からの管軸方向距離を z と定義する。ただし、堆積室側を正にとる。

材料ガスである SiH₄ ガスは、放電管端までステンレス製の内管により導かれ、放電管端で Ar プラズマ、または N₂ プラズマ中に混入され、堆積物を生ずるラジカルに解離される。これまでに、電子温度、電子密度は $z=4$ [cm] までは急激に減少し、その後、緩やかに減少することが明らかになっており、 $z>4$ [cm] で解離される SiH₄ は、内管端付近で解離される SiH₄ に比べわずかであると考えられる。すなわち、ここまでがラジカル生成領域である。

生成されたラジカルは、ガス流や拡散により基板まで輸送される。すなわち、これがラジカル輸送領域である。

外側放電管には Ar 及び N₂ の放電ガスを流し、内管には SiH₄ ガスを流す。放電ガス及び SiH₄ ガスの流入はすべてコンピュータ制御である。また、ショートサーキットターミネーションやメタルスリーブなどの可動部分をプログラム制御してマイクロ波のインピーダンスマッチングをとり、各放電ごとに最適なプラズマ状態が得られるようにしてある。

a-Si:H 層作製時は、放電ガス、材料ガスとしてそれぞれ Ar、SiH₄ を用いる。このとき、Ar ガス流量は 110[ml/min] で SiH₄ ガス流量は 5[ml/min] である。Si₃N₄ 層作製時は放電ガス、材料ガスとしてそれぞれ N₂、SiH₄ を用いる。このとき、N₂ ガス流量は 140[ml/min] で SiH₄ ガス流量は 5[ml/min] である。基板温度は 250[°C] とした。

本論文では、a-Si:H/Si₃N₄ 多層膜の膜質に関する研究だけでなく、本多層膜の応用として、これを光導波路として用い、その偏光特性についての研究も行っている。

まず、a-Si:H/Si₃N₄ 多層膜を用いたスラブ導波路の作製法について述べる。本装置を用いて、Si 基板上にバッファ層として Si₃N₄ 膜を厚さ約 2[μ m] 堆積させ、その上に a-Si:H 層と Si₃N₄ 層を交互に堆積させ多層膜を作製した。これを、ダイヤモンドカッターを用いて切断し、端面を粒度 15[μ m]、5[μ m]、1[μ m] の酸化アルミニウムの砥粒を用いて研磨し、図 2 に示すような a-Si:H/Si₃N₄ 多層膜スラブ導波路を作製した。

図 3 に a-Si:H/Si₃N₄ 多層膜をスラブ導波路として用いた場合の偏光特性を測定する光学系を示す。入射光として、波長 $\lambda=1.55$ [μ m] のレーザー光を用いた。レーザー光をテーパ型先端球ファイバにより、本導波路に入射

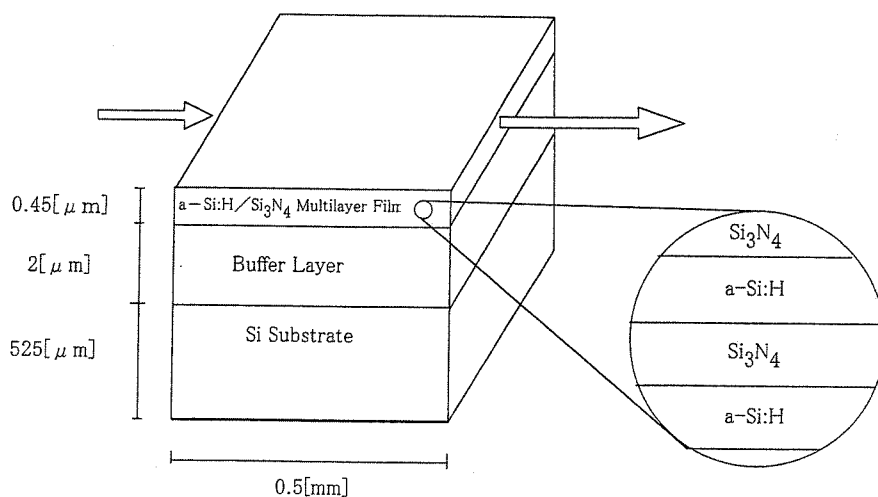


図2 a-Si:H/Si₃N₄ 多層膜スラブ導波路の構造
Fig. 2 Diagram of a-Si:H/Si₃N₄ multilayer slab waveguide.

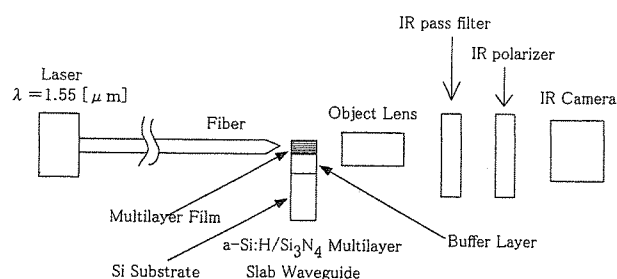


図3 光導波路の測定用光学系
Fig. 3 Experimental setup for measurement of polarization properties.

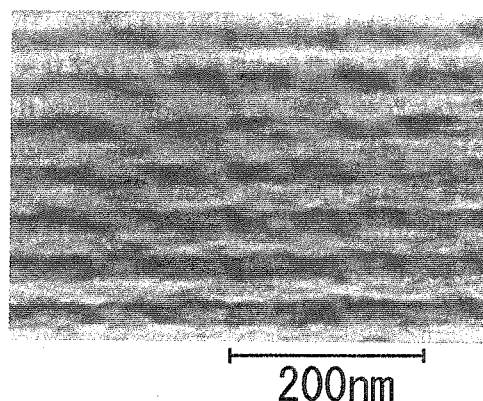


図4 a-Si:H/Si₃N₄ 多層膜の断面 SEM 像
Fig. 4 The SEM image of a-Si:H/Si₃N₄ multilayer film.

させた。導波路からの出射光のニアフィールドパターンを対物レンズで拡大して、赤外線カメラで測定する。対物レンズと赤外線カメラの間には、赤外透過フィルタと赤外偏光フィルタを設置しており、赤外偏光フィルタを回転させることによって導波路内のTE、またはTMモードのみを透過させて観測することができる。導波路長は、0.5[mm]とした。

3. 結果、及び考察

これまで我々が研究してきた a-Si:H 膜は、基板温度 250[°C] で最も良質な膜が作製できることがわかっている [4]。

図4に、基板温度を 250[°C] にして作製した多層膜の断面 SEM 像を示す。図より界面の鮮明な多層膜が作製されていることがわかる。図の SEM 像から読み取った1周期の層の厚さは 45[nm] であり、触針式膜厚計により測定した多層膜のトータル膜厚から算出した1周期の層の厚さ 44[nm] と一致した。なお、使用

した触針式膜厚計は TENCOR 社製 alpha-step100 である。

次に、X線回折ピークを測定するために、1層の厚さを更に薄くした a-Si:H/Si₃N₄ 多層膜を Si 基板上に作製した。その X線回折ピークを図5に示す。図から 1.98[deg] の位置に回折ピークを確認することができる。X線の波長は 1.94[Å] である。この回折ピークから算出した多層膜1周期の層の厚さは 5.6[nm] で、触針式膜厚計により測定した多層膜のトータル膜厚から算出した1周期の層の厚さは 5.8[nm] と非常によく一致した。

そこで、Si₃N₄ 層の厚さを 5.5[nm] と一定にして a-Si:H 層の厚さを 0.9~9[nm] と変化させて作製した多層膜の光学的エネルギーバンドギャップを測定した。トータル膜厚は 450[nm] と一定にした。光学的エネルギーバンドギャップは、紫外可視分光光度計を用いて

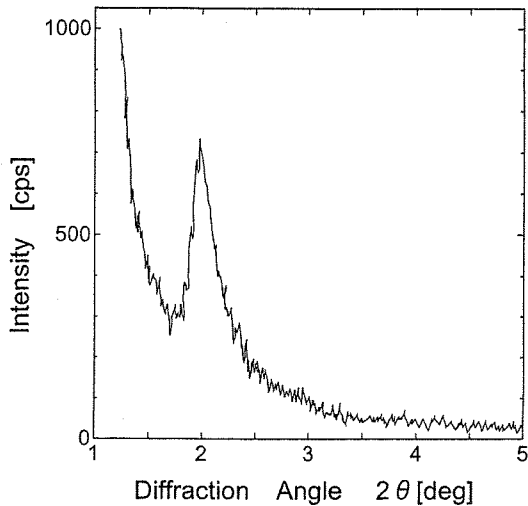


図5 X線回折ピーク
Fig. 5 X-ray diffraction peak of a-Si:H/Si₃N₄ multilayer film.

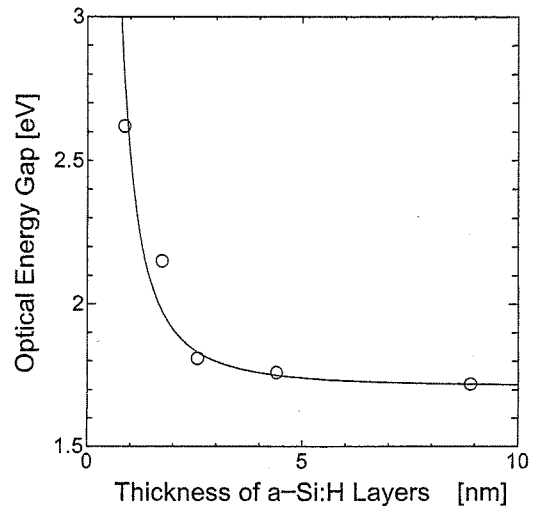


図6 光学的エネルギーバンドギャップの a-Si:H 層の厚さ依存性
Fig. 6 Dependence of the optical energy band gap on the thickness of a-Si:H layers.

透過スペクトルを測定し、これをタウクプロットに変換し、このタウクプロットより算出した。図6に光学的エネルギーバンドギャップ E_0 の a-Si:H 層の厚さ依存性を示す。図より、 E_0 は a-Si:H 層が薄くなるに従い、増加することがわかる。これは、a-Si:H 層中に量子井戸効果による量子準位が形成されているためである。理論式 [5] を用いてカーブフィッティングした結果を図中の実線に示す。理論曲線と実験値はよく一致しており、良質な多層膜が作製できていることがわかる。なお、この理論曲線の算出において、a-Si:H 層の E_0 の値を 1.71[eV] とし、多層膜中の電子の有効質量を自由電子の有効質量の 0.34 倍とした。

図7に、a-Si:H 層の厚さをパラメータとした多層膜の光吸収係数の光子エネルギー依存性を示す。図より、光子エネルギーが大きくなるに従い、光吸収係数は増加することがわかる。これは、光子エネルギーが 1.4~3[eV] の領域では Si₃N₄ の吸収は無視できる程度であるので、a-Si:H の光吸収係数の特性が現れたものである。また同図より、a-Si:H 層が薄くなるに従い、光吸収係数は減少することがわかる。これは多層膜のトータル膜厚を一定にしてあるので、a-Si:H 層が薄くなるに従い、多層膜中の a-Si:H の割合が減り、多層膜全体としては光吸収係数が小さくなるためである。

逆に、a-Si:H 層の厚さを 3[nm] と一定にして、Si₃N₄ 層の厚さを 3~30[nm] と変化させて作製した多層膜の光学的エネルギーバンドギャップを測定した。なお、このとき作製した多層膜のトータル膜厚は 450[nm] と一定にした。図8に光学的エネルギーバンドギャップ E_0

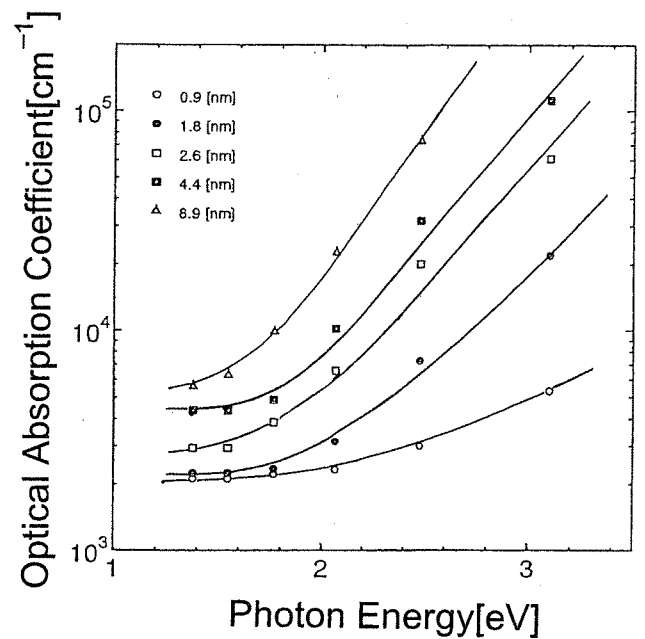


図7 光吸収係数の光子エネルギー依存性
Fig. 7 Dependence of optical absorption coefficient on the photon energy with varying the thickness of a-Si:H layers.

の Si₃N₄ 層の厚さ依存性を示す。図より、 E_0 は Si₃N₄ 層の厚さが約 10[nm] までは約 1.83[eV] と一定であるのに対し、Si₃N₄ 層の厚さがおよそ 10[nm] より厚くなると Si₃N₄ 層が厚くなるに従い増加することがわかる。a-Si:H 層の厚さは 3[nm] であるので、Si₃N₄ 層の厚さが薄いときは、多層膜中ではサブバンドが形成されている [6],[7]。したがって、Si₃N₄ 層が薄いときには、サ

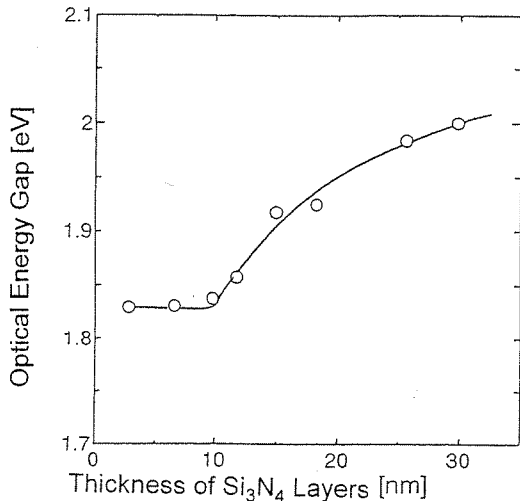


図 8 光学的エネルギーバンドギャップの Si₃N₄ 層の厚さ依存性

Fig. 8 Dependence of the optical energy band gap on the thickness of Si₃N₄ layers.

バンド間での光学遷移が支配的であるので、光学的エネルギーバンドギャップ E₀ は一定になる。それに対して、Si₃N₄ 層がより厚くなると、多層膜中ではサブバンドは形成されず、井戸層である a-Si:H 層にできている量子単位間の光学遷移と、障壁層である Si₃N₄ 層のエネルギーバンドギャップ間での光学遷移が支配的になる。ここで、Si₃N₄ 層が厚くなっていくと、トータル膜厚は一定であるので多層膜中の Si₃N₄ 層の割合が増える。したがって、a-Si:H 層の量子単位間の光学遷移よりも、Si₃N₄ 層のエネルギーバンドギャップ間の光学遷移の方が支配的になってくるので、E₀ は増加していく。

次に、a-Si:H/Si₃N₄ 多層膜を光導波路として用いた場合について検討する。導波光の波長 λ より十分に薄い超薄膜多層構造をもつ光導波路には特異な伝搬特性をもつことが期待できる。図 3 に示した光学系を用いて、光導波路に波長 1.55[μm] の光を伝搬させ光導波路からの出射光のニアフィールドパターンの様子を観察した。赤外偏光フィルタにより TM モードのみを透過させたときの出射光の様子を図 9(a) に、そして赤外偏光フィルタを 90 度回転させ TE モードのみを透過させたときの出射光の様子を図 9(b) に示す。なお、このとき測定した光導波路は a-Si:H 層の厚さを 5[nm]、Si₃N₄ 層の厚さを 10[nm]、トータル膜厚を 450[nm]、導波路長を 0.5[mm] として作製したスラブ導波路である。a-Si:H 層、Si₃N₄ 層の屈折率実部を測定するために、多層膜を作製したときと同じ条件で厚さ約 1[μm]

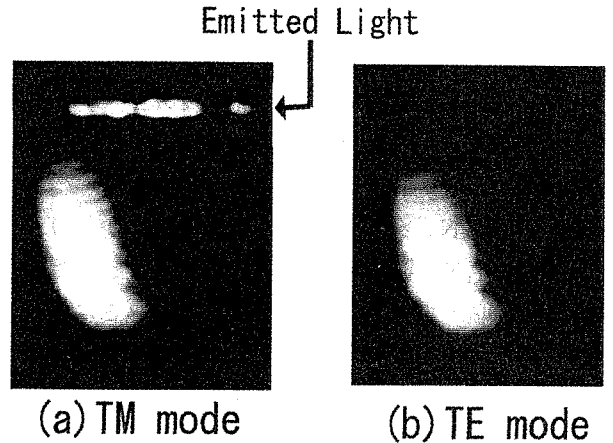


図 9 スラブ型光導波路からの出射光のニアフィールドパターン
Fig. 9 Near field pattern of emitted light from the slab optical waveguides.

の a-Si:H、Si₃N₄ の単層膜をそれぞれ作製し、赤外可視分光光度計を用いて測定したそれぞれの単層膜の透過スペクトルの振幅から屈折率実部を求めた [8],[9]。波長 1.55[μm] において、a-Si:H 層の屈折率は 2.64、Si₃N₄ 層の屈折率は 1.78 であった。屈折率虚部は各単層膜の吸収係数から算出した結果、波長 1.55[μm] において、a-Si:H 層の屈折率虚部は 1.8×10⁻²、Si₃N₄ 層の屈折率虚部は 2.5×10⁻³ であり、Si₃N₄ の屈折率虚部は無視できる。また、多層膜中で Si₃N₄ が多くの割合を占めているので、本導波路の挿入損は小さいものと考えられる。図 9 において、上部の線状の光が超薄膜多層構造をもつ光導波路を導波した光で、下部の楕円状の光が Si 基板中を透過した光である。図より、TM モードは光導波路中を導波しているが、TE モードは導波していないことがわかる。Si 基板中を透過した光は、偏光されていないので、赤外偏光フィルタの影響を受けず、図 9(a),(b) の Si 基板中を透過した光には変化がない。T. Sato らの文献 [10] によると、Al/SiO₂ 多層膜を偏光子として用い、その偏光原理は次のようであると述べられている。「電界が層に対して平行な方向に振動している TE モードに対しては、金属層の電子が加速され、結果としてジュール熱が生じ光損失を引き起こす。一方、電界が層に対して垂直な方向に振動している TM モードに対しては誘電体層があるために電子はほとんど加速されずジュール熱は生じない。ゆえに、TM モードは透過する。」本研究では前述のように a-Si:H/Si₃N₄ 多層膜を用いているが、a-Si:H は障壁層の Si₃N₄ と比べれば比較的高い電気伝導度を持ち、同様の現象が起きていると考えられる。これより、本

超薄膜多層構造をもつ光導波路を用いてTMモード透過偏光フィルタが作製できることがわかった。本スラブ導波路では17[dB]の消光比が得られた。

4. む す び

a-Si:H/Si₃N₄多層膜のX線回折ピークから算出したa-Si:H/Si₃N₄多層膜1周期の層の厚さと多層膜のトータル膜厚から算出した1周期の層の厚さは非常によく一致し、各層の厚さをサブナノオーダーで制御できることを示した。Si₃N₄層の厚さを一定にし、a-Si:H層の厚さを変化させて作製した多層膜の光学的エネルギーバンドギャップの理論曲線と実験値はよく一致しており、良質な多層膜を作製できることが示された。また、a-Si:H層の厚さを一定にし、Si₃N₄層の厚さを変化させて作製した多層膜の光学的エネルギーバンドギャップから、Si₃N₄層の厚さが薄いときはサブバンドが形成され、サブバンド間での吸収が支配的であるが、Si₃N₄層の厚さが厚くなると、光学遷移はSi₃N₄層の影響を大きく受けることがわかった。

更に、本多層膜の光子材料としての応用として、これを光導波路として使い、この導波路がTMモード透過、TEモードカットという偏光特性をもつことを明らかにした。本研究では17[dB]の消光比を得た。よって、TMモード透過型光回路素子になり得ることを示した。

謝辞 本研究は文部省科学研究費の補助を得て行ったものである。

文 献

- [1] I. Kato, S. Wakana, and S. Hara, "Microwave plasma CVD system to fabricate a-Si thin films out of plasma," J.J.A.P., vol.22, no.1, pp.L470-L472, Aug. 1982.
- [2] 加藤 勇, 若菜伸一, "新しいマイクロ波プラズマ科学気相法堆積装置," 真空, vol.26, no.7, pp.628-636, July 1983.
- [3] 加藤 勇, 米田俊之, 松下 亨, "プラズマCVDによって作製されたa-Si:H膜に与えるイオン衝撃の影響," 信学論(C-II), vol.J77-C-II, no.9, pp.384-391, Sept. 1994.
- [4] 加藤 勇, 上田哲也, 畑中和久, "二重管式同軸線路形マイクロ波プラズマCVD法によるa-Si:H薄膜の基板温度特性," 電学論(A), vol.106-A, no.8, pp.35-41, Aug. 1986.
- [5] B. Abeles and T. Tiedje, "Amorphous semiconductor superlattices," Physical Review Letters, vol.51, no.21, pp.2003-2006, Nov. 1983.
- [6] 日本物理学会(編), 半導体超格子の物理と応用, pp.6-8, 培風館, 1986.
- [7] 岡本 紘, 超格子構造の光物性と応用, pp.10-12, コロナ社, 1988.
- [8] J C Manificier, et al., "A simple method for the determination of the optical constants n,k and the thickness of a

weakly absorbing thin film," J. Phys. E, vol.9, pp.1002-1004, 1976.

- [9] R. Swanepoel, "Determination of the thickness and optical constants of amorphous silicon," J. Phys. E, vol.16, pp.1214-1222, 1983.
- [10] T. Sato, et al., "Fabrication techniques and characteristics of Al-SiO₂ laminated optical polarizers," IEEE J. Quantum Electron., vol.29, pp.175-181, 1993.

(平成12年5月30日受付, 9月26日再受付)

加藤 勇 (正員)



昭42早大・理工・電子通信卒。昭48同大大学院博士課程了。同年工博。同年早大勤務。昭53同大助教授。昭54~56マニトバ大客員教授, カナダ国立研究会議の研究費を受け共同研究並びに研究指導。昭58早大教授, 現在に至る。マイクロ波プラズマCVD, 光子工学, レーザ工学, 電子物性工学, 計測工学, 光子材料, プラズマ・エレクトロニクス, 光量子エレクトロニクス, 半導体薄膜工学などの研究に従事。電気学会, 応用物理学会, 映像情報メディア学会, 日本真空協会, IEEE各会員。

匂坂 雅彦



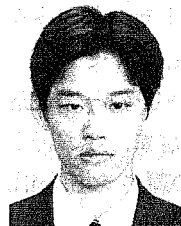
平11早大・理工・電子情報通信卒。現在, 同大大学院修士課程在学中。導波型光回路素子に関する研究に従事。応用物理学会会員。

菅井 貴義



平12早大・理工・電子情報通信卒。現在, 同大大学院修士課程在学中。a-Si:H膜に関する研究に従事。応用物理学会会員。

上垣内岳司



平10早大・理工・電子情報通信卒。平12同大大学院修士課程了。在学中は超薄膜多層構造膜に関する研究に従事。現在, 東芝セミコンダクター社に勤務。

Dependence of PL Characteristics of a-Si:H Nanoball Films Fabricated by Double Tubed Coaxial Line Type MPCVD System on Substrate Position

二重管式同軸線路型 MPCVD 装置を用いて作製した a-Si:H ナノボール膜の PL 特性の基板位置依存性

Takayuki Matsumoto and Isamu Kato

松本 貴之, 加藤 勇

School of Science and Engineering, Waseda University,
3-4-1 Okubo, Shinjuku-ku, Tokyo 169-8555

早稲田大学理工学部, 〒169-8555 東京都新宿区大久保 3-4-1

Using a double tubed coaxial line type microwave plasma CVD system, a-Si:H nanoball films which include Si nanocrystals can be fabricated. The photoluminescence (PL) peaked around 780 nm is observed at the room temperature after the a-Si:H nanoball film is oxidized by heating in the atmosphere. We have fabricated a-Si:H nanoball films with varying the substrate position and DC bias substrate voltage of this system, and discussed the relationship between the film properties and the PL characteristics of a-Si:H nanoball films.

1. Introduction

We have developed a double tubed coaxial line type microwave plasma CVD (MPCVD) system.^{1,2)} Figure 1 shows the configuration of this MPCVD system. In this system the microwave power is confined in the cylindrical cavity region, and in the deposition chamber a spatial afterglow plasma without injection of the microwave power is created by the gas flow and diffusion. The discharge gas (which creates the plasma, but doesn't create a deposited material by itself) is fed to the outer discharge tube which is composed of fused quartz, and the material gas (which is dissociated in the plasma and creates a deposited material) is fed to the inner tube (as shown in Fig. 1). Both gases can be led separately to the deposition chamber. The discharge gas is ionized in the cylindrical cavity region by the microwave power. The material gas is led to the discharge tube end through the inner tube, flows into the plasma and is dissociated by the collision with the plasma particles.

Using Ar gas as a discharge gas and SiH₄ gas as a material gas, a-Si:H films are fabricated. In the case of the low gas pressure in the deposition chamber by the high speed exhaust, a good a-Si:H film is created.^{3,4)} In the case of the high gas pressure in the deposition chamber by the low speed exhaust, because the mean free path becomes short, SiH_x radicals are spatially recombined in the gaseous phase, and forms a spherical cluster (~20 nm in diameter). We name it a a-Si:H nanoball. The

a-Si:H nanoballs deposit on the substrate, and a a-Si:H nanoball film is fabricated. The feature of our system is that it can fabricate both the a-Si:H film and the a-Si:H nanoball film by controlling the speed of exhaustion. It is found by X-ray diffractometer that a-Si:H nanoballs include Si nanocrystals (~5 nm in diameter). The photoluminescence (PL) is observed at the room temperature after the a-Si:H nanoball film is oxidized by heating in the atmosphere.

In this study we have fabricated the a-Si:H nanoball films with varying the substrate position and the DC bias voltage, and discussed the relationship between the film properties and the PL characteristics of a-Si:H nanoball films.

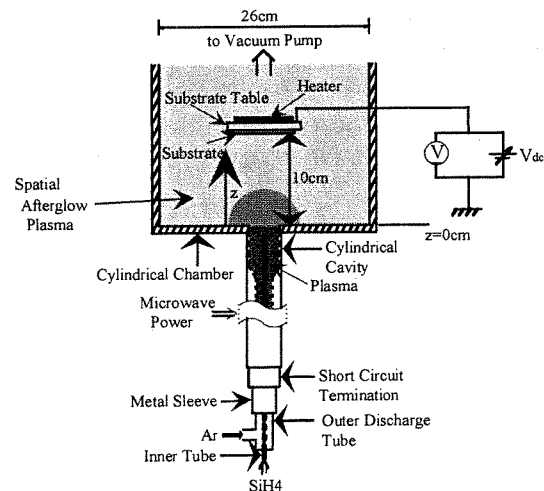


Fig.1 Configuration of the double tubed coaxial line type microwave plasma CVD system

2. Experimental

The experimental conditions are as follows. The axial distance from the discharge tube end is defined as z (as shown in Fig. 1). The Ar gas flow rate is 110 ml/min and the SiH₄ gas flow rate is 30 ml/min. The microwave power is 150 W. The inner tube end is at $z = -1.4$ cm. The gas pressure in the deposition chamber is set at 250 mTorr by controlling the exhaust valve. The substrate temperature is R.T. The discharge time is 10 min. In this study the substrate table is set at $z = 4, 6, 10$ cm and the DC substrate bias voltage is varied from -80 V to $+40$ V.

As deposited, the films are thermally oxidized in the atmosphere. After oxidation the PL spectrum is measured. The excitation light is Ar⁺ laser (514.5 nm). The measurement is done at the room temperature in a vacuum ($\sim 2 \times 10^{-5}$ Torr) in order to avoid the thermal oxidation by the laser irradiation energy. The laser beam is irradiated at an angle of 60° from a normal line of the film. We remove a scattered laser light by a spectrophotometer and observe the PL spectrum from a normal line direction.

3. Results and Discussions

We measured the sheath voltage (V_{sh}) at $z = 3, 5, 9$ cm in the pure Ar⁺ plasma by the single probe method when the substrate is set at $z = 4, 6, 10$ cm. From this result, it is found that the V_{sh} varied from -110 V to -20 V with varying V_{dc} from -80 V to $+40$ V at any substrate position. Therefore, the ion bombardment energy can control from -110 eV to -20 eV regardless of the substrate position.

In order to survey the influence of the variation of the ion bombardment energy on the construction of the film, we calculate the hydrogen concentration from the FTIR spectra. It is found that, as the V_{sh} increases in a negative direction, the ion bombardment energy increases and the C_H decreases at any substrate position. This result is considered to be due to as follows. As the V_{sh} increases, the Ar⁺ ions are more accelerated by the sheath voltage and the Ar⁺ ions with larger energy are struck into the film.

Then we calculate dependence of the deposition rate of the film on the V_{sh} . It is found that, as the V_{sh} increases in a negative direction, the deposition rate decreases at any substrate position. This result is considered to be due to as follows. As the V_{sh} increases, the mobility of the a-Si:H nanoballs attached to the substrate is raised by the film surface heating effect of the ion bombardment, therefore, the a-Si:H nanoballs deposit densely on the substrate.

Figure 2 shows the dependence of the PL intensity on the V_{sh} . It is found that, as the V_{sh} increases in a

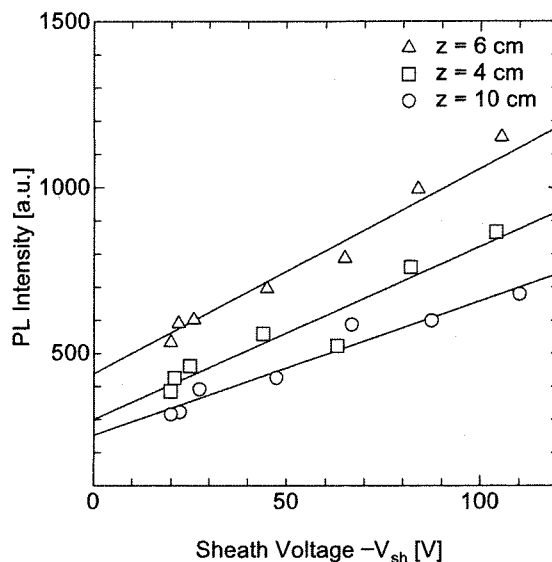


Fig.2 Dependence of the PL intensity on the V_{sh}

negative direction, the PL intensity increases at any substrate position. As the substrate position z decreases, the a-Si:H nanoball deposits more. Therefore the PL intensity should increase. But the PL intensity at $z = 4$ cm is weaker than that at $z = 6$ cm. The reason is considered to be as follows. The SiH_x radicals arrive at the substrate before the a-Si:H nanoballs are created by the spatial recombination. Furthermore, when z decreases, the amount of ion bombardment increases as the plasma density increases. The film surface is heated by ion bombardment during deposition. The hydrogen atoms are disconnected from the a-Si:H nanoball films with increasing the substrate temperature, then this film becomes nearer a-Si film. It is more difficult for the a-Si to be oxidized than the a-Si:H. Therefore the state that the Si nanocrystals are embedded in SiO₂ (Si quantum dot) does not form, hence the PL is weak.

Acknowledgements

This work was supported by the Grant-in-Aid for scientific research from the Ministry of Education, Science and Culture. The authors thank Mr. Saito, research student, for his experimental assistance.

References

- 1) I. Kato, S. Wakana, S. Hara and H. Kezuka: Jpn. J. Appl. Phys. 21 (1982) 470
- 2) I. Kato, S. Wakana and S. Hara: Jpn. J. Appl. Phys. 22 (1983) 40
- 3) I. Kato, T. Ueda and K. Hatanaka: Electron. Commun. Jpn, 2, 70 (1987) No. 11, 73
- 4) K. Kato and I. Kato: Jpn. J. Appl. Phys. 30 (1983) 1245

Quality of a-Si:H/Si₃N₄ multilayer films fabricated by double tubed coaxial line type MPCVD system(II)

二重管式同軸線路形 MPCVD 装置を用いて作製した a-Si:H/Si₃N₄ 多層膜の膜質について(II)

Takayoshi Sugai , and Isamu Kato

菅井貴義, 加藤勇

School of Sci. and Engin. Waseda Univ.

3-4-1,Ookubo,Shinjuku-ku,Tokyo 169-8555

早稲田大学理工学部, 〒169-8555 東京都新宿区大久保 3-4-1

We fabricated a-Si:H/Si₃N₄ multilayer films using the double tubed coaxial line type MPCVD System. We fabricated a-Si:H, Si₃N₄, and a-Si:H/Si₃N₄ multilayer films varying the substrate temperature from R.T. to 500[°C], and evaluate their quality. We measured X-Ray diffraction peak, dangling bond density, and optical band gap. As a result, we can fabricate a-Si:H/Si₃N₄ multilayer films of good value by measuring X-Ray diffraction peak. And we obtained that dangling bond density increase and optical band gap decrease as substrate temperature is higher.

1. Introduction

We have used the double tubed coaxial line type microwave plasma CVD system to make a-Si:H/Si₃N₄ multilayer film and to study about its quality^[1]. We have studied that optical band gap of multilayer film with thickness of Si₃N₄ layer fixed and thickness of a-Si:H layer varying increases as the thickness of a-Si:H layer is decreased. And when thickness of a-Si:H layer is fixed and thickness of Si₃N₄ layer is varied, its optical band gap is invariable in case of thickness of Si₃N₄ layer is under 10[nm], and increases in case of it is over 10[nm].

In this paper, we fabricated a-Si:H, Si₃N₄, and a-Si:H/Si₃N₄ multilayer films varying the substrate temperature and evaluate their quality.

2. Experimental

Figure 1 shows the configuration of the MPCVD system. In the deposition chamber of this system, spatial after-grow plasma is formed by the gas flow and diffusions because the microwave power is not injected into the plasma in the chamber. The discharge gas, such as Ar and N₂, is fed to the outer discharge tube and the SiH₄ gas is fed to the inner tube.

The computer all controls inflow of discharge gas and SiH₄ gas. As movable parts, such as Short Circuit Termination and Metal Sleeve, are controlled by programs, we are able to get best condition of plasma in each discharge. When

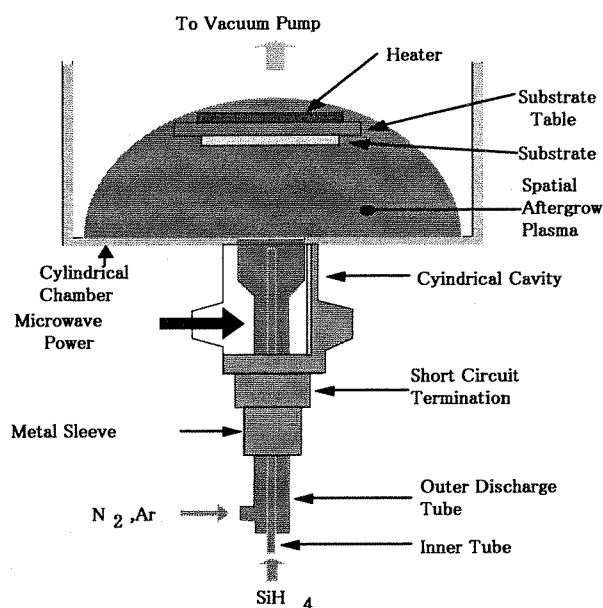


Fig. 1 MPCVD system

Making a-Si:H layer, Ar gas is used as discharge gas, and SiH₄ gas is used as material gas. Ar gas flow rate is 110[ml/min], and SiH₄ gas flow rate is 5[ml/min]. When making Si₃N₄ layer, N₂ gas is used as discharge gas, and SiH₄ gas is used as material gas. N₂ gas flow rate is 140[ml/min], and SiH₄ gas flow rate is 5[ml/min]. We fabricated films varying the substrate temperature from R.T. to 500[°C].

3. Result and discussion

Figure 2 shows the X-ray diffraction peak of a-Si:H/Si₃N₄ multilayer film deposited on Si

substrate. An X-ray wavelength scattering films is 1.54[Å]. The well-defined peak is shown in Fig 2. The thickness of 1 period layer of multilayer film calculated from this diffraction peak is 6.8[nm] in case of the primary peak, and is 5.5[nm] in case of the secondary peak. The other one calculated from the total thickness of multilayer film is 6.8[nm]. The close agreement between the two values is obtain.

Figure 3 shows dependence dangling bond density on substrate temperature. In this figure, dangling bond of a-Si:H films decrease when substrate temperature is under 250[°C], and increase when substrate temperature is over 250[°C]. Dangling bond density of Si₃N₄ films decrease, as substrate temperature is higher. But, dangling bond of multiplayer films increase, as substrate temperature is higher. Although dangling bond density of a-Si:H and Si₃N₄ films decrease with substrate temperature higher, dangling bond of the interface increase in according to no lattice adjustment from crystallization, and distortion from difference of heat expansion rate. So dangling bond density of multilayer films increase.

Figure 4 shows dependence optical band gap on substrate temperature. In this figure, optical band gap of a-Si:H film decrease when substrate temperature is higher. We think that a-Si:H films get near to poly-crystal according to heat the substrate. optical band gap of Si₃N₄ film is about 5[eV] and a little decrease when substrate temperature is higher. We think that Si₃N₄ films also get near to poly-crystal according to heat the substrate. Optical band gap of multiplayer films is almost agreed with that of a-Si:H films. Because a-Si:H layer becomes well layer of multilayer films, and optical transport occurs in well layer, so optical band gap of multilayer films is almost agreed with that of a-Si:H films.

4. Conclusion

We can fabricate good multilayer film because the thickness of 1 period layer of multilayer film calculated from total thickness is agreed with the thickness calculated from X-Ray diffraction peak.

Dangling bond density of multilayer films increases, as the substrate temperature is higher, and optical band gap decrease, as substrate temperature

is higher.

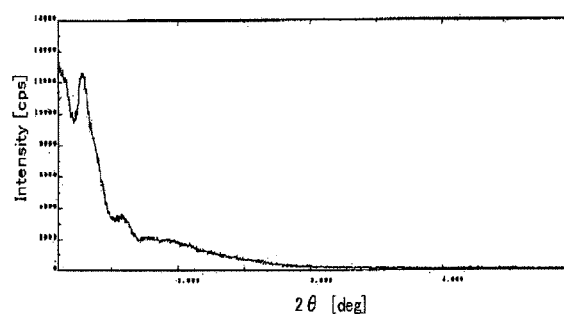


Fig. 2 X-Ray diffraction Peak

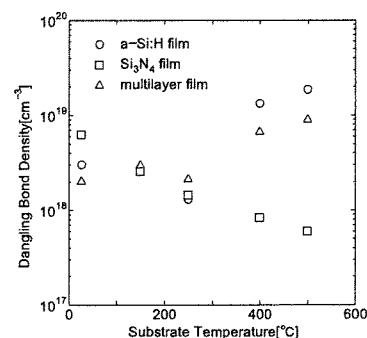


Fig. 3 Dependence of Dangling Bond Density on Substrate temperature

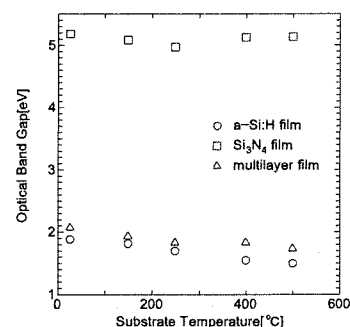


Fig. 4 Dependence of Optical Band Gap on Substrate Temperature

Acknowledgement

This work was supported by the Grant-in-Aid for scientific research from the ministry of Education, Science, and Culture. This work was also supported by a Waseda University Grant for Special Research Projects.

Reference

[1] T.Kamigaichi: *Proc. 17th Sympo. Plasma Processing*, PP239-242

Film quality of a-Si:H/Si₃N₄ multilayer films and propagate properties of optical waveguides using the multilayer films

a-Si:H/Si₃N₄ 多層膜の膜質および本多層膜を用いて作製した
光導波路の伝搬特性

Masahiko Sagisaka, Takayoshi Sugai, Naoyuki Tamaru* and Isamu Kato
匂坂雅彦, 菅井貴義, 田丸直幸*, 加藤勇

*School of Sci. and Engin. Waseda Univ.
3-4-1, Ookubo, Shinjuku-ku, Tokyo 169-8555*

**Otsuma Women's Univ
2-7-1, Karakida, Tama, Tokyo 206-8540*
早稲田大学理工学部, 〒169-8555 東京都新宿区大久保 3-4-1
*大妻女子大学, 〒206-8540 東京都多摩市唐木田 2-7-1

We fabricated a-Si:H/Si₃N₄ multilayer films using the double tubed coaxial line type MPCVD System. We fabricated films varying the substrate temperature from R.T. to 500[°C]. We evaluated the quality of the multilayer films by measuring the optical energy gap E_o, the refractive index, absorption coefficient and so on. As a result, we obtained that we can fabricate the good multilayer when the substrate temperature is more than 250[°C].

We processed the films to slab waveguides, and measured their propagation properties. As a result, we obtained high extinction ratio when the substrate temperature is 250[°C].

1. Introduction

We have used the double tubed coaxial line type microwave plasma CVD system to make a-Si:H/Si₃N₄ multilayer film and to study about its quality. We processed the film to slab waveguides, and as a result, we have confirmed that these optical waveguides have polarization properties that TM mode was transmitted and TE mode was cut. We obtained that fabricated multilayer slab waveguides have high extinction ratio that is 17[dB]. Also we understood that the extinction ratio rise when the slab waveguides are pumped. In this study, the relation between the substrate temperature when we fabricated a-Si:H/Si₃N₄ multilayer and quality of the multilayer has been definitely shown. Also the relation between the substrate temperature and the propagation properties of multilayer film optical waveguides has been definitely shown.

2. Experimental

We fabricated a-Si:H/Si₃N₄ multilayer films by depositing a-Si:H films and Si₃N₄ films alternately on the p-Si substrates and on the quartz substrates using the double tubed coaxial line type microwave plasma CVD system. We fabricated films varying the substrate temperature from R.T. to 500[°C]. The thickness of a-Si:H layers were 10[nm] and the thickness of Si₃N₄ layers were 30[nm]. We took this process 15 cycles, and the total film thickness was 600[nm]. We evaluated the optical energy gap E_o, the refractive index, absorption coefficient from the spectrum transmission of this multilayer films.

Next we explain how to fabricate the slab waveguides. The Si₃N₄ film(about 2 [μm]) was deposited on p-Si substrate as buffer layer. We deposited a-Si:H films and Si₃N₄ films alternately on the buffer layer. We cut the multilayer film using a diamond cutter and polished up its end face. Then we fabricated multilayer film optical waveguide whose length is about 1[mm]. We measured the propagation properties of the fabricated slab waveguides using the lensed fiber(λ=1.55[μm]).

3. Result and discussion

We measured the optical energy gap of multilayer films. The dependence of the optical energy gap on the substrate temperature is shown in Fig.1. By the Fig.1, it is obvious that optical energy gap decreases as the substrate temperature becomes higher. The structure of a-Si:H closes with that of c-Si as the substrate temperature is higher. The optical energy gap of c-Si is smaller than that of a-Si:H. So, the optical energy gap is smaller according as the substrate temperature is higher, and the optical energy gap of the multilayer films is larger. Therefore, it is clear that we can control the optical energy gap by varying the substrate temperature.

To the next, we measured the refractive index of the multilayer films. The dependence of the refractive index on the substrate temperature is shown in Fig.2. It is obvious that the refractive index is higher according as the substrate temperature is higher. This shows that the density

of films is higher according as the substrate temperature is higher. Namely, the structures of a-Si:H and Si₃N₄ close with those of c-Si and c-Si₃N₄ respectively. Therefore, we can control the refractive index by varying the substrate temperature.

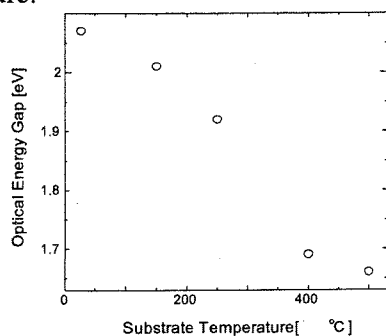


Fig.1 Dependence of the optical energy gap on the substrate temperature

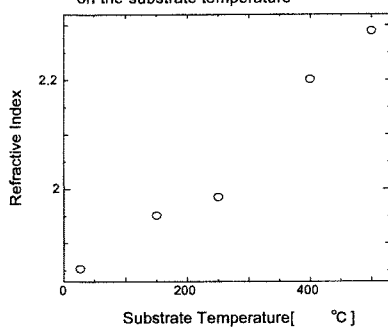


Fig.2 Dependence of the refractive index on the substrate temperature

To the next, we measured the absorption coefficient (at $\lambda = 1.55[\mu\text{m}]$) of the multilayer films. The dependence of the absorption coefficient on the substrate temperature is shown in Fig.3. It is obvious that the absorption coefficient increases as the substrate temperature becomes higher. The absorption coefficient of c-Si is higher than that of a-Si:H in infrared range. This is because the structure of a-Si:H closes with that of c-Si as the substrate temperature is highert. By the Fig.3, the absorption coefficient is very high when the substrate temperature is more than 400[°C]. From this result, the suitable substrate temperature for the optical waveguides is less than 250[°C].

We processed the film to slab waveguides, and measured its polarization properties. The dependence of the extinction ratio of the multilayer film optical waveguides on the substrate temperature is shown in Fig.4. By the Fig.4, the extinction ratio becomes larger according as the substrate temperature is higher. When the substrate temperature is R.T., the interface of a-Si:H and Si₃N₄ is not clear, and a-Si:H and Si₃N₄ are intermixed. So, we cannot fabricate good multilayer films when the substrate temperature is R.T.

Therefore, the optical waveguides cannot reflect the TE mode component of propagation lightwave, and the extinction ratio becomes low. Also, we can obtain higher extinction ratio when the substrate temperature is higher. When the substrate temperature is higher, the structure of a-Si:H closes with that of c-Si, and the conductivity of a-Si:H becomes higher. Therefore, a quantity of reflection of TE mode component increases. As a result, intensity of TE mode transmitted lightwave decrease, and the extinction ratio becomes higher.

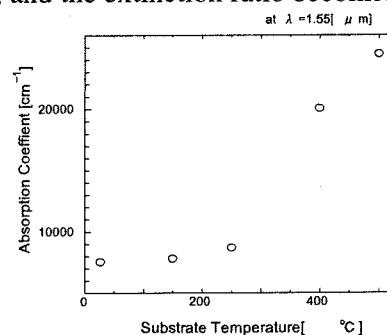


Fig.3 Dependence of the absorption coefficient on the substrate temperature

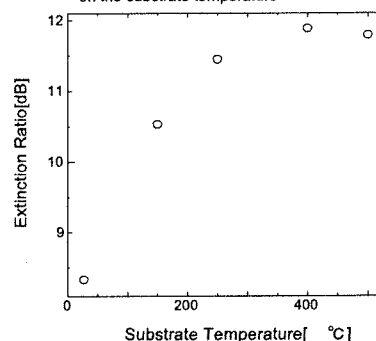


Fig.4 Dependence of the extinction ratio on the substrate temperature

4. Conclusion

It is clear that we can fabricate the good multilayer film with clear interface when the substrate temperature is from 250[°C] to 500[°C]. It is obvious that the optical waveguide has high extinction ratio when the substrate temperature is from 250[°C] to 500[°C]. But the absorption ratio is higher when the substrate temperature is more than 400[°C]. Therefore the suitable substrate temperature for the optical wavguides is 250[°C].

Acknowledgement

This work was supported by the Grant-in-Aid for Scientific Research from the Ministry of Education, Science and Culture of Japan and the Waseda University Grant for Special Research Projects. The author thanks Mr. Koyama and Mr. Shinohara, research student, for his experimental assistance.

Effect of Ar⁺ Ion Bombardment During Hydrogenated Amorphous Silicon Film Growth in Plasma Chemical Vapor Deposition System

Isamu KATO^{1,2}, Yuuki NAKANO¹ and Nobuhiko YAMAGUCHI¹

¹Department of Electronics, Information and Communication Engineering, Waseda University, 3-4-1, Okubo, Shinjuku-ku, Tokyo 169-8555, Japan

²Materials Research Laboratory for Bioscience and Photonics, Waseda University, 3-4-1, Okubo, Shinjuku-ku, Tokyo 169-8555, Japan

(Received May 29, 2000; accepted for publication August 22, 2000)

We have developed the double tubed coaxial line type microwave plasma chemical vapor deposition (MPCVD) system to fabricate hydrogenated amorphous silicon (a-Si:H) films. We have studied the influence of Ar⁺ ion bombardment during a-Si:H film growth and clarified that the ion bombardment causes film surface heating effect and ion implanting effect. It is not sufficient to discuss only whether films are of good quality or not, when the ion bombardment energy is increased. In this study, we show that the effect of ion bombardment can be separated into the film surface heating effect and the ion implanting effect and discuss the influence of each effect on the film properties. We also show that the film surface temperature can be expressed as a function of the sheath voltage. It is clarified that a film with low dangling bond density can be fabricated at low temperatures if there is no ion bombardment.

KEYWORDS: microwave plasma, spatial afterglow plasma, chemical vapor deposition, a-Si:H, ion bombardment, single probe method, ion sheath, film surface heating effect, dangling bond density

1. Introduction

In recent years research studies on plasma chemical vapor deposition (CVD) methods using RF discharge and electron-cyclotron-resonance (ECR) discharge for depositing a-Si:H films have been widely conducted. Among them are reports on the influence of ion bombardment on a-Si:H film properties.^{1,2} We have developed the double tubed coaxial line type microwave plasma CVD (MPCVD) system^{3,4} and studied these effects. In this system, discharge plasma with injected microwave power is confined in a fixed region, and in the deposition chamber downstream, the gas flow forms spatial afterglow plasma without injected microwave power. Substrate is placed in the spatial afterglow plasma, where film deposition takes place. Sheath voltage in front of the film can be controlled because only the plasma spatial voltage changes as the substrate voltage is varied (distribution of electron temperature and electron density does not change). The gas which does not leave deposits after discharge (discharge gas) and the gas which leaves deposits after dissociation or combination in the plasma (material gas) can be separately fed because the system is double tubed. Using a coaxial line type microwave discharge tube, the created plasma is uniformly distributed around the axis⁵ (in this case, the metallic cylindrical cavity works as the outer conductor and the plasma as the inner conductor). We have studied the influences of ion bombardment on a-Si:H film properties when the ions (Ar⁺, H⁺, etc.) that are accelerated by the sheath voltage collide with the growing film surface.

We proposed that the effect of ion bombardment consists of the physical effect (the lattice of film surface is excited to vibrate), which we call film surface heating effect, and the chemical effect (implanted ions react chemically in the film surface, cutting off molecular bonds, and H atoms are pulled out of SiH₂ bond by implanted H⁺ ions), which we call ion implanting effect. The former effect raises the equivalent temperature of film surface, increasing the mobility of arriving radicals on the film surface so that film structure is relaxed. The latter effect leaves Ar atoms as impurities in the film thus increasing the number of dangling bonds and cutting off SiH

and SiH₂ bonds reducing hydrogen in the film. Therefore, it is incomplete to discuss the fabrication of good quality films by considering only the amount of ion bombardment. In this paper, we clarify that the effect of the ion bombardment can be separated into the physical effect (film surface heating effect) and the chemical effect (ion implanting effect) and examine the influence of each on a-Si:H films.

2. Experiment

Figure 1 shows the experimental setup of the MPCVD system. The axial distance from the discharge tube end is defined as z (shown in Fig. 1). In this system, the microwave power is confined in the cavity, and not injected into the plasma in the chamber. Thus, in the deposition chamber, the gas flow forms spatial afterglow plasma with no microwave power injected. The outer discharge tube is composed of fused quartz and the inner tube is made of stainless steel. The Ar gas is fed to the outer discharge tube and the SiH₄ gas is fed to the inner tube.

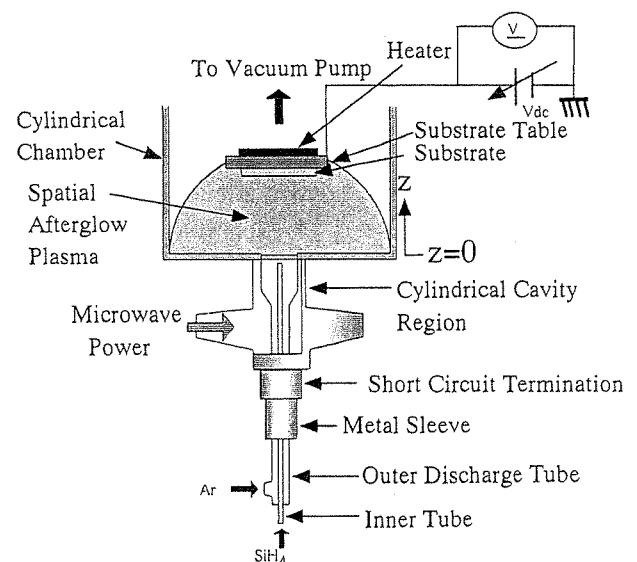


Fig. 1. Experimental setup of the double tubed coaxial line type microwave plasma CVD system.

The Ar gas is ionized in the cylindrical cavity region by the microwave power. The SiH₄ gas flows into the Ar plasma at the discharge tube end through the inner tube, and then the SiH₄ is dissociated by collision with the Ar plasma particles. The substrate table area is 40 cm² and is placed at $z = 10$ cm. The Ar gas flow rate is 110 ml/min and the SiH₄ gas flow rate is 30 ml/min. Sheath voltage (V_{sh}) can be controlled from 0 V to -95 V by varying the DC substrate bias voltage (V_{dc}) from +40 V to -80 V. The value of sheath voltage is obtained from the following equation:

$$V_{sh} = V_{dc} - V_S. \tag{1}$$

Here plasma spatial voltage (V_S) is measured using the single probe method.^{6,7)} The probe of 0.05 cm in diameter and 1 cm in length is used. The measurement is performed at $z = 9$ cm on the deposition chamber axis, which is 1 cm in front of the substrate table. In the case of the measurement of dependence on substrate temperature (T_s), V_{sh} is set to 0 V (namely V_{dc} is +40 V) and T_s is varied from room temperature (R.T.) to 250°C.

The following are measured: Si concentration, deposition rate, SiH bond concentration, SiH₂ bond concentration and dangling bond density. Si concentration is obtained by measuring the energy spectrum of ions that are scattered backward elastically (Rutherford backscattering) by the Coulomb interaction after collision with the targeted nucleus in the film. Deposition rate is obtained by measuring film thickness with a stylus profiler. SiH bond concentration and SiH₂ bond concentration are obtained by measuring the area of the infrared absorption spectra of the a-Si:H film. In the above-mentioned cases, Si wafers are used. To obtain the value of dangling bond density, we use the electron spin resonance (ESR) method to measure the spin angular momentum of non-paired electron that is affiliated to the radicals such as dangling bonds. In this case, Al substrates are used.

3. Results and Discussion

Dependence of Si concentration on substrate temperature (T_s) and that on sheath voltage (V_{sh}) are shown in Fig. 2(a). The dependence of Si concentration on T_s is not affected by ion bombardment because it is measured under the condition of $V_{sh} = 0$ V. Therefore, film surface temperature is equal to the substrate temperature. Here we assume that the dependence of Si concentration on V_{sh} is not influenced by the ion implanting effect but only by the film surface heating effect. In this case, the dependence of Si concentration on T_s is equivalent to that on V_{sh} , and we have the following equation:

$$T_s = aV_{sh} + b^\circ\text{C}. \tag{2}$$

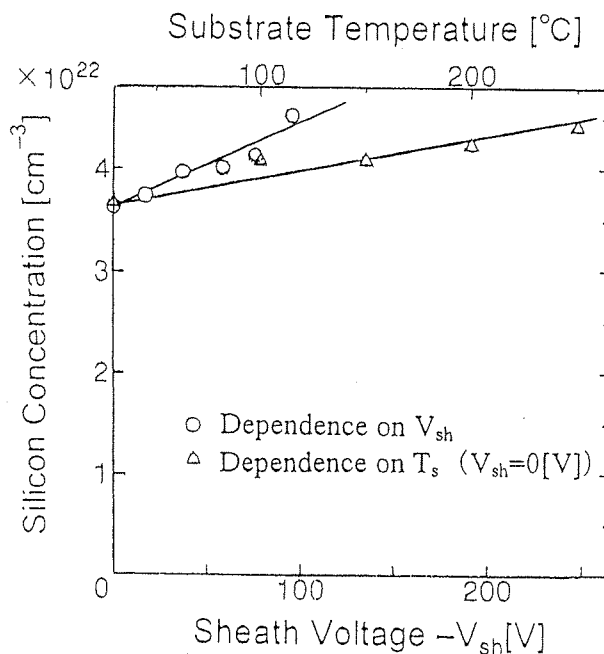
Hence the graph of the dependence of Si concentration on V_{sh} can be fitted to the graph of that on T_s by adjusting the scale of the former graph. First, the Si concentration at $T_s = 28^\circ\text{C}$ in the graph of the dependence of Si concentration on T_s and that at $V_{sh} = 0$ V in the graph of the dependence of Si concentration on V_{sh} are the same because the films are deposited under the same condition (namely $b = 28^\circ\text{C}$). Second, we obtain the value of the coefficient "a" of eq. (2) using the experimental values in Fig. 2(a):

$$T_s = -2.34 \times V_{sh} + 28^\circ\text{C}. \tag{3}$$

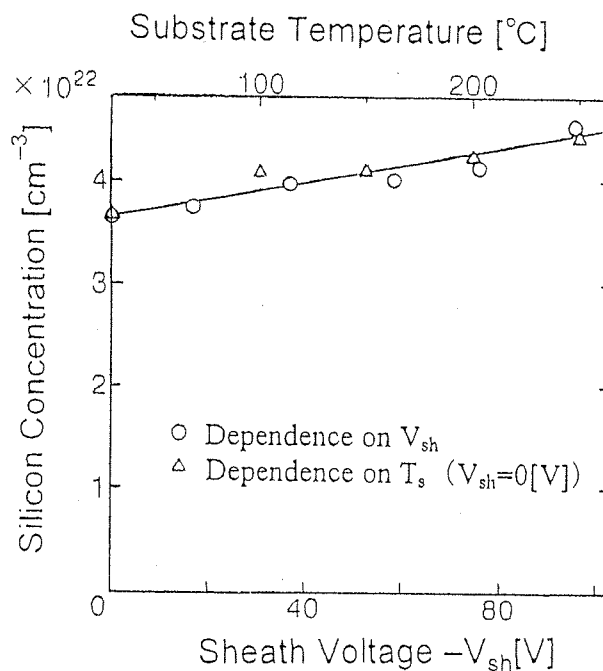
In this equation, 28 denotes the room temperature and

$-2.34 \times V_{sh}$ denotes the rise in the film surface temperature caused by the ion bombardment. The dependence of Si concentration on T_s and that on V_{sh} are shown in Fig. 2(b), using eq. (3). Figure 2(b) shows that the two graphs are in good agreement, which confirms the above-mentioned assumption. Thus, the film surface is heated as a result of the ion bombardment even when the substrate is at room temperature. The film surface equivalent temperature is 68°C when V_{sh} is -17 V, 115°C when V_{sh} is -37 V, and 164°C when V_{sh} is -58 V.

The dependence of Si concentration on T_s is shown in



(a)



(b)

Fig. 2. Dependence of Si concentration on T_s and V_{sh} . (a) original and (b) result of calculation using eq. (3).

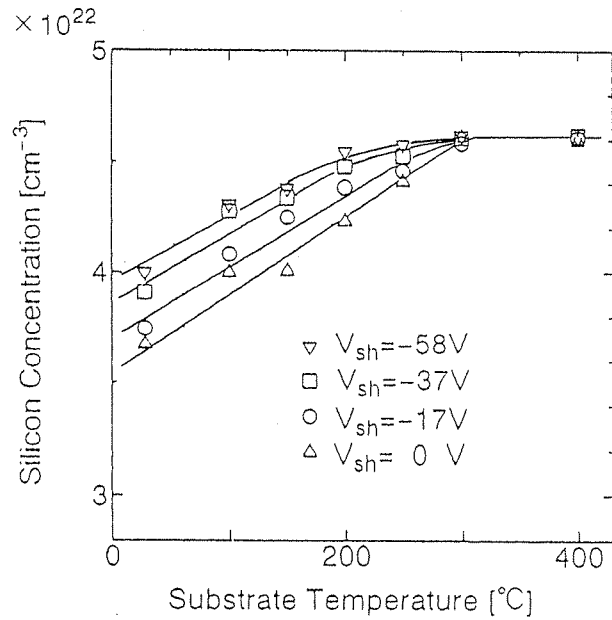
Fig. 3(a). Here the parameter is V_{sh} . The Si concentration increases when T_s is increased. This is because the vibration of the lattice in the film is excited and structural relaxation occurs. The Si concentration increases as a result of the film surface heating effect when V_{sh} is decreased.

Considering the film surface heating effect, T_s must be shifted by 40°C when V_{sh} is -17 V, 87°C when V_{sh} is -37 V, and 136°C when V_{sh} is -58 V [following eq. (3)]. The curve of dependence of Si concentration on T_s in Fig. 3(a) is shifted as mentioned above, and the shifted curve is shown in Fig. 3(b). Figure 3(b) indicates that the four curves are in good agreement. This is because the dependence of Si concentration on V_{sh} is not influenced by the ion implanting effect

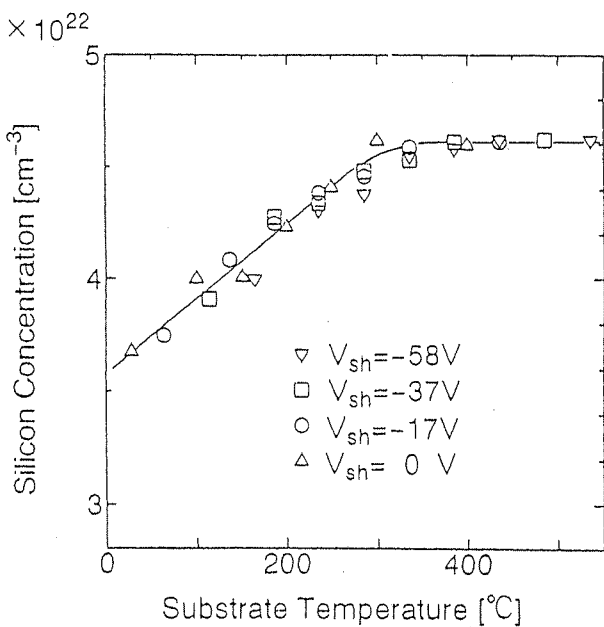
but only by the film surface heating effect, namely eq. (3) is reconfirmed. Figure 3(b) also shows that the Si concentration is constant after T_s reaches about 300°C, which is because the a-Si:H film is sufficiently dense at that temperature.

The dependence of deposition rate on T_s is shown in Fig. 4(a). Here the parameter is V_{sh} . The deposition rate decreases when T_s is increased because the film becomes dense. As V_{sh} is decreased, the deposition rate decreases because the film becomes dense as a result of the film surface heating effect.

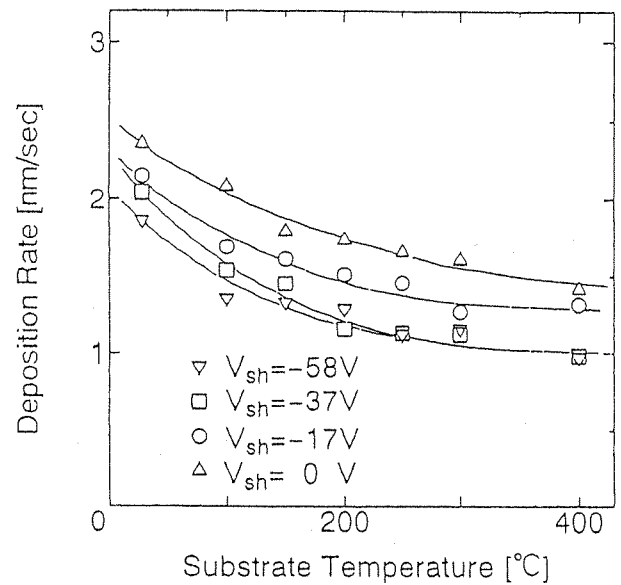
The curves of dependence of deposition rate on T_s in Fig. 4(a) are shifted as mentioned above, and the shifted curves are shown in Fig. 4(b). As shown in the figure, the curves of the deposition rate are in good agreement until T_s reaches about 130°C but subsequently it decreases faster



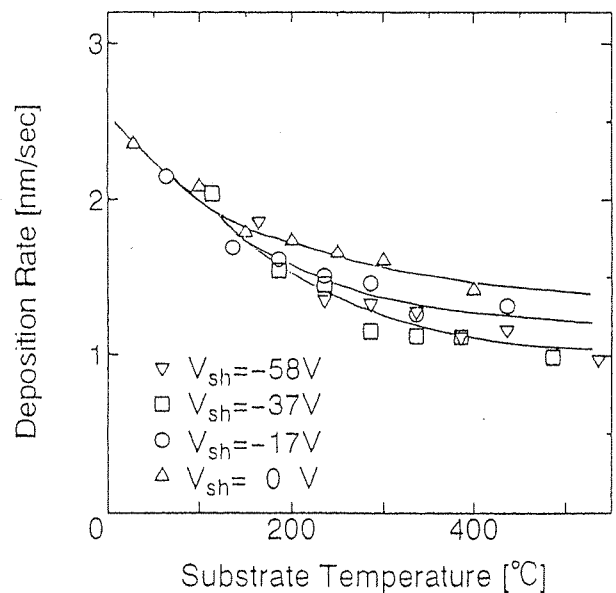
(a)



(b)



(a)



(b)

Fig. 3. Dependence of Si concentration on T_s . (a) original and (b) result of shift using eq. (3).

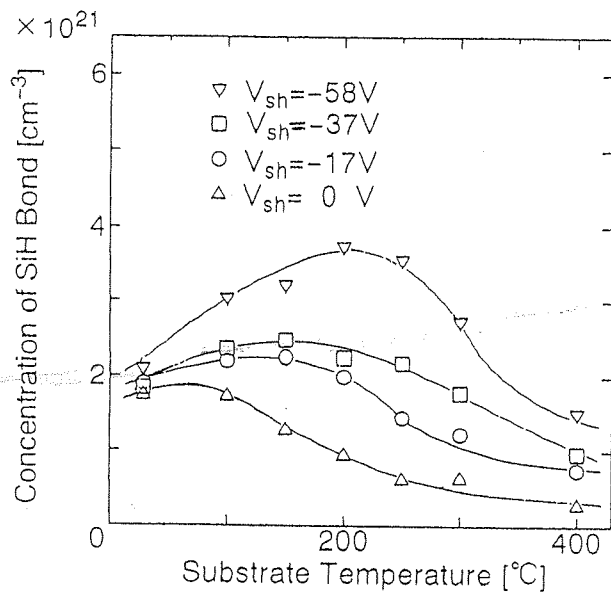
Fig. 4. Dependence of deposition rate on T_s . (a) original and (b) result of shift using eq. (3).

as V_{sh} becomes low. Differences between the curve for $V_{sh} = 0$ V and the curves for other V_{sh} in the region where T_s is larger than 130°C are considered to be affected by the ion implanting. It is experimentally clarified that the ion implanting effect does not appear until T_s reaches about 130°C but appears strongly after that [shown in Fig. 4(b)]. Radicals on the film surface do not migrate before T_s reaches about 130°C but the time of migration becomes greater after that, which means that the film is sputtered more by the Ar^+ ions. Thus the sputtering effect by the Ar^+ ions appears markedly after T_s reaches about 130°C , which leads to a decrease in the deposition rate as V_{sh} decreases.

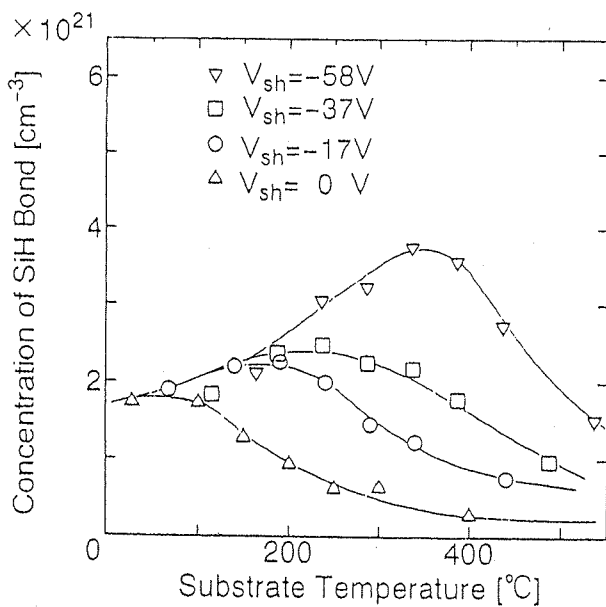
The dependence of SiH bond concentration on T_s is shown in Fig. 5(a). Here the parameter is V_{sh} . Next, the curves of dependence of SiH bond concentration on T_s in Fig. 5(a) are

shifted as mentioned above, and the shifted curves are shown in Fig. 5(b). SiH bond concentration increases when V_{sh} is decreased as a result of the ion implanting effect, which means that the smaller V_{sh} is, the larger the ion implanting effect is. When V_{sh} is not 0 V, SiH bond concentration increases as T_s is increased until it reaches a certain peak value, and decreases after that. The SiH bond concentration increases because the hydrogen constituting the SiH_2 bond is disconnected as a result of the ion implanting effect. Thus, the ion implanting effect causes the SiH bond concentration to increase and then it is considered that the film acquires a better quality.

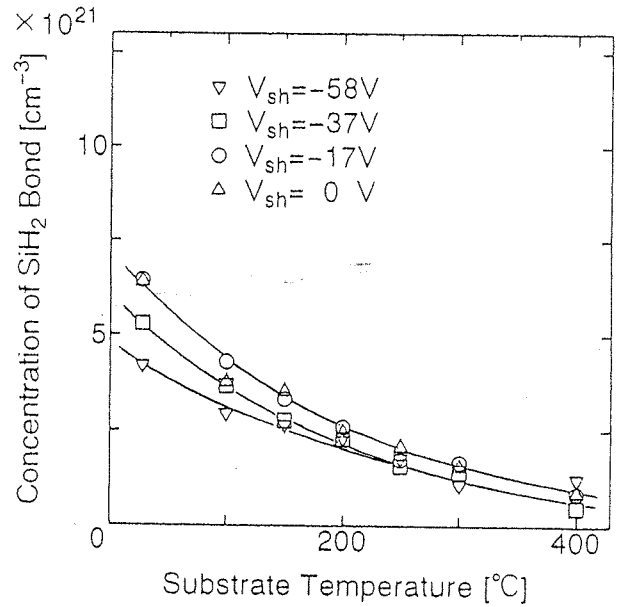
The dependence of SiH_2 bond concentration on T_s is shown in Fig. 6(a). Here the parameter is V_{sh} . SiH_2 bond concentration decreases as T_s is increased. The hydrogen atoms con-



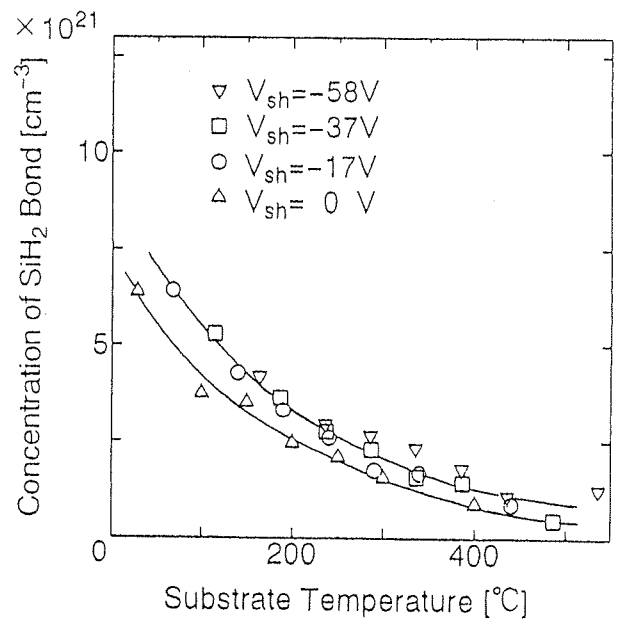
(a)



(b)



(a)



(b)

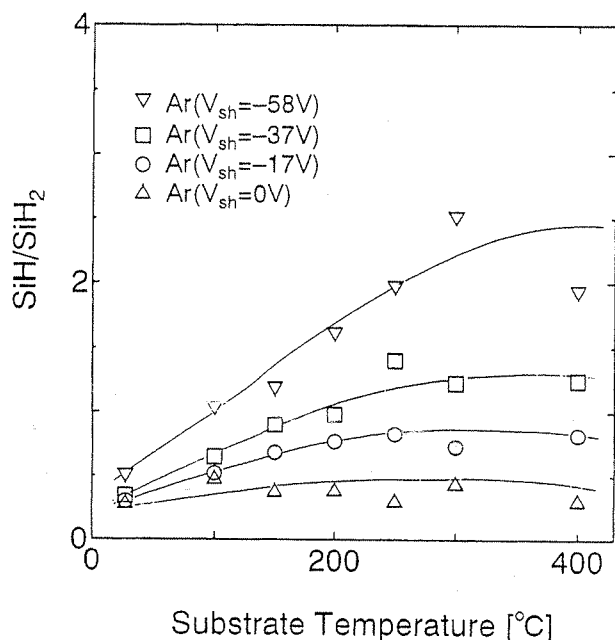
Fig. 5. Dependence of SiH bond concentration on T_s . (a) original and (b) result of shift using eq. (3).

Fig. 6. Dependence of SiH_2 bond concentration on T_s . (a) original and (b) result of shift using eq. (3).

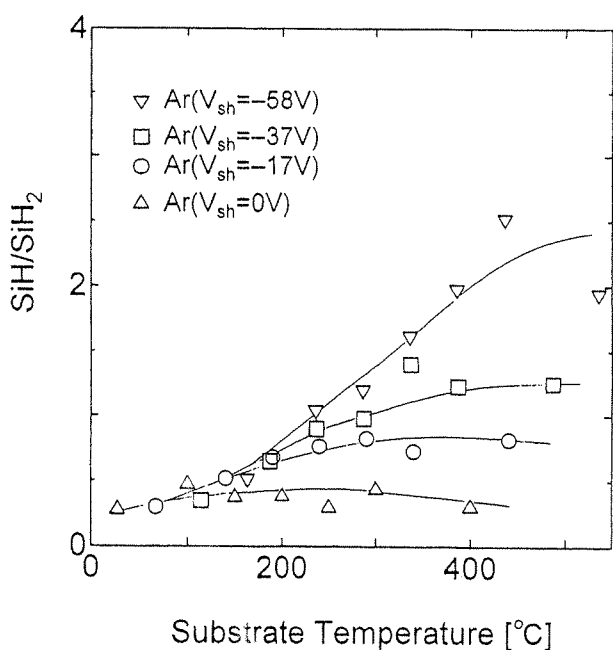
stituting the SiH₂ bond are disconnected as a result of structural relaxation as T_s is increased. SiH₂ bond concentration decreases as V_{sh} is decreased.

The curves of dependence of SiH₂ bond concentration on T_s in Fig. 6(a) are shifted as mentioned above, and the shifted curves are shown in Fig. 6(b). Only the ion implanting effect is considered here. SiH₂ bond concentration is higher when V_{sh} is not 0 V, which means that the film quality is degraded.

The dependence of the ratio of SiH bond concentration to SiH₂ bond concentration (SiH/SiH₂) is shown in Fig. 7(a).



(a)



(b)

Fig. 7. Dependence of the ratio of SiH bond concentration to SiH₂ bond concentration (SiH/SiH₂) on T_s . (a) original and (b) result of shift using eq. (3).

Here the parameter is V_{sh} . The ratio becomes larger as T_s is increased until it gets to about 300°C and decreases gently after that when V_{sh} is low. The ratio becomes larger as V_{sh} is decreased.

The curves of dependence of the ratio of SiH bond concentration to SiH₂ bond concentration (SiH/SiH₂) are shifted as mentioned above, and the shifted curves are shown in Fig. 7(b). The ratio does not change as T_s becomes high when $V_{sh} = 0$ V. When V_{sh} is decreased, the ratio increases because more H atoms are pulled out of the SiH₂ bond by implanted H⁺ ions and the concentration of SiH bond formed from the combination of implanted H⁺ ions and Si atoms with dangling bonds increases.

From these points of view, better quality films can be fabricated for lower V_{sh} . Calculating total H concentration from Fig. 5(b) and Fig. 6(b), it is clarified that total H concentration decreases simply as T_s is increased, which suggests that dangling bond density increases at high substrate temperatures because more H atoms leave the film. Thus we cannot draw a simple conclusion that a-Si:H film acquires a high quality as the SiH/SiH₂ ratio increases.

The dependence of dangling bond density on T_s is shown in Fig. 8. Here the parameter is V_{sh} . The dangling bond density takes the minimum value at $T_s = 150^\circ\text{C}$ when V_{sh} is 0 V. When V_{sh} is not 0 V, it takes the minimum value at 200–230°C. As T_s is increased, structural relaxation occurs and then the dangling bond density decreases. When T_s is larger than $T_{s\text{min}}$ where the dangling bond density is the lowest, the hydrogen atoms are disconnected from the SiH bond so that the dangling bond density increases. When V_{sh} is not 0 V, which means that the Ar⁺ ions are implanted, the film structure is destroyed and the dangling bond density increases. It is clear that the substrate needs to be heated more for more structural relaxation to occur under the ion bombardment. Therefore, the film with a low dangling bond density can be fabricated at lower temperatures avoiding the ion bombardment.

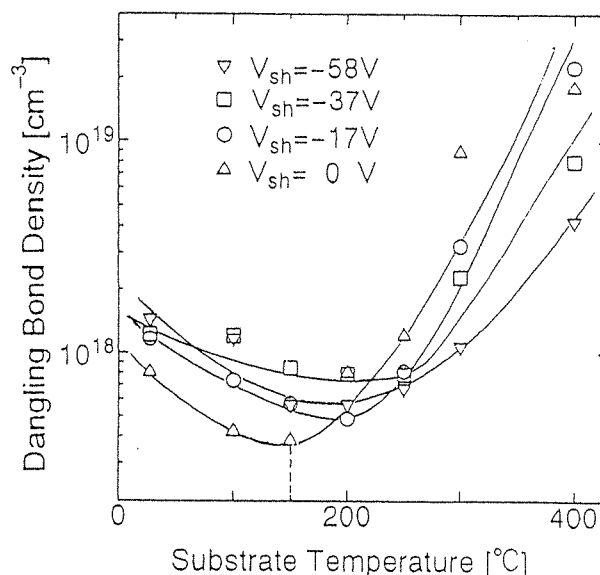


Fig. 8. Dependence of dangling bond density on T_s .

4. Conclusion

- (1) Considering the relationship between the dependence of Si concentration on substrate temperature (T_s) and that on sheath voltage (V_{sh}), we clarified that the relationship between T_s and V_{sh} can be expressed as the following experimental equation:

$$T_s = -2.34 \times V_{sh} + 28^\circ\text{C}. \quad (3)$$

Figure 2(b) shows that the two curves are in good agreement, which confirms eq. (3).

- (2) Figure 3(a) shows the dependence of Si concentration on T_s . Here the parameter is V_{sh} . As we shift T_s , following eq. (3) to take into account the film surface heating effect, all curves are in good agreement as shown in Fig. 3(b). This reconfirms eq. (3).
- (3) Figure 4(a) shows the dependence of deposition rate on T_s . Here the parameter is V_{sh} . As we shift T_s , following eq. (3) to take into account the film surface heating effect, all curves are in good agreement at low temperatures (below 130°C) as shown in Fig. 4(b). This indicates that ion implanting does not affect the dependence of the deposition rate on T_s at low temperatures.
- (4) Both SiH bond concentration and SiH_2 bond concentration increase when V_{sh} is decreased as a result of ion implanting effect [shown in Fig. 5(b) and Fig. 6(b)].
- (5) From the perspective that better quality film can be

achieved as the ratio of SiH bond concentration to SiH_2 bond concentration (SiH/SiH_2) is increased, the best condition would be that V_{sh} is low and T_s is 400°C [shown in Fig. 7(b)]. On the contrary, the dangling bond density increases as V_{sh} becomes lower (shown in Fig. 8). Thus we cannot draw a simple conclusion that the a-Si:H film acquires a high quality as the SiH/SiH_2 ratio increases.

- (6) We clarified that the film with low dangling bond density can be fabricated at low temperatures avoiding ion bombardment (shown in Fig. 8).

Acknowledgment

This work was supported by the Grant-in-Aid for scientific research from the Ministry of Education, Science, Sports and Culture.

- 1) S. Kaushal, V. Dalal and J. Xu: *J. Non-Cryst. Solids* **198–200** (1996) 563.
- 2) W. M. M. Kessels, C. M. Lewis, M. C. M. van de Sanden and D. C. Schram: *J. Appl. Phys.* **86** (1999) 4029.
- 3) I. Kato, S. Wakana, S. Hara and H. Kezuka: *Jpn. J. Appl. Phys.* **21** (1982) 470.
- 4) I. Kato, S. Wakana and S. Hara: *Jpn. J. Appl. Phys.* **22** (1983) 40.
- 5) K. Noguchi, K. Ebashi and I. Kato: *Proc. 3rd Symp. Plasma Processing* (1986) p. 155.
- 6) I. Kato, T. Ueda and T. Sakamoto: *Trans. IEE Jpn. A* **112** (1992) 355 [in Japanese].
- 7) K. Kato and I. Kato: *Proc. 9th Symp. Plasma Processing* (1992) p. 91.

POLARIZATION PROPERTIES OF a-Si:H/a-Si₃N₄
MULTILAYERS OPTICAL WAVEGUIDES

a-Si:H/Si₃N₄ 多層膜光導波路の偏光特性

Masahiko SAGISAKA and Isamu KATO

匂坂雅彦、加藤勇

School of Science and Engineering, Waseda University

3-4-1, Okubo, Shinjuku-ku, Tokyo, 169-0072

早稲田大学理工学部、〒169-0072 東京都新宿区大久保 3 - 4 - 1

Abstract

We fabricated a-Si:H/Si₃N₄ Multilayers films using the Double Tubed Coaxial Line Type MPCVD System. We processed the film to slab waveguides, and measured its propagation properties. As a result, these optical waveguides have polarization properties that TM mode was transmitted and TE mode was cut. Also, TE/TM extinction ratio was changed by irradiating light to the waveguides.

1. Introduction

In recent years, the development of optical communication devices is going on rapidly. But the research of new photonic materials and new thought devices using the materials is not advancing much. Our laboratory have studied new photonic materials using the Double Tubed Coaxial Line Type MPCVD System. One of them, we succeeded in fabricating the slab waveguides with ultra thin films multilayer structure by depositing good a-Si:H films and good Si₃N₄ films alternately. We think the optical waveguides with ultra thin films multilayer structure that much thinner than wavelength λ of propagation light have specific properties, but there are few experimental example. In this study, we researched the propagation properties of the optical waveguides. Also, we study the change of propagation properties of the optical waveguides by pumping. Therefore functionability can be given to the optical waveguides, and we can expect the application to optical modulators and optical switching devices.

2. Experimental

We fabricated the a-Si:H/Si₃N₄ multilayers films using the Double Tubed Coaxial Line Type MPCVD System⁽¹⁾. In the deposition chamber of this system, spatial after-grow plasma is formed by the gas flow and diffusions because the microwave power is not injected into the plasma in the chamber. The discharge gas, such as Ar and N₂, is fed to the outer discharge tube and the SiH₄ gas is fed to the inner tube.

The computer all controls inflow of discharge gas and SiH₄ gas. Because movable

parts, such as Short Circuit Termination and Metal Sleeve, are controlled by programs, we able to get best condition of plasma in each discharge.

First, Si_3N_4 film (about $2 \mu\text{m}$) was deposited on Si substrates as buffer layers. To the next, We deposited a-Si:H films and Si_3N_4 films alternately on the buffer layers. Tab.1 shows the condition of fabricating each film. To the next, we cut the multilayers films and fabricated the slab waveguides shown in Fig.1.

Tab.1 Condition of fabricating the films

	Discharge Gas Flow Rate	SiH_4 Gas Flow Rate	Substrate Temperature
Buffer Layers	N_2 140 [ml/min]	15 [ml/min]	R.T.
a-Si:H Layers	Ar 110 [ml/min]	5 [ml/min]	250°C
Si_3N_4 Layers	N_2 140 [ml/min]	5 [ml/min]	250°C

We measured the propagation properties of the fabricated slab waveguides using the system shown in Fig.2. We used a black light or a blue LED for pumping the waveguides.

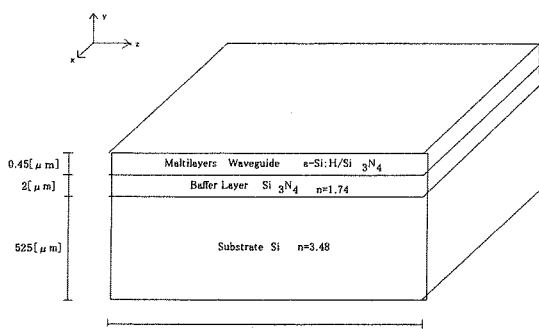


Fig.1 Multilayers Slab Waveguide

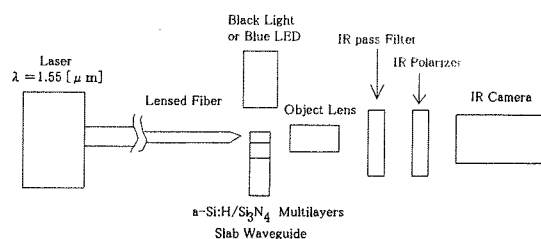


Fig.2 Experimental setup for measurement of the extinction ratio

3. Result and Discussion

Fig.3 shows that pictures of the light out from the end of slab waveguide. Fig(a) is the light of TM mode and Fig(b) is the light of TE mode. In pictures, the lines of lights are the lights that have propagated in the optical waveguides. And the things of ellipse are the lights that have propagated in the Si substrates. It is obvious that TM mode can pass and TE mode cannot pass. The lights that have propagated in the Si substrates is not polarized, so these lights can pass in both Fig(a) and (b). As we have seen, it is obvious that a-Si:H/ Si_3N_4 multilayers optical waveguides have the polarization properties that TE mode cut.

Fig.4 shows that the dependence of the extinction ratio on the thickness of a-Si:H layers, when the thickness of Si_3N_4 layers were stabilized with 20nm. The total film thickness are 450nm. It is obvious that as a-Si:H layer become thin, the extinction ratio

rise. It is conceivable as a reason that TM mode light is absorbed to a-Si:H layers more, when a-Si:H layers become thick. Therefore the extinction ratio become worse when a-Si:H layers become thick.

Also, Fig.4 shows the extinction ratio when the slab waveguides was pumped by the black light. It is obvious that the extinction ratio rise when the waveguides is pumped. Because a-Si:H layer in the waveguides become more metallic by pumping, TE mode become difficult to transmit. Also, by a-Si:H layers absorb pumping lights, the absorption of propagation lights decreases, therefore transmittance of TM mode increases.

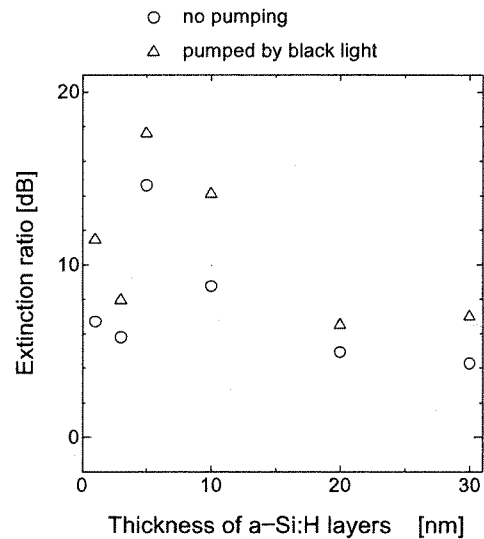


Fig.4 Dependence of the extinction ratio on the thickness of a-Si:H layers

To the next, we pumped the a-Si:H/Si₃N₄ slab waveguides by blue LED. Its thickness of a-Si:H layers were 5nm, Si₃N₄ layers were 50nm, total film thickness were 450nm. Fig.5 shows the dependence of the intensity of TM mode on the intensity of the pumping lights. Fig.6 shows the dependence of the intensity of TE mode on pumping lights. Fig.7 shows the dependence of the extinction ratio on the intensity of the pumping lights. In this experiments, the LED was 1800mcd, whose directivity angle was 15 degree.

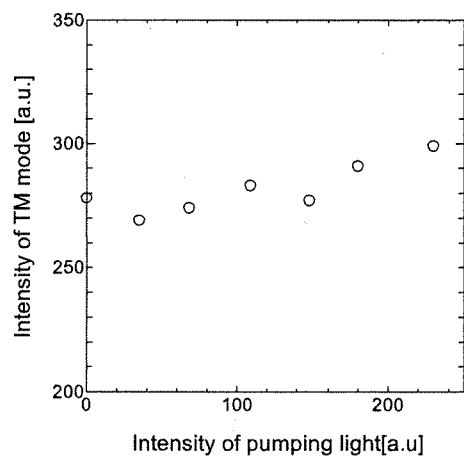


Fig.5 Dependence of the intensity of TM mode on the intensity of pumping light

By the Fig.5, it is obvious that the intensity of TM mode increase as the pumping light intensity increase. It is conceivable in the following reason. Because a-Si:H layer absorb the pumping lights, the absorption volume of TM mode of propagation lights decrease. So the intensity of TM mode increase.

By the Fig.6, it is obvious that the intensity of TE mode decreases, as the intensity of pumping lights more increases. Because a-Si:H layer in the waveguides become more metallic by pumping, TE mode become difficult to transmit.

By the Fig.7, it is obvious that the extinction ratio become better when the pumping lights increases. Such result was obtained by the change of TM mode and TE mode shown in Fig.5 and Fig.6.

4. Conclusion

a-Si:H/Si₃H₄ multilayers films have polarization properties, TE-mode-cut and TM-mode-pass. The extinction ratio rises by pumped by lights. When intensity of pumping lights increase, the extinction ratio rises.

Acknowledgement

This work was supported by the Grant-in-Aid for Scientific Research from the Ministry of Education, Science and Culture of Japan and the Waseda University Grant for Special Research Projects.

The author thanks Mr. Hoshihara, research student, for his experimental assistance, and Udaka Laboratory for permission to use their measurement systems.

References

- (1) Isamu Kato, Takashi Usui, Tadashi Sakamoto : Trans.IEE of Japan Vol.112-A No.5, 355-362, (1992)

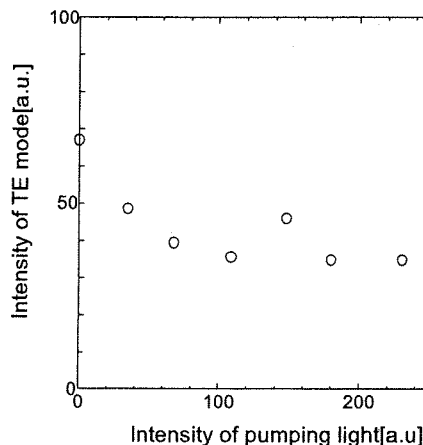


Fig.6 Dependence of the intensity of TE mode on the intensity of pumping light

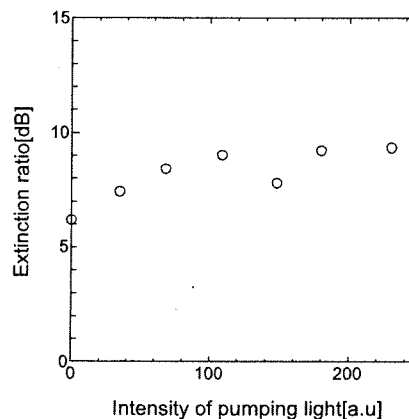


Fig.7 Dependence of the extinction ratio on the intensity of pumping light

QUALITY OF a-Si:H/Si₃N₄ MULTILAYER FILMS FABRICATED
BY DOUBLE TUBED COAXIAL LINE TYPE MPCVD SYSTEM

二重管式同軸線路形 MPCVD 装置を用いて作製した a-Si:H/Si₃N₄ 多層膜の膜質について

Takeshi KAMIGAICHI and Isamu KATO
上垣内岳司, 加藤勇

School of Science and Engineering, Waseda University
3-4-1, Okubo, Shinjyuku-ku, Tokyo, 169
早稲田大学理工学部、〒169 東京都新宿区大久保 3-4-1

Abstract

We were able to control the thickness of a membrane with nano-meter unit from X-ray diffraction peak of a-Si:H/Si₃N₄ multilayer film. We understood that the defect density in the multilayer film increases, as the thickness of a-Si:H layer decreases, from optical absorption coefficient of multilayer films that changes and produces the thickness of a-Si:H layer.

1. Introduction

We have used the double tubed coaxial line type microwave plasma CVD system⁽¹⁾ to make a-Si:H/Si₃N₄ multilayer film and to study about its quality. We have studied that optical band gap of multilayer film with thickness of Si₃N₄ layer fixed and thickness of a-Si:H layer varying increases as the thickness of a-Si:H layer is decreased. And when thickness of a-Si:H layer is fixed and thickness of Si₃N₄ layer is varied, its optical band gap is invariable in case of thickness of Si₃N₄ layer is under 10[nm], and increases in case of it is over 10[nm]. In this paper, we report that we measured the optical absorption coefficient, and examined about the quality of a-Si:H/Si₃N₄ multilayer films.

2. Experiment

Figure.1 shows the configuration of the MPCVD system. In the deposition chamber of this system, spatial after-grow plasma is formed by the gas flow and

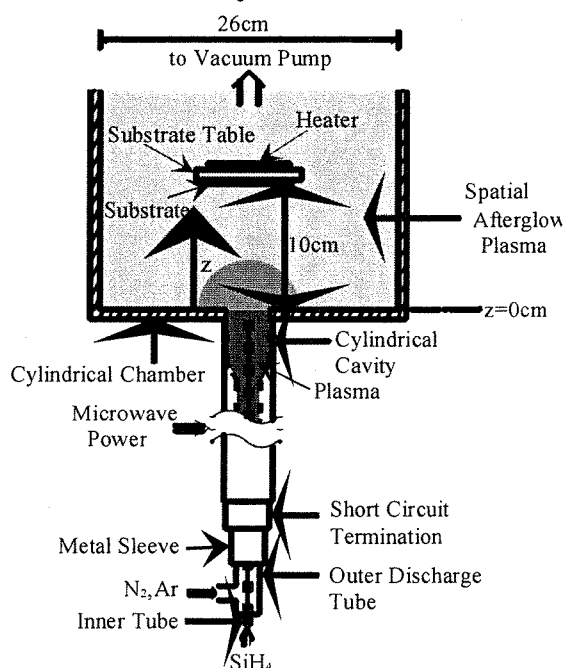


Fig1. MPCVD System

diffusions because the microwave power is not injected into the plasma in the chamber. The discharge gas, such as Ar and N₂, is fed to the outer discharge tube and the SiH₄ gas is fed to the inner tube.

The computer all controls inflow of discharge gas and SiH₄ gas. Because movable parts, such as Short Circuit Termination and Metal Sleeve, are controlled by programs, we able to get best condition of plasma in each discharge.

When making a-Si:H layer, SiH₄ gas flow rate is 5[ml/min] and Ar gas flow rate is 110[ml/min]. When making Si₃N₄ layer, SiH₄ gas flow rate is 5[ml/min] and Ar gas flow rate is 140[ml/min]. And substrate temperature is 250[C].

3. Result and Discussion

Figure 2 shows the X-ray diffraction peak of a-Si:H/Si₃N₄ multilayer film deposited on Si substrate. An X-ray wavelength scattering films is 1.94[Å]. The well-defined peak is shown in Fig 2. The thickness of 1 period layer of multilayer film calculated from this diffraction peak is 5.6[nm], and the other one calculated from the total thickness of multilayer film is 5.8[nm]. The close agreement between the two values is obtained.

The multilayer films with thickness of Si₃N₄ layer (5.5[nm]) fixed and a range of the thickness of a-Si:H layer varying from 0.9 to 9[nm] were fabricated, and the optical energy band gap and the optical-absorption coefficient of these multilayer films were measured.

Figure 3 shows the dependence of the optical energy band gap E_0 on the thickness of a-Si:H layer. As the thickness of a-Si:H layer is decreased, E_0 increases. This shows that the quantum level is made for quantum size effects in the a-Si:H layers and shows the making of quantum wells. The solid line in Fig 3 represents a curve-fitted by a theoretical formula. The close agreement between the theoretical curve and the experimental values is obtained, and this figure shows that the multilayer films of fine quality can be

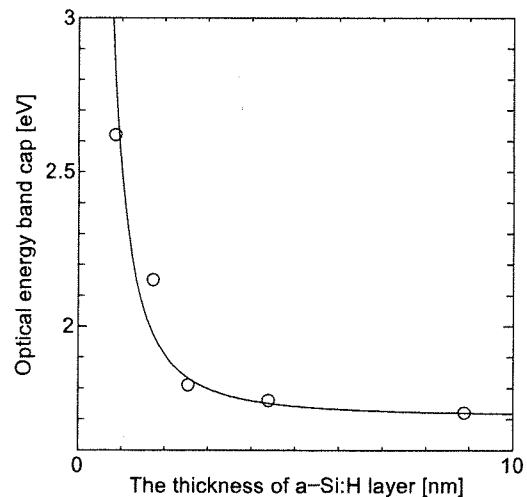


Fig.3. Dependence of optical energy band gap on the thickness of a-Si:H layer

fabricated. When this theoretical curve was estimated, 1.71[eV] was used for E_0 of the a-Si:H layers and the effective mass of the electron in these multilayer films was used 0.34 times as heavy as the one of free electron.

Figure 4 shows the dependence of the optical-absorption coefficient on the photon energy for multilayer films with the thickness of a-Si:H layers varied. As the photon energy is increased, the optical absorption coefficient increased. And then as the thickness of a-Si:H layers is decreased, the optical absorption coefficient decreased. However, as the thickness of a-Si:H layer is decreased, the proportion of the increase of the optical absorption coefficient associated with the increase of photon energy is decreasing. We suggested that the optical transport is prevented, because the defect density in a multilayer film increases with the thickness of a-Si:H layers increased.

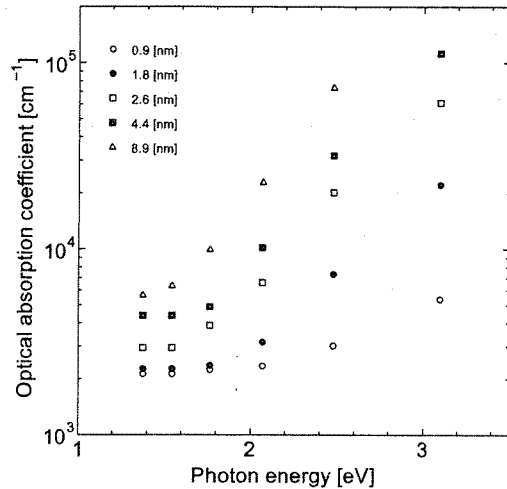


Fig.4 The dependence of optical absorption coefficient on photon energy with varying the thickness of a-Si:H layer

On the other hand, multilayer films with thickness of a-Si:H layer (3[nm]) fixed and a range of the thickness of Si_3N_4 layer varying from 3 to 30[nm] were fabricated, and the optical energy band gap and the optical-absorption coefficient of these multilayer films were measured.

Figure 5 shows the dependence of the optical energy band gap E_0 on the Si_3N_4 layer thickness. E_0 is constant with about 1.83 [eV] in case of the thickness of Si_3N_4 layer is under about 10 [nm], but as the thickness of Si_3N_4 layer is increased, E_0 increases in case of the thickness is over 10[nm]. While the optical transport between the quantum level in a-Si:H is dominant in case of the thickness of Si_3N_4 layers is under 10[nm], its transport exerts an influence largely to Si_3N_4 layers in case of the thickness is over 10[nm].

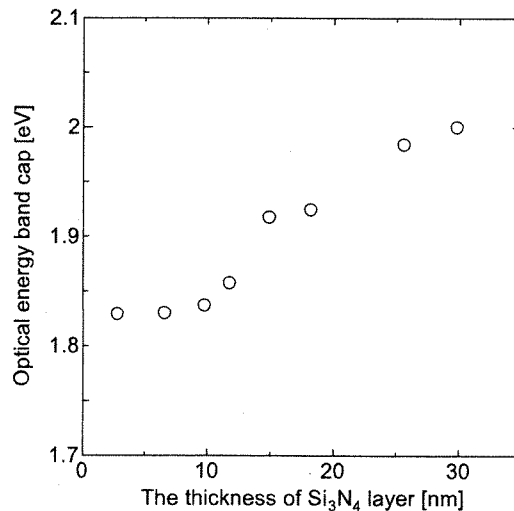


Fig.5. Dependence of the optical energy band gap on the thickness of Si_3N_4 layer

Figure 6 shows the dependence of the optical-absorption coefficient on the photon energy for multilayer films with thickness of Si_3N_4 layers varied. As the photon energy is increased, the optical absorption coefficient increased. And then as the thickness of

Si_3N_4 layers is increased, the optical absorption coefficient decreased. In this figure, there is almost no difference between the curves of the 2 thinnest Si_3N_4 layers, because a sub band by a tunnel effect is formed. However, other curves show the value of the optical absorption coefficient that relied on the thickness of Si_3N_4 layer, because the sub band is not formed.

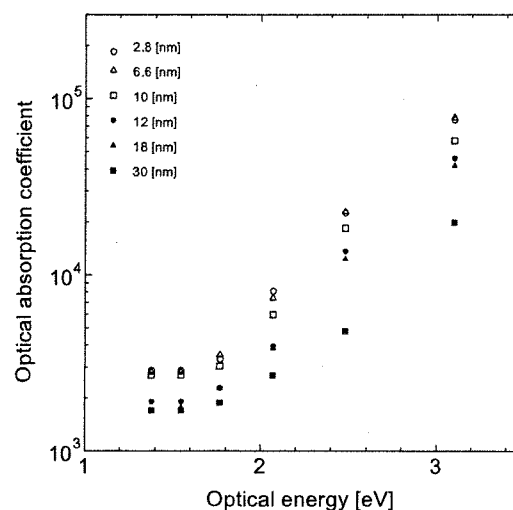


Fig.6 The dependence of optical absorption coefficient on photon energy with varying the thickness of Si_3N_4 layer

4. Conclusion

The thickness of the 1 period layer of a-Si:H/ Si_3N_4 multilayer film calculated from the total thickness of the multilayer film and the thickness calculated from a X-ray diffraction peak of the multilayer film agreed very well.

A theoretical curve and an experiment value of optical energy band gap of multilayer films with thickness of Si_3N_4 layer fixed and a range of the thickness of a-Si:H layer varying were agreeing well, and we able to fabricated the multilayer films of good quality.

That the defect density in the multilayer films increases, as the thickness of a-Si:H layer decreases from the optical absorption coefficient of the same multilayer films, understood.

We understood that optical transport exerts an influence to Si_3N_4 layer largely in case of the thickness is over 10[nm] from optical energy band gap and optical absorption coefficient of the multilayer films with thickness of a-Si:H layer fixed and a range of the thickness of Si_3N_4 layer varying.

5. Acknowledgment

This work was supported by the Grant-in-Aid for scientific research from the ministry of Education, Science, and Culture. This work was also supported by a Waseda University Grant for Special Research Projects in 1999. The authors thank Mr.Sugai, research student, for his experimental assistance.

6. References

(1)

DEPENDENCE OF PL CHARACTERISTICS OF a-Si:H NANOBALL FILMS
FABRICATED BY DOUBLE TUBED COAXIAL LINE TYPE MPCVD SYSTEM
ON ION BOMBARDMENT ENERGY

Yoshio KAWAHARA and Isamu KATO

河原吉男, 加藤勇

School of Science and Engineering, Waseda University,
3-4-1 Okubo, Shinjuku-ku, Tokyo 169-8555
早稲田大学理工学部, 〒169-8555 東京都新宿区大久保 3-4-1

Abstract

Using a double tubed coaxial line type microwave plasma CVD system, a-Si:H nanoball films which include Si nanocrystals can be fabricated. The photoluminescence (PL) is observed at the room temperature after the a-Si:H nanoball film is oxidized by heating in the atmosphere or the pure oxygen gas. We have fabricated a-Si:H nanoball films with varying the DC bias substrate voltage of this system and discussed the influence of the ion bombardment energy on the film properties and the PL characteristics. We have also analyzed the mechanism of the creation of Si nanocrystals and estimated theoretically the number of the Si nanocrystals.

Introduction

We have developed a double tubed coaxial line type microwave plasma CVD (MPCVD) system^{1,2}. Figure 1 shows the configuration of this MPCVD system. In this system the microwave power is confined in the cavity region, and in the deposition chamber a spatial afterglow plasma without injection of the microwave power is created by the gas flow and diffusions. The discharge gas (which creates the plasma, but doesn't create a depositional material by itself) is fed to the outer discharge tube and the material gas (which is dissociated in the plasma and creates a depositional material) is fed to the inner tube (as shown in Fig. 1). Both gases can be led separately to the deposition chamber. The discharge gas is ionized in the cavity region by the microwave power. The material gas is led to the discharge tube end through the inner tube, flows into the plasma and is dissociated by the collision with the plasma particles.

Using Ar gas as a discharge gas and SiH₄ gas as a material gas, a-Si:H films are fabricated. In the case of the low gas pressure in the deposition chamber by the high speed exhaust, a good a-Si:H film is created^{3,4}. This film is suitable for a solar battery and a thin film transistor. In the case of the high gas

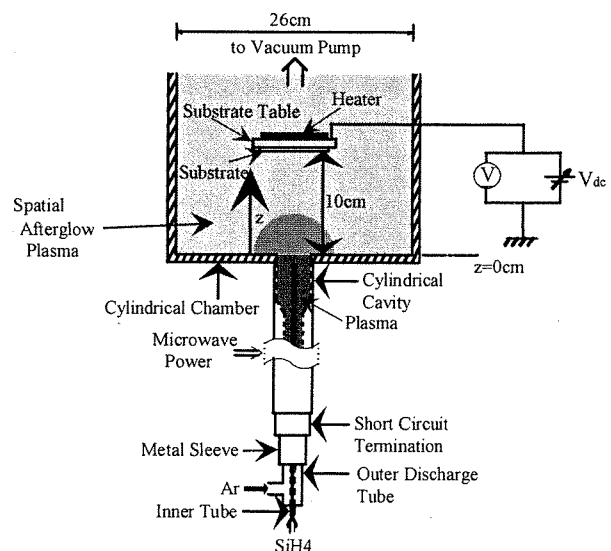


Fig.1 Configuration of the double tubed coaxial line type microwave plasma CVD system

pressure in the deposition chamber by the low speed exhaust, because the mean free path becomes short, SiH_x radicals are spatially recombined in the gaseous phase, and become a-Si:H nanoballs (~20 nm in diameter). The a-Si:H nanoballs deposit on the substrate, and an a-Si:H nanoball film is fabricated⁵. It is found by X-ray diffractometer that a-Si:H nanoballs include Si nanocrystals (several nm in diameter). The photoluminescence (PL) is observed at the room temperature after the a-Si:H nanoball film is oxidized by heating in the atmosphere or the pure oxygen gas.

In this study we have fabricated the a-Si:H nanoball films with varying the DC bias substrate voltage and discussed the influence of the ion bombardment energy on the film properties and the PL characteristics. We have analyzed the mechanism of the creation of Si nanocrystals and estimated theoretically the number of the Si nanocrystals from the results .

Experimental

The experimental conditions are as follows. The axial distance from the discharge tube end is defined as z (as shown in Fig. 1). The Ar gas flow rate is 110 ml/min and the SiH_4 gas flow rate is 30 ml/min. The microwave power is 150 W. The substrate table is set at $z = 10$ cm. The inner tube end is at $z = -1.4$ cm. The gas pressure in the deposition chamber is set at 250 mTorr by controlling the exhaust valve. The substrate temperature is R.T.. The discharge time is 10 min. In this study The DC substrate bias voltage is varied from -80 V to $+40$ V.

As deposited, the FTIR absorption is measured in order to calculate the hydrogen concentration of the film, the X-ray diffractometer in order to calculate the diameter of Si nanocrystals included in the film by the Scherrer's formula, and the SEM image in order to observe the film surface and the cross section.

The other films are oxidized in the atmosphere at 220 °C for 60 hours. After oxidation the PL spectrum is measured. The excitation light is Ar^+ laser (514.5 nm). The measurement is done at the room temperature in a vacuum ($\sim 2 \times 10^{-5}$ Torr) in order to avoid the thermal oxidation by the laser irradiation energy.

Results and discussions

We measured the sheath voltage (V_{sh}) at $z = 9$ cm in the pure Ar^+ plasma by the single probe method when the substrate is set at $z = 10$ cm. Figure 2 shows the dependence of the V_{sh} on the V_{dc} . It is found that the V_{sh} was varied from -110 V to -20 V with varying V_{dc} from -80 V to $+40$ V. Therefore, the ion bombardment energy is varied from -110 eV to -20 eV because the Ar^+ ion hardly collides with any other plasma particles in the sheath.

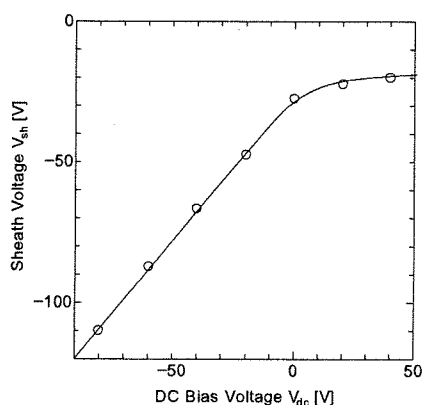


Fig. 2 Dependence of the V_{sh} on the V_{dc}

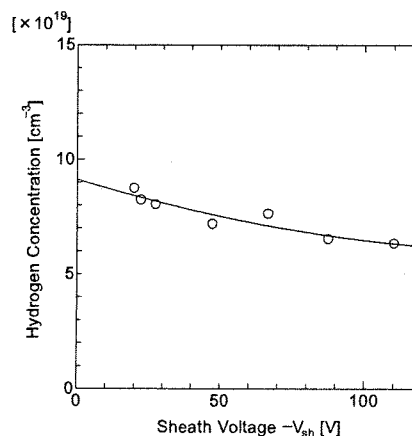


Fig. 3 Dependence of the C_H on the V_{sh}

In order to survey the influence of the variation of the ion bombardment energy on the construction of the film, we calculated the hydrogen concentration (C_H) from the FTIR spectra. Figure 3 shows the dependence of the C_H on the V_{sh} . It is found that, as the V_{sh} increases in a negative direction, i.e. the ion bombardment energy increases, the C_H decreases. This result is considered to be due to as follows. As the V_{sh} increases, the Ar^+ ions are more accelerated by the sheath voltage and the Ar^+ ions with larger energy are struck into the film.

Figure 4 shows the dependence of the deposition rate of the film on the V_{sh} . It is found that, as the V_{sh} increases in a negative direction, the deposition rate decreases. This result is considered to be due to as follows. As the V_{sh} increases, the mobility of the a-Si:H nanoballs attached to the substrate is raised by the film surface heating effect of the ion bombardment⁷, therefore, the a-Si:H nanoballs deposit densely on the substrate.

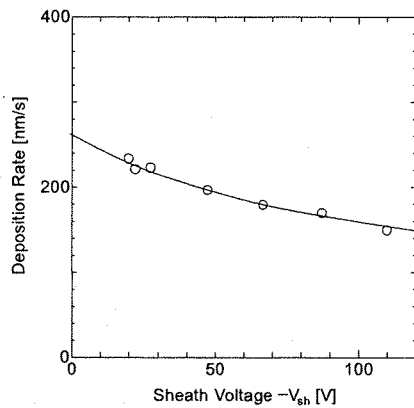


Fig. 4 Dependence of the deposition rate of the film on the V_{sh}

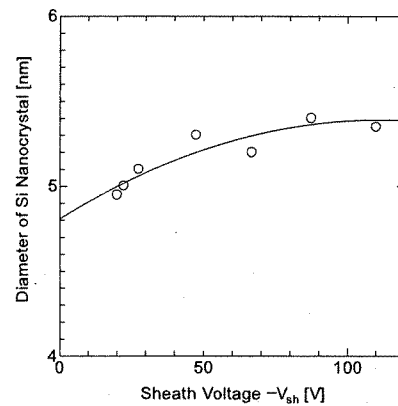


Fig. 5 Dependence of the diameter of the Si nanocrystal on the V_{sh}

Figure 5 shows the dependence of the diameter of the Si nanocrystal on the V_{sh} . It is found that, as the V_{sh} increases in a negative direction, the diameter of the Si nanocrystal increases. This result is considered to be due to as follows. As the ion bombardment energy increases, the diameter increases because the Si nanocrystal is created by the ion bombardment (as mentioned later).

Figure 6 shows the dependence of the PL intensity on the V_{sh} . It is found that, as the V_{sh} increases in a negative direction, the PL intensity increases. From this result it is considered that the number of the Si nanocrystals in the a-Si:H nanoball film increases, because the PL

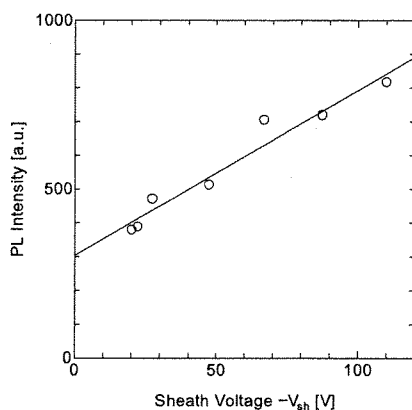


Fig. 6 Dependence of the PL intensity on the V_{sh}

intensity is supposed to be in proportion to the number of Si nanocrystals in the film. This result is explained by the analysis of the mechanism of the creation of Si nanocrystals as follows. The Ar^+ ions are struck into the a-Si:H nanoball deposited on the substrate and provide their energy to the a-Si:H nanoball. Moreover the a-Si:H nanoball itself has the thermal energy when created in the gaseous phase. Then the energies is used to disconnect some hydrogen atom connected to the a-Si:H, and, moreover, to crystallize the a-Si. Therefore, the Si nanocrystal is created in the a-Si:H nanoball film by the Ar^+ ion bombardment.

In order to confirm this analysis, we estimated the number of Si nanocrystals existing per unit area of the a-Si:H nanoball film i.e. the concentration of Si nanocrystals per unit area ($n(V_{sh})$) from the measured results mentioned above. $n(V_{sh})$ is expressed as follows.

Acknowledgement

This work was supported by the Grant-in-Aid for scientific research from the Ministry of Education, Science and Culture. The authors thank Mr. Matsumoto, research student, for his experimental assistance.

Reference

1. I. Kato, S. Wakana, S. Hara and H. Kezuka, Japanese Journal of Applied Physics, 21 (1982) L470
2. I. Kato, S. Wakana, S. Hara, Japanese Journal of Applied Physics, 22 (1983) L40
3. I. Kato, T. Ueda, K. Hatanaka, Electronics & Communications in Japan Part 2, 70 (1987) No. 11, 73
4. K. Kato and I. Kato, Japanese Journal of Applied Physics, 30 (1983) 1245
5. I. Kato and Y. Kawahara, Proc. 51st International Conference on Reactive Plasmas and 16th Symposium on Plasma Processing (1998) 109
6. O. P. Agnihotri, R. Tyagi and I. Kato, Japanese Journal of Applied Physics, 36 (1997) 6711
7. M. Yamashita, H. Ogihara and I. Kato, Proc. 13th Symposium on Plasma Processing (1996) 109
8. L. Pauling, The Chemical Bond (Cornell Univ. 1967) 65
9. E. P. Donovan, F. Spaepen, D. Turnbull, J. M. Poate and D. C. Jacobson, Applied Physics Letters, 42 (1983) 698

FABRICATION OF POLYMER-LIKE a-C:H FILMS BY DOUBLE TUBED
COAXIAL LINE TYPE MPCVD SYSTEM

二重管式同軸線路形 MPCVD 装置を用いたポリマー状 a-C:H 膜の作製

Takashi Otsuka and Isamu Kato

大塚 崇、加藤 勇

School of Science and Engineering, Waseda University

3-4-1, Okubo, Shinjuku-ku, Tokyo, 169-8555

早稲田大学理工学部、〒169-8555 東京都新宿区大久保 3-4-1

Abstract

We have fabricated a-C:H films using the double tubed coaxial line type MPCVD system. H₂ gas was used as the discharge gas and CH₄ gas was used as the material gas. In this study, in order to deposit the polymer-like a-C:H films, the gas pressure in the deposition chamber is made high by exhausting using only the rotary pump. (between 180 mTorr and 500 mTorr). Also the substrate temperature is R.T. . Under this condition we are able to deposit transparent and soft polymer-like a-C:H films. We discuss the influence that the H₂ gas flow rate gives to the pure H₂ plasma parameter, the deposition rate, the hardness, and the optical energy band gap.

1.Introduction

Figure 1 shows the double tubed coaxial line type microwave plasma CVD (MPCVD) system. The discharge gas is fed to the fused quartz outer discharge tube and the material gas is fed to the stainless steel inner tube. H₂ gas was used as the discharge gas and CH₄ gas was used as the material gas. H₂ gas is ionized in the discharge region by the microwave power. The inner tube leads CH₄ gas to the discharge tube end, and CH₄ gas is dissociated by the collision with the H₂ plasma particles.

An iris is put on the end of the outer discharge tube (figure 2). This is in order to make the gas pressure high in the discharge tube. In this way, we could create high density H₂ plasma and deposit the a-C:H films fast at the low pressure.[1]. Furthermore, the coil is set up around the cavity of the system in order to create the stable and high density plasma. And the magnetic field along the gas flow is applied to the discharge area to suppress the diffusion to the discharge tube wall. Using this system, we fabricate the polymer-like a-C:H films at the high pressure.

2.Experiment

The axial distance from the end of the discharge tube is defined as z. At z=2 cm in the deposition chamber, the plasma parameters of pure H₂ plasma are measured, where the H₂ gas flow rate is varied from 110 to 400 ml/min and the magnetic flux density at the center of the

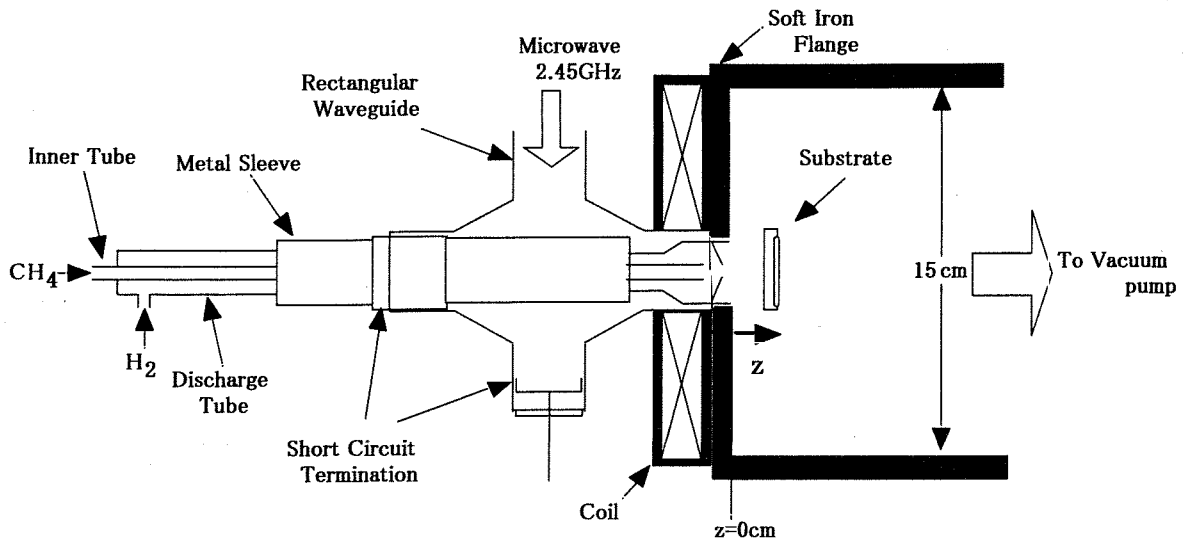


Fig.1 The double tubed coaxial line type MPCVD system

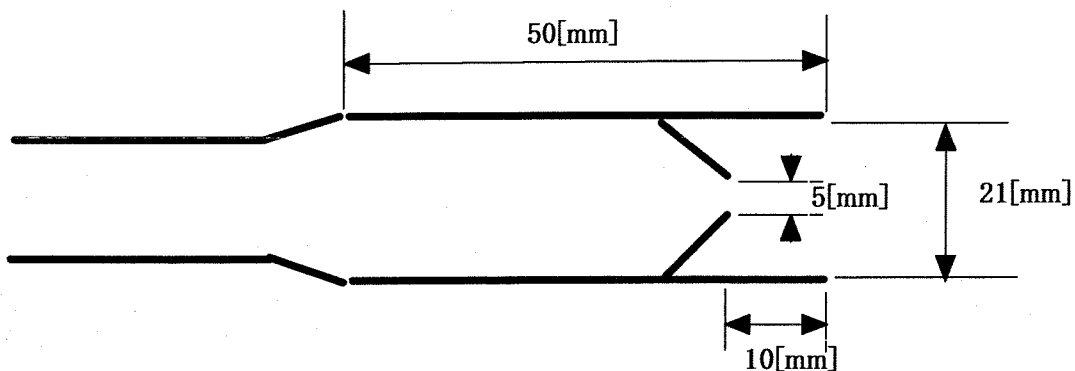


Fig.2 The outer discharge tube

coil is varied from 0 to 2000 Gauss. The microwave power is 220 W. A probe of 0.05 cm diameter and 1.0 cm length is used.

The polymer-like a-C:H film is fabricated on the substrate table at $z=2$ cm, where the magnetic flux density is 1500 Gauss, the H_2 gas flow rate is 110 to 400 ml/min, and the CH_4 gas flow rate is 20 ml/min. The substrate temperature is R.T., and the DC substrate bias voltage is 0V.

3.Result and Discussion

Fig 3 shows the dependence of the gas pressure on z in H_2 gas flow rate=400 ml/min. The gas pressure in the discharge tube is high when we used the outer

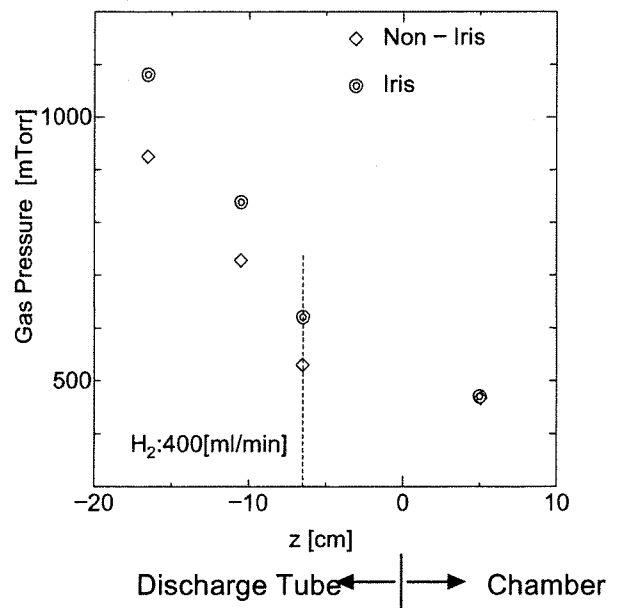


Fig.3 Dependence of Gas Pressure on z

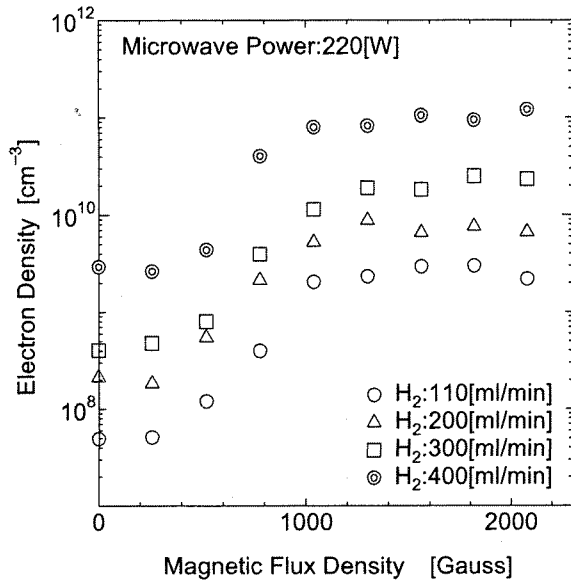


Fig.4 Dependence of Electron Density on Magnetic Flux Density

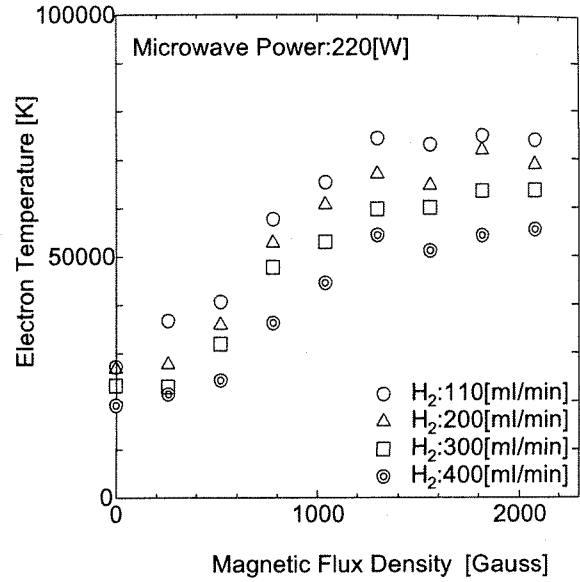


Fig.5 Dependence of Electron Temperature on Magnetic Flux Density

discharge tube with the iris. But the gas pressure at $z=5$ cm in the deposition chamber is same. The plot at $z=-7$ cm is the gas pressure in the discharge region. We can create the stable and high density plasma, because the gas pressure in the discharge region is high.

Fig 4 shows the dependence of the electron density on the magnetic flux density at $z=2$ cm. The electron density increases with increasing the magnetic flux density. And the electron density is saturated when the magnetic flux density is more than 1300 Gauss. The electron density is increased because it is suppressed by applying the magnetic field that the electron diffuses to the discharge tube wall. So we fabricate a-C:H films under the condition of magnetic flux density =1500 Gauss.

Fig 5 shows the dependence of the electron temperature on the magnetic flux density at $z=2$ cm. The electron temperature increases with increasing the magnetic flux density. The electron that has high energy is easy to diffuse to the discharge tube wall without the magnetic field. With applying the magnetic field, it decreases that such an electron disappearing by the surface reconnection on the discharge tube wall. As a result, the electron temperature increases because the ratio of such an electron is increased.

Fig 6 shows the dependence of the deposition rate on the H_2 gas flow rate. The deposition rate decreases with increasing the H_2 gas flow rate. This is because the electron temperature decreases with increasing the H_2

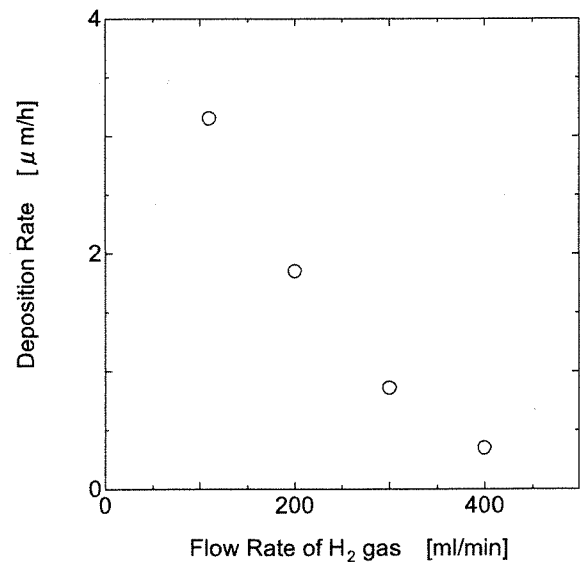


fig.6 Dependence of Deposition Rate on Flow Rate of H_2 gas

gas flow rate.

Figure 7 shows the dependence of the hardness of a-C:H films on the H₂ gas flow rate. The hardness was measured by micro vickers hardness tester. The hardness of diamond-like carbon film is known to be about 1000~4000 kg/mm². The a-C:H films fabricated by this system are softer than it.

Figure 8 shows the dependence of the optical energy band gap on the H₂ gas flow rate. The optical energy band gap doesn't depend on the H₂ gas flow rate. It is about 2.8 eV. The optical energy band gap of a-C:H films deposited at the low pressure (4mTorr) were about 2.2 eV. We could deposit the transparent polymer-like a-C:H films at the high pressure. The color was light yellow.

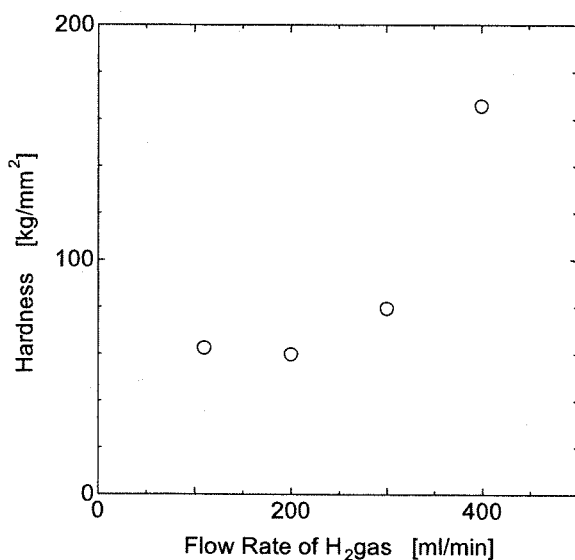


Fig.7 Dependence of Hardness on Flow Rate of H₂ gas

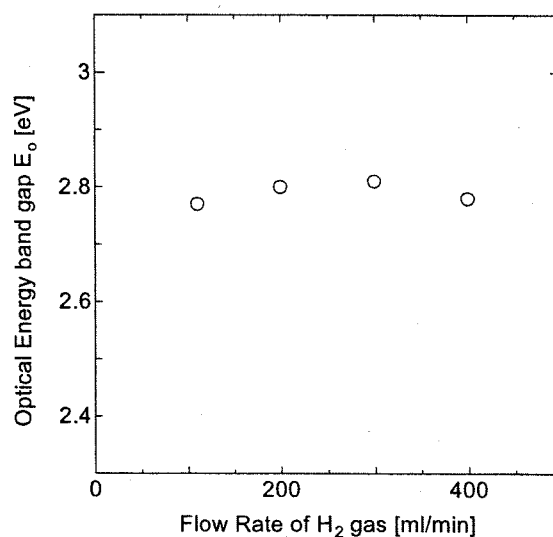


Fig.8 Dependence of Optical Energy band gap (E₀) on Flow Rate of H₂ gas

4. Conclusion

The gas pressure of the discharge region in the discharge tube is able to be high by using the outer discharge tube with the iris. As a result, we can create the stable and high density H₂ plasma when the magnetic flux density is more than 1300 Gauss.

At the high pressure and room temperature, the transparent and soft polymer-like a-C:H films are fabricated. The optical energy band gap is about 2.8 eV.

Acknowledgement

This research was supported by the Grant-in-Aid for Scientific Research from the Ministry of Education, Science and Culture of Japan. The authors thank Mr. Noda, research student, for their experimental assistance.

Reference

- [1] T. Otsuka et al : The 46th Spring Meeting of Jpn. Soc. Appl. phys. ,30p-D-1 (1999)

Fabrication of a-Si:H Film using H₂/SiH₄ Plasma by Longitudinal Magnetic Field Applied MPCVD System (II)

縦磁界印加MPCVDによる H₂/SiH₄ プラズマを用いた a-Si:H 膜の作製 (II)

Yuuki Nakano、Isamu Katou
中野 有喜、加藤 勇

School of Science and Engineering, Waseda University,
3-4-1 Okubo, Shinjuku-ku Tokyo 169

早稲田大学理工学部、〒169-0072 東京都新宿区大久保3-4-1

Abstract

We have fabricated a-Si:H films using double tubed coaxial line type microwave plasma CVD system. We fabricated a-Si:H films using Ar plasma, but there were some problems, one of which was that Ar atoms were implanted as the impurities. To solve these problems, we have used H₂ plasma to fabricate them. This time we use the sheath voltage (V_{sh}) on the film surface as the parameters, fabricate a-Si:H films varying substrate temperature (T_s). The sheath voltage is obtained by subtracting the plasma space potential from DC substrate bias voltage (V_{dc}).

1. Introduction

We have studied the influence that each parameter, which are magnetic flux density, SiH₄ flow rate, H₂ flow rate, substrate temperature and sheath voltage, exert on a-Si:H film quality using H₂ plasma. ^{[1] [2] [3] [4] [5]} We learned that the dangling bond density can be minimized at $V_{sh}=-30[V]$ ($V_{dc}=0V$), $T_s = 150^{\circ}C$, and can be made smaller by putting V_{sh} closer to 0V from minus region^{[4][5]}.

In this paper, we fabricated a-Si:H film varying substrate temperature and use V_{sh} as a parameter, study the influence of T_s on its quality. Also we compare the quality of it with that of one which was fabricated using Ar plasma in a same condition.

2. Experiment

Fig.1 shows the configuration of longitudinal magnetic field applied double tubed coaxial line type MPCVD system. In this system the microwave power is confined in the cavity. The H₂ gas is fed to the outer discharge tube and the SiH₄ gas is fed to the inner tube. The H₂ gas is ionized in the cavity region by the microwave power. The SiH₄ gas flows to the discharge tube end through the inner tube, then the SiH₄ is dissociated by the collision with the H₂ plasma particles.

The coil is set up around the cavity of the system, so we can create stable and dense H₂ plasma. This is because the magnetic field along the gas flow (longitudinal magnetic field) is applied to the discharge area to suppress the diffusion to the discharge tube wall. The axial distance from the discharge tube end is defined as z .

The substrate table area is 40 cm^2 and the table is placed at $z=10 \text{ cm}$. The magnetic flux density is 1750 Gauss. H_2 gas flow rate is 400 ml/min and SiH_4 gas flow rate is 30 ml/min. The DC substrate bias voltage is +40V, 0V and -20V. Then each V_{sh} is 0V, -17V and -37V. [5] The substrate temperature is varied from R.T. to 300°C .

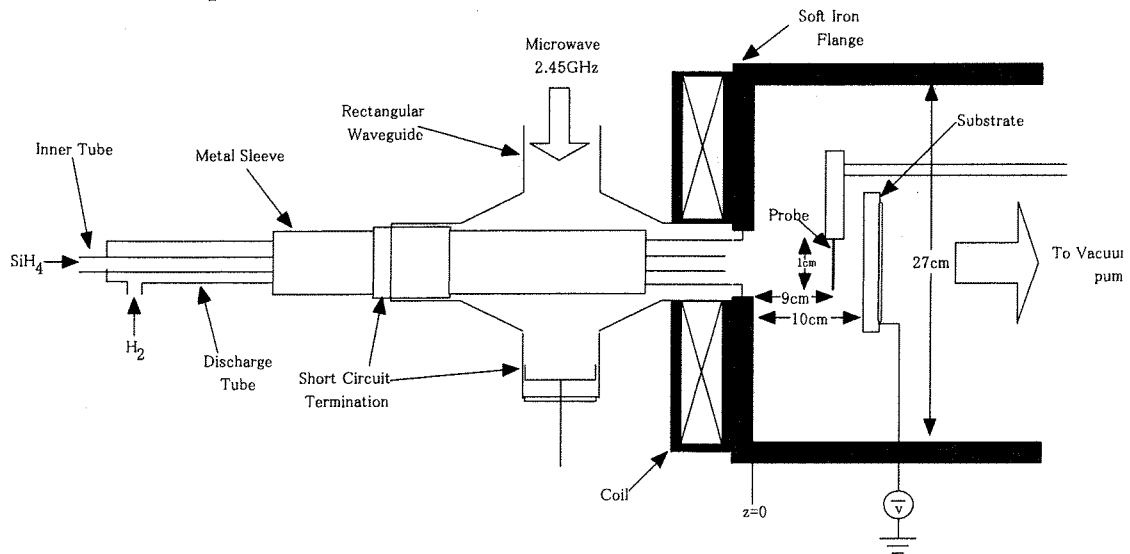


図 2. 1. 1 縦磁界印加二重管式同軸線路形MPCVD装置

3.Result and Discussion

We have studied influences of the ion bombardment on a-Si:H films and clarified that an ion bombardment has a film surface heating effect (ions excite vibration of lattice of atom surface) and ion implanting effect (ions accelerated by V_{sh} implant into the substrate) on the film. First of all, in the case of using H_2 gas as the discharge gas, we assume that the latter is neglected, and we consider only the former. But in the case of using Ar gas as the discharge gas, we should consider both effects. So the film surface heating effect and the ion implanting effect of the ion bombardment should be separately studied and discussed. [6] When we study the film quality in the case of using Ar plasma, we shift T_s by the heat which the substrate is given through the film surface heating effect. For example, T_s is shifted 40°C when V_{sh} is -17V, 87°C when V_{sh} is -37V and 136°C when V_{sh} is -58V. So in this paper, T_s is shifted in the case of using Ar plasma.

Fig.2 shows the dependence of the deposition rate on the substrate temperature with V_{sh} as the parameter. In the cases of both using Ar plasma and using H_2 plasma, the deposition rate decreases for all parameters when T_s is increased. This is because the film

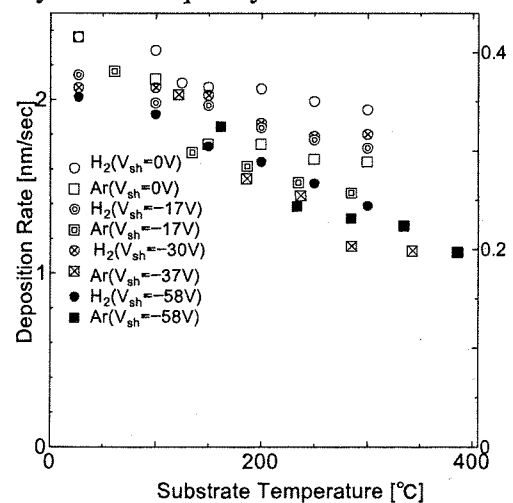


図1 シース電圧をパラメータとした堆積速度の基板温度依存性

density increases as the substrate is heated.

Fig.3 shows the dependence of the concentration of SiH bond on the substrate temperature with V_{sh} as the parameter. In the case of using H_2 plasma, the concentration of SiH bond increases until T_s gets to $100^\circ C$ because the hydrogen constituting the SiH_2 bond is disconnected. But after that it decreases because amount of the hydrogen disconnected from SiH_2 is larger than that of the hydrogen disconnected from SiH. In both cases of using H_2 plasma and using Ar plasma, the concentration of SiH bond increases because of ion implanting effect.

Fig.4 shows the dependence of the concentration of SiH_2 bond on the substrate temperature with V_{sh} as the parameter. In the cases of both using Ar plasma and using H_2 plasma, the concentration of SiH_2 bond decreases for all parameters as T_s becomes higher. This is because the hydrogen constituting the SiH_2 bond is disconnected when the substrate temperature is increased. In both cases of using H_2 plasma and using Ar plasma, the concentration of SiH bond increases because of ion implanting effect.

Fig.5 shows the dependence of the ratio of the concentration of SiH bond to the concentration of SiH_2 bond on the substrate temperature with V_{sh} as the parameter. In the case of using H_2 plasma, it increases until T_s gets to about $200^\circ C$, and after that it decreases gradually. It is considered that this is because the concentration of SiH_2 bond decreases steeply at around $200^\circ C$, but the concentration of SiH bond does not so.

Fig.6 shows the dependence of the dangling bond density on the substrate temperature with V_{sh} as the parameter. In the case of using H_2 plasma, it remains minimum at $T_s=150^\circ C$ for all parameters. And it increases when V_{sh} is

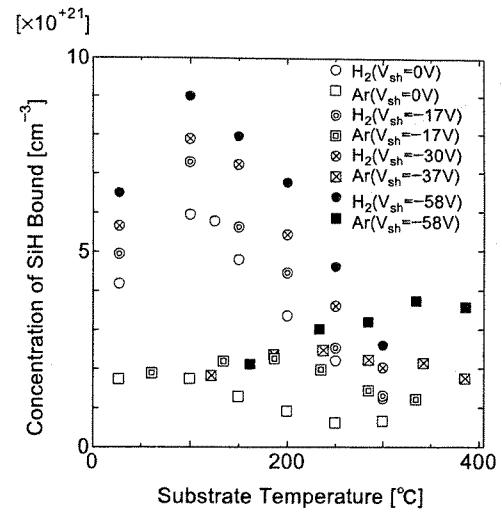


図2 シース電圧をパラメータとした SiH結合量の基板温度依存性

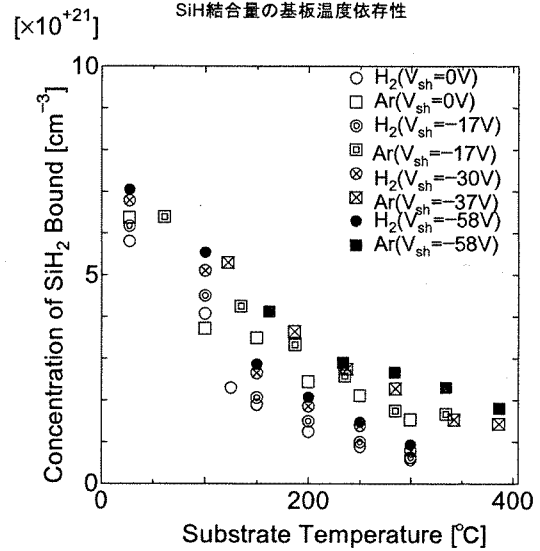


図3 シース電圧をパラメータとした SiH_2 結合量の基板温度依存性

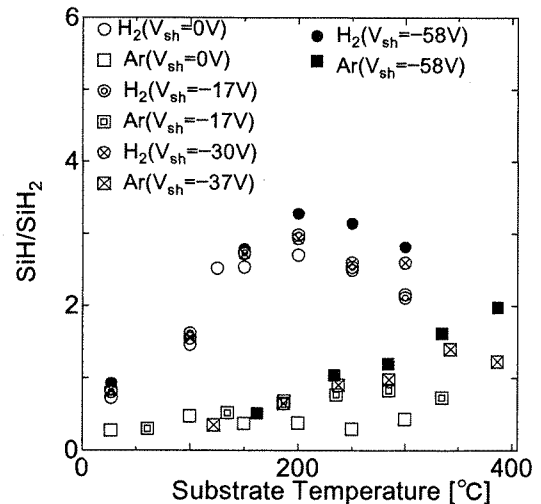


図4 シース電圧をパラメータとした SiH_2 結合量に対するSiH結合量の基板温度依存性

increased. It is considered that this is because hydrogen ions accelerated by V_{sh} cut off Si-Si bond and Si-H bond.

Fig.7 shows the dependence of the optic energy band gap on the substrate temperature with V_{sh} as the parameter. In the cases of both using Ar plasma and using H_2 plasma, the optic energy band gap decreases for all parameters when T_s is increased.

4. Conclusion

We fabricated a-Si:H film using double tubed coaxial line type microwave plasma CVD system. In the case of using H_2 gas as the discharge gas, the deposition rate decreases when T_s is increased, and decreases when V_{sh} is increased. The concentration of SiH bond takes a maximum value at $T_s=150$, and it increases when V_{sh} is increased. The concentration of SiH_2 bond decreases when T_s is increased. The dangling bond density can be minimized at $T_s=150^\circ C, V_{sh}=0V$. The optic energy band gap decreases for all parameters when T_s is increased.

5. Acknowledgment

This work was supported by the Grant-in-Aid for scientific research from the ministry of Education, Science, and Culture. And this work was also supported by Waseda University Grant for Special Research Projects. The authors thank Mr. Yamaguchi, research student, for his experimental assistance.

References

- [1]H.Iizuka et al: The 15th Sympo. Plasma Processing ,406(1998)
- [2]M.Usuda et al: The 46th Spring Meeting of Jpn.Soc.Sppl.phys. ,30p-H-13(1998)
- [3]M.Usuda et al: The 46th Autumn Meeting of Jpn.Soc.Sppl.phys. ,15a-Q-3(1998)
- [4]M.Usuda et al: The 46th Spring Meeting of Jpn.Soc.Sppl.phys. ,31p-YB-3(1999)
- [5]Y.Nakano et al: The 46th Spring Meeting of Jpn.Soc.Sppl.phys. ,31p-YB-5(1999)
- [6]H.Ogiwara et al: The 15th Sympo. Plasma Processing ,84(1998)

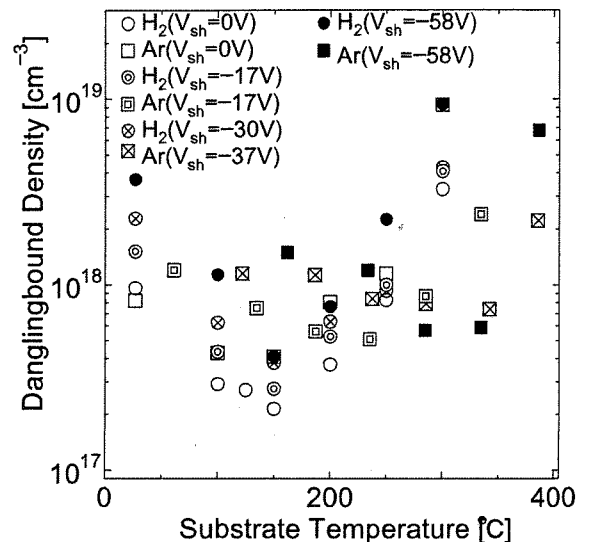


図6 シース電圧をパラメータとした
ダングリングバンド密度の基板温度依存性

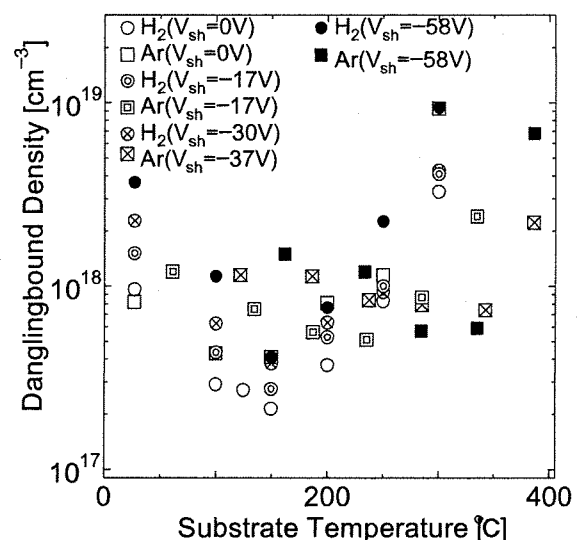


図6 シース電圧をパラメータとした
ダングリングバンド密度の基板温度依存性

Photoluminescence from a:Si-H Nanoball Films Fabricated by Double Tubed Coaxial Line Type Microwave Plasma CVD System

Isamu Kato^{1,2}, Yoshio Kawahara¹ and O.R. Agnihotri³

¹Department of Electronics,
Information and Communication Engineering,
Waseda University,
Tokyo 169-8555,
Japan

²Materials Research Laboratory for Bioscience and Photonics,
Waseda University, Tokyo 169-8555,
Japan

³Semiconductor Engineering Laboratory,
Department of Physics,
Indian Institute of Technology,
New Delhi-110 016

Using a double tubed coaxial line type microwave plasma CVD system, a-Si:H nanoball films which include Si nanocrystals can be fabricated. The photoluminescence (PL) is observed at the room temperature after the a-Si:H nanoball film is oxidized by heating in the atmosphere or the pure oxygen gas. We have fabricated a-Si:H nanoball films with varying the parameters of fabrication conditions and oxidation conditions, and discussed the film properties and the PL characteristics of a-Si:H nanoball films. We have also discussed the influence of the ion bombardment energy and analyzed the mechanism of the creation of Si nanocrystals and estimated theoretically the number of the Si nanocrystals.

INTRODUCTION

We have developed a double tubed coaxial line type microwave plasma CVD (MPCVD) system^{1,2}. Figure 1 shows the configuration of this MPCVD system. In this system the microwave power is confined in the cavity region, and in the deposition chamber a spatial afterglow plasma without injection of the microwave power is created by the gas flow and diffusions. The discharge gas (which creates the plasma, but doesn't create a depositional material by itself) is fed to the outer discharge tube and the material gas (which is dissociated in the plasma and creates a depositional material) is fed to the inner tube (as shown in Fig. 1). Both gases can be led separately to the deposition chamber. The discharge gas is ionized in the cavity region by the microwave power. The material gas is led to the discharge tube end through the inner tube, flows into the plasma and is dissociated by the collision with the plasma particles.

Using Ar gas as a discharge gas and SiH₄ gas as a material gas, a-Si:H films are fabricated. In the case of the low gas pressure in the deposition chamber by the high speed exhaust, a good a-Si:H film is created^{3,4}. This film is suitable for a solar battery and a thin film transistor. In the case of the high gas pressure in the deposition chamber by the low speed exhaust, because the mean free path becomes short, SiH_x radicals are spatially recombined in the gaseous phase, and become a-Si:H nanoballs (~20 nm in diameter). The a-Si:H nanoballs deposit on the substrate, and an a-Si:H nanoball film is

fabricated⁵. It is found by X-ray diffractometer that a-Si:H nanoballs include Si nanocrystals (several nm in diameter). The photoluminescence (PL) is observed at the room temperature after the a-Si:H nanoball film is oxidized by heating in the atmosphere or the pure oxygen gas. This Si luminescent material is suitable for optoelectronic monolithic integrated circuits by combination with the SiON waveguides about which we published elsewhere⁶.

In this study we have fabricated the a-Si:H nanoball films with varying the parameters of fabrication conditions and discussed the film properties and the PL characteristics of a-Si:H nanoball films. We peculiarly have discussed the influence of the ion bombardment energy on the film properties and the PL characteristics. We have analyzed the mechanism of the creation of Si nanocrystals and estimated theoretically the number of the Si nanocrystals from the results .

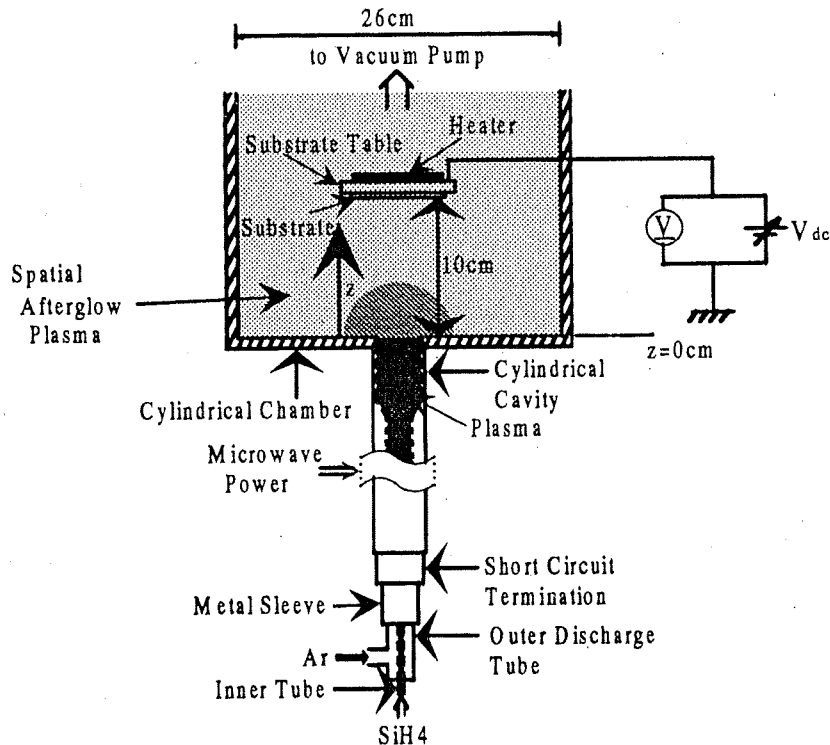


Fig. 1. Configuration of the double tubed coaxial line type microwave plasma CVD system

EXPERIMENTAL

The basic experimental conditions are as follows. The axial distance from the discharge tube end is defined as z (as shown in Fig. 1). The Ar gas flow rate is 110 ml/min and the SiH_4 gas flow rate is 30 ml/min. The microwave power is 150 W. The substrate table is set at $z = 10$ cm. The inner tube end is at $z = -1.4$ cm. The gas pressure in the deposition chamber is set at 250 mTorr by controlling the exhaust valve. The DC bias substrate voltage is 0 V. The substrate temperature is R.T.. The discharge time is 10 min.

The parameters of the fabrication conditions are varied as follows. The Ar gas flow rate is varied from 90 ml/min to 130 ml/min. The SiH_4 gas flow rate is varied from 10 ml/min to 50 ml/min. The microwave power is varied from 110 W to 190 W. The substrate position is varied from $z = +2.5$ cm to 17.5 cm. The substrate temperature is varied from R.T. to 400 °C. The discharge time is varied from 1 s to 1800 s. The DC substrate bias voltage is varied from -80 V to +40 V.

As deposited, the FTIR absorption is measured in order to calculate the hydrogen concentration of the film, the X-ray diffractometer in order to calculate the diameter of Si nanocrystals included in the film by the Scherrer's formula, and the SEM image in order to observe the film surface and the cross section.

The other films are oxidized in the atmosphere at 220 °C for 60 hours or in the pure oxygen gas at

200 °C for 2 hours. The oxidation temperature and time are varied in order to clarify their influence on the PL characteristics. After oxidation the PL spectrum is measured. The excitation light is Ar⁺ laser (514.5 nm). The measurement is done at the room temperature in a vacuum ($\sim 2 \times 10^{-5}$ Torr) in order to avoid the thermal oxidation by the laser irradiation energy.

RESULTS AND DISCUSSIONS

The dependence on the oxidation time and temperature

Figure 2 shows the PL spectra from the a-Si:H nanoball film which is oxidized at 200 °C in the pure oxygen gas. In the figure the parameter indicates the oxidation time. The PL spectra have a peak at about 780 nm. The PL cannot be observed from the films before oxidation, but after oxidation the PL is observed at the room temperature and its intensity increases as the oxidation time gets longer.

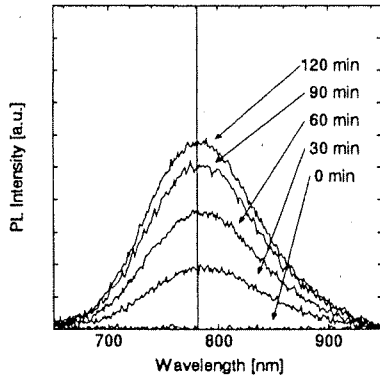


Fig. 2 PL spectra from the a-Si:H nanoball film the other hand, in the case of the pure oxygen gas (b), the PL intensity of each temperature saturates sooner than those in the case of the atmosphere.

From the above result it is considered that the a-Si:H is oxidized and becomes SiO₂, so that the Si nanocrystals are buried in the SiO₂.

In order to see the dependence of the oxidation temperature on the PL characteristics, we also measured the PL intensity from the films oxidized at the different temperatures (i.e. 80, 150, 220 °C in the atmosphere and 200, 300, 400, 500 °C in the pure oxygen gas). Figure 3 show the dependence of the PL intensity on the oxidation time. In the figures the parameters indicate the oxidation temperature. It is found that, in the case of the atmosphere (a), as the temperature is higher, the PL intensity is stronger and saturates sooner. On

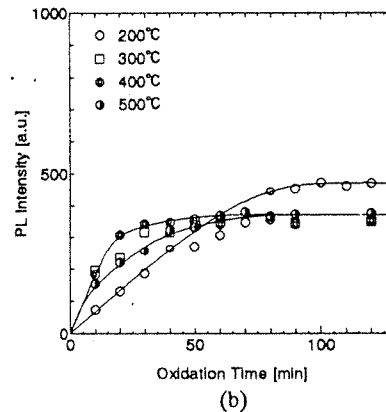
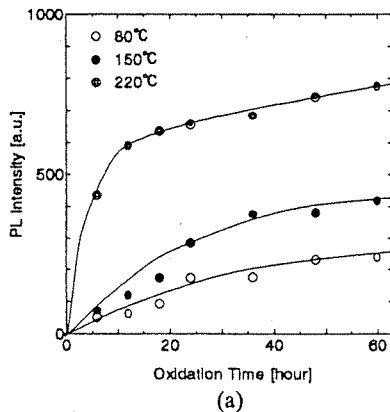


Fig.3 Dependence of the PL intensity on the oxidation time in (a) the atmosphere and (b) the pure oxygen gas

The influence of the substrate temperature

We fabricated the films with varying the substrate temperature from R.T. to 400 °C. From the SEM image, we observed the structure of the films. The ones at 200 °C and below consist of the distinct balls depositing, but, about the ones at 300 °C and 400 °C, the balls seem to break in smaller particles and they deposit. Figure 4 shows the dependence of the PL intensity on the substrate temperature. The PL is observed from the films fabricated only below 100 °C and the PL intensity increases as the substrate temperature becomes lower. From this result it is considered that, as the substrate temperature is higher than 100 °C, the film becomes hard to be oxidized, so that the PL from the films fabricated only below 100 °C can be observed.

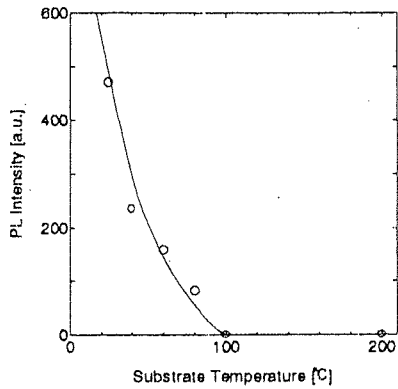


Fig. 4 Dependence of the PL intensity on the substrate temperature

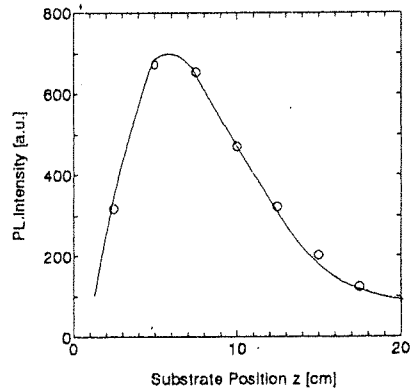


Fig. 5 Dependence of the PL intensity on the substrate position

The dependence on the substrate position

We fabricated the films with varying the substrate position from $z = +2.5$ cm to $+17.5$ cm. Figure 5 shows the dependence of the PL intensity on the substrate position. It is found that, as the substrate is set nearer to the discharge tube end, the PL intensity increases and has its maximum nearby $z = 5, 7.5$ cm and decreases drastically at $z = 2.5$ cm. This result is considered to be due to as follows. As the substrate position z decreases, the density of SiH_x radical in front of the substrate increases, so the film thickness increases. Therefore the PL intensity increases. But when the z is as small as 2.5 cm, SiH_x radicals arrived on the substrate before the a-Si:H nanoballs are created by the spatial recombination, and, in addition, the substrate was heated by the ion bombardment. Therefore, the PL intensity decreases. The effect mentioned above and these two effects are considered to lead the result of Fig. 5.

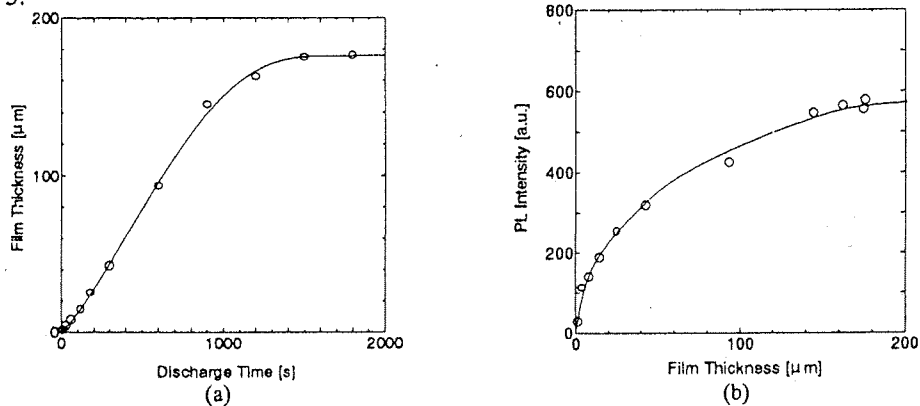


Fig.6 (a) Dependence of the film thickness on the discharge time
(b) Dependence of the PL intensity on the film thickness

The dependence on the discharge time

In order to estimate the process of the deposition of the film, we observed the SEM image of the surface and the cross section of the films fabricated with varying the discharge time from 1s to 1800 s. Figure 6 (a) shows the dependence of the film thickness on the discharge time. It is found that, as the discharge time increases, the thickness increases and saturates nearby 1500 s. From the SEM image of the cross section a-Si:H nanoballs are found to have deposited on the substrate taking the form of pillars with a space. From the above results it is considered that, as the discharge time increases, the pillars grow upward to some extent of height, and after that they get fat, hence, the film thickness saturates. Figure 6 (b) shows the dependence of the PL intensity on the film thickness. It is found that, as the film thickness increases, the PL intensity increases not in proportion to the thickness and

saturates. This result is considered to be due to as follows. When the film is thin, the whole film can be oxidized, but, when the film is thick, the space between the pillars become narrow, then the film is hard to be oxidized totally, hence, the PL intensity saturates.

The influence of the ion bombardment energy

In order to see the influence of the ion bombardment energy on the film properties and the PL characteristics, we fabricated the films with varying the DC bias substrate voltage (V_{dc}) from -80 V to $+40$ V.

We measured the sheath voltage (V_{sh}) at $z = 9$ cm in the pure Ar^+ plasma by the single probe method when the substrate is set at $z = 10$ cm. Figure 7 shows the dependence of the V_{sh} on the V_{dc} . It is found that the V_{sh} was varied from -110 V to -20 V with varying V_{dc} from -80 V to $+40$ V. Therefore, the ion bombardment energy is varied from -110 eV to -20 eV because the Ar^+ ion hardly collides with any other plasma particles in the sheath.

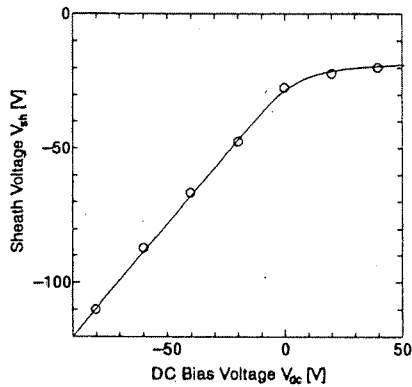


Fig. 7 Dependence of the V_{sh} on the V_{dc}

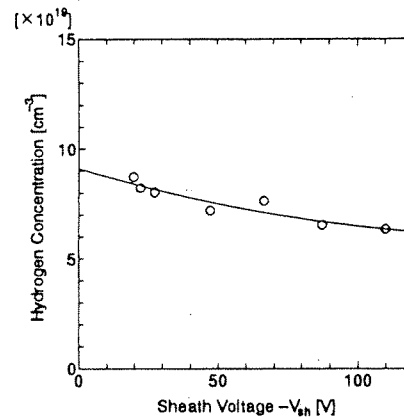


Fig. 8 Dependence of the C_H on the V_{sh}

In order to survey the influence of the variation of the ion bombardment energy on the construction of the film, we calculated the hydrogen concentration from the FTIR spectra. Figure 8 shows the dependence of the C_H on the V_{sh} . It is found that, as the V_{sh} increases in a negative direction, i.e. the ion bombardment energy increases, the C_H decreases. This result is considered to be due to as follows. As the V_{sh} increases, the Ar^+ ions are more accelerated by the sheath voltage and the Ar^+ ions with larger energy are struck into the film.

Figure 9 shows the dependence of the deposition rate of the film on the V_{sh} . It is found that, as the V_{sh} increases in a negative direction, the deposition rate decreases. This result is considered to be due to as follows. As the V_{sh} increases, the mobility of the a-Si:H nanoballs attached to the substrate is raised by the film surface heating effect of the ion bombardment⁷, therefore, the a-Si:H nanoballs deposit densely on the substrate.

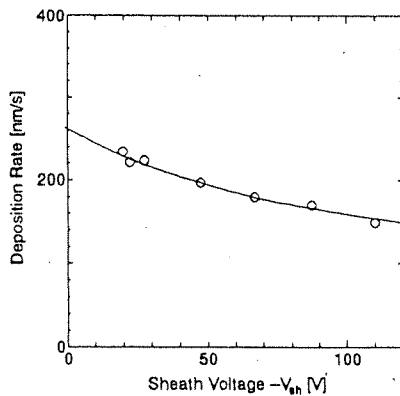


Fig. 9 Dependence of the deposition rate of the film on the V_{sh}

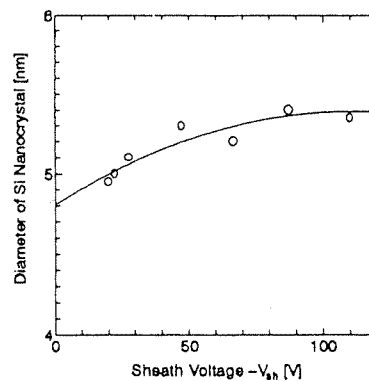


Fig. 10 Dependence of the diameter of the Si nanocrystal on the V_{sh}

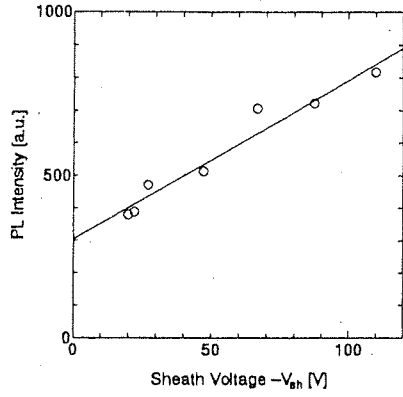


Fig. 11 Dependence of the PL intensity on the V_{sh}

nanoball film increases, because the PL intensity is supposed to be in proportion to the number of Si nanocrystals in the film. This result is explained by the analysis of the mechanism of the creation of Si nanocrystals as follows. The Ar^+ ions are struck into the a-Si:H nanoball deposited on the substrate. Then its energy is used to disconnect some hydrogen atom connected to the a-Si:H, and, moreover, to crystallize the a-Si. Therefore, the Si nanocrystal is created in the a-Si:H nanoball film by the Ar^+ ion bombardment. In order to confirm this analysis, we estimated the number of Si nanocrystals existing per unit area of the a-Si:H nanoball film from the measured results mentioned above. The method of calculation is shown as follow.

The energy ($E_{Ar}(V_{sh})$) provided by the bombardments of the Ar^+ ions per unit time and unit area of the substrate is expressed as follows by the sheath voltage (V_{sh}), the current (I_s) which flows into the substrate table while deposition and the area of the substrate table (S). The measured I_s is a certain value of $3 \mu A$ independent of the V_{sh} .

$$E_{Ar}(V_{sh}) = \frac{V_{sh} I_s}{S} \quad [J/m^2 \cdot s] \quad (1)$$

The energy which is necessary for the disconnection of the hydrogen atoms per unit time and unit area is defined as $E_H(V_{sh})$. Where the number of the hydrogen atoms which are disconnected per unit time and unit area ($D_H(V_{sh})$) is expressed as the function of V_{sh} by the hydrogen concentration ($C_H(V_{sh})$) and the deposition rate ($R_d(V_{sh})$) as follows. The $C_H(V_{sh})$ and $R_d(V_{sh})$ is obtained from Figs. 8 and 9.

$$D_H(V_{sh}) = C_H(V_{sh} = 0) \cdot R_d(V_{sh} = 0) - C_H(V_{sh}) \cdot R_d(V_{sh}) \quad [1/m^2 \cdot s] \quad (2)$$

The binding energy of Si-H is 295 kJ/mol⁸. Therefore,

$$E_H(V_{sh}) = \frac{295 \times 10^3}{6.02 \times 10^{23}} \cdot (C_H(V_{sh} = 0) \cdot R_d(V_{sh} = 0) - C_H(V_{sh}) \cdot R_d(V_{sh})) \quad [J/m^2 \cdot s] \quad (3)$$

It is considered that the energy of $E_{Ar} - E_H$ is consumed to create the Si nanocrystals.

Next, the energy which is necessary for the creation of a Si nanocrystal is defined as $E_{ac}(V_{sh})$. As the lattice constant of Si crystal is 5.43 Å and a unit lattice has 8 Si atoms, the number of Si atoms consisting a Si nanocrystal ($N_{Si}(V_{sh})$) is expressed as the function of V_{sh} by the radius of the Si nanocrystal ($r(V_{sh})$). The $r(V_{sh})$ is obtained from Fig. 10 as the half value of the diameter.

$$N_{Si}(V_{sh}) = \frac{8}{(5.43 \times 10^{-10})^3} \cdot \frac{4\pi r(V_{sh})^3}{3} \quad (4)$$

The energy necessary for the phase transition from a-Si to Si crystal is 11.9 kJ/mol⁹. Therefore,

$$E_{ac}(V_{sh}) = \frac{11.9 \times 10^3}{6.02 \times 10^{23}} \cdot \frac{8}{(5.43 \times 10^{-10})^3} \cdot \frac{4\pi(V_{sh})^3}{3} \quad [\text{J}] \quad (5)$$

The number of Si nanocrystals created per unit time and unit area is calculated as the $E_A - E_H$ divided by the E_{ac} . Therefore the number of Si nanocrystals existing per unit area of the a-Si:H nanoball film, i.e. the concentration of Si nanocrystals per unit area ($n(V_{sh})$), is expressed as follows by multiplying it by the discharge time of 600 s.

$$n(V_{sh}) = \frac{E_A - E_H}{E_{ac}} \times 600$$

$$= \left\{ \frac{V_{sh} I_s}{S} - \frac{295 \times 10^3}{6.02 \times 10^{23}} \cdot (C_H(0) \cdot R_d(0) - C_H(V_{sh}) \cdot R_d(V_{sh})) \right\} \cdot \frac{6.02 \times 10^{23}}{11.9 \times 10^3} \cdot \frac{(5.43 \times 10^{-10})^3}{8} \cdot \frac{3}{4\pi(V_{sh})^3} \times 600$$

[1/m²] (6)

Where, the $C_H(0)$ and $R_d(0)$ are estimated from the Figs. 8 and 9 by extrapolation.

Now the $n(V_{sh})$ can be estimated from Figs. 8, 9 and 10 by above method. Where, the solid lines of those figures are drawn as the curve of secondary degree obtained by the method of least squares, and are used for the calculation. Figure 12 shows the dependence of the $n(V_{sh})$. It is found that, as the V_{sh} increases in a negative direction, the $n(V_{sh})$ increases almost linearly.

Figure 13 shows the dependence of the PL intensity (I) on the $n(V_{sh})$ calculated from Figs. 11 and 12. Where, the plots present the experimental result and the solid line presents the theoretical one which is obtained by vertical transition of the solid line of Fig. 12 in order to agree with the plots. Comparing the two results from the figure, it is found that they are in a good agreement. But it is found also that the analysis is not perfect because the PL intensity is not 0 when the concentration of Si nanocrystals is 0 as shown in Fig. 13. However, the agreement of their tendencies shows the appropriateness of our theoretical analysis. Now we are improving this analysis.

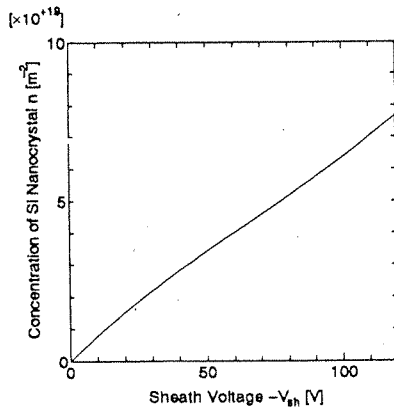


Fig. 12 Dependence of the concentration of the Si nanocrystals on the V_{sh}

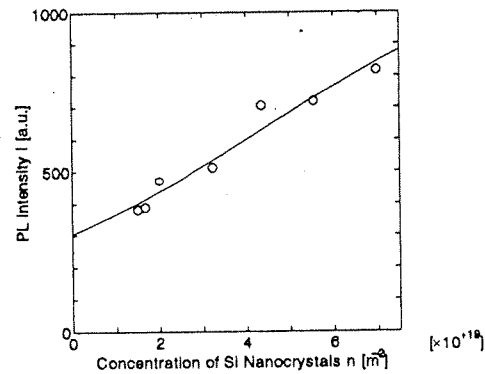


Fig. 13 Dependence of the PL intensity on the concentration of Si nanocrystals

CONCLUSION

We fabricated a-Si:H nanoball films by a double tubed coaxial line type microwave plasma CVD system with varying fabrication conditions and oxidation conditions and discussed the PL characteristics and the film properties.

- (1) After the films are oxidized by heating, the PL is observed at the room temperature. The PL intensity from the films oxidized in the pure oxygen gas saturates sooner with the increase of the

oxidation time than that in the atmosphere.

- (2) As the substrate temperature during deposition is higher, the PL intensity decreases, and the PL cannot be observed at 100 °C or over, because the films become hard to be oxidized.
- (3) When the substrate is set at 5~7 cm away from the discharge tube end, the PL intensity is strongest.
- (4) As the discharge time increases, the film thickness increases and then saturates nearby 1500 s. As the film thickness increases, the PL intensity increases and then saturates.

We also fabricated a-Si:H nanoball films with varying the DC bias substrate voltage in order to discuss the effect of the ion bombardment energy on the PL characteristics and the film properties.

- (5) The sheath voltage (V_{sh}) was varied from -110 V to -20 V with varying the DC bias substrate voltage from -80 V to +40 V.
- (6) As the V_{sh} increases in a negative direction, the hydrogen concentration decreases, the deposition rate decreases and the diameter of the Si nanocrystal increases.
- (7) Analyzing the mechanism of the creation of Si nanocrystals in the film, we estimated experimentally and theoretically the relation between the PL intensity and the number of Si nanocrystals. The experimental result and the theoretical one are found to be qualitatively in a good agreement.

ACKNOWLEDGEMENT

This work was supported by the Grant-in-Aid for scientific research from the Ministry of Education, Science and Culture. The authors thank Mr. Matsumoto, research student, for his experimental assistance.

REFERENCE

1. I. Kato, S. Wakana, S. Hara and H. Kezuka, Japanese Journal of Applied Physics, 21 (1982) L470
2. I. Kato, S. Wakana, S. Hara, Japanese Journal of Applied Physics, 22 (1983) L40
3. I. Kato, T. Ueda, K. Hatanaka, Electronics & Communications in Japan Part 2, 70 (1987) No. 11, 73
4. K. Kato and I. Kato, Japanese Journal of Applied Physics, 30 (1983) 1245
5. I. Kato and Y. Kawahara, Proc. 51st International Conference on Reactive Plasmas and 16th Symposium on Plasma Processing (1998) 109
6. O. P. Agnihotri, R. Tyagi and I. Kato, Japanese Journal of Applied Physics, 36 (1997) 6711
7. M. Yamashita, H. Ogihara and I. Kato, Proc. 13th Symposium on Plasma Processing (1996) 109
8. L. Pauling, The Chemical Bond (Cornell Univ. 1967) 65
9. E. P. Donovan, F. Spaepen, D. Turnbull, J. M. Poate and D. C. Jacobson
Applied Physics Letters, 42 (1983) 698

Photo Luminescence from Si Films Fabricated by Double Tubed Coaxial Line Type Microwave Plasma CVD Apparatus

Isamu Kato and Yoshio Kawahara

*Department of Electronics, Information and Communication Engineering, School of Science and Engineering,
Waseda University, 3-4-1 Okubo, Shinjuku-ku, Tokyo 169-0072, Japan*

Using a microwave plasma CVD apparatus we fabricate a-Si:H nanoball films. It is found by X-ray diffraction that there are nanocrystal Si in the a-Si:H nanoball. When the a-Si:H nanoball films are oxidized in the atmosphere, the photo luminescence is observed at room temperature. In this study, we fabricate films with varying the fabrication conditions (i.e. SiH₄ gas flow rate, microwave power and substrate temperature), and discuss how the variations affect the photo luminescence characteristics.

1. Introduction

We have developed a double tubed coaxial line type microwave plasma CVD (MPCVD) apparatus. Figure 1 shows the configuration of this MPCVD apparatus. In this apparatus the microwave power is confined in the cylindrical cavity region, and in the deposition chamber a spatial afterglow plasma without injection of the microwave power is created by the gas flow and diffusion. The discharge gas (which creates the plasma, but doesn't create a deposition material by itself) is fed to the outer discharge tube and the material gas (which is dissociated in the plasma and creates a deposition material) is fed to the inner tube (as shown in Fig. 1). Both the gases can be separately led to the deposition chamber. The discharge gas is ionized in the cylindrical cavity region by the microwave power. The material gas is led to the discharge tube end through the inner tube and flows into the plasma and is dissociated by the collision with the plasma particles.

Using Ar gas as a discharge gas and SiH₄ gas as a material gas, a-Si:H films are fabricated. In the case of the low gas pressure in the deposition chamber by the high exhaust speed, a fine a-Si:H film is created. This film is suitable for a solar battery and a thin film transistor. In the case of the high gas pressure in the deposition chamber by the low exhaust speed, because the mean free path becomes short, SiH_x radicals are spatially recombined in the gaseous phase and become a-Si:H nanoballs. The a-Si:H nanoballs deposit on the substrate and an a-Si:H nanoball film is fabricated^[1]. It is found by X-ray diffraction that there are nanocrystal Si (several nm

in diameter) in the a-Si:H nanoball (~20 nm in diameter). After the a-Si:H nanoball film is thermally oxidized in the atmosphere, the photo luminescence (PL) is observed at room temperature. In this study we fabricate the a-Si:H nanoball films with varying the parameters of various fabrication conditions and discuss the characteristics of the photo luminescence.

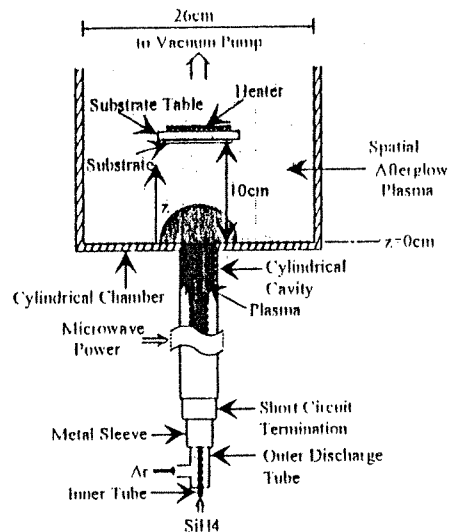


Fig. 1. Configuration of the MPCVD apparatus

2. Experiment

The basic experimental conditions are as follows. The axial distance from the discharge tube end is defined as z (as shown in Fig. 1). The microwave power is 150W. The substrate table is placed at $z=10$ cm. The inner tube end is at $z=-1.4$ cm. The gas pressure in the deposition chamber is set at 250mTorr by controlling the exhaust speed. The DC

substrate bias voltage is 0V. The substrate temperature is R.T. The Ar gas flow rate is 110ml/min and the SiH₄ gas flow rate is 30ml/min.

The parameters of the fabrication conditions are varied as follows. The SiH₄ gas flow rate is varied from 10ml/min to 50ml/min, the microwave power from 110W to 190W, the substrate temperature from R.T. to 400°C.

The pumping light is Ar⁺ laser beam (514.5nm).

3. Results and Discussion

Figure 2 shows the spectrum of the PL from the a-Si:H nanoball films which are oxidized at 150°C in the atmosphere. In the figure the parameter is the oxidization time. The PL spectrum has a peak at about 800nm. The PL cannot be observed from the films before oxidization, but after oxidization the PL is observed at R.T. and its intensity increases as the oxidization time gets longer.

Therefore, in order to see the dependence of the PL intensity on the oxidization temperature, we also measured the PL from the films oxidized at different oxidization temperatures (i.e. 80, 150, 220°C). From the result, it is found that, as the temperature is higher within the measurements, the PL intensity is stronger and becomes saturated earlier.

From the above result it is considered that, when the a-Si:H nanoball film is oxidized, the a-Si:H becomes SiO₂, so that the nanocrystal Si is buried in the SiO₂.

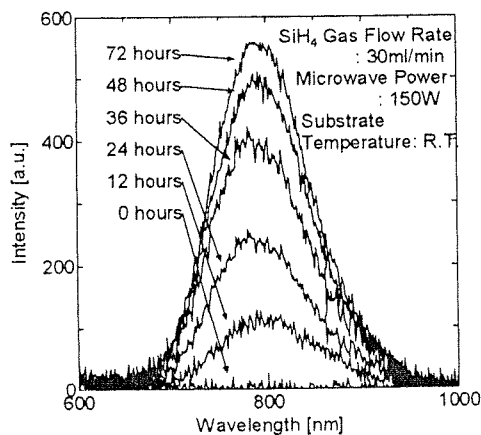


Fig.2. PL spectrum

We fabricated the films with varying the substrate temperature from R.T. to 400°C. From the SEM picture, we observed the structure of the films. The ones at 200°C and below consist of the a-Si:H nanoball, but about the ones at 300°C and 400°C, the a-Si:H nanoballs seem to have broken and the

smaller particles seem to have deposited. The PL is observed from the films fabricated only below 100°C and the PL intensity increases as the substrate temperature becomes lower. From this result it is considered that, as the substrate temperature is higher than 100°C, the a-Si:H nanoball film becomes the fine a-Si:H film, which is suitable for a solar battery and a thin film transistor, so that the PL from the films fabricated at 100°C or over cannot be observed.

We fabricated the films with varying the SiH₄ gas flow rate (i.e. 10, 20, 30, 40, 50ml/min). Figure 3 shows the dependence of the PL wavelength on the SiH₄ gas flow rate. From the figure, it is found that the PL wavelength is very long at 10ml/min and becomes shorter as the SiH₄ gas flow rate increases. The surface of the film at 10ml/min looks smooth. From these results, it is considered that at 10ml/min in SiH₄ gas flow rate the probability of the spatial recombination is small and the a-Si:H nanoballs don't grow up so large. The film surface becomes smooth and the PL intensity is small.

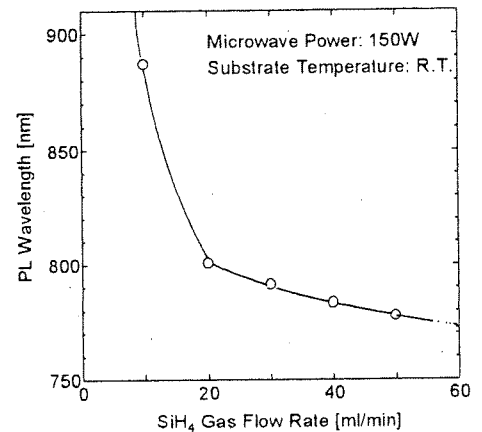


Fig.3. Dependence of the PL wavelength on SiH₄

Conclusion

We fabricated a-Si:H nanoball films using a MPCVD apparatus at the high gas pressure. After the films are thermally oxidized in the atmosphere, the PL (~800nm) is observed at room temperature.

Acknowledgement

This work is partly supported by the Grant-in-Aid for scientific research from the ministry of Education, Science and Culture in Japan.

Reference

- [1] N. Koshiji, K. Watanabe and I. Kato: Proc. 15th Sympo. Plasma Processing (1998) 140

Stabilization of Ar Plasma by Applying Longitudinal Magnetic Field

Isamu Kato

Materials Research Laboratory for Bioscience and Photonics, Waseda University, Tokyo, Japan 169

Toshihiro Yamagishi, Yoshinori Morita, and Taro Kamiko

School of Science and Engineering, Waseda University, Tokyo, Japan 169

SUMMARY

This research is intended to obtain a stable plasma with a low gas pressure by applying a magnetic field parallel to the gas flow in the discharge region of a double-tubed coaxial line-type microwave plasma CVD system so that the diffusion of the plasma in the radial direction is suppressed. The stability of the plasma is studied by the width of variation and temporal change of the electron saturation current. In the case where the Ar gas flow rate is 30, 20, and 15 ml/min, the stability of the plasma is good. Improved stability is seen on application of a magnetic field. Also, in the case of Ar gas flow rate of 10 and 8 ml/min, the plasma is unstable without a magnetic field. By applying a magnetic field of more than about 500 gauss, the diffusion of electrons to the discharge tube wall is suppressed and as a result the extinction of electrons at the wall is reduced. Hence, a stable microwave plasma is obtained even at a low gas pressure (low gas flow). © 1998 Scripta Technica, Electron Comm Jpn Pt 2, 81(3): 10-16, 1998

Key words: Microwave plasma CVD; longitudinal magnetic field; stability; radial diffusion; low gas pressure.

1. Introduction

Plasma CVD is used for fabrication of thin films and is a method indispensable for fabrication of electron devices and photonic devices. In order to realize plasma suitable for CVD, much research has been carried out on the plasma intended to be used for CVD. The authors have been carrying out research on plasma for fabrication of high-quality hydrogen amorphous silicon films and silicon nitride films [1, 2].

In the plasma generation equipment such as the RF plasma CVD widely used as a plasma source, electric power is injected into the film deposition region and hence the film quality is degraded due to ion bombardment on the film surface. In the authors' laboratory, research and development have been carried out for a double-tubed coaxial line-type microwave plasma CVD system in which a spatial afterglow plasma without the electric power injection into the film deposition chamber can be generated [3-7]. As fundamental data for fabrication of thin films, measurement of plasma parameters in the deposition chamber has been carried out [1-3].

Recently, for advancement of the plasma process, the following three points are required: density enhancement of plasma, uniformity of plasma in line with a large aperture, and film fabrication under a low gas pressure. In order to realize these objectives, extensive research has been

carried out on various types of plasma generation equipment such as ECR plasma equipment [9]. In the authors' laboratory, the uniformity of the plasma in line with a large aperture diameter and the film fabrication under a low gas pressure have almost been attained using present equipment [1, 2, 6, 7, 9, 10]. Hence, in the present study, in order to obtain a stable plasma with a high density under a low gas pressure, stabilization of the plasma is investigated by a longitudinal magnetic field (parallel to the gas flow) applied in the discharge region of the present equipment so that the diffusion of plasma in the radial direction of the discharge tube is suppressed.

2. Experiment

In the experiment, the double-tubed coaxial line-type microwave plasma CVD equipment shown in Fig. 1 is used [4, 5, 10]. As the plasma generation condition, the microwave input power and the microwave reflected power are 100 and 30 W constant. In the outer discharge tube, Ar gas is flowing as the discharge gas. The gas flow rate is varied between 8 and 30 ml/min. In the inner tube made of stainless steel, the material gas such as SiH_4 can flow which is not used in the present experiment. The gas pressure in the deposition chamber varies linearly between 0.5 and 3.0 mTorr by the Ar gas flow rate. The current in the longitudinal magnetic field application coil (shown in Fig. 1) is between 0 and 6 A. Then the magnetic flux density generated at the center of the coil is between 0 and 1986 gauss.

The deposition chamber in this equipment is a cylinder with an internal diameter of 15 cm. The distance along the axial direction of the deposition chamber from the discharge tube edge, or the interior wall of the flange of the

deposition chamber, is defined as z while the distance in the radial direction from the center axis is r (see Fig. 1). The single probe method is used for measurement of stability. The probe has a diameter of 0.05 cm and a length of 1 cm and is cylindrical. Also, the measurement position is $z = 1.5$ cm and $r = 0$ cm. The location of the inner tube edge is $z = -2.0$ cm as the state of the film fabrication by the present equipment [5].

3. Coil Characteristics

The present research is intended for studying possible variations in the plasma when a magnetic field is applied to the plasma and for obtaining stable plasma suitable for CVD. Therefore, it is necessary to eliminate as much as possible the problem areas not existing in the absence of the applied magnetic field. Hence, there are possibilities for problems such as the loss of uniformity of the film quality due to anisotropy in the plasma if a strong magnetic field leaks into the film fabrication region.

In the present equipment, the coil is surrounded by a soft iron plate that forms a magnetic circuit. In addition, the flange between the deposition chamber and the coil is made of a 1.5-cm-thick soft iron plate (shown in Fig. 1) so that the magnetic field does not leak into the deposition chamber.

In Fig. 2, the spatial distribution of the magnetic flux density in the deposition chamber is shown. The figure is for the case where the coil current is 3.0 A. It is seen that the magnetic flux density on the z axis decays quickly from 82.3 gauss to 6.6 gauss for z ranging between 0 and 2 cm. Subsequently, as z is increased, the density gradually decays to 2.5 gauss. Also, in the range of $z > 4$ cm, the variation of

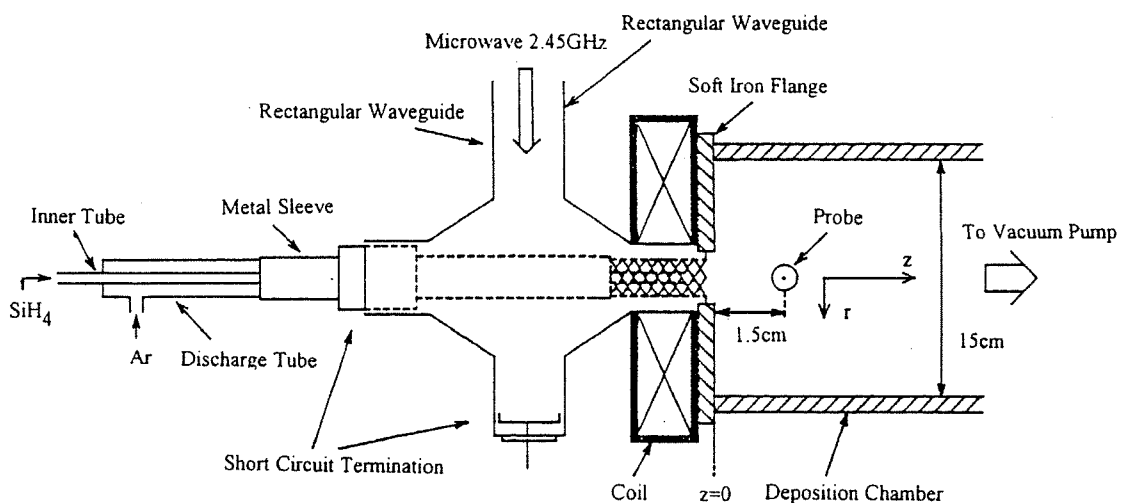


Fig. 1. Double tube coaxial line-type microwave plasma CVD system.

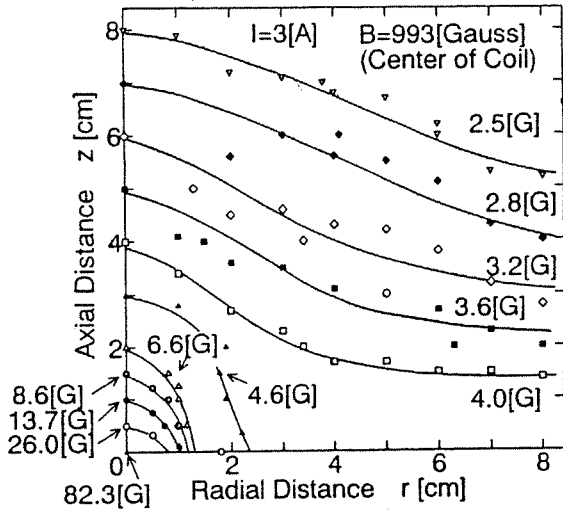


Fig. 2. Spatial distribution of magnetic flux density (outside of coil).

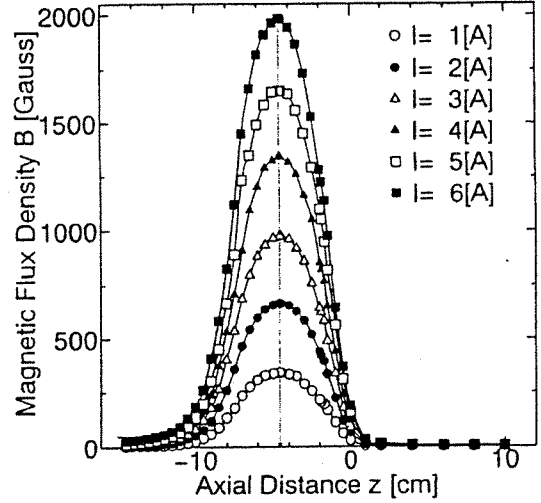


Fig. 3. Spatial distribution of magnetic flux density (on z axis).

the magnetic flux density in the r direction is slight. From the above, it is concluded that no magnetic field leaks that generates anisotropy to the plasma in the deposition chamber.

Next, in order to study the effect of the longitudinal magnetic field on the plasma in the discharge region (the meshed area in Fig. 1), the magnetic flux density is measured in the discharge region.

Figure 3 shows the measured results of the magnetic flux density on the z axis where $r = 0$ cm. It is seen that the magnetic flux density increases in proportion to the current I in the coil. Also, the magnetic flux density reaches a maximum on the z axis when $z = -4.6$ cm. This value almost coincides with the center of the coil. In the following, the value of the magnetic flux used in this paper is defined to be that at the center of the coil.

From the above results, it is considered that the applied magnetic field does affect the discharge plasma in the area meshed at the end of the discharge shown in Fig. 1 but does not affect the plasma in the deposition chamber, or the spatial afterglow plasma.

Let us investigate the effect of the magnetic field on the probe measurement. First, the reason why the probe is located at $z = 1.5$ cm as described above is to make the probe current sufficient for measurement as shown later in Fig. 7. Next, the magnetic flux density at $z = 1.5$ cm and $r = 0$ cm is 17.2 gauss even when the coil current is a maximum at 9 A as is clear from Figs. 2 and 3. Since the magnetic field is very low at this probe location, the effect of the applied magnetic field on the probe measurement is nil.

4. Results and Discussion

Under no magnetic field, the I_p-V_p characteristics of the probe are observed in the measurement of the plasma parameters in a low-gas-pressure Ar plasma when the Ar gas flow rate is 8 and 10 ml/min. It is then found that the waveform varies significantly in time in the electron current refuted region and in the electron current saturation region. Figure 4 shows an example of the I_p-V_p characteristics for the probe in the case where the Ar gas flow is 8 ml/min.

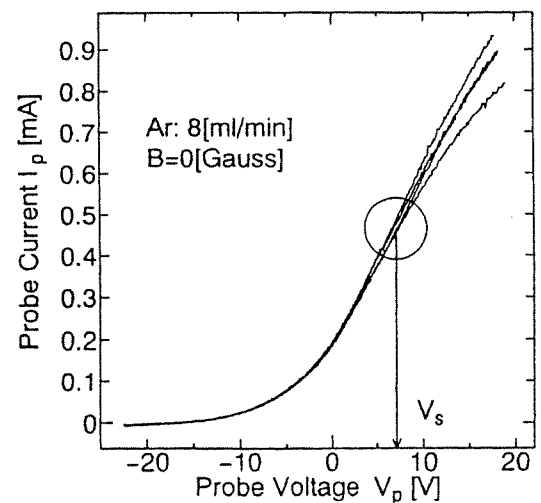


Fig. 4. Probe I_p-V_p characteristic in unstable plasma.

These four waveforms are arbitrarily selected from continuously swept waveforms at every 10 ms. It is seen that there are fluctuations in the waveforms. Hence, the fluctuations of the space potential V_s of the plasma (Fig. 4) are first noted and the stability of the plasma is discussed. Figure 5 shows the dependence of the fluctuation range of the space potential on the magnetic flux density. In this figure, the measured values of V_s at each magnetic flux density are averaged, and this averaged value is determined to be V_s at each magnetic flux. Then, the difference ΔV_s between each measured value and the average value V_s is shown. From the figure, it is found that V_s has an almost constant fluctuation range regardless of the applied magnetic flux density at any gas flow rate. Also, it is found that the fluctuation range is only $\pm 1-2$ V and is slight. We thus conclude that the fluctuation of the measured data is not dependent on the magnetic flux density but on the error caused in the processing of data. Hence, the plasma stability due to the strength of the applied magnetic field cannot be discussed from the fluctuation of V_s . However, since the fluctuation range is larger for a plasma with a lower gas pressure (and hence a lower gas flow rate), the stability is considered to be better in the case of Ar gas flow of 30 ml/min than for one of lower gas pressure.

Since the fluctuation of the I_p-V_p characteristics of the probe does not significantly affect the fluctuation of V_s , it is not possible to discuss the plasma stability due to the intensity of the applied magnetic field based on the fluctuation of V_s . Hence, the plasma stability is discussed by studying the fluctuation along the longitudinal direction in the I_p-V_p characteristics of the probe in Fig. 4.

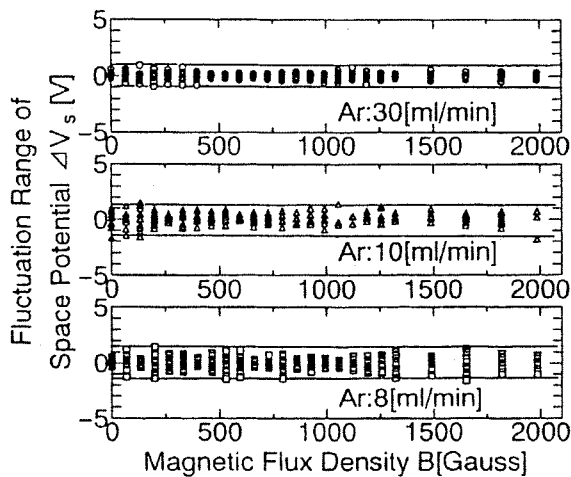


Fig. 5. Dependence of fluctuation range of space potential V_s on magnetic flux density.

Figure 6 shows the dependence of the fluctuation range of the electron saturation current I_{esat} , or the probe current I_p at $V_p = V_s$, on the magnetic flux density. In this figure, I_{esat} is normalized by the average value of I_{esat} at each magnetic flux density. It is seen that the fluctuation range of I_{esat} becomes smaller by application of a magnetic field stronger than about 500 gauss at any gas flow rate. Namely, for any gas flow rate, the plasma stability can be improved by applying a magnetic field stronger than about 500 gauss. If the gas flow rate is large (30 ml/min), the plasma is already stable and its fluctuation range is small.

From the above experimental results, it is found that the fluctuation range of I_{esat} is reduced by the application of a magnetic field. In order to study this phenomenon in more detail, a constant voltage equal to V_s (the average value of measured space potentials described above) at each gas flow rate and magnetic flux density is applied to the probe and the time variation of I_{esat} is measured so that the effect of the applied magnetic field on the plasma stability is discussed. As shown in Fig. 7, V_s changes significantly depending on the gas flow rate and the applied magnetic flux density. Therefore, if the probe voltage V_p is identical at all experimental conditions, no objective measurement of stability is accomplished unless V_p is equal to V_s , since the electron saturation current is not measured. Hence, the value of V_p is made equal to V_s under each experimental condition. As shown in Fig. 7, when the Ar gas flow rate is 30 ml/min and the applied magnetic flux density is 0 gauss, the probe measurement resulted in $V_s = 25$ V. Under this condition, the time variation of the probe current is measured with $V_p = 25$ V. Under other experimental conditions, V_p is similarly determined.

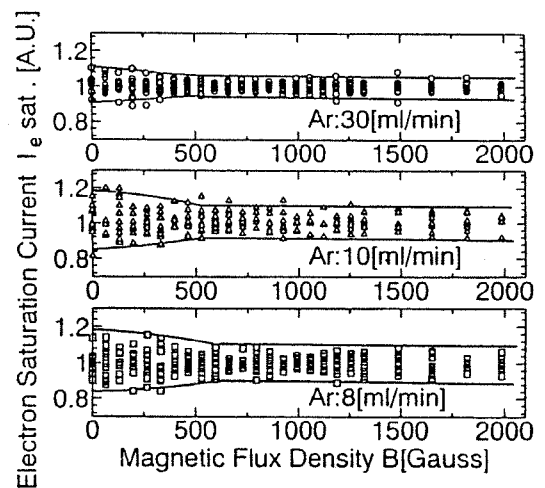


Fig. 6. Dependence of fluctuation range of electron saturation current on magnetic flux density.

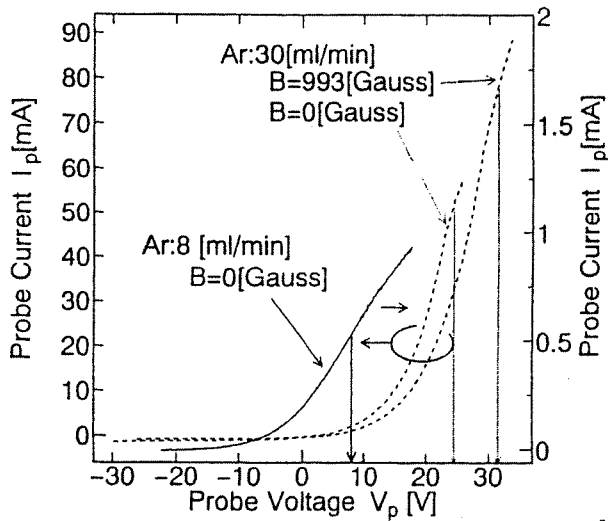
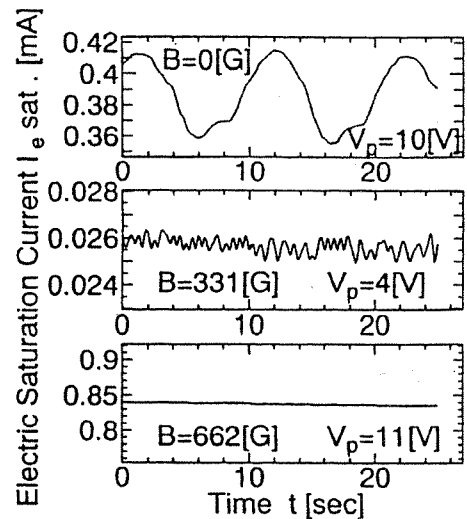


Fig. 7. Difference in probe I_p - V_p characteristic by gas flow rate and magnetic flux density.

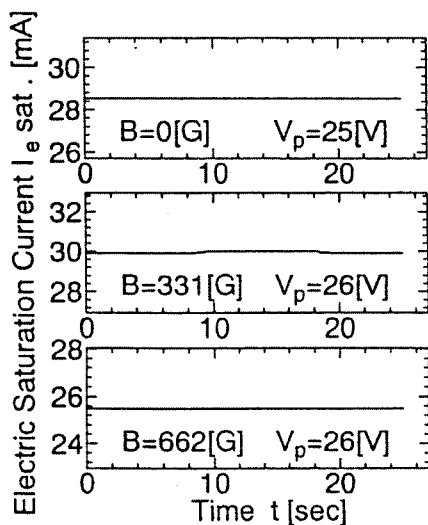
The results are shown in Figs. 8(a), 8(b), and 8(c). From Fig. 8(a), it is found that I_{esat} is constant in time at any magnetic flux density when the Ar gas flow rate is 30 ml/min. Hence, the plasma stability is considered excellent regardless of the applied magnetic flux density when the Ar gas flow rate is 30 ml/min. From Figs. 8(b) and 8(c), it is found that I_{esat} varies significantly in time with no applied magnetic field but the fluctuation range is decreased by

applying a magnetic field in the case of Ar gas flow rate of 10 and 8 ml/min. Hence, it is concluded that unstable Ar gas plasma with a low gas pressure and low gas flow rate under no magnetic field can be stabilized by applying a longitudinal magnetic field.

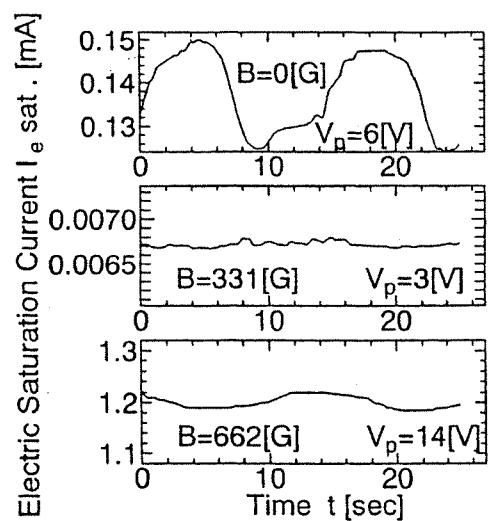
A similar experiment has been carried out in the case where the Ar gas flow rate is 15 and 20 ml/min. Like the case of Ar gas flow rate of 30 ml/min, the stability is excellent without a magnetic field. No significant change is observed by applying a magnetic field.



(b) Ar: 10 [ml/min]



(a) Ar: 30 [ml/min]



(c) Ar: 8 [ml/min]

Fig. 8. Variation of probe current with time.

When the gas pressure is reduced, the generation rate of electrons is decreased so that the discharge becomes unstable and halted. Hence, by applying a longitudinal magnetic field, the diffusion of electrons in the radial direction is suppressed. Then, a stable discharge can be maintained even at a low gas pressure, since the extinction rate of the electron decreases.

By way of this stabilization, the deposition speed at an Ar gas flow rate of 8 ml/min becomes more than ten times faster than one without a magnetic field so that a sufficiently practical deposition speed (about 0.5 nm/s) can be obtained.

5. Conclusions

A method has been studied for evaluation of the plasma stability from the current-voltage characteristics of the probe. By choosing the probe voltage at the average value of the plasma space potential V_p , the time fluctuations of the probe current (electron saturation current) are measured to evaluate the plasma stability equally under various conditions.

From this method, the following results are obtained.

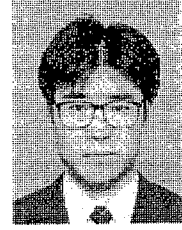
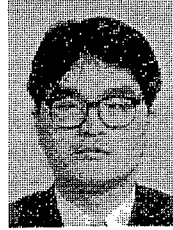
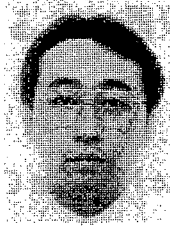
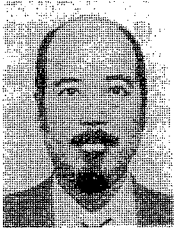
(1) When the Ar gas flow rate is 15, 20, and 30 ml/min, the plasma stability is excellent even without any magnetic field. By applying a longitudinal magnetic field, the stability is improved. (2) In the case of a low gas pressure with an Ar gas flow rate of 8 and 10 ml/min, the plasma is unstable without any magnetic field. By applying a longitudinal magnetic field, the plasma can be stabilized. Hence, by applying a longitudinal magnetic field to the plasma, the diffusion of electrons into the discharge tube wall can be suppressed so that the extinction rate of electrons at the discharge tube wall is reduced. Hence, a stable microwave plasma can be obtained at a low gas pressure.

Acknowledgment. This work was supported by a Scientific Research Grant from the Ministry of Education.

REFERENCES

1. I. Kato, T. Shirai, and T. Sakamoto. Spatial distribution of plasma parameters in microwave plasma CVD. *Trans. I.E.E. Japan (A)*, **112-A**, No. 5, pp. 355-362 (May 1992).
2. I. Kato, T. Shimoda, and T. Yamagishi. Spatial distribution of parameters for N_2/SiH_4 plasma in double-tubed coaxial line type microwave plasma CVD. *Trans. I.E.E. Japan (A)*, **116-A**, No. 7, pp. 617-622 (July 1996).
3. I. Kato, S. Wakana, S. Hara, and H. Kezuka. Microwave plasma CVD system for the fabrication of thin solid films. *J.J.A.P.*, **21**, No. 8, pp. L470-L472 (Aug. 1982).
4. I. Kato, S. Wakana, and S. Hara. Microwave plasma CVD system to fabricate α -Si thin films out of plasma. *J.J.A.P.*, **22**, No. 1, pp. L40-L42 (Jan. 1983).
5. I. Kato and S. Wakana. New plasma chemical vapor deposition equipment. *Vacuum*, **26**, No. 7, pp. 628-636 (July 1983).
6. I. Kato, S. Hara, and S. Wakana. Analysis of radial distribution of plasma parameters in a coaxial-line microwave discharge tube. *J.A.P.*, **54**, No. 9, pp. 4883-4888 (Sept. 1983).
7. I. Kato, K. Kato, and T. Sakamoto. Plasma chemical vapor deposition method using microwave discharge. *Radiat. Res.*, **ED-91-60**, pp. 141-150 (1991).
8. H. Sugai. New development in low pressure high density plasma—ECR, Helicon wave and induction coupled plasma. *J. Appl. Phys.*, **63**, No. 6, pp. 559-567 (June 1994).
9. I. Kato, K. Noguchi, and K. Numada. Preparation of silicon nitride films at room temperature using double-tubed coaxial line-type microwave plasma chemical vapor deposition system. *J.A.P.*, **62**, No. 2, pp. 492-497 (1987).
10. I. Kato, T. Ueda, and K. Hatanaka. Substrate temperature characteristics of a-Si:H thin film by double-tubed coaxial line-type microwave CVD method. *Trans. I.E.E. Japan (A)*, **106-A**, No. 8, pp. 35-41 (Aug. 1986).

AUTHORS (from left to right)



Isamu Kato (member) graduated from Waseda University in 1967 and completed the doctoral course in 1973. In that year, he obtained his D.Eng. degree. He then joined the staff of Waseda University. In 1978, he became an associate professor. From 1979 to 1981, he was on leave as a visiting professor at the University of Manitoba. With a research grant from the Canadian National Research Council, he carried out collaborative research and research supervision. In 1983, he became a professor at Waseda University. He has been engaged in research on microwave plasma CVD, photonics, laser engineering, electronic materials, measurement engineering, photonic materials, plasma electronics, optical quantum electronics, and semiconductor thin film engineering. He is a member of the Institute of Electrical Engineers of Japan, the Applied Physics Society, the Institute of Television Engineering, the Japan Vacuum Society, and IEEE.

Toshihiro Yamagishi (nonmember) graduated from Waseda University in 1994 and completed the master's course in 1996. Presently, he is with Hitachi, General Computer Works. He was engaged in research on microwave plasma. He is a member of the Applied Physics Society.

Yoshinori Morita (nonmember) graduated from Waseda University in 1992 and completed the master's course in 1994. In 1997, he withdrew from a doctoral course. He was engaged in research on microwave plasma.

Taro Kamiko (nonmember) graduated from Waseda University in 1993 and completed the master's course in 1997. Presently, he is with Toshiba, Information and Communication Systems Technology Laboratory. He was engaged in research on microwave plasma. He is a member of the Applied Physics Society.

FABRICATION OF a-Si:H FILM USING H₂/SiH₄ PLASMA BY LONGITUDINAL
MAGNETIC FIELD APPLIED MPCVD SYSTEM

縦磁界印加MPCVDによるH₂/SiH₄プラズマを用いた a-Si:H 膜の作製

Hidetaka IIDUKA, Masayuki USUDA and Isamu KATO
飯塚英孝、臼田雅之、加藤勇

School of Science and Engineering, Waseda University
3-4-1, Okubo, Shinjuku-ku, Tokyo, 169
早稲田大学理工学部、〒169 東京都新宿区大久保3-4-1

Abstract

The longitudinal magnetic field is applied to the cavity of the double tubed coaxial line type MPCVD system to decrease the surface recombination of electrons and ions on the discharge tube wall. And the stable and high density H₂ plasma is created. Therefore, using H₂/SiH₄ plasma to fabricate the a-Si:H film, the deposition rate of a-Si:H films becomes fast enough for practical use. The SiH bond density of the film fabricated in H₂/SiH₄ plasma becomes numerically superior to that of the film fabricated in Ar/SiH₄ plasma.

1. Introduction

The double tubed coaxial line type MPCVD system has the double tube structure that consists of the fused quartz outer discharge tube and the stainless steel inner tube. The discharge gas is fed to the outer discharge tube and the material gas is fed to the inner tube. The discharge gas is ionized in the discharge region by the microwave power. The inner tube leads the material gas to the discharge tube end, and the material gas is dissociated by the collision with the plasma particles. In this system, when pure H₂ gas was used as the discharge gas and SiH₄ gas was used as the material gas, the deposition rate of a-Si:H film was much slower, because the electron density of H₂ plasma was low. Then, in order to create the stable and high density plasma, the coil is set up around the cavity of the system. And the magnetic field along the gas flow (longitudinal magnetic field) is applied to the discharge area to suppress the diffusion to the discharge tube wall. Using this stable and high density plasma, the a-Si:H films are fabricated .

2. Experiment

Figure 1 shows the setup of the longitudinal magnetic field applied double tubed coaxial line type MPCVD system. This system has the structure that the magnetic field does not come in the deposition chamber, because the coil is covered by a soft iron and the flange of a chamber is made of a soft iron to form the magnetic closed circuit [1]. The microwave electric field in the discharge area is the fundamental mode of the coaxial line and is parallel with the gas flow, namely, with the applied magnetic field. Therefore, the electron cyclotron resonance (ECR) doesn't fundamentally occur.

The axial distance from the end of the discharge tube is defined as z . At $z=1,5,10$ cm

in the deposition chamber, the plasma parameters of H_2 plasma are measured, where the H_2 gas flow rate is 400 ml/min and the magnetic flux density at the center of the coil is varied from 0 to 2600 Gauss. A probe of 0.05 cm diameter and 1.0 cm length is used. The a-Si:H film is fabricated on the substrate table at $z=10$ cm, where the magnetic flux density is 1750 Gauss, the H_2 gas flow rate is 400 ml/min, and the SiH_4 gas flow rate is 10 to 50 ml/min. The substrate is not heated by a heater.

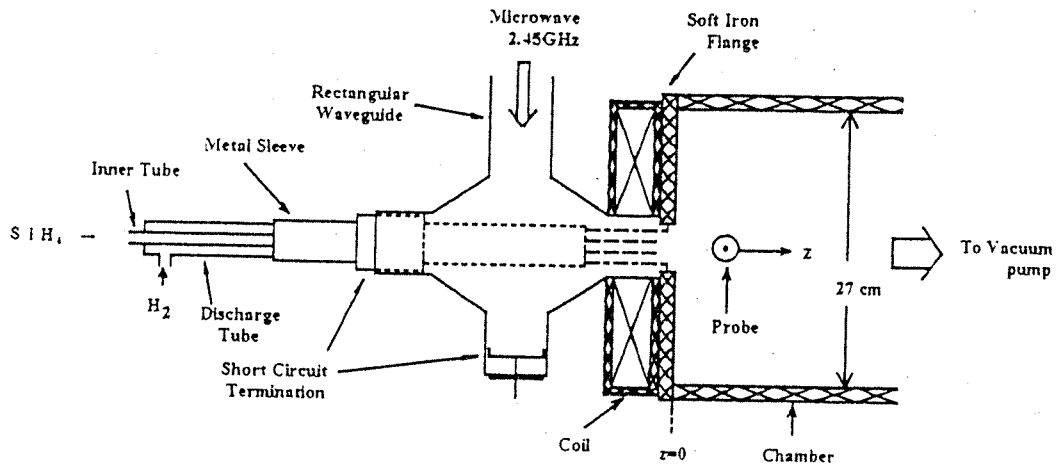


Figure 1 Setup of Longitudinal Magnetic Field Applied MPCVD System

3. Result and Discussion

Figure 2 shows the dependence of electron density on the magnetic flux density at $z=1, 5, 10$ cm. The electron density increases with increasing the magnetic flux density. And electron density is saturated when magnetic flux density is more than 1600 Gauss. This is because that the effect of suppressing the diffusion of electrons is saturated [2]. The stable and high density H_2 plasma can be created when magnetic flux density is more than 1600 Gauss. The a-Si:H films are created under the condition of magnetic flux density = 1750 Gauss.

Figure 3 shows the dependence of the deposition rate at $z = 10$ cm on the SiH_4 gas flow rate.

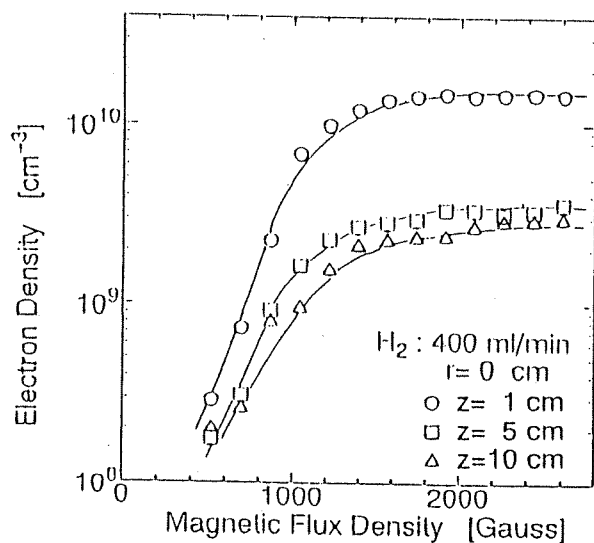


Figure 2 Dependence of Electron Density on Magnetic Flux Density

In this figure, \square plot shows the value of the deposition rate in the case Ar gas flow rate is 110 ml/min, SiH_4 gas flow rate is 30 ml/min. The deposition rate when H_2 gas is used as the discharge gas is one fourth of the deposition rate when Ar gas is used as this discharge gas. This deposition rate is fast enough for practical use.

Figure 4 shows the dependence of the ratio of the SiH bond density to the SiH_2 bond density on SiH_4 gas flow rate. As the SiH_4 gas flow rate is increased, the SiH bond density becomes numerically inferior to the SiH_2 bond density. Namely, when the deposition rate becomes faster, the disconnection of Hydrogen atoms from the film surface hardly occurs.

The SiH bond density of the film fabricated in the H_2/SiH_4 plasma is numerically superior to that of the film fabricated in the Ar/SiH_4 plasma.

Figure 5 shows the dependence of the total hydrogen concentration on the SiH_4 gas flow rate. When the SiH_4 gas flow rate is increased, the total hydrogen concentration decreases and increases. The effect of H_2 plasma during the film deposition decreases with increasing the deposition rate. But, as the deposition rate becomes much faster, the surface reaction like the disconnection of hydrogen atoms from film surface becomes slow, so the hydrogen concentration in the film increases. Compared with the case of Ar/SiH_4 plasma, the total hydrogen concentration of a-Si:H film fabricated by H_2/SiH_4 plasma is less than that of a-Si:H film fabricated by Ar/SiH_4 . Because H_2 plasma has the great effect on the disconnection of hydrogen atoms on the surface of a-Si:H film.

Figure 6 shows the dependence of the dangling bond density on the SiH_4 gas flow rate. The relaxation of the dangling bond decreases with increasing the deposition rate. When the SiH_4 gas flow rate is 30 ml/min, the dangling bond density is the same in the cases of Ar/SiH_4 plasma and H_2/SiH_4 plasma.

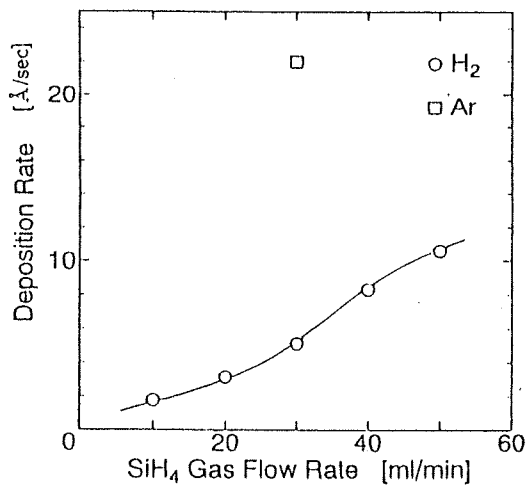


Figure 3 Dependence of Deposition Rate on SiH_4 Gas Flow Rate

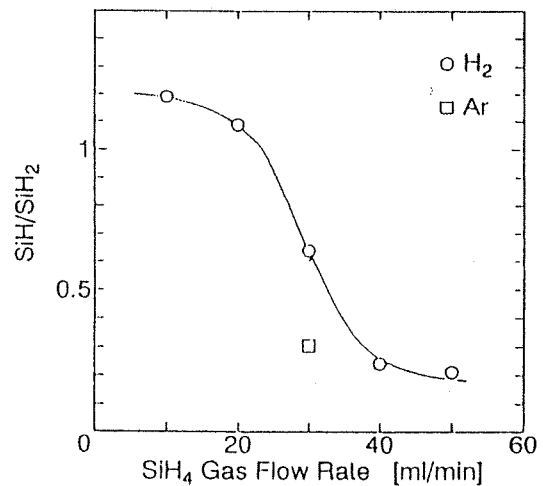


Figure 4 Dependence of SiH/SiH_2 on SiH_4 Gas Flow Rate

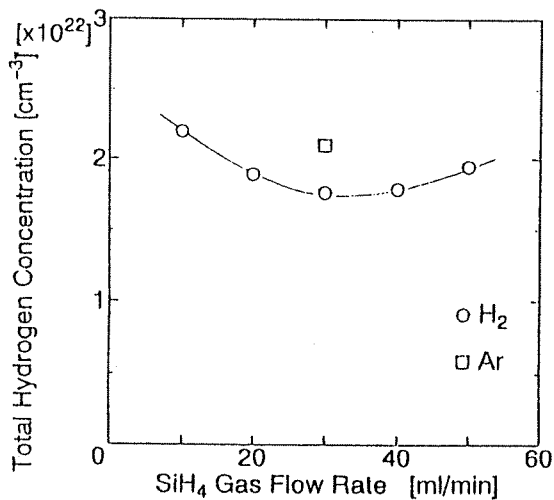


Figure 5 Dependence of Total Hydrogen Concentration on SiH₄ Gas Flow Rate

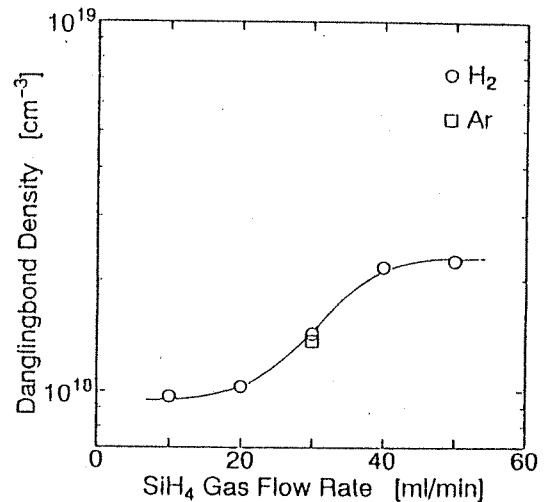


Figure 6 Dependence of Dangling Bond Density on SiH₄ Gas Flow Rate

4. Conclusion

The stable and high density H₂ plasma is created by the applied longitudinal magnetic field.

The high speed deposition rate is possible by using the stable and high density H₂ plasma and SiH₄ gas. And the a-Si:H film whose SiH bond is numerically superior can be fabricated, compared with the film fabricated by Ar/SiH₄ plasma.

Acknowledgement

This research was supported by the Grant-in-Aid for Scientific Research from the Ministry of Education, Science and Culture of Japan and the Waseda University Grant for Special Research Projects.

The authors thank Mr. Mori, research student, for their experimental assistance.

References

- [1] I. Kato et al : Trans. IEICE, C- II , J80, 11, 101-110(1997)
- [2] T. Kamiko et al : The 13th Symposium on Plasma Processing, 1A1-4(1996)

Si LUMINESCENCE MATERIAL FABRICATED USING MPCVD COAXIAL LINE TYPE

Nobuyuki KOSHII, Kazuhiro WATANABE and Isamu KATO
越地 信行、渡部 一博、加藤 勇

School of Science and Engineering,
Waseda University, 3-4-1 Ohkubo, Shinjuku-ku, Tokyo 169, JAPAN
早稲田大学理工学部 〒169 東京都新宿区大久保 3-4-1

Abstract

In this study, using MPCVD coaxial line type we fabricate the Si nanoball films with varying DC substrate bias voltage (V_{dc}) in order to vary an ion bombardment energy, and discuss how the ion bombardment affects the properties and optical characteristics of the Si nanoball. As a result, the size of nanocrystal Si(nc-Si) in the Si nanoball increases a little with increasing the ion bombardment energy. And it is considered that the PL intensity increases because the number of nc-Si in the Si nanoball increases by the ion bombardment.

1. Introduction

We have developed the double tubed coaxial line type microwave plasma CVD (MPCVD) apparatus. Using this apparatus we have reported that an ion bombardment energy can be controlled by varying V_{dc} when a-Si:H films are fabricated in the low pressure (which is about 4.2mTorr) in the deposition chamber⁽¹⁾. Also we have reported that a Si nanoball film is fabricated in the high pressure (which ranges between 55mTorr and 400mTorr) in the deposition chamber. In this paper we report that how the ion bombardment affects the qualities and optical characteristics of the Si nanoball film which is grown by the volume reaction in the high pressure. In addition, at the day of presentation we will report the characteristic of Si nanoball deposited with varying the rate of dissociation of SiH_4 .

2. Experiment

Figure 1 shows the configuration of the MPCVD apparatus. In this apparatus, a discharge plasma is only created in the cavity region. In the deposition chamber, a spatial afterglow plasma without supply of the microwave power is created by gas flow and diffusion. The discharge region of the apparatus has the double tubed structure that consists of the fused quartz outer discharge tube and the

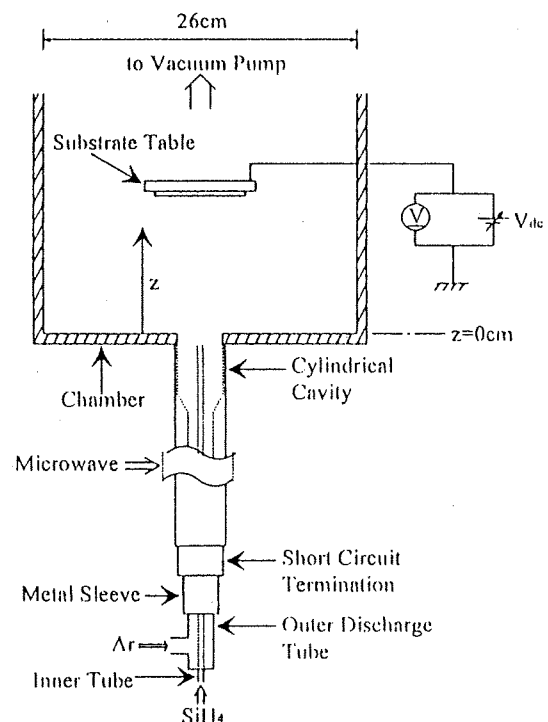


Fig.1 The double tubed coaxial line type MPCVD apparatus

stainless steel inner tube. The Ar gas is fed to the outer discharge tube and the SiH₄ gas is fed to the inner tube. Ar atoms are ionized in the cavity region by the microwave power. The inner tube leads the SiH₄ gas to the discharge tube end, then the SiH₄ is dissociated by the collision with the Ar plasma particles. When the gas pressure is high in the deposition chamber, SiH_x radicals are spatially reacted several times in the process of the transportation to the substrate table, and become the Si nanoball. After that, the Si nanoballs are deposited on the substrate table.

The experimental conditions are as follows. The axial distance from the discharge tube end is defined as z. The microwave power is 150W. Ar gas flow rate is 110ml/min and SiH₄ gas flow rate is 30ml/min. The substrate table is placed at z=10cm. The gas pressure in the deposition chamber is set at 250mTorr by controlling the exhaust valve. Under these conditions, Si nanoball films are fabricated when V_{dc} is varied from -80V to +40V. The Photoluminescence(PL) spectrum from these films is measured under R.T. at the vacuity of 5 × 10⁻²Torr to avoid an oxidation of the films by laser heating. The excitement light is Ar⁺ laser whose wavelength is 514.5nm.

3. Results and Discussion

From SEM picture, Si nanoballs are observed, and the size of Si nanoballs are about 20nm. Figure 2 shows the dependence of the size of the Si nanoball on V_{dc}. The plots in this figure are measured from SEM pictures. The size of the particles are almost constant with varying V_{dc}.

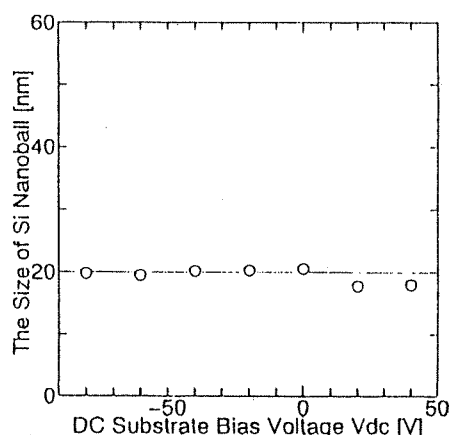


Fig.2 Dependence of the size of Si nanoball on V_{dc}

Figure 3 shows the PL spectra from Si nanoball films which are oxidized by heating at 80°C in the atmosphere for 48 hours. Before the oxidation films, the PL intensity can be seen a little, but the PL intensity increases as the oxidation time becomes longer. From now, we express that “the films just after leak” is “the films before the oxidation”, and “the films after heating at 80°C in the atmosphere for 48 hours to oxide” is “the films after the oxidation”.

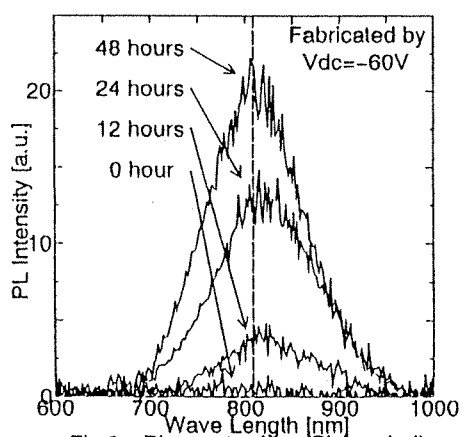


Fig.3 PL spectra from Si nanoball oxidized for 0,12,24,48 hours

Figure 4 shows the two FTIR spectra of the films before the oxidation and the films after the oxidation. From the absorption spectrum of the film before the oxidation, much absorption of the SiH₃ and (SiH₂)_n can be seen. But from the absorption spectrum after the oxidation, absorption of SiH₃ and (SiH₂)_n cannot be seen and much absorption of SiO can be

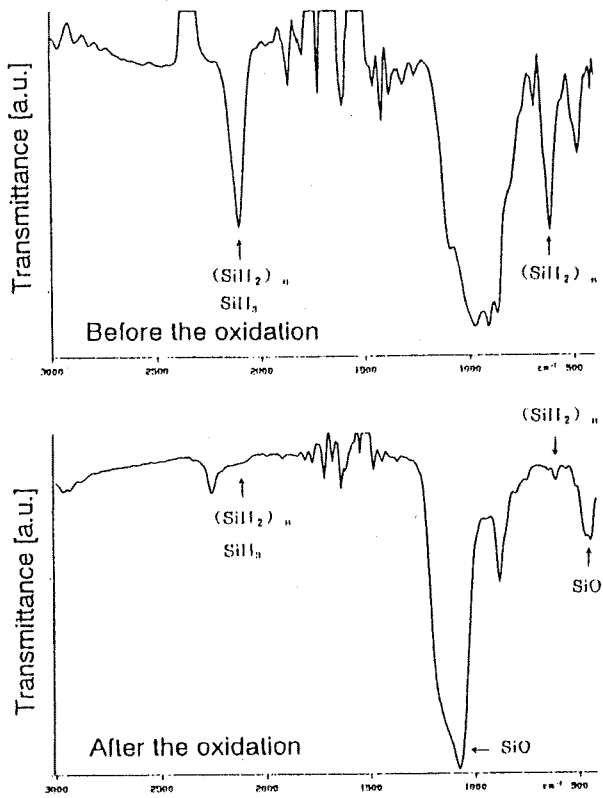


Fig.4 FTIR spectra from films before the oxidation and after the oxidation

seen. This is because $(SiH_2)_n$ and SiH_3 become SiO by the oxidation. The figs.3 and 4 are measured about the film fabricated at $V_{dc}=-60V$, the same tendency can be seen from the films fabricated at other values of V_{dc} .

From the profile of X-ray diffraction, it is clear that the nc-Si exist in the Si nanoball. Then, the size of the nc-Si is estimated from integral width of profile by using equation of Scherrer. Figure 5 shows the dependence of the size of nc-Si on V_{dc} . The size varies from 3.7nm to 4.3nm when V_{dc} are varied from +40V to -80V. Namely, the size of nc-Si increases with increasing the ion bombardment energy.

Figure 6 shows the dependence of the size of nc-Si on the peak position at PL spectra. The peak positions are about 810nm without regard to the size of nc-Si.

Figure 7 shows the dependence of the PL intensity at peak position on the PL spectrum of the size of nc-Si. Figs. 6 and 7 are measured about the films after the oxidation. The PL

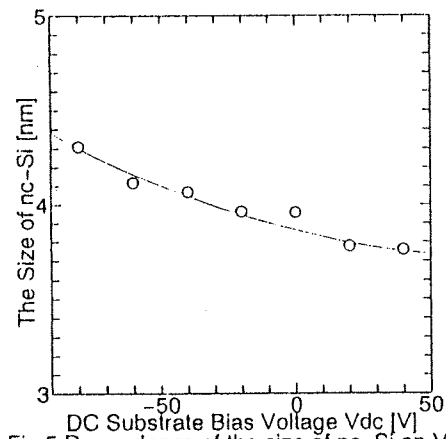


Fig.5 Dependence of the size of nc-Si on V_{dc}

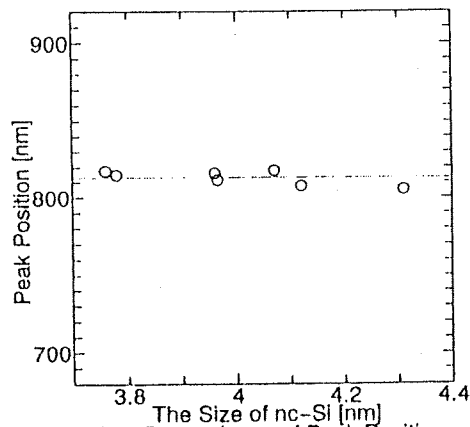


Fig.6 Dependence of Peak Position on the size of nc-Si

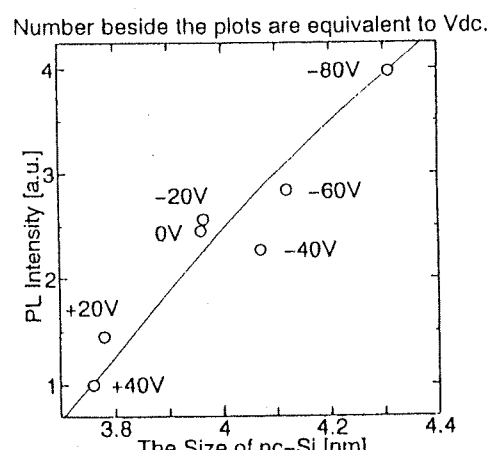


Fig.7 Dependence of PL intensity on the size of nc-Si

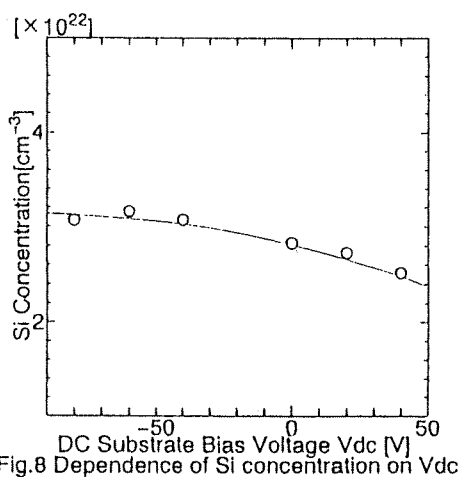


Fig.8 Dependence of Si concentration on Vdc

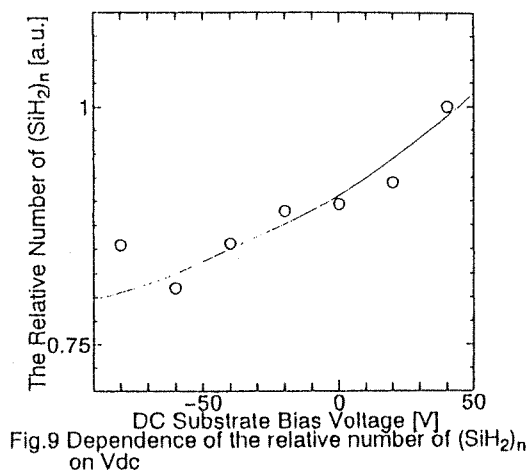


Fig.9 Dependence of the relative number of (SiH₂)_n on Vdc

intensity increases with increasing Vdc negatively. As a result, the PL intensity at 4.3nm is 4 times as much as that at 3.7nm. Namely, the PL intensity increases when the ion bombardment energy increases. Generally, it is said that the PL intensity does not change, even if the size of nc-Si varies about 1nm. And then it is estimated that the number of nc-Si in the Si nanoball increases 4 times.

We have reported that film surface heating effect of an ion bombardment has an increasing effect of Si concentration and disconnection effect of H atoms⁽³⁾. Then, figure 8 shows the dependence of Si concentration which is measured by RBS on Vdc. Si concentration increases with increasing Vdc negatively. Figure 9 shows the dependence of relative number of (SiH₂)_n which becomes SiO by oxidation on Vdc. The relative number of (SiH₂)_n decreases with increasing Vdc negatively. According to figs.8 and 9, Si concentration increases and (SiH₂)_n concentration decreases by the ion bombardment. As the results, it is estimated that the number of nc-Si in the Si nanoball increases. Namely it is considered that the PL intensity increases depending on the number of nc-Si.

4. Conclusion

The size of nc-Si increases a little with increasing an ion bombardment energy. The PL intensity increases with increasing an ion bombardment energy, because the number of nc-Si in the Si nanoball increases by an ion bombardment.

5. Acknowledgement

A part of this work was supported by the Grant-in-Aid for scientific research from the ministry of Education, Science, and Culture, Also a part of this work was supported by a Waseda University Grant for Special Research Project in 1997. The authors thank Mr.Kawahara, research student, for his experimental assistance.

Reference

- (1) M.Yamashita, H.Ogihara, and I.Kato: Proc.13th Sympo. Plasma Processing, 109(1996)
- (2) N.Koshiji, I.Kato: JSAP, Extended Abstracts 30-p-B-15, (The 44th spring Meeting, 1997)
- (3) H.Ogihara, H.Iizuka, N.Koshiji and I.Kato: ICRP-3/SPP-14, Iva-6(1997)

EFFECT OF ION BOMBARDMENT DURING a-Si:H FILM GROWTH

a-Si:H 膜成長中のイオン衝撃効果

Hiroataka OGIHARA, Naoyuki IWATA and Isamu KATO

荻原博隆、岩田直之、加藤勇

School of Science and Engineering, Waseda University,

3-4-1 Okubo, Shinjuku-ku Tokyo 169

早稲田大学理工学部、〒169 東京都新宿区大久保3-4-1

Abstract Generally in a plasma CVD method, a substrate table is placed in the discharge plasma and films are fabricated under the ion bombardment. We have studied influences of the ion bombardment on a-Si:H films and clarified that an ion bombardment has a film surface heating effect that excite vibration of lattice of atom surface and ion implanting effect in films [1][2][3]. In this paper we use the sheath voltage (V_{sh}) on the film surface subtracted the plasma space potential from DC substrate bias voltage as parameter, fabricate a-Si:H films with varying substrate temperature and study the effect of ion bombardment.

1. Introduction

We have used the double tubed coaxial line type microwave plasma CVD system to study the effect of ion bombardment during fabrication of a-Si:H films. In this system, the microwave power is confined in the cavity. In the deposition chamber, a spatial after-glow plasma is formed by the gas flow and diffusions because the microwave power is not injected into the plasma in the chamber. Figure 1 shows the configuration of the MPCVD system. The Ar gas is fed to the outer discharge tube and the SiH_4 gas is fed to the inner tube. The Ar gas is ionized in the cavity region by the microwave power. The SiH_4 gas flows to the discharge tube end through the inner tube, then the SiH_4 is dissociated by the collision with the Ar plasma particles. In this paper, the sheath voltage (V_{sh}) on the film surface subtracted the plasma space potential from DC substrate bias voltage is set on several points, and the a-Si:H films are fabricated with varying substrate temperature.

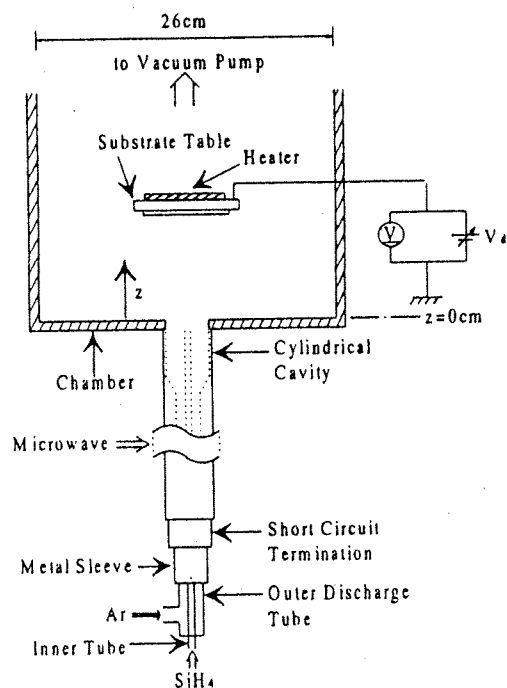


Fig.1. Configuration of the MPCVD system

2. Experiment

The axial distance from the discharge tube end is defined as z shown in Fig.1. The

substrate table area is 40 cm² and the table is placed at z=10 cm. Ar gas flow rate is 110 ml/min and SiH₄ gas flow rate is 30 ml/min. The DC substrate bias voltage is varied +40V, 0V and -20V. Then each V_{sh} is 0V, -17V and -37V[2]. The substrate temperature (T_s) is varied from R.T. to 400°C.

3. Result and Discussion

The dependence of Si concentration on T_s and V_{sh} is shown in Fig.2. Because the dependence of Si concentration on T_s is measured under the condition of V_{sh} = 0 V, there is no ion bombardment on the film surface. This dependence is equivalent to the dependence of Si concentration on the film surface temperature. Here we suppose that the dependence of the Si concentration on V_{sh} is not influenced by ion implanting effect but only influenced by film surface heating effect. Therefore the dependence of Si concentration on T_s is equivalent to that on V_{sh}. So we have the following equation.

$$T_s = f(V_{sh}) \quad (1)$$

Hence the graphs of the dependence of Si concentration on T_s and that on V_{sh} can be fitted together by adjusting the scale of the dependence of Si concentration on V_{sh}. First, the Si concentration at T_s = 28°C and that at V_{sh}=0V are the same because they are deposited under the same condition. The two points at V_{sh} = -95 V and T_s = 250 °C in the curves of the dependence of Si concentration on T_s and V_{sh} in Fig.2 are fitted together, then the two curves of the dependence of Si concentration on T_s and V_{sh} are shown in Fig.3. Hence, the above-mentioned supposition is confirmed to be correct. We can get the following equation using the experimental values.

$$T_s = -2.32 \times V_{sh} + 28 \quad (2)$$

In this equation, 28 means the room temperature and $-2.32 \times V_{sh}$ means the amount of rising film surface temperature caused by the ion bombardment. Namely, the film surface temperature is equivalent to 68 °C when V_{sh} is -17V and 115 °C when V_{sh} is -37V.

The dependence of Si concentration on T_s is shown in Fig.4. Here the parameter is V_{sh}.

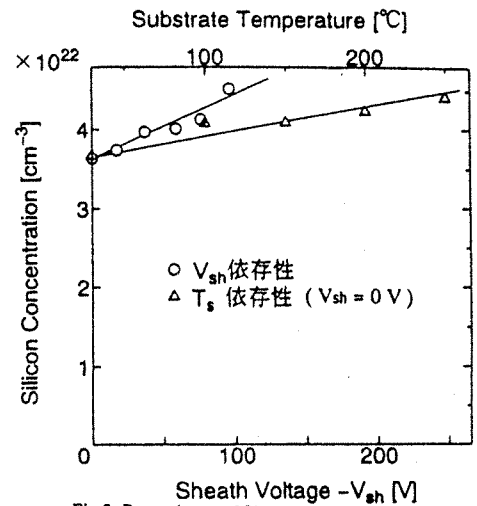


Fig.2. Dependence of Si concentration on T_s and V_{sh}.

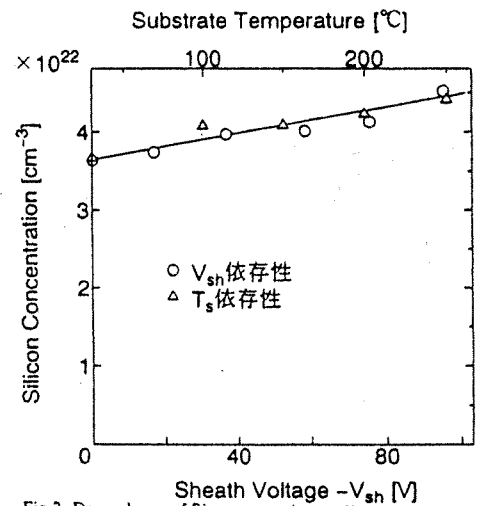


Fig.3. Dependence of Si concentration on T_s and V_{sh} (shift)

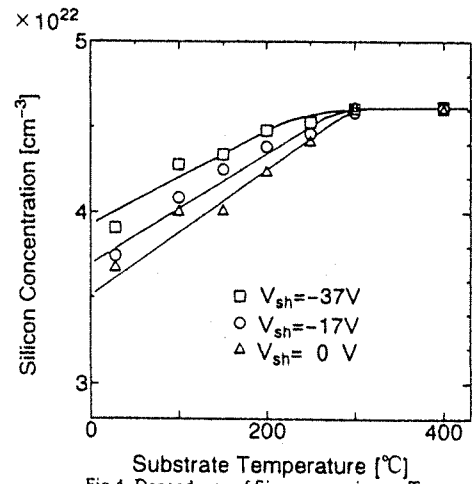


Fig.4. Dependence of Si concentration on T_s.

The Si concentration increases when T_s is increased. This is a reason why the vibration of lattice in the film is excited and the structure relaxation is occurred. The Si concentration is increased by the film surface heating effect when V_{sh} is increased.

The dependence of Si concentration on T_s is shifted 40 °C when V_{sh} is -17V and 87 °C when V_{sh} is -37V considering the film surface heating effect in fig.5. We can fit together three curves as shown in fig.5. This reason is that the Si concentration is influenced by not the ion implanting effect but the film surface heating effect. From this, the above-mentioned equation appearing the rise of film surface temperature is reconfirmed to be correct.

The dependence of deposition rate on T_s is shown in Fig.6. Here the parameter is V_{sh} . The deposition rate decreases when T_s is increased. The deposition rate decreases because the the film density increases by the film surface heating effect mentioned above when V_{sh} as parameter increases.

The dependence of deposition rate on T_s is shifted 40 °C when V_{sh} is -17V and 87. °C when V_{sh} is -37V considering the film surface heating effect in Fig.7. From the figure each graph of the deposition rate is fitted until T_s gets to 130 °C. But after that T_s gets to 130 °C, it decreases faster when V_{sh} becomes high. This effect of the decrease of the deposition rate when V_{sh} increases is the ion bombardment effect. It is clear that ion implanting effect does not appear until T_s gets to about 130°C but appears markedly after that T_s gets to about 130 °C.

The dependence of the dangling bond density on T_s is shown in Fig.8. Here the parameter is V_{sh} . The dangling bond density decreases until T_s gets to 150 °C, but after that it increases when V_{sh} is 0 V. The dangling bond density decreases until T_s gets to 200 °C, but after that it increases when V_{sh} is -17 V.

The dangling bond density decreases until T_s gets to 250 °C, but after that it increases when V_{sh} is -37 V. When T_s increases, the structure relaxation occurs and then the dangling bond density decreases. When T_s increases more than T_s that is minimum point of the dangling bond density, the hydrogen atoms are disconnected and then the dangling bond destiny increases. When V_{sh} increases and the ion bombardment energy increases,

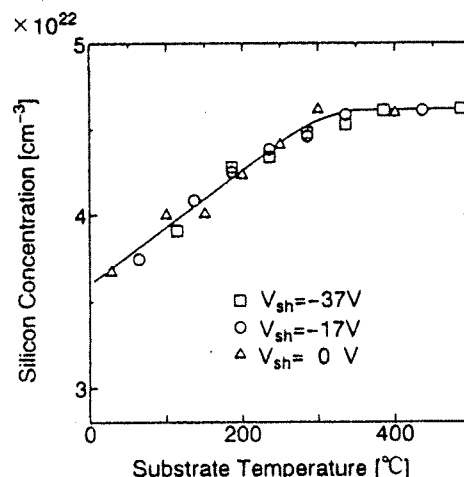


Fig.5. Dependence of Si concentration on T_s (shift)

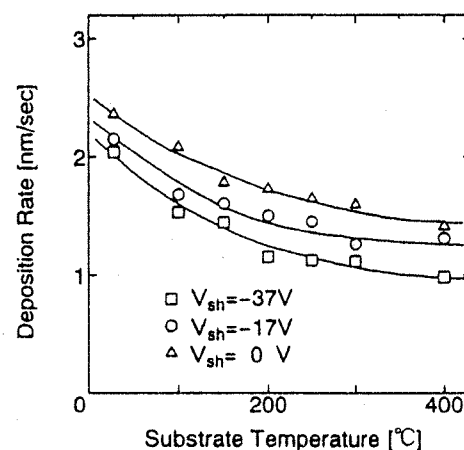


Fig.6. Dependence of deposition rate on T_s

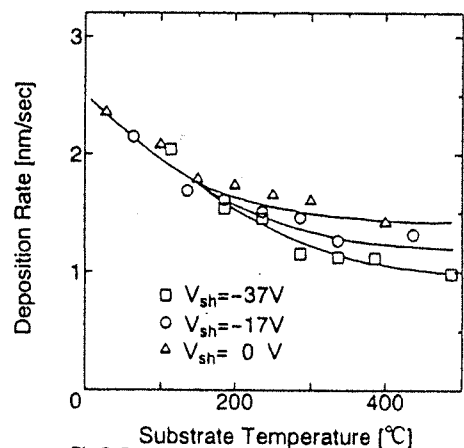


Fig.7. Dependence of deposition rate on T_s (shift)

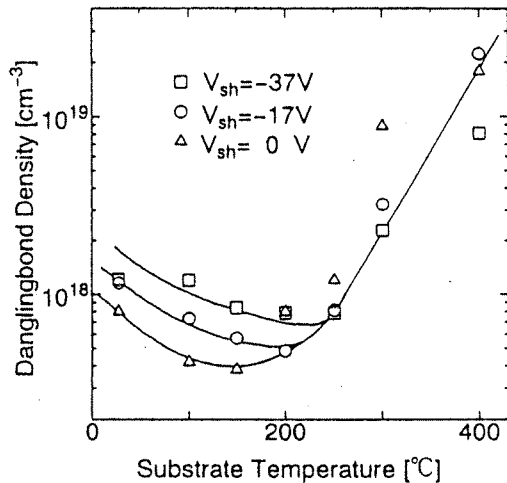


Fig.8. Dependence of dangling bond density on T_s

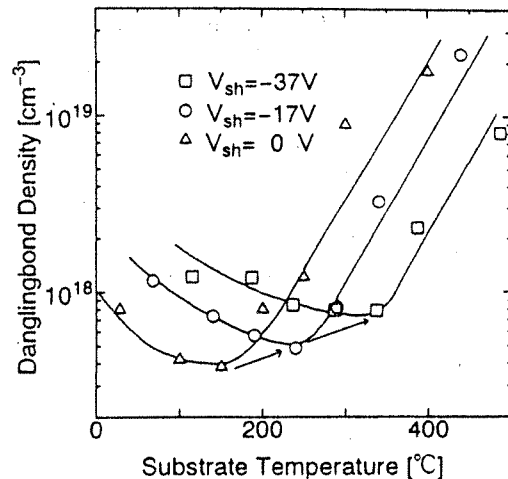


Fig.9. Dependence of dangling bond density on T_s (shift)

the film structure is destroyed and the dangling bond density increases. It is clear that the substrate needs to be heated higher to occur the structure relaxation under this ion bombardment.

The dependence of dangling bond density on T_s is shifted 40 °C when V_{sh} is -17 V and 87 °C when V_{sh} is -37 V considering the film surface heating effect are shown in Fig.9. When the curves at $V_{sh} = 0$ V in the fig.9 is shifted along the arrows, that is fitted with curves at $V_{sh} = -17$ V and $V_{sh} = -37$ V. This amount of shift is that of the destruction of the film structure caused by the ion implanting effect. Namely, the film of which dangling bond density is low can be fabricated at lower temperature avoiding the ion bombardment.

4. Conclusion

From the relation between the dependence of Si concentration on T_s and V_{sh} , a relation between T_s and V_{sh} is shown the following experimental equation,

$$T_s = - 2.32 \times V_{sh} + 28$$

From the figure of the deposition rate, it is clear that the ion implanting effect does not appear at low temperature but appears after that T_s gets to about 130 °C.

It is clear that if there is no ion bombardment, the film of which dangling bond density is low can be fabricated at lower temperature.

5. Acknowledgment

This work was supported by the Grant-in-Aid for scientific research from the ministry of Education, Science, and Culture. And this work was also supported by Waseda University Grant for Special Research Projects in 1997. The authors thank Mr. Kamigaichi, research student, for his experimental assistance.

References

- [1] I. Kato, T. Yoneda and T. Matsushita: Trans. IEICE, C- II, J77, 9, 384-391 (1994)
- [2] M. Yamashita, H. Ogihara and I. Kato: Proc. 13th Sympo. Plasma Processing, 109 (1996)
- [3] H. Ogihara, H. Iizuka, N. Koshiji and I. Kato: ICRP-3/SPP-14, Iva-6 (1997)

縦磁界印加による Ar プラズマの安定化

加藤 勇[†] 山岸 俊浩^{††} 森田 義則^{††} 神子 太郎^{††}

Stabilization of Ar Plasma by Applying Longitudinal Magnetic Field

Isamu KATO[†], Toshihiro YAMAGISHI^{††}, Yoshinori MORITA^{††}, and Taro KAMIKO^{††}

あらまし 本研究は、2重管式同軸線路形マイクロ波プラズマCVD装置の放電領域部分にガス流に平行な磁界(縦磁界)を印加して、プラズマの径方向への拡散を抑制することにより、低ガス圧で安定なプラズマを得ることを目的とする。プラズマの安定性は、電子飽和電流の変動幅および経時変化により検討した。Arガス流量が30, 20, 15 [ml/min]の場合は、無磁界においてもプラズマの安定性は良いが、磁界を印加することにより安定性の向上が見られる。また、Arガス流量が10, 8 [ml/min]の場合、無磁界ではプラズマは不安定であるが、約500 [Gauss]以上の磁界を印加することにより放電管壁への電子の拡散が抑制され、その結果放電管壁での電子の消滅が減少することにより、低ガス圧(低ガス流量)においても安定なマイクロ波プラズマが得られることを明らかにした。

キーワード マイクロ波プラズマCVD, 縦磁界, 安定性, 径方向拡散, 低ガス圧

1. ま え が き

プラズマCVDは薄膜の作製に用いられ、電子デバイス、光子デバイスの作製に欠かせない手法として注目されている。そこで、CVDに適したプラズマを実現するために、CVDに用いることを前提としたプラズマの研究が多くの研究機関において行われている。当研究室も、良質な水素化アモルファスシリコン膜や窒化シリコン膜を作製するためのプラズマの研究を行っている[1], [2]。

従来、プラズマ源として一般によく用いられているRFプラズマCVD装置などのプラズマ発生装置では、膜堆積領域に電力が注入されているため、膜表面へのイオン衝撃が大きいことで膜質が劣化するという問題があった。そこで当研究室では、マイクロ波を所定の領域に閉じ込めて、膜堆積室内には電力注入のない空間的アフターグロープラズマを生成できる2重管式同軸線路形マイクロ波プラズマCVD装置の研究開発を

行ってきた[3]~[7]。そして、本装置で薄膜を作製するための基礎的なデータとして、堆積室内におけるプラズマパラメータ等の測定を行っている[1]~[3]。

近年、プラズマの高密度化、大口径化に伴うプラズマの均一化、低ガス圧下での製膜の3点がプラズマプロセスの発展のために要求されており、これを実現するために、ECRプラズマ装置をはじめとした各種のプラズマ発生装置に関する研究が盛んに行われている[9]。当研究室では本装置により、低ガス圧下での製膜と大口径化に伴うプラズマの均一化については、ほぼ達成できるという結果を得ている[1], [2], [6], [7], [9], [10]。そこで、本研究においては、より低いガス圧において、高密度で安定なプラズマを得るために、本装置の放電領域に縦方向磁界を印加し、放電管の径方向へのプラズマの拡散を抑えることによるプラズマの安定化について検討する。

2. 実 験

実験には、図1に示す2重管式同軸線路形マイクロ波プラズマCVD装置を用いる[4], [5], [10]。プラズマ生成条件として、マイクロ波入射電力、マイクロ波反射電力をそれぞれ100, 30 [W]一定とした。外側放電管には放電ガスとしてArガスを流し、ガス流量は

[†] 早稲田大学バイオ・フォトリクス新素材研究施設, 東京都 Materials Research Laboratory for Bioscience and Photonics, Waseda University, Tokyo, 169 Japan

^{††} 早稲田大学理工学部電子・情報通信学科, 東京都 School of Science and Engineering, Waseda University, Tokyo, 169 Japan

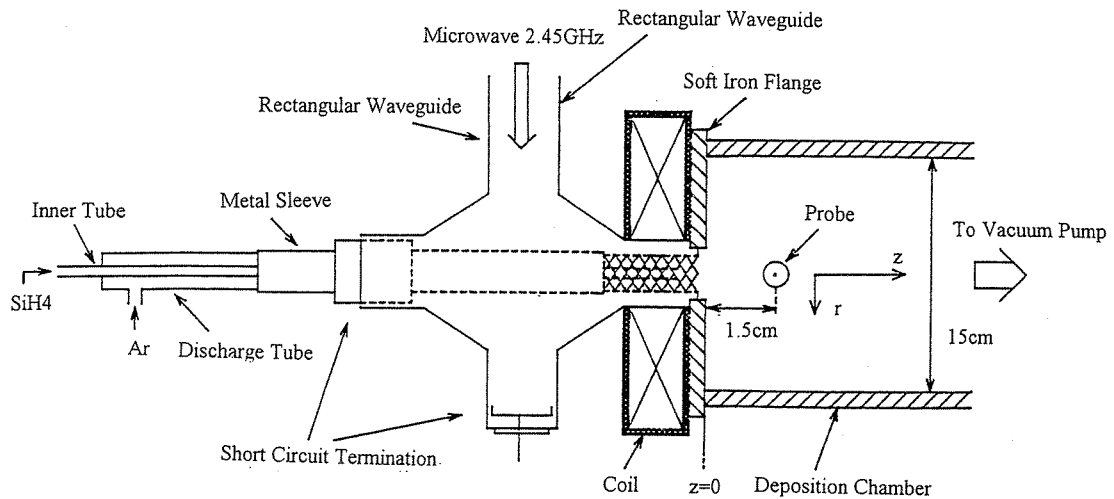


図1 2重管式同軸線形マイクロ波プラズマCVD装置
Fig. 1 Double tubed coaxial line type microwave plasma CVD system.

8~30 [ml/min] と変化させた。ステンレス鋼製の内側管には SiH₄ などの材料ガスを流せるようにしているが、本実験においては使用していない。堆積室内のガス圧は、Ar ガス流量によって、0.5~3.0 [mTorr] まで直線的に変化した。縦磁界印加コイル(図1参照)に流す電流は 0~6 [A] とした。そのときに、コイルの中心で発生する磁束密度は 0~1986 [Gauss] である。

本装置の堆積室は、内直径 15 [cm] の円筒形である。放電管端、すなわち堆積室のフランジの内壁面の位置から堆積室の軸方向への距離を z 、中心軸からの径方向への距離を r と定義する(図1参照)。安定性の測定にはシングルプローブ法を用いている。プローブは直径 0.05 [cm]、長さ 1 [cm] の円筒プローブである。また、測定位置は、 $z=1.5$ [cm]、 $r=0$ [cm] とした。なお、内管端の位置は、本装置による製膜時の状態である、 $z=-2.0$ [cm] の点とした[5]。

3. コイル特性

本研究は、プラズマに磁界を印加したときにプラズマにどのような変化があるかを調べ、CVD に適した安定なプラズマを得ることを目的としているので、本装置を CVD に利用する場合に、磁界を印加しないときには現れなかった問題点は極力なくすようにすべきである。すなわち、製膜領域に強い磁界が漏れているとプラズマが異方性をもち、膜質の均一性が失われる等の問題を生じる可能性がある。

そこで本装置においては、まずコイルの周囲を軟鉄板で覆うことにより磁気回路を形成させ、更に堆積室とコイルの間にあるフランジを厚さ 1.5 [cm] の軟鉄製

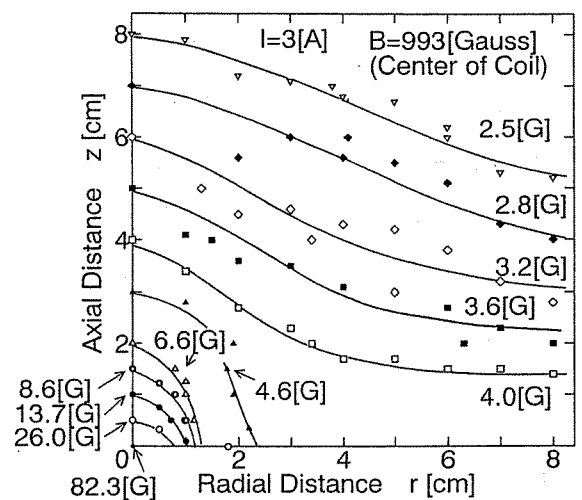


図2 磁束密度の空間分布(コイル外部)
Fig. 2 Spatial distribution of magnetic flux density. (outside of coil)

とすることにより(図1参照)、堆積室内に磁界が漏れないように設計してある。

図2に堆積室内における磁束密度の空間分布を示す。図はコイル電流を 3.0 [A] としたときのものである。図より z 軸上における磁束密度は $z=0\sim 2$ [cm] の範囲で 82.3~6.6 [Gauss] と急激に減少し、その後 z が増加するに従い 2.5 [Gauss] まで徐々に減少することがわかる。また $z > 4$ [cm] の範囲では磁束密度の r 方向への変化はわずかであることがわかる。以上のことから、堆積室内のプラズマに異方性を生じさせるような磁界は漏れていないと言える。

次に、縦磁界が放電領域(図1の網掛け領域)におけるプラズマに及ぼす効果を検討するために、放電領域

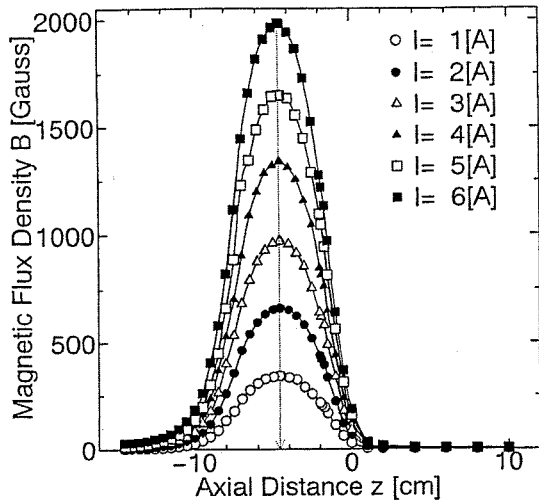


図3 磁束密度の空間分布 (z 軸上)
Fig. 3 Spatial distribution of magnetic flux density. (on z axis)

における磁束密度の測定を行った。

図3に $r=0$ [cm], すなわち z 軸上における磁束密度の測定結果を示す。図より磁束密度はコイルの電流値 I に比例して増加していることがわかる。また z 軸上で磁束密度が最大となるのは、 $z=-4.6$ [cm] の点であり、ほぼコイルの中心と一致している。以後、本論文において用いる磁束密度の値は、すべてコイルの中心での磁束密度と定義する。

以上の結果から、印加磁界は放電プラズマ、すなわち図1の放電端の網線をかけた部分のプラズマに影響を及ぼし、堆積室内におけるプラズマ、すなわち空間的アフターグロープラズマには影響を及ぼさないと考えられる。

ここで磁界がプローブ測定に与える影響について検討しておく。まず、前述のようにプローブ位置を $z=1.5$ [cm] としたのは、後述の図7に示すように、プローブ電流を測定上十分な値にするためである。次に $z=1.5$ [cm], $r=0$ [cm] における磁束密度は図2, 3から明らかのように、コイル電流が9[A]と最大の場合においても17.2[Gauss]である。すなわち、このプローブ位置においては、このような低磁界であるので、プローブ測定に及ぼす磁界印加の影響はないと言える。

4. 結果と考察

無磁界時において、Arガス流量が8, 10 [ml/min]のときの、低ガス圧のArプラズマのプラズマパラメータを測定する際にプローブ I_p-V_p 特性を観察したところ、電子電流反駁領域および電子電流飽和領域におい

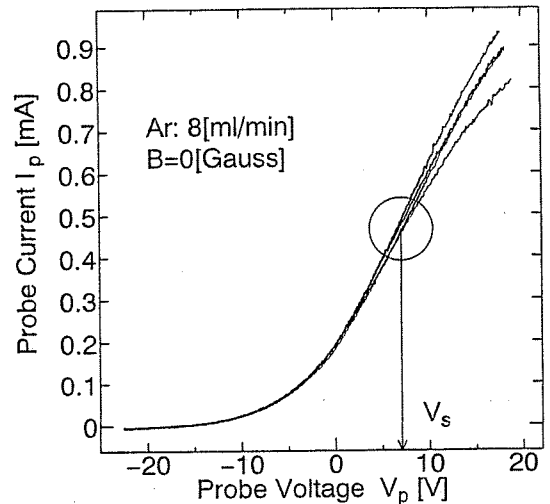


図4 不安定なプラズマにおけるプローブ I_p-V_p 特性
Fig. 4 Probe I_p-V_p characteristic in unstable plasma.

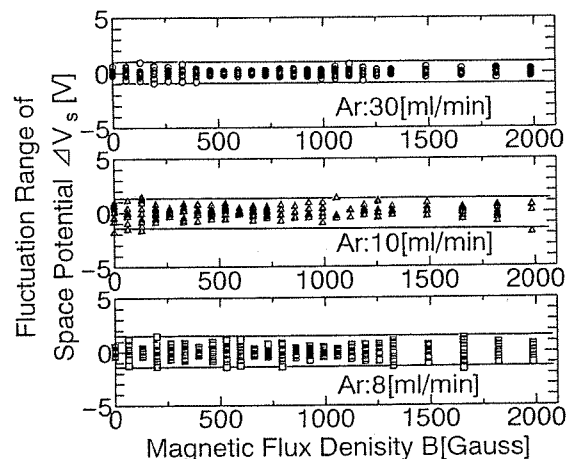


図5 空間電位 V_s の変動幅の磁束密度依存性
Fig. 5 Dependence of fluctuation range of space potential V_s on magnetic flux density.

て波形が時間的に大きく変動することがわかった。図4にArガス流量が8 [ml/min]の場合のプローブ I_p-V_p 特性を一例として示す。これらの波形は、10 [ms]ごとに連続的にスイープした波形から任意に四つ選んだものであり、波形にばらつきがあることがわかる。そこで、まずプラズマの空間電位 V_s (図4参照) の変動に注目してプラズマの安定性を検討することを試みた。図5に空間電位 V_s の変動幅の磁束密度依存性を示す。これは各々の磁束密度での V_s の測定値を平均し、その平均値を各々の磁束密度での V_s と決めたとときに、個々の測定値と平均値 V_s との差 ΔV_s を示したものである。図より、どのガス流量においても、 V_s は印加する磁束密度によらずほぼ一定の変動幅をもち、また、その変

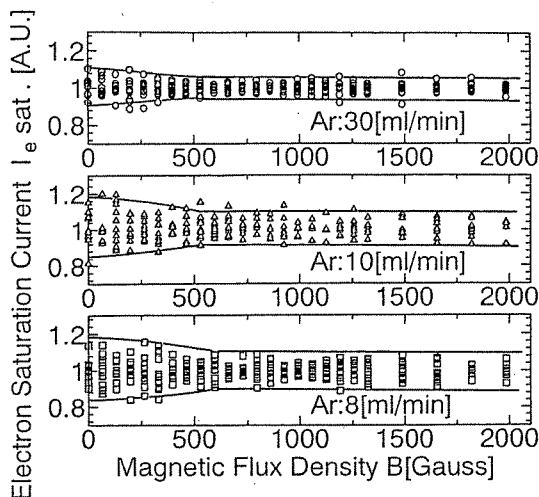


図6 電子飽和電流 I_{esat} の変動幅の磁束密度依存性
 Fig. 6 Dependence of fluctuation range of electron saturation current on magnetic flux density.

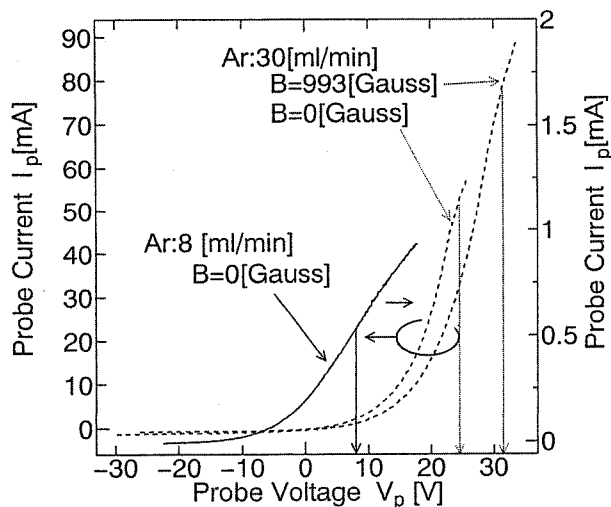


図7 プローブ I_p-V_p 特性のガス流量と磁束密度による違い
 Fig. 7 Difference in probe I_p-V_p characteristic by gas flow rate and magnetic flux density.

変動幅は $\pm 1 \sim 2$ [V] 程度でわずかであることがわかる。このことより、 V_s における測定値の変動は印加する磁束密度に依存するよりも、むしろデータを処理する際に生じる誤差に起因していると考えられる。従って、 V_s の変動からは印加磁界の強弱によるプラズマの安定性は議論できない。但し、低ガス圧(すなわち、低ガス流量)のプラズマの方が変動幅が大きいことから、Ar ガス流量が 30 [ml/min] の場合には印加磁界の有無にかかわらず低ガス圧のものより安定性が良いと言える。

このように、プローブ I_p-V_p 特性の変動は V_s の変動には大きく影響していないので、 V_s の変動から印加磁界の強弱によるプラズマの安定性を検討することには

無理があることがわかった。そこで、次に図4のプローブ I_p-V_p 特性における縦軸方向の変動を調べることにし、プラズマの安定性を検討することにする。

図6に電子飽和電流 I_{esat} 、すなわち $V_p = V_s$ のときのプローブ電流 I_p の変動幅の磁束密度依存性を示す。この図における I_{esat} は、各々の磁束密度での I_{esat} の平均値で規格化してある。この図より、どのガス流量においても約 500 [Gauss] 以上の磁界を印加することにより、 I_{esat} の変動幅が小さくなることがわかる。すなわち、どのガス流量においても約 500 [Gauss] 以上の磁界を印加することによりプラズマの安定性が向上することがわかる。なお、ガス流量が大きい場合 (30 [ml/min]) においては、もともとプラズマがほぼ安定であるので、その変化量は小さい。

上述の実験結果から、磁界を印加することにより I_{esat} の変動幅が減少することがわかったので、このことを更に詳しく検討するために、各々のガス流量および磁束密度における V_s (前述の空間電位の測定値の平均値) に等しい一定電圧をプローブに印加し、 I_{esat} の経時変化を測定することにより、印加磁界がプラズマの安定性に及ぼす効果を次に検討する。すなわち図7に示すようにガス流量および印加する磁束密度により V_s が大きく変化するので、すべての実験条件においてプローブ電圧 V_p を同一とすると、 V_p の値が V_s とはならない場合には、電子飽和電流を測定していることにはならないので客観的な安定性の測定にはならない。そこで、 V_p の値をそれぞれの実験条件での V_s とした。図7に示すように、例えば、Ar ガス流量が 30 [ml/min] で印加磁束密度が 0 [Gauss] のときには、 $V_s = 25$ [V] であるという結果がプローブ測定により得られているので、この実験条件のときには $V_p = 25$ [V] としてプローブ電流の経時変化を測定している。他の実験条件においても V_p を同様に決定している。

図8(a), (b), (c)にその結果を示す。図8(a)より、Ar ガス流量が 30 [ml/min] の場合には、どの磁束密度においても I_{esat} は時間的に一定であることがわかる。このことより Ar ガス流量が 30 [ml/min] の場合には印加する磁束密度によらずプラズマの安定性は良好であると言える。図8(b), (c)より Ar ガス流量が 10, 8 [ml/min] の場合には、無磁界時には I_{esat} は時間的に大きく変化するが、磁界を印加することにより変動割合が小さくなることがわかる。このことより、無磁界時には不安定な低ガス流量、すなわち低ガス圧の Ar プラズマにおいて縦磁界を印加することにより安定化で

ることがわかる。

また、Ar ガス流量が 15, 20 [ml/min] の場合にも同様の実験を行っているが、Ar ガス流量が 30 [ml/min] の場合とほぼ同様、無磁界においても安定性はよく、磁界を印加しても大きな変化は見られなかった。

すなわち、ガス圧を低下させれば、電子の生成割合が減少し、放電は不安定となり、更には放電しなくなる。そこで、縦磁界を印加して、電子の径方向への拡散を抑制すれば、電子の消滅割合が小さくなるので、より低いガス圧でも放電を安定に維持できることになる。

なお、この安定化により、Ar ガス流量 8 [ml/min] に

おいて、堆積速度が無磁界時の 10 数倍以上速くなり、十分実用的な堆積速度 (約 0.5 nm/s) が得られている。

5. むすび

プローブ電流-電圧特性より、プラズマの安定性を評価する方法を検討し、プローブ電圧をプラズマ空間電位の平均値 V_s として、プローブ電流 (電子飽和電流) の時間的変動特性を測定することにより、各種条件下でのプラズマの安定性が同等に評価できることを示した。

この方法を用いて、本同軸線路型マイクロ波プラズマ発生装置 (図 1) において、① Ar ガス流量が 15, 20, 30 [ml/min] の場合には、無磁界でもプラズマの安定性は良いが、縦磁界を印加することにより安定性の向上が見られる、② Ar ガス流量が 8, 10 [ml/min] の低ガス圧の場合には、無磁界ではプラズマは不安定であるが、縦磁界を印加することにより安定するという結果を得た。これにより、プラズマに縦磁界を印加することにより放電管壁への電子の拡散が抑制され、その結果、放電管壁での電子の消滅割合が減少するので、低ガス圧においても安定なマイクロ波プラズマが得られることを明らかにした。

謝辞 本研究は文部省科学研究費の補助を得て行ったものである。

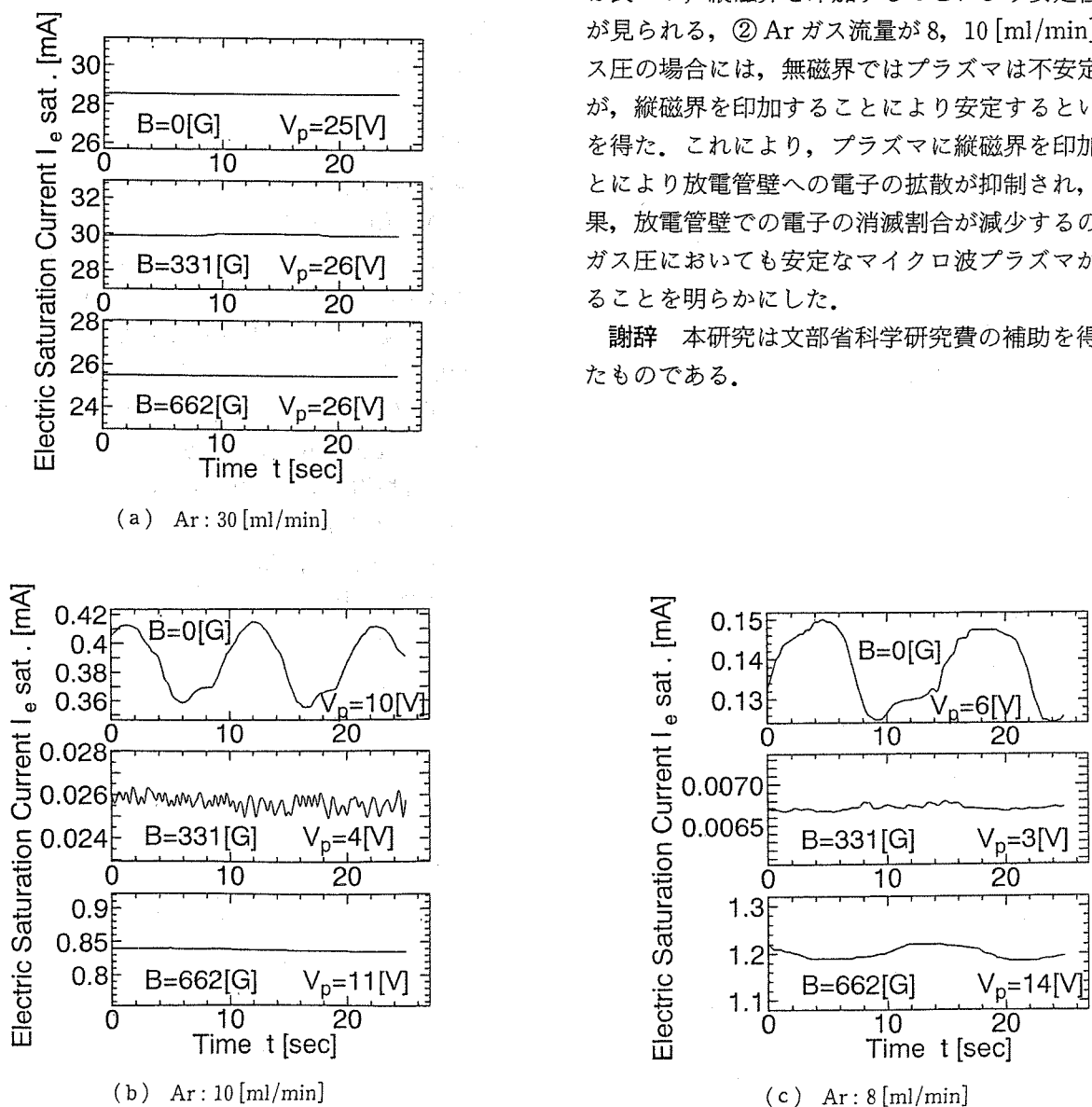


図 8 プローブ電流の経時変化
Fig. 8 Variation of probe current with time.

文 献

- [1] 加藤 勇, 白井隆志, 阪本 匡, “マイクロプラズマ CVD におけるプラズマパラメータの空間分布,” 電学論(A), vol. 112-A, no. 5, pp. 355-362, May 1992.
- [2] 加藤 勇, 下田 毅, 山岸俊浩, “二重管式同軸線路形マイクロ波プラズマ CVD における N_2/SiH_4 プラズマのパラメータの空間分布,” 電学論(A), vol. 116-A, no. 7, pp. 617-622, July 1996.
- [3] I. Kato, S. Wakana, S. Hara, and H. Kezuka, “Microwave plasma CVD system for the fabrication of thin solid films,” J. J. A. P., vol. 21, no. 8, pp. L470-L472, Aug. 1982.
- [4] I. Kato, S. Wakana, and S. Hara, “Microwave plasma CVD system to fabricate α -Si thin films out of plasma,” J. J. A. P., vol. 22, no. 1, pp. L40-L42, Jan. 1983.
- [5] 加藤 勇, 若菜伸一, “新しいプラズマ化学気相堆積装置,” 真空, vol. 26, no. 7, pp. 628-636, July 1983.
- [6] I. Kato, S. Hara, and S. Wakana, “Analysis of radial distribution of plasma parameters in a coaxial-line microwave discharge tube,” J. A. P., vol. 54, no. 9, pp. 4883-4888, Sept. 1983.
- [7] 加藤 勇, 加藤聖隆, 阪本 匡, “マイクロ波放電を用いたプラズマ化学気相堆積法,” 放電研究会資料, ED-91-60, pp. 141-150, 1991.
- [8] 菅井秀郎, “低圧力・高密度プラズマの新しい展開—ECR, ヘリコン波および誘導結合型プラズマ,” 応用物理学会誌, vol. 63, no. 6, pp. 559-567, June 1994.
- [9] I. Kato, K. Noguchi, and K. Numada, “Preparation of Silicon Nitride films at room temperature using double-tubed coaxial line-type microwave plasma chemical vapor deposition system,” J. A. P., vol. 62, no. 2, pp. 492-497, 1987.
- [10] 加藤 勇, 上田哲也, 畑中和久, “二重管式同軸線路形マイクロ波プラズマ CVD 法による a-Si:H 薄膜の基板温度特性,” 電学論(A), vol. 106-A, no. 8, pp. 35-41, Aug. 1986.

(平成 8 年 12 月 17 日受付, 9 年 5 月 23 日再受付)



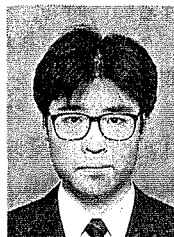
山岸 俊浩

平 6 早大・理工・電子通信卒, 平 8 同大大学院修士課程了。現在, 日立製作所汎用コンピュータ事業部勤務。在学中はマイクロ波プラズマに関する研究に従事。応用物理学会会員。



森田 義則

平 4 早大・理工・電子通信卒, 平 6 同大大学院修士課程了。平 9 同大学院博士課程退学。在学中はマイクロ波プラズマに関する研究に従事。



神子 太郎

平 5 早大・理工・電子通信卒, 平 9 同大大学院修士課程了。現在東芝情報・通信システム技術研究所勤務。在学中はマイクロ波プラズマに関する研究に従事。応用物理学会会員。



加藤 勇 (正員)

昭 42 早大・理工・電子通信卒。昭 48 同大大学院博士課程了。同年工博。同年早大勤務。昭 53 同大助教授。昭 54~56 マントバ大客員教授, カナダ国立研究会議の研究費を受け共同研究ならびに研究指導。昭 58 同大教授, 現在に至る。マイクロ波プラズマ CVD, 光子工学, レーザ工学, 電子物性工学, 計測工学, 光子材料, プラズマ・エレクトロニクス, 光量子エレクトロニクス, 半導体薄膜工学などの研究に従事。電気学会, 応用物理学会, テレビジョン学会, 日本真空協会, IEEE 各会員。

ナノ加工基板上への MBE 成長のための基礎検討

Fundamental study of MBE growth on nano-pattern-fabricated substrates

早稲田大学理工学部 ○池田晴申¹、高畑正浩¹、井巻克哉¹、宇高勝之^{1,*}、坂田治久²

¹Waseda University, ²KDD R&D Labs. ○H. Ikeda¹, M. Takahata¹, K. Imaki¹, K. Utaka^{1,*} and H. Sakata²
○600d0076@mn.waseda.ac.jp

【はじめに】化合物半導体微細量子構造は、量子ドットレーザに代表されるように従来にはない優れた特性を得られることが期待されており、現在サイズの揺らぎの改善や密度の増加、さらに位置制御に関して様々な方法による検討が行われている。そこで本研究では、微細量子構造の高密度化、サイズ均一化、および位置制御を目的とした、加工基板上への MBE による結晶成長を試みた。

【実験及び結果】EB リソグラフィと SiN 膜をマスクとした CH₄ 系 RIE により、直径 400nm~600nm 程度、深さ 20nm 程度のホールを 4μm 間隔で 2次元アレー状に作成した GaAs 基板上へ、MBE により InAs を 1nm~3.5nm 程度成長させた。この時の基板温度は 400°C、460°C、700°C であり、バッファ層、およびクラッド層は成長しなかった。その結果、全ての成長条件において、図 1 のようにホール部の淵に沿ってリング状の微細構造が優先的に成長した結果が得られた。この時、基板平坦部において、基板温度 400°C、460°C で成長させた基板では自己形成量子 (SK) ドットが現れたのに対し、700°C で成長させた基板では SK ドットは観察されなかった。

次に、同様の加工基板上に GaAs バッファ層、InAs 単層または 5 層積層構造、クラッド層の成長を行った。その結果、上記リング部で積層されたと思われる盛り上がりが見られた。これらの結果から基板加工のサイズをナノオーダーに微細化することにより位置制御された積層構造の成長が可能と期待される。リング内側で溝や、加工プロセス時の基板のダメージによると思われる表面荒れも見られ、今後改善の余地がある。

【謝辞】本研究は文部省ハイテクリサーチセンター整備事業の援助のもとで行われた。

【参考文献】 1) T. Ishikawa, et al. Apply. Phys. Lett. 76(2000)167

*早大バイオ・フォトリソクス新素材研究施設

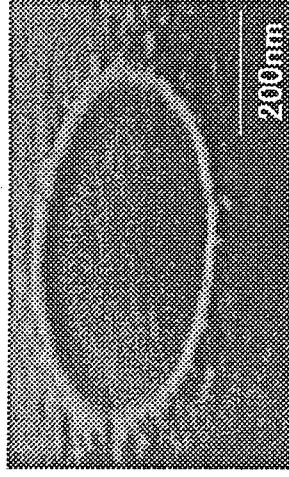


図 1 InAs 成長後の基板の様子

InGaAsP/InP Multi-Mode Interference Photonic Switches for Monolithic Photonic Integrated Circuits

Shuichi NAGAI, Goh MORISHIMA, Mikito YAGI and Katsuyuki UTAHA

Department of Electronics, Information and Communication Engineering, School of Science and Engineering, Waseda University, 3-4-1 Ohkubo, Shinjuku, Tokyo 169-8555, Japan

(Received June 22, 1998; accepted for publication November 12, 1998)

InGaAsP/InP semiconductor photonic switches using multi-mode interference (MIPS) are proposed for monolithic photonic integrated circuits. Changing the refractive indices of index-modulated regions located in the center of a multi-mode waveguide, controls its switching functions. It is predicted from calculations by an FD-TD (finite difference time domain) method that these devices can operate in various kinds of output schemes with typical device dimensions of about $8\ \mu\text{m}$ width and $540\ \mu\text{m}$ length. 1×2 InGaAsP/InP MIPS's with a high-mesa structure have been fabricated, and fundamental switching characteristics were measured. At the preliminary stage, switching was observed at 20 mA current injection with about 37% extinction ratio. Switching efficiency and cross talk of the MIPS can be improved by optimizing the device dimensions and structure. The flexibility of setting the index-modulated regions suggests versatile operation of the MIPS, such as a photonic space division switch, a variable power splitter, or as an optical modulator.

KEYWORDS: photonic switch, multi-mode interference, photonic integrated circuit, FD-TD, switching characteristics

1. Introduction

For advanced multi-media communications, network systems consisting of mixed point-to-point and broadcasting connections will be needed to satisfy huge transmission capacity demand, and to provide flexible network configurations, lightwave communication network systems are essential. Photonic switches and couplers are indispensable for the realization of optical cross-connection, interconnection and distribution, and will become more and more important in advanced large-scale systems. Photonic switches used in these systems are needed to be versatile, high-speed, compact and suitable for monolithic integration. For the actual application to lightwave communications at long wavelength range InP-based photonic devices are desirable.

Multi-mode interference¹⁾ effects are used in many kinds of optical passive devices such as ultra-compact couplers,²⁾ filters³⁾ or free splitting ratio couplers.⁴⁾ For instance, semiconductor multi-mode interference (MMI) couplers,^{5,6)} are very attractive devices for monolithic photonic integrated circuits because of compactness, polarization and wavelength insensitive characteristics, fabrication process tolerances, and moreover, versatile operation. Thus using multi-mode interference is very advantageous, even in optical switches such as the digital optical switch.⁷⁾

In this paper, we propose InGaAsP/InP multi-mode interference photonic switches (MIPS), which are based on a different operation principle than that of ref. 7. Since the proposed devices have a simple electrode structure, it is easier to design and fabricate. Moreover, functional operation such as 3dB-coupling is also possible. The structure and various kinds of switching operations of the MIPS are described in §2. In §3 fundamental switching characteristics are analyzed by an FD-TD method, and preliminary experimental results of the fabricated MIPS are shown in §4. Conclusions are summarized in §5.

2. Structure

Switching operation of an MIPS is obtained by changing the effective multi-mode interference waveguide width and length by reducing the refractive indices of index-modulated

regions. The fundamental beat length of multi-mode interference⁸⁾ is related to the waveguide parameters as

$$L_\pi = \frac{\pi}{\beta_0 - \beta_1} \equiv \frac{4nW_e^2}{3\lambda_0}, \quad (1)$$

where β_0 and β_1 are the propagation constants of the fundamental and first order lateral modes, respectively, λ_0 is the free space wavelength, n is the effective index, and W_e is the effective width. The field intensities in the multi-mode interference waveguide exhibit various distributions, as they propagate, related to the beat-length L_π .

Figure 1 shows a schematic structure of the proposed MIPS device, equipped with two index-modulated regions at the center of the multi-mode waveguide. The width of the index-modulated regions is s , and the refractive indices are n_2 and n_3 . The length and the width of the multi-mode waveguide are designed such that output light emits from a cross port, which requires $L = 3L_\pi$, in case of uniform index structure, i.e., $n_1 = n_2 = n_3 = n_4$. The output light can be switched from the cross port to the straight one by reducing the indices n_2 and n_3 , and can even emit from both ports when either n_2 or n_3 is reduced. This partial index reduction can be attained by current injection into the InGaAsP waveguide layer through the electrodes formed at the top of the respective index-modulated regions. The switching speed of the MIPS is expected to be rather high determined by carrier lifetime of less than a few ns.

3. Analysis

Switching characteristics of the MIPS are analyzed by an FD-TD method.⁹⁾ The length and width of the multi-mode waveguide are $L = 540\ \mu\text{m}$ and $W = 8\ \mu\text{m}$, respectively. The refractive indices of the waveguide and the cladding regions are $n_1 = 3.358$ for InGaAsP with a bandgap wavelength of $1.24\ \mu\text{m}$ and $n_5 = 1.45$ for SiO_2 , respectively, in a high-mesa structure. The lengths of the index-modulated regions are chosen to be half of the length of the multi-mode waveguide, and the widths are $2\ \mu\text{m}$. The input field intensity at a wavelength $\lambda = 1550\ \text{nm}$ is assumed to be in Gaussian distribution with a spot size of $s = 2.0\ \mu\text{m}$, and is coupled at a position separated from the side edge of the multi-mode

waveguide by $x = 1.5 \mu\text{m}$. The peak intensity of the input field is set to 1.0. In this analysis reduction of the refractive index of the index-modulated regions is assumed to be 1%, which is a reasonable reduction value attainable by current injection.

Calculated results of the two-dimensional (2D) propagated field intensity distributions and the relative output intensities are shown in Fig. 2. In the case that all regions have the same refractive indices such that $n_1 = n_2 = n_3 = n_4$, the input field intensity propagates in the multi-mode waveguide as shown in Fig. 2(a-1), and the output field intensity coupled to the cross output port is shown in Fig. 2(a-2) with a very small cross talk as is expected from the characteristics of the multi-mode interference. On the other hand, when both n_2 and n_3 are reduced to 3.324 (by 1% reduction), the output is obtained from the straight port as a result of formation of a nearly single mode waveguide, as shown in Fig. 2(b-1)

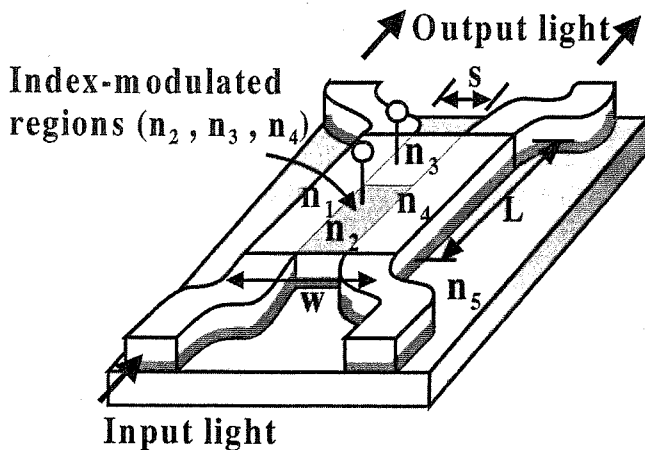


Fig. 1. Schematic structure of the proposed multi-mode interference photonic switch (MIPS).

and (b-2). Although a cross talk of about 11.3% appears in this case, it can be much reduced by optimizing the waveguide structures as addressed later. When either n_2 or n_3 are reduced to 3.324, the output field intensity is obtained from both output ports as shown in Fig. 2(c-1) and (c-2) since the length of the multi-mode waveguide becomes about half of that for the case of the cross-port output. As the propagation field in the multi-mode interference region does not become single mode in the case of the index reduction, a beating of the excited modes in the multi-mode interference region appears in Fig. 2. This beating effect leads to a perturbation in the output field intensity distribution. However, the beating of the propagating modes would disappear when the input field intensity had a wider spot size.

These results show the potential of the MIPS as functional photonic switches with not only line switching but also broadcasting behavior. These operations may be attained by only a few tens of mA current injection into each index-modulated region if the width and the lengths of these regions are as described above.

In order to reduce the cross talk that appeared for the high mesa structure, we calculated the characteristics of the MIPS by changing the structural parameters. First, when a ridge waveguide structure is adopted, which means an increase of the cladding index from 1.45 to 3.250, the cross talk can be reduced from 11.3% to 9.2%. The reason why the cross talk is reduced is that the distribution of propagated field intensity is shifting less toward the index-modulated regions due to the almost symmetric waveguide structure to the propagated field. Second, by increasing the width of the index-modulated regions from $2 \mu\text{m}$ to $4 \mu\text{m}$, the cross talk can also be reduced from 11.3% to 6.8%. This is because the evanescent field extending into the region of n_4 can be reduced.

Although using these methods optimization of its structural parameters can reduce the cross talk of the MIPS, it may still remain a few %, as mentioned above, as long as the index-

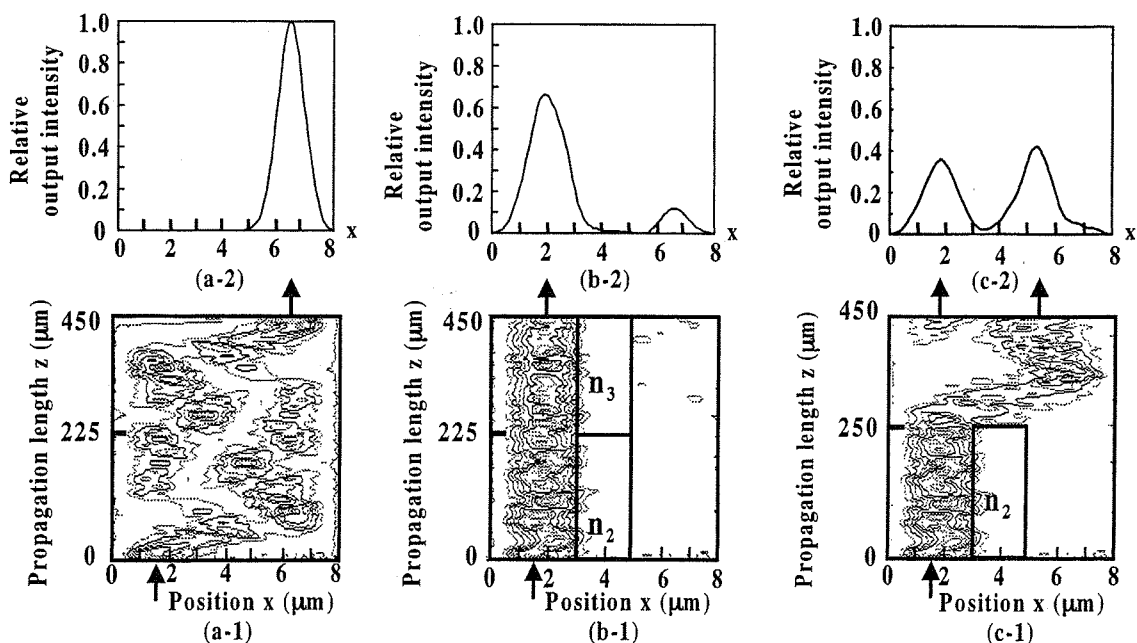


Fig. 2. 2D intensity distributions in the multi-mode waveguide (* - 1), and output intensities (* - 2) of the MIPS for various index changes: (a - *) no index-change ($n_1, n_2, n_3, n_4 = 3.358$), (b - *) n_2 and n_3 reduced by 1% ($n_2, n_3 = 3.324$), (c - *) only n_2 reduced by 1% ($n_2 = 3.324$).

modulated regions are located at the center of the multi-mode waveguide, which is aimed for a 2×2 MIPS configuration. On the other hand, if the n_4 region also plays a role as an index-modulated one, and its index is reduced to 3.324 (by 1% reduction), the cross talk can be much reduced down to -20 dB, as shown in Fig. 3. In this case, the MIPS operates as a 1×2 switch. Although the other input port cannot be used in this structure, good switching characteristics are expected from this calculation. Although excess loss due to free carrier absorption is not taken into account in this analysis, it may contribute to further reduction of the cross talk in the actual case under current injection.

4. Experimental Results and Discussions

1×2 MIPS's were fabricated with a high-mesa structure as shown in Fig. 4, with a single electrode controlling index regions n_2 , n_3 , and n_4 . The wafers of the MIPS were grown by liquid phase epitaxy (LPE) method, and the waveguide structures were made by conventional photolithography and wet chemical etching. The thickness of an n-InP buffer layer, an InGaAsP waveguide layer of the bandgap wavelength of $1.24 \mu\text{m}$, an InP cladding layer, a p^+ -InGaAsP cap layer and a SiO_2 film were about $0.5 \mu\text{m}$, $0.2 \mu\text{m}$, $0.8 \mu\text{m}$, $0.3 \mu\text{m}$ and $0.1 \mu\text{m}$, respectively. Due to the preliminary stage, we fab-

ricated the MIPS with the length deviated from the intended dimensions ($L = 3L_\pi$) as a result of unwanted side etching or so on in the process. The width and the length of the multi-mode waveguide were $W = 13 \mu\text{m}$ and $L = 870 \mu\text{m}$, respectively, and the dimensions of the index-modulated region were $s = 4 \mu\text{m}$ and $l = 820 \mu\text{m}$. The index-modulated region was formed along one side end of the multi-mode waveguide as shown in Fig. 4.

Considering that the actual current flow injected through the electrode may spread laterally in the InGaAsP waveguide layer, we made the width of the index-modulated region electrode of the 1×2 MIPS narrower than that used in the simulation in order to compensate for this current spread. The light of $1.55 \mu\text{m}$ wavelength was input into the MIPS at the straight-side input port by a lensed single mode fiber as in Fig. 4(a), and the output light was observed by an infrared camera through a low-pass optical filter, not to detect the emitted light at $1.24 \mu\text{m}$ wavelength. In the measurements, direct current was injected in the MIPS's.

The propagated light through the InGaAsP multi-mode waveguide layer of the MIPS was observed at the cross port under no current injection, as shown in Fig. 5(a). On the other hand, the output light was switched to the straight port by an injected current of 20 mA, as shown in Fig. 5(b).

Figure 6 shows the switching characteristics of the relative peak intensity of the output light from each port as a function of injected current with approximate fitting curves. Although the total output power equals the spatial integral of the output light intensity, we have plotted the peak values only for convenience. Because the length of the fabricated MIPS did not correspond to $3L_\pi$, some optical power appeared at the straight port under no current injection corresponding to a cross talk of 52%. Its value can be reduced by fabricating the MIPS with a length more closely to $L = 3L_\pi$.

The output field intensity at the straight port increased in proportion to the injected current, and that at the cross port decreased abruptly as the current increased, then saturated under more than 5 mA current injection. The cross talk and extinc-

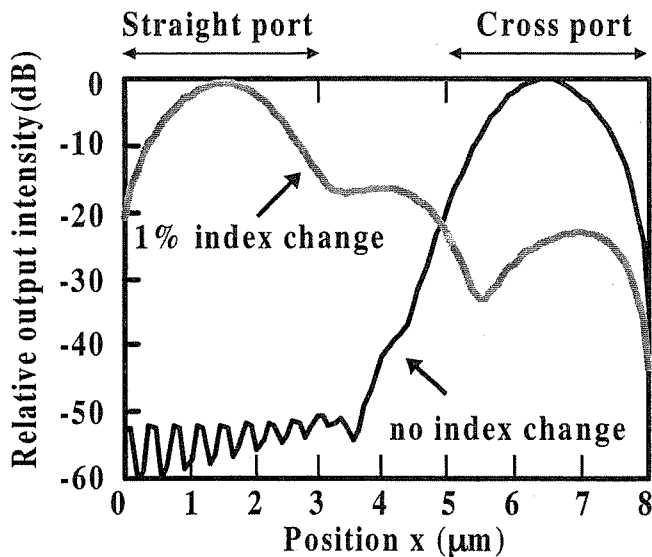


Fig. 3. Output intensity distributions of a 1×2 MIPS with additional index change of n_4 .

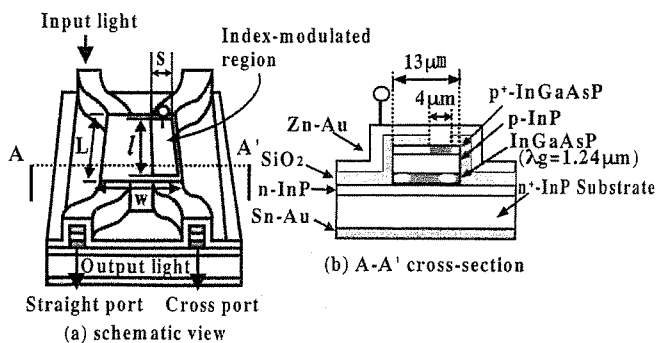


Fig. 4. Structure of the fabricated MIPS (a) and a waveguide cross-section in the multi-mode interference region (b).

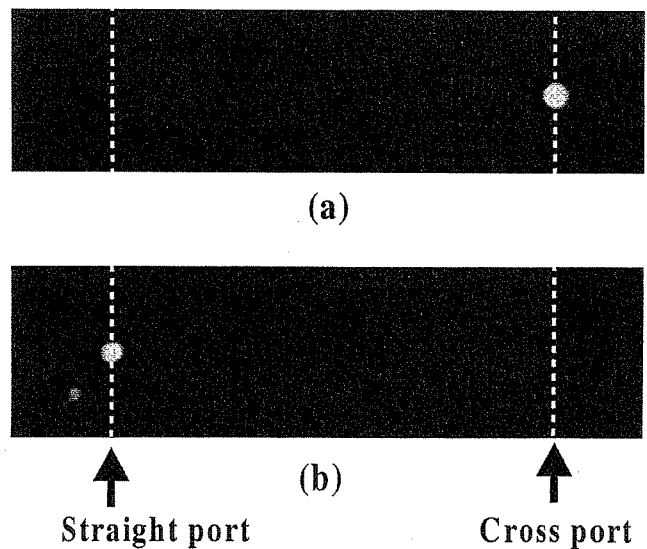


Fig. 5. Measured output field intensities from the MIPS under no current injection (a) and under 20 mA current injection (b).

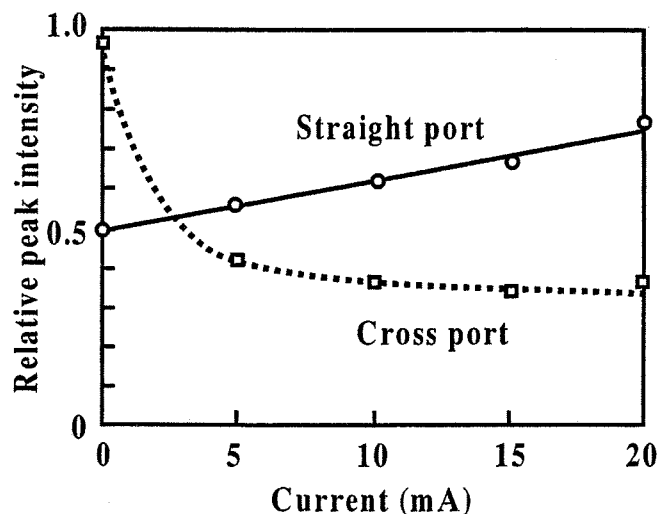


Fig. 6. Measured peak intensities of the output light as a function of injected current. Data shown by circles and squares are for the straight and the cross ports, respectively.

tion ratio at the cross port were 46% (relative to the straight port) and 37%, respectively, under 20 mA current injection. It should be noted that this rather inefficient switching behavior may be attributed to the fabricated device structure deviating from the designed one due to technical limitations in the fabrication process, such as wide access waveguides of about $7\ \mu\text{m}$, and almost no separation between the access waveguides at the interface of the multi-mode waveguide. The access waveguide should be single mode, located at a well-defined input position of the multi-mode waveguide for the predicted operation. In addition, the existence of higher-order modes in the fabricated access waveguides was also responsible for the poor cross talk at the off-state. The steep decrease of the output power at the cross port under small current injection was clear evidence of refractive index reduction due to current injection, but unwanted field coupling at the cross port waveguide led to the saturating cross talk level in the on-state.

As for the output at the straight port, since the coupling relied on the field distribution which was dependent on the index profile resulting from current injection, lateral spread of the index reduced region in accordance to the increase of current released the mismatch of the field distributions between of the multi-mode waveguide and of the access waveguide, and the output field intensity increased only slightly as a result. The index-modulated region has to be fabricated such as to take out the straight output light efficiently under current injection.

We could not measure the characteristics under more than 25 mA current injection because of spontaneous emission from the waveguide layer, which was not able to cut by the low-pass filter anymore since the wavelength of the emitted light increased due to the increase of temperature. As for insertion loss, it was predicted that absorption loss due to free carriers would lead to excess loss of the device, since the

switching operations of the device were controlled by carrier injection. A precise evaluation is left to study.

5. Conclusion

In summary, we proposed novel InGaAsP/InP multi-mode interference photonic switches (MIPS), in which various kinds of switching operation can be attained by introducing index-modulated regions in multi-mode interference waveguides. The fundamental characteristics analyzed by an FDTD method show that the MIPS's are quite promising as functional photonic switching devices. It is predicted that the switching characteristics can be improved by optimizing the waveguide structure, such as using a higher cladding index, wider index-modulated regions and so on. From these calculations, small cross talk of less than $-20\ \text{dB}$ and large extinction ratio are expected for a 1×2 MIPS.

We have fabricated a 1×2 MIPS, and switching operation was confirmed. The cross talk and the extinction ratio were 46% and 37%, respectively, under an injected current of 20 mA. These switching characteristics are expected to be surely improved by fabricating the designed device structure more accurately. This preliminary experiment also revealed that it is important to restrict current flow for index-modulated regions especially at the center of the multi-mode waveguide by some method such as partial pnpn regions, semi-insulating regions, and so on. Though there remain several problems to be overcome yet, we have demonstrated the advantage of the MIPS as a versatile photonic switching device for monolithic photonic integrated circuits.

Acknowledgment

The authors would like to sincerely thank Dr. S. Tanaka of KDD R&D Laboratories Inc. for his experimental support. They are also grateful to Mr. H. Inayoshi, Mr. J. Suzuki and Mr. M. Hirajima of Waseda University for their help in the experiment. This work was supported by Grant-in-Aid 09650368 for Scientific Research from the Ministry of Education, Science, Sports and Culture, and by International Communications Foundation.

- 1) R. Ulrich and G. Ankele: *Appl. Phys. Lett.* **27** (1975) 337.
- 2) D. S. Levy, R. Scarmozzino, Y. M. Li and R. M. Osgood: *IEEE Photon. Technol. Lett.* **10** (1998) 96.
- 3) M. R. Paiam and R. I. MacDonald: *Electron. Lett.* **33** (1997) 1219.
- 4) P. A. Besse, E. Gini, M. Bachmann and H. Melchior: *J. Lightwave Technol.* **14** (1996) 2286.
- 5) E. C. M. Pennings, R. J. Deri, A. Scherer, R. Bhat, T. R. Hayes, N. C. Andreadakis, M. K. Smit, L. B. Soldano and R. J. Hawkins: *Appl. Phys. Lett.* **59** (1991) 1946.
- 6) J. M. Heaton, R. M. Jenkins, D. R. Wight, J. T. Parker, J. C. H. Birbeck and K. P. Hilton: *Appl. Phys. Lett.* **61** (1992) 1754.
- 7) H. Okayama, H. Yaegashi and M. Kawahara: *Tech. Dig. Fifth Optoelectronic Conf. (OEC'94)* 15B3-6.
- 8) L. B. Soldano and E. C. M. Penning: *J. Lightwave Technol.* **13** (1995) 615.
- 9) D. S. Katz, E. T. Thiele and A. Taflove: *Microwave & Guided Wave Lett.* **4** (1994) 268.

PROPOSAL OF NOVEL InGaAsP/InP MULTI-MODE INTERFERENCE PHOTONIC SWITCHES

Shuuichi NAGAI, Norihito KOGURE,
Goh MORISHIMA, and Katuyuki UTAKA

Waseda University, 3-4-1 Ohkubo, Shinjuku, Tokyo 169-8555, Japan

Abstract

We propose novel InGaAsP/InP semiconductor photonic switches using multi-mode interference (MIPS). Switching functions are controlled by changing the refractive indices of the index-modulated regions which are located at the center of the multi-mode waveguide. It is predicted from the calculations by FD-TD (finite difference time domain) method¹⁾ that these devices can operate in various kinds of output schemes, with device sizes of about $8\mu\text{m}$ wide and $540\mu\text{m}$ long. The characteristics can be improved by optimizing cladding index and/or index-modulated region's width. Actually we fabricated the InGaAsP/InP MIPS with partial current injection regions, and at present preliminary transmission property with no index change was observed.

I. Introduction

In advanced lightwave communication network systems, as like wavelength division multiplexing (WDM), photonic switches are very important besides optical filters. These devices are needed to be versatile and high-speed, compact and suitable for monolithic integration.

Semiconductor multi-mode interference couplers (MMIC) are very attractive devices for monolithic photonic integrated circuits because of compactness, polarization-insensitive characteristics²⁾⁻⁴⁾ and, moreover, versatile operations.

In this paper we propose novel InGaAsP/InP multi-mode interference photonic switches (MIPS), in which various kinds of switching operations are realized by changing the refractive indices of the partial waveguide regions. Fundamental switching characteristics are evaluated by FD-TD method. And actually InGaAsP/InP MIPS's were fabricated.

II. Structure

Figure 1 shows the structure of the proposed MIPS device, and it is equipped with two index-modulated regions at the center of the multi-mode waveguide, of which width is s and refractive indices are n_2 and n_3 . The dimensions of the multi-mode waveguide are $540\mu\text{m}$ long and $8\mu\text{m}$ wide, and are designed so that an output light emits from a cross port in case of uniform index structure, i.e., $n_1 = n_2 = n_3 = n_4$. The output light can switch from the cross port to the straight one and can even emit from the both ports when both and either

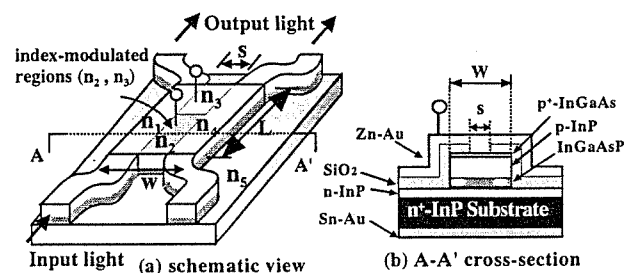


Fig.1 Structure of the proposed multi-mode interference photonic switch (MIPS)

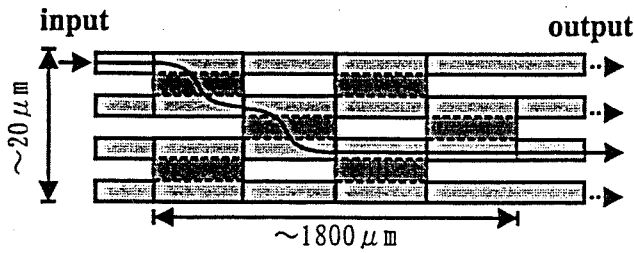


Fig.2 Structure of non-blocking 4×4 matrix switch with four-stage MIPS's

indices of n_2 and n_3 are reduced, respectively. This index reduction can be attained by current injection into the InGaAsP waveguide layer by forming electrodes at the top of the index-modulated regions. The switching speed of the MIPS will be high determined by carrier life time of a few ns.

Figure 2 shows one of the applications of the MIPS's to a non-blocking 4×4 matrix switch with as small as $20\mu\text{m} \times 1800\mu\text{m}$ dimensions. It shows that the MIPS is suitable for monolithic photonic integrated circuits.

III. Analysis

The analysis of switching characteristics is based on FD-TD method. The input light of the wavelength $\lambda = 1550\text{nm}$ is assumed to be in Gaussian distribution with a spot size of $2.0\mu\text{m}$, and is input at the position away from the side end of the multi-mode waveguide by $x = 1.5\mu\text{m}$. The peak intensity of the input light is set 1.0. The refractive indices of the waveguide and the cladding regions are $n_1=3.358$ for InGaAsP layer of the bandgap wavelength of $1.24\mu\text{m}$ and $n_5=1.45$ for SiO_2 , respectively, as a high-mesa structure. The lengths of the index-modulated regions are chosen to be half of the length of the multi-mode waveguide, and the widths of these are $2\mu\text{m}$. In this analysis the reduction of the index of the index-modulated regions is assumed to be 1% as reasonable reduction limit by current injection.

In the case that all regions have the same refractive indices such as $n_1 = n_2 = n_3 = n_4$, the input light propagates in the multi-mode waveguide as

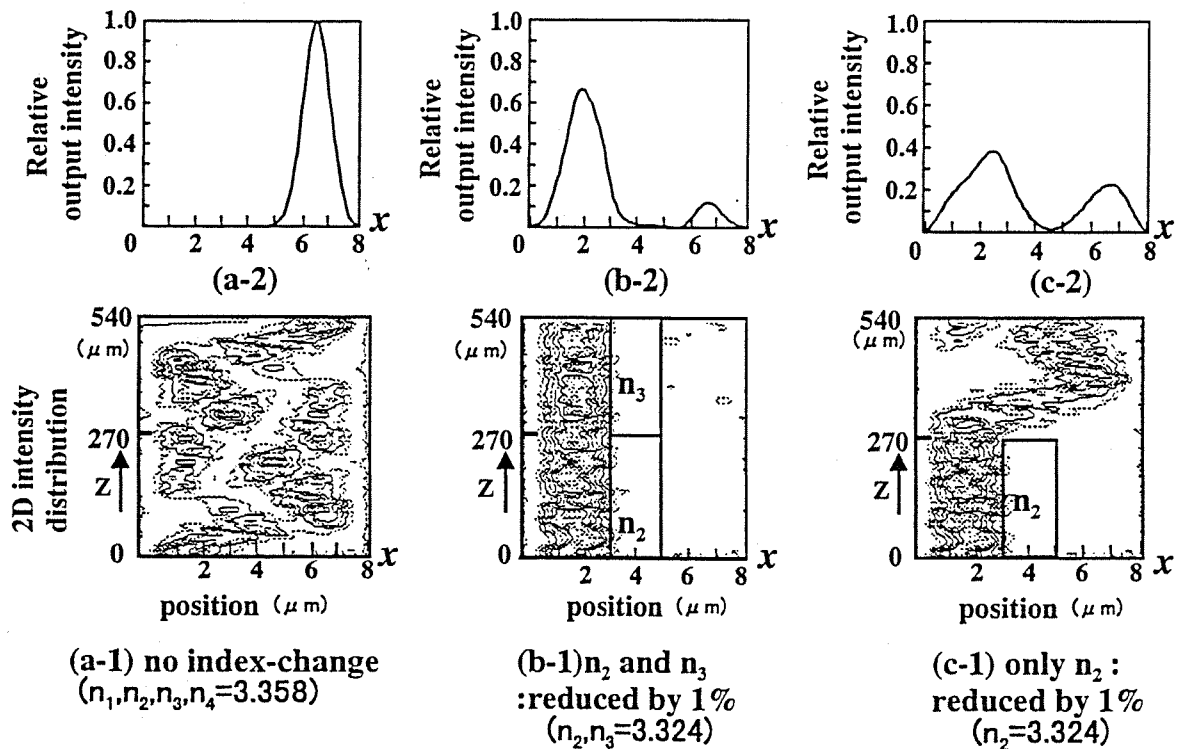


Fig.3 2D intensity distributions in multi-mode waveguides: (a-1), (b-1), (c-1), And output intensity: (a-2), (b-2), (c-2) of MIPS by changing indices

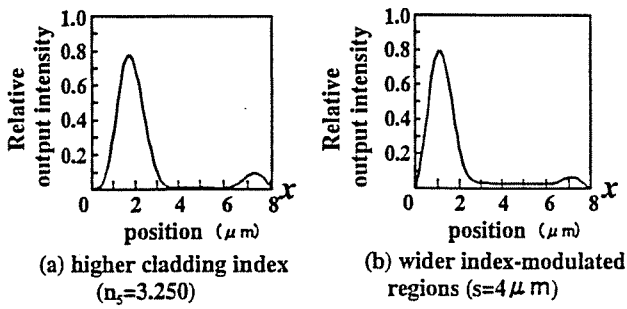


Fig.4 Output intensity of MIPS by changing indices

shown in Fig.3 (a-1), and the output light is obtained from the cross output port as shown in Fig.3 (a-2) with very small cross talk as is estimated by the characteristics of the multi-mode interference.

On the other hand, when both of n_2 and n_3 are reduced to be 3.324 (by 1% reduction), the output is obtained from the straight port as a result of formation of single mode waveguides, as shown in Fig.3 (b-1) and (b-2). Though the cross talk of about 11.3% appears in this case, it can be much reduced by optimizing the waveguide structures as addressed later.

And when only n_2 or n_3 are reduced to 3.324, the output light is obtained from both output ports as shown in Fig.3 (c-1) and (c-2) since the length of the multi-mode waveguide is made half of that for the case of the cross-port output. Though the output intensity of both ports is not equal, it may be able to be improved by optimizing the length of the region of n_2 . These results show the potential of the MIPS as functional photonic switches with not only line switching but broadcasting behavior, and these operations can be attained by about 35mA current injection to each index-modulated region if the width and the lengths of these region are $2\mu\text{m}$ and $270\mu\text{m}$, respectively.

In order to reduce the cross talk of the MIPS when n_2 and/or n_3 are reduced as described above, we calculate the characteristics of the MIPS by changing the structure parameters. Figure 4(a) shows the case when the ridge waveguide structure is adopted. The cross talk can be reduced to 9.2% from 11.3%

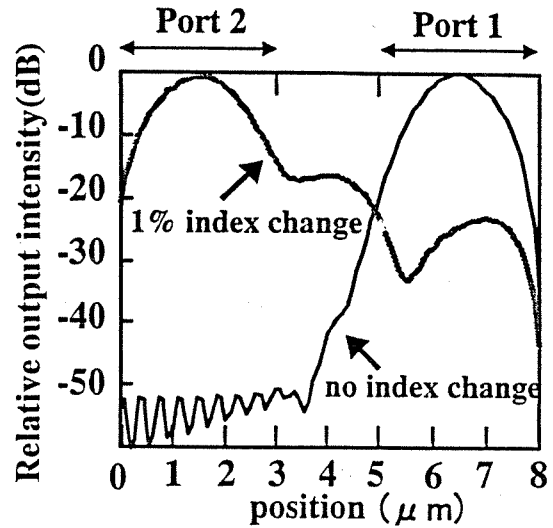


Fig.5 Output intensity of 1×2 MIPS (n_2 , n_3 and n_4 are reduced by 1%)

by increasing the cladding index to be 3.250 from 1.45. The reason why the cross talk is reduced is that the distribution of propagated light is less inclining toward the index-modulated regions due to the almost symmetric waveguide structure to the propagated light.

And by increasing the width of the index-modulated regions to $4\mu\text{m}$ from $2\mu\text{m}$, the cross talk can also be reduced to 6.8% from 11.3% as in Fig.4 (b). This is due to that, the evanescent field to the region of n_4 is reduced. In those methods, the cross talk of the MIPS can be reduced by optimizing its structure.

The cross talk is still remained a few %, as mentioned above, if the index-modulated regions are located in the center of the multi-mode waveguide, which is aimed for 2×2 MIPS configuration. On the other hand, if the n_4 region is also made as an index-modulated one and its index is reduced to 3.324 (by 1% reduction), the cross talk can be much reduced down to -20dB. In this case, the MIPS operates as 1×2 switch, Figure 5 shows its characteristics. Though the other input port cannot be used in this structure, the good switching characteristics as the 1×2 MIPS are expected from this calculation.

IV. Experiment

We fabricated the MIPS with the structure in Fig.1. The width and the length of the fabricated MIPS is $13\mu\text{m}$ and $1200\mu\text{m}$, respectively. The thicknesses of an InGaAsP waveguide layer of the bandgap wavelength of $1.24\mu\text{m}$ and a p-InP and a p^+ -InGaAs layers are $0.3\mu\text{m}$, $1.5\mu\text{m}$ and $0.05\mu\text{m}$, respectively.

The propagated light through the InGaAsP multi-mode waveguide layer of the MIPS was observed by an infrared camera as expected under no current injection, as shown in Fig.6. But switching operation of the MIPS has not obtained by current injection, because the injected current may have spread laterally in the whole InGaAsP layer, and the index changed uniformly. This preliminary experiment claims that some methods to restrict the current flows only through the center index-modulated regions are needed, such as partial pnpn regions, semi-insulating regions and so on. And a 1×2 MIPS may be rather easier to fabricate under sacrifice of one input port.

V. Conclusion

In summary, we proposed novel InGaAsP/InP multi-mode interference photonic switches (MIPS), in which various kinds of switching are attained by introducing patterned index-modulated regions. The fundamental characteristics evaluated by FD-TD method show that the MIPS is quite promising as

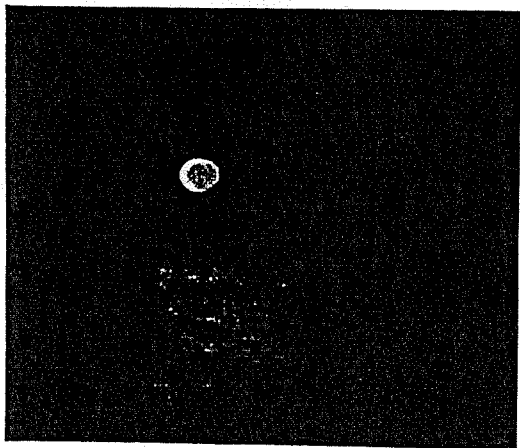


Fig.6 Output light from MIPS under no current injection

functional photonic switching devices. It is predicted that the switching characteristics can be improved by optimizing the waveguide structures such as higher cladding index, wider index-modulated region and so on.

We fabricated the MIPS actually, but it was found that the region where the injected current flows is needed to be restricted in the MIPS. And we are attempting to fabricate the improved MIPS and the 1×2 MIPS and expecting to demonstrate the fundamental experimental results at the conference.

Acknowledgements

The authors would like to thank Dr.S.Tanaka of KDD R&D Laboratories for providing wafers. This work was partially supported by Grant-in-Aid for Scientific Research and International Communications Foundation.

References

- (1.) D.S.Katz, E.T.Thiele, and A.Taflove, "Validation and Extension to Three Dimensions of the Berenger PML Absorbing Boundary Condition for FD-TD Meshes," IEEE Microwave and Guided Wave Lett., vol.4, pp 268-270, August 1994
- (2.) E.C.M.Pennings, R.J.Deri, A.Scherer, R.Bhat, T.R.Hayes, N.C.Andreadakis, M.K.Smit, L.B.Soldano, and R.J.Hawkins, "Ultracompact, low-loss directional couplers on InP based on self-imaging by multimode interference," Appl. Phys. Lett., vol.59, pp 1926-1928, October 1991
- (3.) J.M.Heaton, R.M.Jenkins, D.R.Wight, J.T.Parker, J.C.H.Birbeck, and K.P.Hilton, "Novel 1-to-N way integrated optical beam splitter using symmetric mode mixing in GaAs/AlGaAs multimode waveguides," Appl. Phys. Letter, vol.61, pp 1754-1756, October 1992
- (4.) L.B.Soldano and E.C.M.Penning, "Optical Multi-Mode Interference Devices Based on Self-Imaging: Principles and Applications," J. Lightwave Technol., vol.13, pp 615-627, April 1995

Analysis and Fabrication of Current-defined Multi-mode Interference Photonic Switches with Partial-index Modulation Regions (MIPS-P)

H. Inayoshi, S. Yagi, S. Nagai, and K. Utaka

Department of Science and Engineering, Waseda University

3-4-1 Ohkubo, Shinjuku, Tokyo 169-8555, Japan

TEL +81-3-5286-3394, FAX +81-3-3200-2567, e-mail : utaka@mn.waseda.ac.jp

Abstract

We propose two types of MIPS-P's for current-definition. Both types of MIPS-P's can be expected to realize switching operation with very low crosstalks of less than -20dB clarified by wide-angle finite-difference beam propagation method (WA-FD-BPM) analysis. Experimentally a fabricated MIPS-P with a groove region exhibited preliminary switching behavior according to current injection.

Introduction

Photonic switching is gathering increasing expectation in accordance to recent explosive development of photonic networks. For these applications, photonic switches may be needed to be versatile, high-speed, low power operation, polarization insensitive, wavelength insensitive, compact and suitable for monolithic integration. Multi-mode interference (MMI) waveguide devices are attractive candidates for such functional photonic devices [1]. Previously we proposed a new structure of multi-mode interference photonic switches with partial index-modulation regions (MIPS-P) to realize versatile power switching among multi ports [2],[3]. For proper operation of the MIPS-P, formation of the index-modulation regions with desirable sizes and positions is important. Actually positioning in accuracy in the fabrication process of the device and carrier diffusion of current injection for the index-modulation may deform the effective sizes of the index-modulation regions. In this paper, we discuss current-defining structures for the partial index-modulation regions in terms of low crosstalk operation, and report preliminary experimental characteristics of a MIPS-P with the current-defining structure.

Device Structure

A schematic of the 2x2 MIPS-P we investigated is shown in Fig.1. The width and the length of an MMI waveguide are $W=12\ \mu\text{m}$ and $L=1296\ \mu\text{m}$, respectively. L is selected to be $3L_{\pi}$, which is the coupling length of the MMI waveguide, where $L_{\pi}=4n_{\text{MMI}}W^2/3\lambda$. n_{MMI} is the equivalent refractive index, and λ is the wavelength of light in vacuum. This means that an asymmetric output light is emitted from

a cross port in the case of no index modulation. The length of the index-modulation region is $l=24\ \mu\text{m}$, and its width w_2 is adjusted in accordance with the current-defining width w_1 . The length l is selected so as to obtain a phase change of $-\pi$ with a refractive index change of -1%.

The switching principle is as follows. By setting the index-modulation region at an appropriate position and utilizing mode conversions in it, the multi-mode interference patterns after passing the region can be manipulated, and the output light can be switched to arbitrary output ports. Both 2x2 MIPS-P and 3x3 MIPS-P can realize switching operation with low crosstalks of less than -20dB as a result of the analysis by wide-angle finite-difference beam propagation method (WA-FD-BPM) using (3,3) Pade approximate operators with transparent boundary conditions.

Structure of Current-Definition

For the MIPS-P, index-modulation only at appropriate positions is essential. So we propose two types of structures for current-definition, that is, a groove region and proton-bombarded regions, as shown in Fig.2 (a) and (b), respectively.

The MIPS-P with a groove region is fabricated by etching the side of an index-modulation region in an MMI waveguide, as shown in Fig.2 (a), and consequently lateral diffusion of carriers by current injection can be avoided. The effect on switching characteristics against the sizes of the groove is analyzed by WA-FD-BPM for a 2x2 MIPS-P. Fig.3 shows the relation between the crosstalk and the width of the groove w_1 with its length of $l=24\ \mu\text{m}$. We also calculate the relation between the crosstalk and the length of the groove l . These results indicate that the 2x2 MIPS-P with a groove region can attain a very low crosstalk of less than -30dB on the condition that $w_1=0\sim 4\ \mu\text{m}$ and $l<35\ \mu\text{m}$.

On the other hand, proton-bombarded regions exhibit high resistivity due to depletion of carriers, and prevent the carrier diffusion as like the groove region. It is noted that the carrier depletion associates a refractive index increase at the same time, therefore its influence on switching characteristics is analyzed by WA-FD-BPM for a 3x3 MIPS-P. The change ratio of refractive index against carrier density is assumed -

$7.2 \times 10^{21} \text{cm}^{-3}$ [4], and the initially doped carrier density of an InP-cladding layer is assumed $5 \times 10^{17} \text{cm}^{-3}$. The calculated results show very low crosstalks of less than -20dB as well as low insertion losses less than -0.2dB. The MIPS-P with proton-bombarded regions is expected to the application to larger switching scale of NxN.

Experiments

The preliminary switching characteristics of the fabricated 2x2 MIPS-P with a groove region were measured. The width and the length of the MMI waveguide were $W=12 \mu\text{m}$ and $L=1250 \mu\text{m}$, respectively. And those of the groove were $w_1=2 \mu\text{m}$ and $l=24 \mu\text{m}$, respectively. The relative output intensities as a function of injection current are shown in Fig.4. By current injection, the relative output intensity of the cross port decreased by 6.8dB, and that of the straight port increased by 5.5dB. The crosstalk value at no current injection was far from the desired one, since the fabricated device sizes were deviated from the designed values. But the preliminary switching was obtained, and the effect of the current-defining structure was confirmed. The device characteristics can be improved by forming the groove more properly and by avoiding the heat problem due to current injection. MIPS-P's with proton-bombarded regions are under investigation.

Conclusion

We proposed two types of MIPS-P's for current-definition, that is, a groove region and proton-bombarded regions. Both types of MIPS-P's can be expected to realize switching operation with very low crosstalks of less than -20dB by WA-FD-BPM analysis. Besides a fabricated MIPS-P with a groove region exhibited preliminary switching behavior according to current injection. It is expected that desirable switching operation can be realized by to optimizing the device structures of MIPS-P's.

References

[1] L. B. Soldano and E. C. M. Pennings, J. Lightwave Technol., vol. 13, No. 4, pp. 615-627, 1995.
 [2] K. Utaka, S. Nagai, M. Yagi, H. Inayoshi, and G. Morishima, OECC'99, Beijing, C2S4, 1999.
 [3] M. Yagi, S. Nagai, H. Inayoshi, and K. Utaka, Electron. Lett., vol. 36, No. 6, pp. 533-534, 2000.
 [4] K. Stubkjaer, M. Asada, S. Arai, and Y Suematsu, Jpn. J. Appl. Phys., vol. 20, No. 8, pp. 1499-1505, 1981.

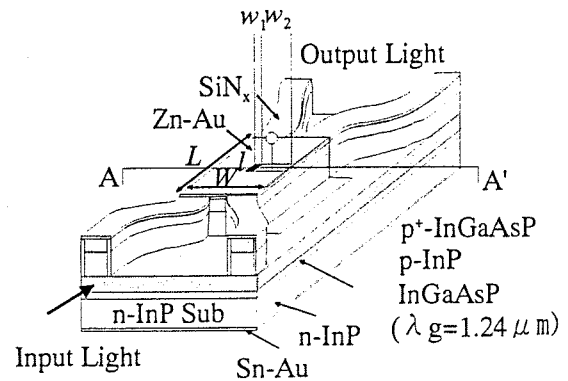
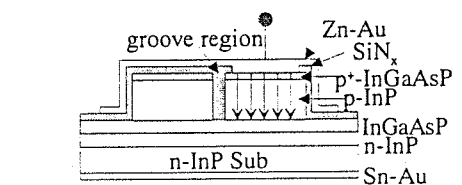
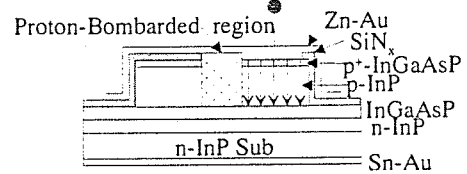


Fig.1 Schematic of the 2x2 MIPS-P



(a) MIPS-P with a groove region



(b) MIPS-P with a proton-bombarded region

Fig.2 Cross sections of A-A'

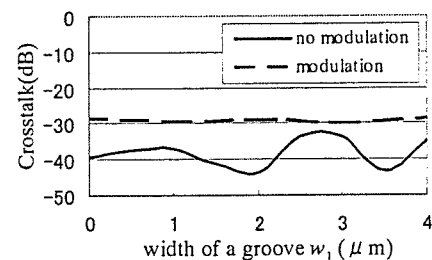


Fig.3 Relation between the crosstalk and w_1

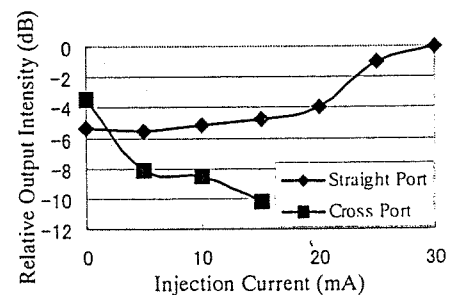


Fig.4 Output Intensities of a 2x2 MIPS-P with a groove region

Versatile multimode interference photonic switches with partial index-modulation regions

M. Yagi, S. Nagai, H. Inayoshi and K. Utaka

A new structure is proposed for multimode interference photonic switches which have partial index-modulation regions to obtain control of the power switching between multiple output ports. The switching characteristics for a 3×3 configuration are analysed by the wide-angle finite-difference beam propagation method. This analysis confirms that complete switching can be obtained with low crosstalk levels of ~ 23 dB.

Introduction: 2×2 multimode interference photonic switches (MIPS), the switching operation of which is achieved by controlling the confinement of the propagating light, have been proposed, and 1×2 switching operation has been experimentally demonstrated [1]. The advantages of utilising multimode interference (MMI) waveguides for photonic devices are that they are compact and polarisation-insensitive, have large optical bandwidth and improved fabrication tolerances, and that they are flexible to scale-extensions [2–5].

In this Letter we propose a new structure for multimode interference photonic switches, the switching operation of which is controlled via phase modulation. By changing the refractive indices of these index-modulation regions installed in the multimode waveguide, $N \times N$ switching functions can be controlled. Fundamental switching characteristics are analysed by the wide-angle finite-difference beam propagation method (WA-FD-BPM) [6], and the potential for a wide range of applications is described.

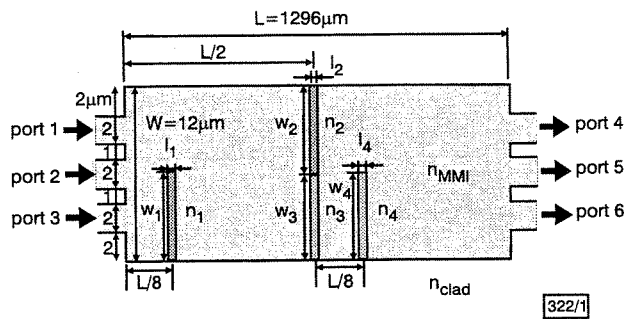


Fig. 1 Structural parameters of MIPS-P for 3×3 configuration

Device structure: A schematic structure of the multimode interference photonic switch with partial index-modulation regions (MIPS-P) is shown in Fig. 1 for a 3×3 configuration. The width and the length of the MMI waveguide are $W = 12$ and $L = 1296$ μm , respectively. L is selected to be $3 L_\pi$, where the coupling length of the MMI waveguide $L_\pi = 4n_{MMI}W^2/3\lambda$ with the equivalent refractive index n_{MMI} and λ is the wavelength of light in a vacuum [2]. This means that the asymmetric input light is emitted from a cross port without any index modulation. The lengths l_1 , l_2 , l_4 and the widths w_1 , w_2 , w_3 , w_4 of the index-modulation regions are 24 and $6 \mu\text{m}$, respectively. The equivalent refractive index of the MMI region n_{MMI} and the cladding region n_{clad} are 3.219 and 3.058, respectively, assuming an InGaAsP/InP ridge structure for $\lambda = 1.55 \mu\text{m}$. The lengths of the index-modulation regions are selected so as to obtain a phase change of $-\pi$ for a refractive index change of -1% .

The index-modulation regions denoted by (n_1, n_4) and (n_2, n_3) are placed at the positions in the MMI waveguide where a pair of images of an input signal are obtained for symmetric and asymmetric interference, respectively [2]. For example, in the case of a change in phase of one of the pair images in the MMI waveguide by $-\pi$, an even mode is transformed into an odd mode, and vice versa ('transformation'). Also the unification of modes (i.e. both modes become the same type) ('unification') or the division of both modes ('division') can be realised by changing the phase of either symmetric image by $-\pi/2$. By utilising these mode conversions, the multimode interference patterns after further propagation in the MMI waveguide can be manipulated, and the output light is switched to arbitrary ports by setting the partial index-modulation regions at appropriate positions.

Analysis: The fundamental switching characteristics of the MIPS-P were analysed by WA-FD-BPM using (3, 3) Padé approximant operators with transparent boundary conditions. TM polarisation was considered.

The light propagation characteristics and output intensities for the case where the input light was fed from port 1 are shown in Fig. 2. Without the index modulation the propagating light is emitted from port 6, as shown in Fig. 2c, since $L = 3 L_\pi$. When the refractive index n_2 or n_3 is decreased by -1% , a transformation between the even and odd modes takes place at $z = L/2$, and the multimode interference patterns for further propagation after $z = L/2$ are inverted. Therefore, the light is emitted out from port 4, as shown in Fig. 2a. Simultaneous decreases in the refractive indices n_3 and n_4 by -0.5 and -1% , respectively, give rise to a unification of modes such that both become odd at $z = L/2$ and subsequently to even modes at $z = 5L/8$, so that the light is emitted out from port 5, as shown in Fig. 2b.

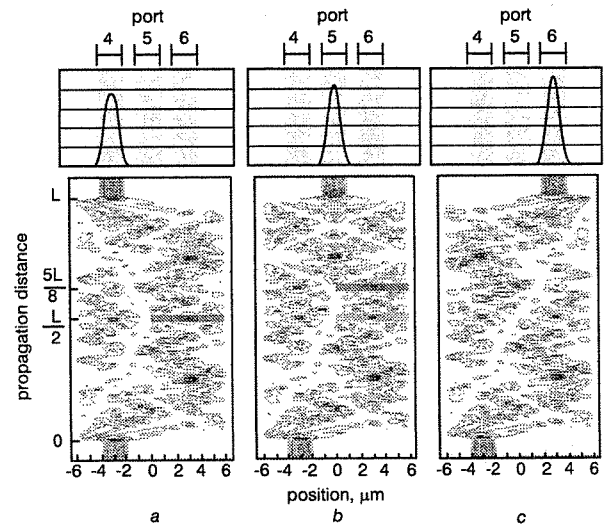


Fig. 2 Light propagation behaviour and output intensities

(Input: port 1)

Black and grey regions indicate where refractive indices are decreased by -1 and -0.5% , respectively

- a n_2 or n_3 decreased by -1%
- b n_3 decreased by -0.5 , n_4 decreased by -1%
- c Without index modulation

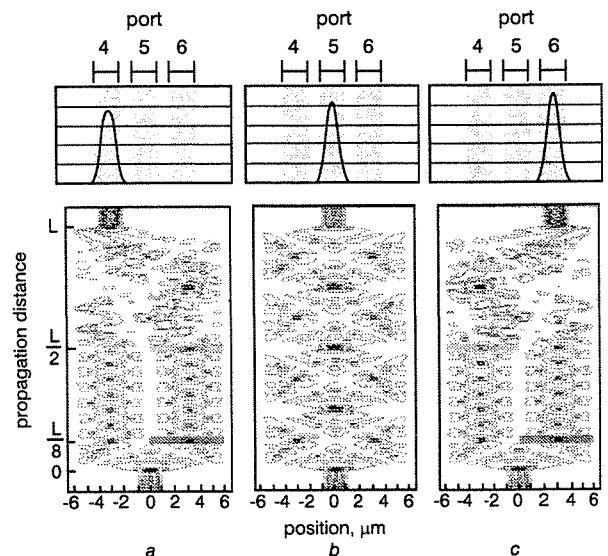


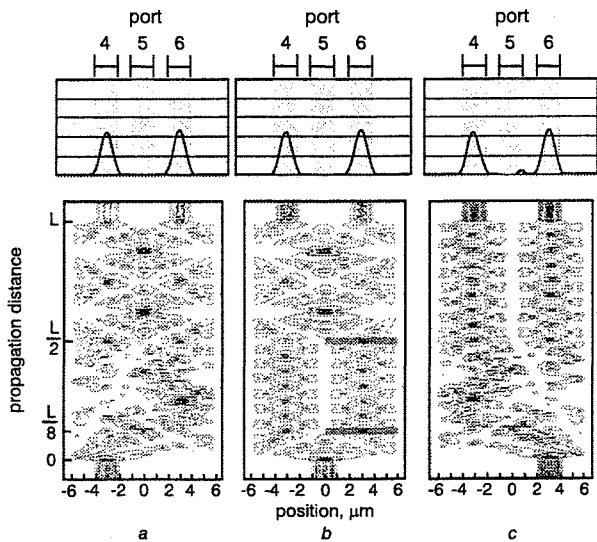
Fig. 3 Light propagation behaviour and output intensities

(Input: port 2)

- a n_1 decreased by -1% , n_3 decreased by -0.5%
- b Without index modulation
- c n_2 decreased by -0.5%

Fig. 3 shows the calculated results for the case where the input light is fed from port 2. Since the input light is fed from the centre

of the MMI waveguide, only even modes are excited. Without index modulation the light output is obtained from the centre port 5, after four cyclic self-imaging-length propagations, as shown in Fig. 3b. Refractive index changes in n_1 by -1% and n_3 by -0.5% cause the unification to odd modes and the division of both modes at the respective positions, resulting in an output from port 4, as shown in Fig. 3a. Fig. 3c depicts the case where n_2 is decreased by -0.5% , instead of n_3 , showing the output from port 6.



322/4

Fig. 4 Light propagation behaviour and output intensities as 3dB coupler

- a Even modes
- b Even modes (different input port from Fig. 4a)
- c Odd modes

The MIPS-P can be operated as a 3dB coupler that branches out the input light into two ports, ports 4 and 6, even if the input light is fed from any port. These functions are realised by finally converting the modes into even modes, as shown in Fig. 4a and b, or odd modes as shown in Fig. 4c.

A decrease in the refractive indices can be easily attained by current injection, and increases can also lead to the same characteristics.

Conclusion: We have proposed a new structure for multimode interference photonic switches with partial index-modulation regions (MIPS-Ps), and demonstrated the possibility of complete switching and also 3dB branching with low crosstalk levels of $< -20\text{dB}$. The proposed MIPS-Ps can be expected to be used as versatile functional photonic switching devices for advanced photonic network systems.

Acknowledgment: This work was supported by a Grant-In-Aid for Scientific Research from the Ministry of Education, Science, Sports and Culture.

© IEE 2000

4 January 2000

Electronics Letters Online No: 20000412

DOI: 10.1049/el:20000412

M. Yagi, S. Nagai, H. Inayoshi and K. Utaka (Waseda University, 3-4-1 Ohkubo, Shinjuku, Tokyo 169-8555, Japan)

E-mail: 698d0577@mn.waseda.ac.jp

References

- 1 NAGAI, S., MORISHIMA, O., YAGI, M., and UTAKA, K.: 'InGaAsP/InP multi-mode interference photonic switches for monolithic integrated circuits', *Jpn. J. Appl. Phys.*, 1999, **38**, Pt.1, (2B), pp. 1269-1272
- 2 SOLDANO, L.B., and PENNING, E.C.M.: 'Optical multi-mode interference devices based on self-imaging principles and applications', *J. Lightwave Technol.*, 1995, **13**, (4), pp. 615-627

- 3 PENNING, E.C.M., DERI, R.J., SCHERER, A., BHAT, R., HAYES, T.R., ANDREADAKIS, N.C., SMIT, M.K., SOLDANO, L.B., and HAWKINS, R.J.: 'Ultracompact, low-loss directional couplers on InP based on self-imaging by multimode interference', *Appl. Phys. Lett.*, 1991, **59**, (14), pp. 1926-1928
- 4 BESSE, P.A., BACHMANN, M., MELCHIOR, H., SOLDANO, L.B., and SMIT, M.K.: 'Optical bandwidth and fabrication tolerances of multimode interference couplers', *J. Lightwave Technol.*, 1994, **LT-12**, (6), pp. 1004-1009
- 5 LEVY, D.S., SCARMOZZINO, R., LI, Y.M., and OSGOOD, R.M.: 'A new design for ultracompact multimode interference-based 2x2 couplers', *IEEE Photonics Technol. Lett.*, 1998, **10**, (1), pp. 96-98
- 6 HADLEY, G.R.: 'Wide-angle beam propagation using Padé approximate operators', *Opt. Lett.*, 1992, **17**, (20), pp. 1426-1428

NEW STRUCTURE OF MULTI-MODE INTERFERENCE PHOTONIC SWITCH WITH PARTIAL INDEX-MODULATION REGIONS (MIPS- P)

K. Utaka ^{1*}, S. Nagai, M. Yagi, H. Inayoshi, and G. Morishima

School of Science and Engineering,

¹also with Materials Research Laboratory for Bioscience and Photonics

Waseda University

3-4-1 Ohkubo, Shinjuku, Tokyo 169-8555, Japan

e-mail : utaka@mn.waseda.ac.jp, tel. :+81-3-5286-3394, fax.:+81-3-3200-2567

Abstract: We propose a new structure of multi-mode interference photonic switches with partial index-modulation regions to realize flexible power switching among multi-ports. The switching characteristics for 3x3 configuration are analysed to show potential for versatile functions.

Introduction

Photonic switching is gathering increasing expectation in accordance to recent explosive development of photonic networks. For these applications, photonic switches may be needed to be versatile, high-speed, low operation power, polarization insensitive, wavelength insensitive, compact and suitable for monolithic integration. Multi-mode interference (MMI) waveguide devices are attractive candidates for such functional photonic devices [1]- [3] and we developed multi-mode interference photonic switches (MIPS) to demonstrate 1x2 switching and 3dB branching theoretically and experimentally [4].

In this paper we propose a new structure of multi-mode interference photonic switch (MIPS-P), which accommodates index-modulation regions at appropriate partial regions in the MMI waveguide. It can operate in versatile functions as flexible power switching among multi-port output waveguides. Fundamental operational characteristics are analysed by wide-angle finite-difference beam propagation method (WA-FD-BPM) [5], and potential for versatile wide application is described.

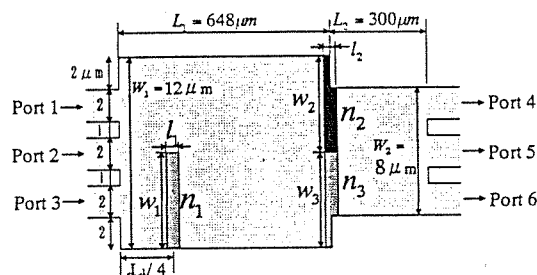
Device structure

A fundamental structure of a multi-mode interference photonic switch with partial index-modulation regions (MIPS-P) is shown in Fig.1 for a 3x3 configuration. It accommodates partial index-modulation regions at such regions in the multi-mode interference (MMI) waveguide as those where propagated beams tend to be focused in order to effectively modulate the phases of specific guided modes, and consequently propagation behaviors can be controlled due to the change of interference among the propagated modes. Here, a 3x3 configuration is drawn as an example, but this operation concept can adapt to larger-scale multi-port structures. Fundamental switching characteristics are analysed by WA-FD-BPM using (3,3) Pade approximate operators with transparent boundary condition.

In the analyses, the device structure which is composed of two MMI regions with different lengths and widths is used, as shown in Fig.1, for improved output beam profiles. The total device length is about 950 μ m. The refractive indices of the core and the cladding regions of the MMI waveguide are $n_{\text{MMI}}=3.219$ and $n_{\text{clad}}=3.058$, respectively. The input light at the wavelength of 1550nm is assumed to

be in Gaussian distribution with a spot size of 1 μ m, and TM polarization is considered. As partial modulation regions, three regions are taken, as shown in the figure denoted by n_1 , n_2 and n_3 , to demonstrate various output behaviors from three ports. The lengths l_1 , l_2 and the widths w_1 , w_2 , w_3 of all these regions are 24 μ m and 6 μ m, respectively.

Figure 1: Schematic structure of 3x3 configuration MIPS-P

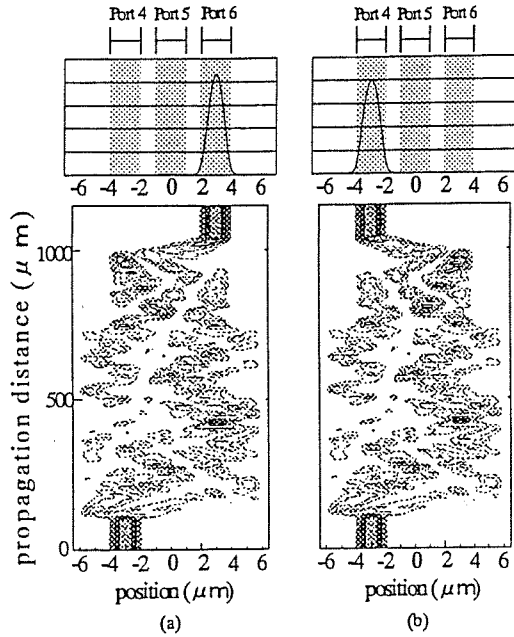


Analyses

Figures 2 show the beam propagation characteristics for the case that the input light is fed into Port 1 without (a) and with (b) partial index-modulation at the region denoted by n_3 . Without index modulation an input light propagates and emits out from a cross port, Port 6, since the effectively total length of the MMI waveguides $L (=L_1+L_2)$ is selected to be effectively $3L_{\pi}$, where $L_{\pi}=4n_{\text{MMI}}W^2/3\lambda$ (λ : the wavelength in the vacuum) is the coupling length determined by the lowest two-ordered modes. This means L_1 and L_2 are chosen to be $3L_{\pi}/2$ for each MMI width W_1 and W_2 . When the refractive index of the index-modulation region n_3 is decreased by 1%, the output is switched from the cross to the straight ports, as shown in Fig.2 (b). The switching characteristics as a function of refractive index change $-\Delta n_3$ are shown in Fig.3 with two cases of the lengths of the partial modulation regions l_2 , 25 μ m and 50 μ m. It is seen that these switching behaviors are quite similar to those of a Mach-Zender interferometer. By decreasing n_3 to attain the corresponding phase change of π , complete switching is realized with a low cross-talk of about -25dB with a wide tolerance in l_2 . It is noted that the

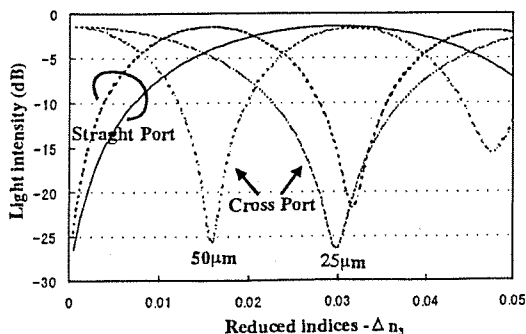
same characteristics are obtained even if the index-modulation region is formed at the opposite side of the MMI waveguide n_2 , giving the same phase effect to the propagated modes.

Figure 2: Beam propagation for the input light in Port 1: without (a) and with (b) index-modulation of n_3



Figures 4 show the output light distributions under the various modulation schemes on n_1 , n_2 and n_3 for the case of the center-fed input light into Port 2. The structure is designed so as to include four equivalent units to project the same center-fed input image after one-unit-length propagation. Therefore, an output light emits out from the center port, Port 5, for the case of no index-modulation. By decreasing the refractive indices n_1 , n_2 and n_3 appropriately, the output switching among three ports can be realized. The switching behaviors by various modulation schemes $(-\Delta n_1, -\Delta n_2, -\Delta n_3)$ of (a)(1%, 0, 0.5%), (b)(0, 0, 0), and (c)(1%, 0.5%, 0) are shown in Fig.4. Here, the refractive index n_2 is not changed. A 1x3 switching operation is realized by just a single chip. It is noted that there are several choices for the positions of the partial index-modulation regions and the length of the MMI waveguide to attain the same operations. Adoption of two MMI regions realizes complete single-mode outputs from the access waveguides. These results evidently show the potential for versatile switching functions.

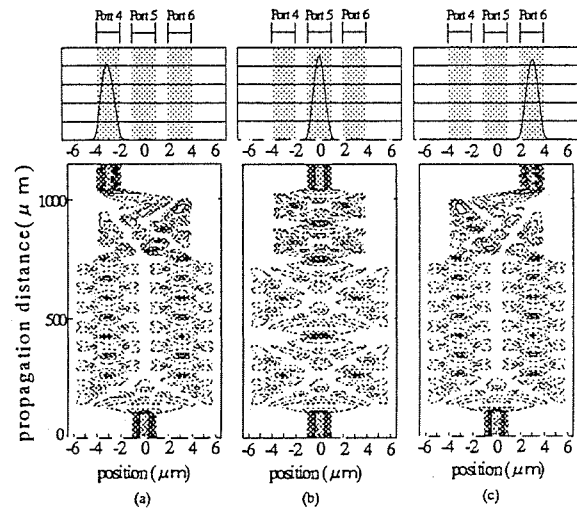
Figure 3: Switching characteristics as a function of the decrease of n_3



Conclusion

We proposed a novel structure of multi-mode interference photonic switches with partial index-modulation regions (MIPS-P). By forming the partial index-modulation regions in the MMI waveguide and appropriately changing the refractive indices, versatile photonic switching operation can be realized to get the outputs from arbitrary waveguides of the multi-port structure with very compact chip size. The proposed MIPS-P's are expected as versatile functional photonic switching devices for advanced photonic network systems.

Figure 4: Various switching behaviors for the input light in Port 2



Acknowledgement

This work was supported by Grant-In-Aid for Scientific Research from the Ministry of Education, Science, Sports and Culture, and by International Communications Foundations.

References

- /1/ E.C.M.Pennings, R.J.Deri, A.Scherer, R.Bhat, T.R.Hayes, N.C.Andreadakis, M.K.Smit, L.B.Soldano, and R.J.Hawkins, "Ultracompact, low-loss directional couplers on InP based on self-imaging by multimode interference", Appl. Phys. Lett., vol.59, No.14, pp.1926-1928, 1991.
- /2/ P.A.Besse, M.Bachmann, H.Melchior, L.B.Soldano, and M.K.Smit, "Optical bandwidth and fabrication tolerances of multimode interference couplers", J. Lightwave Tech., vol.12, No.6, pp.1004-1009, 1994
- /3/ D.S.Levy, R.Scarmozzino, Y.M.Li, and R.M.Osgood, Jr., "A new design for ultracompact multimode interference-based 2x2 couplers", IEEE Photonics Tech. Lett., vol.10, No.1, pp.96-98 1998
- /4/ S.Nagai, G.Morishima, M.Yagi, and K.Utaka, "InGaAsP/InP multi-mode interference photonic switches for monolithic integrated circuits", Jpn. J. Appl. Phys., vol.38, Pt 1, No.2B, pp.212-215, 1999.
- /5/ G.R.Hadley, "Wide-angle beam propagation using Padé approximate operators", Opt. Lett., vol.17, No.20, pp.1426-1428, 1992

NOVEL WAVELENGTH CONVERTER USING MULTI-MODE INTERFERENCE SEMICONDUCTOR OPTICAL AMPLIFIER (MIWC)

S. NAGAI, M. YAGI, J. SUZUKI, K. UTAKA¹ and S. TANAKA*

School of Science and Engineering,

¹ also with Materials Research Laboratory for Bioscience and Photonics, Waseda University

3-4-1 Ohkubo, Shinjuku, Tokyo 169-8555, Japan

e-mail :698d5041@mn.waseda.ac.jp, tel. :+81-3-5286-3394, fax.:+81-3-3200-2567, *KDD R&D Labs.

Abstract: Compact and simple-structured wavelength converter using multi-mode interference semiconductor optical amplifier is proposed. Fundamental characteristics of cross gain modulation with gain suppression of about 3dB were observed.

Introduction

For future advanced wavelength division multiplexing (WDM) optical network systems, a wavelength converter (WC) is expected to be one of the important devices, since it can remove wavelength blocking and provide flexible high capacity network by effectively managing finite wavelengths in interconnections. For this purpose, semiconductor optical amplifiers (SOA's) are promising. So far, a lot of studies on wavelength converters using cross gain modulation (XGM) /1/, cross phase modulation (XPM) /2/, four wave mixing (FWM) /3/ and so on /4/ have been reported. On the other hand, photonic devices using multi-mode interference (MMI)/5-7/ are very attractive from the viewpoint of compactness, polarization and wavelength insensitive characteristics.

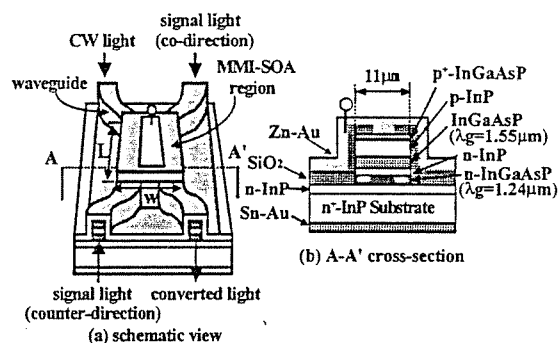
We propose a novel multi-mode interference wavelength converter (MIWC) based on XGM in an MMI-SOA. Although conventional wavelength converters, in most cases, need additional optical components like a filter or a coupler for separating a converted light from a signal light, the MIWC does not need these components, so compact WC configuration is attainable.

Structure

The proposed MIWC has an active multi-mode interference region integrated with passive 2x2 access waveguides, as shown Fig.1. In the MMI-SOA region, a large optical cavity structure was adopted. As the length of the MMI region is chosen $3L\pi$, where $L\pi$ is defined as $L\pi = 4nW^2/3\lambda$ (W and n : the width and refractive index of the MMI waveguide, respectively, λ : the wavelength in the vacuum), input lights from any ports can be taken out from its cross ports. Therefore, efficient separation between a signal light and a converted light is possible without additional filters even for both cases of co-directional and counter-directional configurations, as long as they are fed from different ports. Moreover, since the amplified signal light emitted from one MIWC can be reused in the next MIWC arranged in the cascade, wavelength conversion from one wavelength to multiple ones can be realized. The width and length of the MMI-SOA are $W = 8\mu\text{m}$ $L = 540\mu\text{m}$, respectively, so the MIWC is quite a compact WC.

It is noted that since the MIWC is wider than conventional single-mode SOA's, larger gain is expected.

Figure 1: Structure of the MIWC



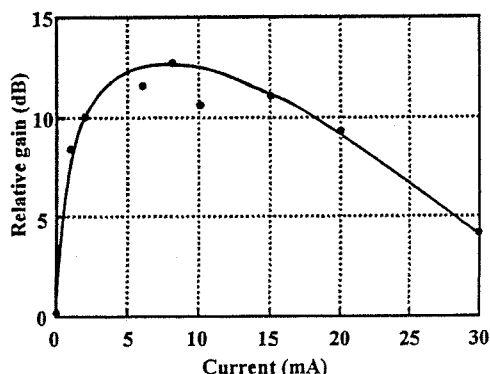
Experimental results

The MIWC were fabricated with a high-mesa structure, for 1550nm wavelength range operation as shown in Figure 1, by liquid phase epitaxy (LPE) method, and the waveguide and MMI-SOA structures were made by conventional photolithography and wet chemical etching. The thickness of an n-InGaAsP waveguide layer of the bandgap wavelength of 1.24 μm , an n-InP buffer layer, an active layer of the bandgap wavelength of about 1.55 μm and a p-InP cladding layer, a p+-InGaAsP cap layer were about 0.25 μm , 0.15 μm , 0.20 μm , 0.50 μm , and 0.20 μm , respectively. The width and the length of the multi-mode waveguide were $W = 11\mu\text{m}$ and $L = 870\mu\text{m}$, respectively.

The gain characteristics of the fabricated MIWC as a function of injection current are shown in Fig.2. In this case, the wavelength and the power of the input light in the launching fiber were 1536nm and -10dBm, respectively. The gains were measured by the change of the output light power from the MIWC, so it corresponds to a small signal gain characteristics since the coupling from the input fiber into the high-mesa waveguide was estimated to be small. The gain reached a peak and then decreased as the current increased, which was attributed to heat rise since the device was not bonded on a heat sink. The maximum gain was about 12dB around 8mA current injection, and the peak of

the ASE spectrum was about 1515nm. The reason why the gain of the MIWC varied by changing the current may be due to the refractive index change associated with current injection.

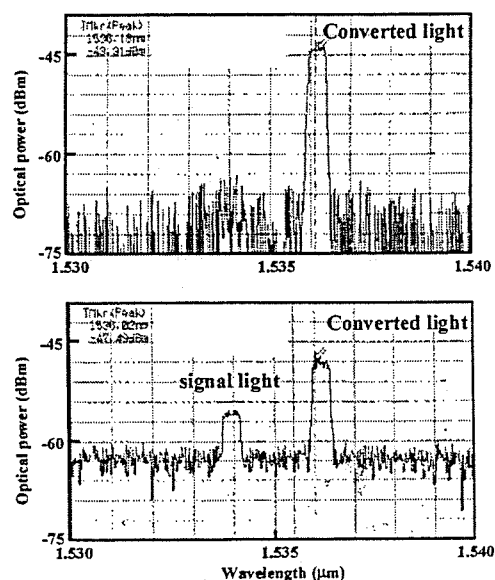
Figure 2: Gain characteristics of the MIWC



In Fig. 3 the gain suppression of the MIWC by 5mA current injection was observed. The wavelength of a CW light was 1536nm and that of a signal light was 1534nm. The input powers of the CW light and the signal light in the launching fibers were about -20dBm and -10dBm, respectively. In this case, the transmitted light power of the CW output light corresponding to the converted light was less than -60dBm without current injection to the MIWC.

The power of the converted light was -43.9dBm when the signal light did not fed to the MIWC, but it reduced to -47.5 dBm by feeding the signal light. The gain suppression rate was about 3dB. The signal light appeared in Fig. 3 because a co-directional configuration was adopted and the length of the MMI region was different from that corresponding to $3L\pi$. It should be noted that in the case of a counter-directional configuration, the signal light can be eliminated entirely at the converted output port.

Figure 3: Gain suppression of the MIWC by feeding signal light



Summary

We proposed a novel wavelength converter (MIWC) with an active multi-mode interference region, which does not need to be equipped with an additional filter to separate a signal from a converted lights. The maximum optical gain of the fabricated MIWC was about 12dB. Though the experiments are still at preliminary stage, the cross gain modulation between the wavelengths of 1534nm and 1536nm was obtained with cross gain suppression of 3dB. Higher performances are expected by improving the launched power in the MMI-SOA and the device reliability, adopting a ridge or a buried heterostructure waveguides, and also optimizing the device dimension parameters.

Acknowledgement

The authors would like to thank to Mr. H. Inayoshi of Waseda University for his help in the experiment. This work was supported by Grant-in-Aid 09305021 for Scientific Research from the Ministry of Education, Science, Sports and Culture, and by International Communications Foundation.

References

- /1/ T. Durhuus, B. Mikkelsen, C. Joergensen, S. L. Danielsen, and K. E. Stubkjaer : "All-Optical Wavelength Conversion by Semiconductor Optical Amplifiers" *Journal of Lightwave Technology*, Vol. 14, No. 6, pp. 942-954 (1996)
- /2/ C. Joergensen, S. L. Danielsen, T. Durhuus, B. Mikkelsen, K. E. Stubkjaer, N. Vodjdani, F. Ratovelomanana, A. Enard, G. Glastre, D. Rondi, and R. Blondeau : "Wavelength Conversion by Optimized Monolithic Integrated Mach-Zehnder Interometer" *IEEE Photonics Technology Letters*, Vol. 8, No. 4, pp. 521-523(1996)
- /3/ R. Schanabel, W. Pieper, R. Ludwig and H. G. Weber : "Multiterahertz frequency conversion of a picosecond pulse train using nonlinear gain dynamics in a 1.5mm MQW semiconductor laser amplifier" *Electronics Letters*, Vol. 29, No. 9, pp. 821-822(1993)
- /4/ K. Inoue : "Dependence of Frequency Chirping on Bias Current in LD Wavelength Conversion" *IEEE Photonics Technology Letters*, Vol. 8, No. 6, pp. 767-769 (1996)
- /5/ L. B. Soldano and E. C. M. Pennings : "Optical Multi-Mode Interference Devices Based on Self-Imaging: Principles and Applications" *Journal of Lightwave Technology*, Vol. 13, No. 4, pp. 615-627 (1995)
- /6/ E. C. M. Pennings, R. J. Deri, A. Scherer, R. Bhat, T. R. Hayes, N. C. Andreadakis, M. K. Smit, L. B. Soldano, and R. J. Hawkins : "Ultracompact, low-loss directional couplers on InP based on self-imaging by multimode interference" *Applied Physics Letters* Vol. 59, No. 16, pp. 1926-1928 (1991)
- /7/ S. Nagai, G. Morishima, M. Yagi, K. Utaka : "InGaAsP/InP Multi-Mode Interference Photonic Switches For Monolithic Photonic Integrated Circuits" *Japanese Journal of Applied Physics*, Vol. 38, Pt. 1, No. 2B, pp. 212-215 (1999)

Fundamental Evaluation of Semiconductor Waveguide-type In-line Wavelength Selective Filter with Fabry-Perot Etalon Resonator

M. Otaka, S. Takahashi, K. Utaka, M. Horita*, and T. Yazaki*

*Department of Electronics, Information and Communication Engineering, Waseda University
3-4-1 Okubo Shinjuku Tokyo, 169-8555 JAPAN*

(Tel) +81-3-5286-3394 (Fax) +81-3-3200-2567 (E-mail) utaka@mn.waseda.ac.jp

** KDD R&D Laboratories*

Abstract

As compact filtering devices easily integrated with semiconductor waveguides and also for the application to a multi-wavelength light source, we fabricated an InGaAsP/InP semiconductor waveguide-type in-line wavelength selective filter with a Fabry-Perot etalon resonator. Filtering effect was obtained with an almost-designed transmission wavelength interval of 0.8nm. Fundamental characteristics of the fabricated devices were evaluated, and the structures to improve a method of the contrast ratio are discussed.

I. Introduction

There are accelerating demands to expand the communication capacities associated with explosive deployment of internet, mobile phone and other media. For this purpose the modulation rate in the communication systems are also increasing, and 40Gb/s systems are expected for the next generation ones. However, further high-bit rate systems seem difficult due to the limit of operation speed of electronic circuits at present, and instead Wavelength Division Multiplexing (WDM) systems are promising. Especially, Dense Wavelength Division Multiplexing (DWDM) networks have been intensively investigated on the basis of ITU-T Recommendation G.692. To increase the channel numbers, the interval of adjacent two wavelengths is made extremely narrow, and the center wavelength should be properly defined in the systems. For example, the standard values of the interval and the center wavelength are 0.8nm (100GHz) and 1552.524nm, respectively. Wavelength selective filters that are highly stable and accurately locked at the allocated wavelengths are essential to realize these systems. In addition, these filters should also be easy for tuning of the interval and the center wavelength, easy for integration with other optical devices such as a light source, a detector and a channel waveguide, and independent of polarization of light. To satisfy these requirements semiconductor waveguide-type in-line wavelength selective filters are quite promising. These kinds of filters are also effective in the respect that a multiple resonator configuration can manipulate the transmission characteristics and realize wide-range wavelength tuning. In this paper, we present the structure, fabrication process and fundamental filtering characteristics of an InGaAsP semiconductor waveguide-type in-line

wavelength selective filter with a Fabry-Perot etalon resonator operating at the 1550nm wavelength range.

II. Fabrication

A structure of the device we fabricated is shown in Fig.1. The devices were fabricated by liquid phase epitaxial (LPE) growth method on InP substrates. The thickness of each layer was as follows: an InP buffer layer of 0.4 μ m, an InGaAsP waveguide layer ($\lambda_g=1.24\mu$ m) of 0.3 μ m, an InP cladding layer of 1.0 μ m, and an InGaAsP cap layer of 0.1 μ m. These layers were not doped intentionally. After the growth, a SiO₂ film was deposited on the surface as a mask before photo-resist coating. In the photolithography, line patterns were first exposed to define waveguides, and then groove patterns forming the resonator regions were exposed by Laser Beam Direct Drawing (LBDD). This two-time exposure was adopted because of the difficulty to form narrow grooves by the simultaneous photolithography for waveguides and resonators. The waveguides and resonators were inclined up to 7 degrees from the <011> direction to suppress spurious resonant modes generated between the cleaved facets.^[1] The width of the grooves, that is, the spacing between the waveguide and the resonator became about 1 μ m after the development process. After the photolithography process, the InGaAsP cap layer, the InP cladding layer and the InGaAsP waveguide layer were etched down by the combination of Reactive Ion Etching (RIE) and wet chemical etching methods in order to eliminate introduced damages and to reduce roughness of the dry-etched surface. The dry etching process was carried out under the conditions of mixed gases of CH₄:H₂=10sccm:40sccm, an RF etching power of 100W, a pressure of 6.4Pa and the etching time of 15 minutes.^[2] After the dry etching process, the surface of the InP

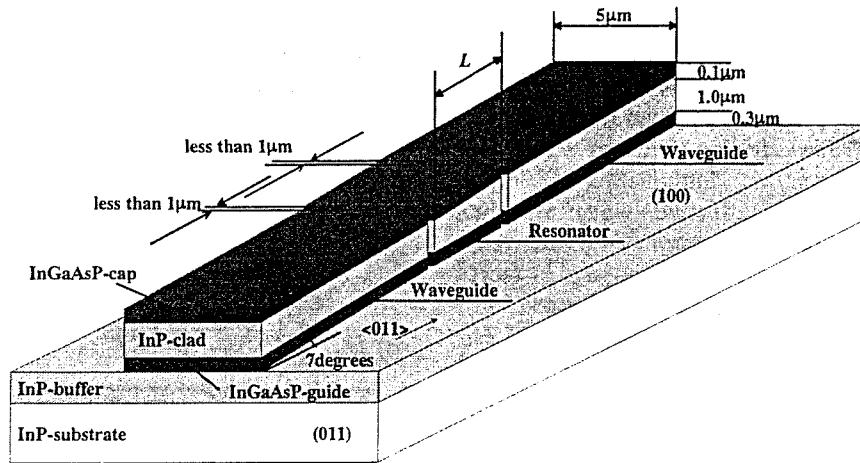


Fig.1 Schematic device structure

buffer layer and the sidewall of the InP cladding layer were etched by an etchant of $\text{HCl}:\text{H}_3\text{PO}_4=1:3$ for 5 seconds, and the sidewall of the InGaAsP waveguide layer by an etchant of $\text{H}_2\text{SO}_4:\text{H}_2\text{O}_2:\text{H}_2\text{O}=1:8:4$ for 30 seconds. Though these wet chemical etching processes helped the dry-etched rough facet to become smooth, it also posed a side etching, which led to a narrower waveguide and a wider spacing between the waveguide and the resonator than the designed ones. The spacing expanded to about $1.3\mu\text{m}$ (though a designed value was $1.0\mu\text{m}$) because of these etching processes, as shown in Fig.2. As a waveguide, a high mesa structure with a width of $5\mu\text{m}$ was adopted. In order to attain a desired wavelength interval $\Delta\lambda$, a length of the resonator L is determined as $L=\lambda^2/2n_{\text{eff}}\Delta\lambda$, where λ is the input wavelength and n_{eff} the effective refractive index of the resonator. Here, L was designed to be $469.2\mu\text{m}$ for $\Delta\lambda=0.8\text{nm}$ using $n_{\text{eff}}=3.20$ at 1550nm wavelength. A spacing between the waveguide and the resonator was designed to be less than $1.0\mu\text{m}$ for low-loss coupling.

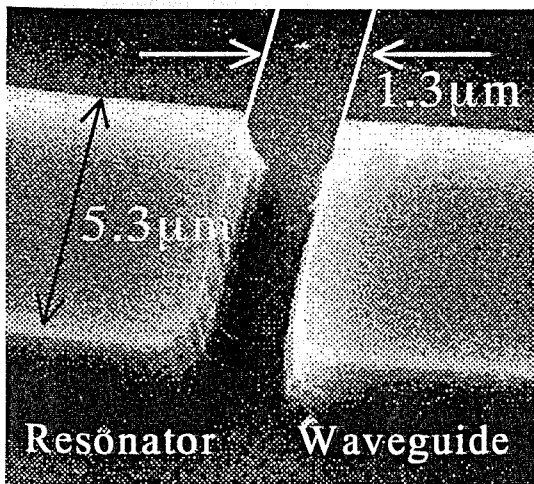


Fig.2 Surface of the device

III. Characteristic Evaluation

Fundamental filtering characteristics of the fabricated device with a total device length of 5-6mm were measured. As an input light source, amplified spontaneous emission of Erbium Doped Fiber Amplifier whose emission wavelength range was from $1.3\mu\text{m}$ to $1.6\mu\text{m}$ was used. An output spectrum of the device is shown in Fig.3. Fabry-Perot resonant characteristics were observed with a designed equal wavelength interval of 0.8nm (100GHz) and a pass-stop contrast ratio of 1.5dB . The low contrast ratio is considered to be due to rather poor facet flatness, as shown in Fig.2, as well as a propagation loss in the resonator, which came from a residual absorption loss and a side-wall scattering loss of about 2.7dB/mm (6.4cm^{-1}). This facet roughness led to reduction of the reflection coefficient.^{[1][3]} The power reflection and transmission coefficients were estimated to be 12% and 51% , respectively, on the basis of these evaluated loss value and contrast ratio. Since the power reflection coefficient at a cleaved mirror facet is 27% , it is one of the issues to further reduce roughness of the mirror facets and to make them like cleaved ones. To flatten the resonator facets, the etching processes have to be optimized, which can reduce a scattering loss at the same time. We are able to reduce the scattering loss

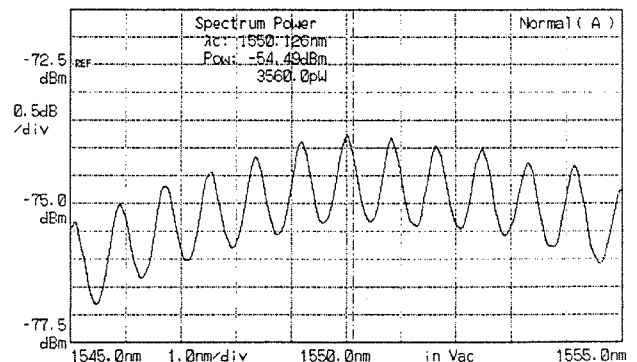


Fig.3 Output Spectrum of the device

also by adopting a ridge structure. The fabrication process optimization will also lead to the realization of a narrower spacing between a waveguide and a resonator, which leads to a lower coupling loss than the estimated value of about 6.7dB^[4] for a spacing of 1.3 μ m. In order to realize a higher contrast, introduction of high reflection (HR) structures is effective, which will be discussed later. It is noted that spurious ripples were successfully suppressed by introducing the angled facet relative to the waveguide, which might degrade the coupling losses between the waveguide and fibers. In order to tune the wavelength intervals and the resonant wavelengths for practical applications, we are trying to introduce the mechanism to change the refractive index of the resonator region by heat control.

IV. Discussion

In order to evaluate the effect of HR structures and design the structures, we simulated the filtering characteristics. Usually HR coatings are composed of the multilayer deposition of metal films or dielectric films. However, for application of the devices which use a transmitted light like this case, metal film coating is not effective because of large absorption loss. Therefore, this simulation premises on dielectric thin films generally used. These kinds of dielectric materials, i.e., silicon dioxide (SiO₂), amorphous silicon (a-Si) and InGaAsP/InP, are used. Their refractive indices n are assumed 1.40, 3.65 and 3.22, respectively, and that of air is set to 1.0. These three thin dielectric films and air gaps with each thickness of $\lambda/4n$ or $3\lambda/4n$ are deposited or installed on the facet of the resonator. The calculated results of reflectivity are shown in Fig.4. In the calculation, existence of the waveguide was also taken into account for actual situations. As for the cases of Fig.4 (c) and (d), a-Si films are assumed to be deposited only on the facets of the resonator. According to Fig.4, even when a single film of a-Si is deposited, the reflectivity of the mirror facet increases to be about 74%. A semiconductor post with two air gaps realizes quite high reflectivity of about 96%, as shown in Fig.4 (a) and (b). It is noted that deposition of films or installation of posts with thicknesses of $\lambda/4n$ are covering quite a wide band for high reflectivity, as shown in Fig.4 (a) and (c), though they may need precise fabrication process, such as Electron Beam Lithography (EB). On the other hand, thick films of $3\lambda/4n$ are easier to fabricate and still keep high reflectivity band at 1500nm wavelength range, as shown in Fig.4 (b) and (d). But, the spacings between the resonator and the waveguide render wide, which may degrade coupling efficiencies. Actual spacings are 895nm, 2686nm, 494nm and 1481nm for the cases of Fig.4 (a), (b), (c) and (d), respectively. If the spacings are smaller than 1 μ m, the coupling loss is not so large. Under the conditions of the power reflectivity of 96% and 74% for HR structures as the cases of Fig.4 and using an experimentally evaluated transmission loss of 2.7dB/mm (6.4cm⁻¹), filtering characteristics are calculated as shown in Fig.5. The contrast ratios are mostly

determined by the reflectivity of the facets, and high contrast ratios of 16dB and 11dB are attainable for Fig.5 (1) and (2), respectively. It is noted that existence of the propagation loss in the resonator seriously degrades the transmissivity. Therefore, the loss has to be reduced as much as possible, and compensation of the loss by a semiconductor optical amplifier is also very effective.

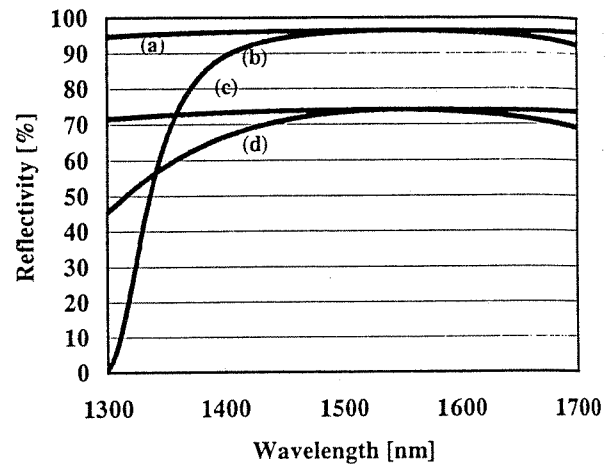


Fig.4 Reflective characteristics of HR structures ;
 (1) The case of a semiconductor post with two air gaps. Respective thicknesses are (a) $\lambda/4n$ and (b) $3\lambda/4n$.
 (2) The case that a single film of a-Si is deposited. Thicknesses of the film and an air gap are (c) $\lambda/4n$ and (d) $3\lambda/4n$, respectively.

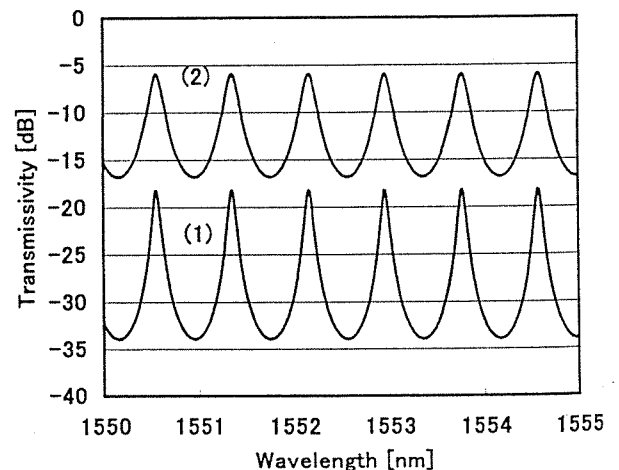


Fig.5 Transmission spectra with a propagation loss of 2.7dB/mm (6.4cm⁻¹) ;
 The reflectivity is (1) 96% and (2) 74%.

V. Conclusion

We reported the structure, fabrication process and fundamental filtering characteristics of an InGaAsP semiconductor waveguide-type in-line wavelength selective filter with a Fabry-Perot etalon resonator. Experimentally, we obtained a designed 0.8nm wavelength interval with a contrast ratio of 1.5dB. Low

contrast ratio can be improved by optimizing the fabrication process and the waveguide structure, and by introducing HR structures. Design consideration for HR structures were discussed.

References

- [1]K. Iga, K. Wakao, and T. Kunitake, Appl. Optics, Vol.20, No.14, pp.2367-2371 (1981).
- [2]C. Cremer and M. Schienle, Electron. Lett., Vol.25, No.17, pp.1177-1178 (1989).
- [3]H. Saito and Y. Noguchi, Jpn J. Appl. Phys. Vol.10, pp.1836-1842 (1989))
- [4] K. Utaka, S. Akiba, K. Sakai, and Y. Matsushima, J. Quantum. Electron, Vol.QE-20, No.3, pp.236-245 (1984)

FABRICATION AND FUNDAMENTAL EVALUATION OF SEMICONDUCTOR WAVEGUIDE-TYPE IN-LINE WAVELENGTH SELECTIVE FILTERS WITH FABRY-PEROT ETALON RESONATOR

Shuichi Takahashi, Masaru Otaka, Katsuyuki Utaka, Masayoshi Horita* and Tomonori Yazaki*
Waseda University, KDD R&D Laboratories*
Japan

1. ABSTRACT

We propose an InGaAsP waveguide-type in-line wavelength selective filters with a Fabry-Perot etalon resonator that correspond to the ITU grid of the DWDM system. Designed wavelength intervals 0.8nm was achieved, and fundamental pass band-stop band contrast ratio 1.5dB was obtained. In this paper, we present the structure, fabrication process, fundamental evaluation of filtering characteristics operating at the 1550nm-wavelength range, and the discussion on the evaluation result is given.

2. INTRODUCTION

The systems of the next generation Dense Wavelength Division Multiplexing (DWDM) networks have already been ruled by ITU-T Recommendation G.692. To increase the density of multiplexing, the interval of adjacent two wavelengths is made extremely narrow, and the center wavelength should be properly defined in the systems. For example, the standard values of the interval and the center wavelength are 0.8nm and 1552.524nm, respectively. In addition to these strict definitions, the allowable deviation of each wavelength is within ± 0.2 nm, so wavelength selective filters that are highly stable and appropriately tunable at the allocated wavelengths are desired in the systems.

As one of the devices that can fulfill those requirements, an InGaAsP waveguide-type in-line wavelength selective filters with a Fabry-Perot etalon resonator is promising in terms of easy tuning and easy integration with other optical devices such as a light source, a detector and a channel waveguide. These kinds of filters are also effective in the respect that a multiple resonator configuration can realize the control of the pass band shape and manipulate the transmission characteristics.

3. DEVICE STRUCTURE

The structure of the fabricated device is shown in Fig.1. The thickness of each layer is as follows: an InP buffer layer of $0.4\mu\text{m}$, an InGaAsP waveguide layer ($\lambda_g=1.24\mu\text{m}$) of $0.3\mu\text{m}$, an InP clad layer of $1.0\mu\text{m}$, and an InGaAsP cap layer of $0.1\mu\text{m}$. As a channel

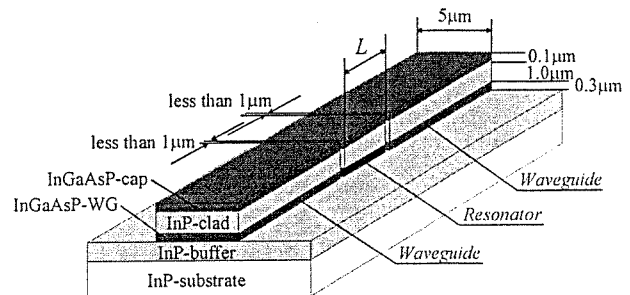


Fig.1: Schematic device structure

waveguide, a high mesa structure with a width of $5\mu\text{m}$ was adopted for single mode propagation. In order to attain a desired interval $\Delta\lambda$ of adjacent two wavelengths, the length of the resonator (L) is determined as

$$L = \frac{\lambda^2}{2N_{eff}\Delta\lambda} \quad (1)$$

where λ is the input wavelength and N_{eff} the effective refractive index of the resonator. Here, L is designed to be $469.2\mu\text{m}$ for $\Delta\lambda=0.8\text{nm}$ using $N_{eff}=3.20$ at 1550nm wavelength. The space between a waveguide and a resonator was designed to be less than $1.0\mu\text{m}$ for low-loss coupling. Furthermore, waveguides and resonators were inclined up to 7 degrees from the $\langle 011 \rangle$ direction to suppress spurious resonant modes generated between the cleaved facets^[1].

4. FABRICATION PROCESSES

The device was fabricated by liquid phase epitaxial (LPE) growth method on a (100) InP substrate. Each layer was not doped intentionally to reduce transmission loss.

After the growth, SiO_2 was deposited on the surface as a mask before photo-resist coating. We adopted the Laser Beam Direct Drawing (LBDD) method for minute photolithography processes. Firstly, line patterns for waveguides were exposed with a certain exposing condition. Then, isolation patterns to separate resonator regions from waveguides were exposed with a different condition. The individual proper selection of the exposure conditions were inevitable and quite effective for the fabrication of a narrower space and saving exposure time. The actual space between the waveguide

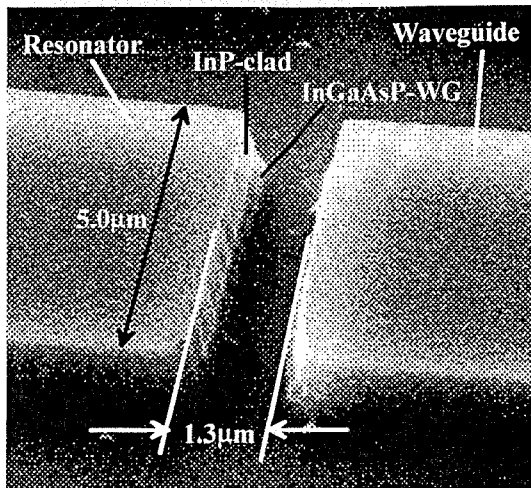


Fig.2: Scanning Electron Microscopic image of the fabricated device

and the resonator became about $1.0\mu\text{m}$ after the development process.

After the photolithography process, an InGaAsP cap layer, an InP clad layer and an InGaAsP waveguide layer were etched down by the combination of Reactive Ion Etching (RIE) and wet chemical etching methods in order to eliminate introduced damages and to suppress roughness of the etched surface. First, the dry etching process was carried out under the conditions of the mixed gas of $\text{CH}_4:\text{H}_2=10\text{sccm}:40\text{sccm}$, the power of 100W, the pressure of 6.4Pa, and the time of 15 minutes^{[2][3]}. Second, to remove carbonized remains the ashing process was carried out under the conditions of the 30sccm O_2 gas, the power of 50W, the pressure of 6.4Pa, and the time of 10 minutes. Third, this device was immersed in HF solution for 60 seconds to remove the oxygenated layers generated by the ashing process. Finally, the dry-etched mirror facets of the InP clad layer and the InGaAsP waveguide layer were etched by the successive wet chemical etchant of $\text{HCl}:\text{H}_3\text{PO}_4=1:3$ for 5 seconds and of $\text{H}_2\text{SO}_4:\text{H}_2\text{O}_2:\text{H}_2\text{O}=1:8:4$ for 10 seconds. Though this wet chemical etching process can help the etched rough facets to become flatter mirror facets, it can also pose side etching, which leads to a narrower waveguide and a wider space between a waveguide and a resonator than the designed one. After this etching process, the space expanded to about $1.3\mu\text{m}$ in contrast to the designed value of $1.0\mu\text{m}$, as shown in Fig.2.

5. FILTERING CHARACTERISTICS

The fundamental filtering characteristics of the fabricated device with a total device length of 2-3mm were measured. As an input light source, amplified spontaneous emission (ASE) of Erbium Doped Fiber Amplifier (EDFA) whose emission wavelength range was from $1.3\mu\text{m}$ to $1.6\mu\text{m}$ was used. The output

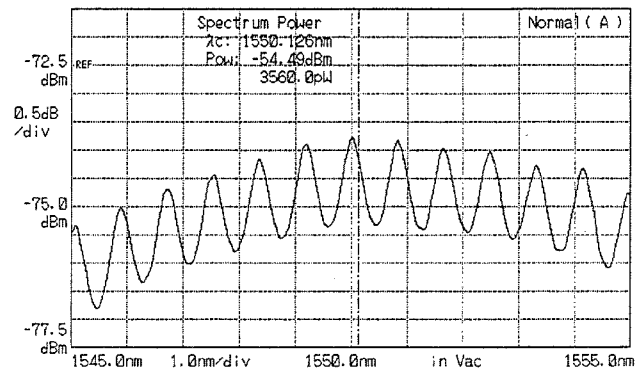


Fig.3: Output Spectrum

spectrum of the device is shown in Fig.3. Fabry-Perot resonant characteristics were achieved with an equal wavelength interval of the designed 0.8nm , and a pass band - stop band contrast ratio of 1.5dB. In the measurement, no current or heat was injected to the device. It is also noted that spurious ripples were successfully suppressed by introducing the angled facet. The extremely low contrast ratio is considered to be attributed to a low reflectivity of the mirror facets of the resonator due to rather poor facet flatness, as can be seen in Fig.2, as well as a high transmission loss estimated about 2.7dB/mm in a resonator, which came from a residual absorption loss and a side-wall scattering loss.

We calculated the dependence of the power reflectivity R , power transmissivity T and attenuation constant α of a mirror facet on the transmission characteristics, as shown in Fig.4. In theory, the power reflectivity of a completely flat semiconductor mirror facet without any reflection films is about 0.27 on the condition that effective refractive index of the waveguide N_{eff} is 3.20 and refractive index of air N_{air} 1.00. The calculation based on the values of $R=0.27$, $T=0.73$ and $\alpha=0\text{cm}^{-1}$ denotes that the pass band - stop band contrast ratio of a resonator without any reflection films is at most 4.8dB (Fig.4 (a)). The calculation enabled us to estimate the values of R , T and α for the fabricated device. The result indicates that R was about 0.12 at the highest, which was also based on the estimated T of 0.51 and α of 6.4cm^{-1} , corresponding to measured 2.9dB/facet and 2.7dB/mm, respectively. This brings the result that the excess loss on the facet was estimated to be 0.37 (Fig.4 (b)). The calculation also proved that high reflection coating (HR coating) on the etched mirror facet is a promising technique to obtain higher contrast ratio. For example, the high contrast ratio as high as 11.8dB can be attained with the coating films for $R=0.80$, $T=0.20$, and $\alpha=6.4\text{cm}^{-1}$ (Fig.4 (c)). The total insertion loss from fiber to fiber was estimated to be 34dB, in which the one of this in-line Fabry-Perot etalon resonator itself was 6.4dB at present.

We have adopted the combination of dry etching and wet chemical etching to fabricate reflection mirror facets, but the latter etching process will cause the

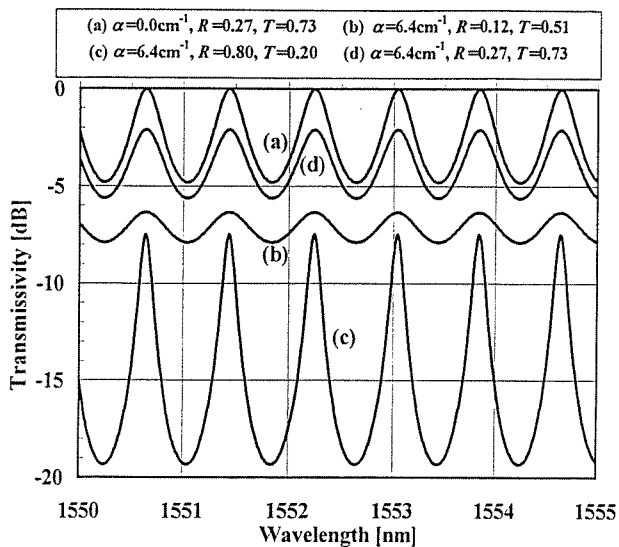


Fig.4: Transmission characteristics

expansion of the space between a waveguide and a resonator. To solve this problem, the dry etching conditions such as gas flow or RF power should be optimized, and this will be conducive to elimination of the wet etching process. The fabrication process optimization will make the space between a waveguide and a resonator narrower, which can improve an insertion loss, and it will also lead to flattening of resonator facets, which can increase facet reflectivity and decrease waveguide scattering loss at the same time.

In order to tune the wavelength intervals and the resonant wavelengths for practical applications, we are introducing the mechanism to change the refractive index of the resonator region by heat control. The experiment is under way.

6. CONCLUSION

We report the structure, fabrication process and fundamental filtering characteristics of a semiconductor waveguide-type in-line wavelength selective filter with a Fabry-Perot etalon resonator. We achieved the designed 0.8nm wavelength interval, and observed 1.5dB contrast ratio. Low contrast ratio and adjustment to the ITU-T recommendation wavelength allocation can be improved by optimizing the fabrication process and the waveguide structure.

ACKNOWLEDGMENTS

This work was supported by Grant-in-Aid for Scientific Research on Priority Areas (A)#410 from the Ministry of Education, Culture, Sports, Science and

Technology, and Waseda University Grant for Special Research Projects.

REFERENCES

- [1] K. Iga, K. Wakao, and T. Kunikane, "Mode reflectivity of tilted mirrors in semiconductor lasers with etched facets," *Appl. Opt.*, **20**, 2367-2371 (1981).
- [2] C. Cremer and M. Schienle, "RIE etching of deep Bragg grating filters in GaInAsP/InP," *Electron. Lett.*, **25**, 1177-1178 (1989).
- [3] H. Saito and Y. Noguchi, "InGaAsP/InP Etched Mirror Lasers Fabricated by Inclined RIE," *Japanese J. Appl. Phys.*, **10**, 1836-1842 (1989).